Universidad de Alcalá

PhD. Program in Electronics: Advanced Electronic Systems. Intelligent Systems

Predictive Techniques for Scene Understanding by using Deep Learning in Autonomous Driving

PhD. Thesis Presented by

Carlos Gómez Huélamo

2023

Universidad de Alcalá

PhD. Program in Electronics: Advanced Electronic Systems. Intelligent Systems

Predictive Techniques for Scene Understanding by using Deep Learning in Autonomous Driving

PhD. Thesis Presented by

Carlos Gómez Huélamo

Advisors

Dr. Luis Miguel Bergasa Pascual

Dr. Rafael Barea Navarro

Alcalá de Henares, 28th of September, 2023

A mi Madre, allá donde esté ...

"En este vasto mundo
navegáis en pos de un sueño,
surcando el ancho mar
que se extiende frente a vosotros.
El puerto de destino es el mañana
cada día más incierto.
¡Encontrad el camino!,
¡Cumplid vuestros sueños!,
¡Estáis todos en el mismo barco!
y vuestra bandera
¡Es la libertad¡"
Opening 3 de One Piece
Autor: The Babystars

Acknowledgements

Esta Tesis Doctoral supone el culmen a cuatro años (Abril 2019 - Septiembre 2023) realmente duros, cargado de emociones, triunfos, pandemias, estafas y tropiezos, todo a partes iguales. Este es probablemente (aunque como diría Sean Connery interpretando a James Bond en 1983, *Never Say Never Again*) mi último gran documento individual, académicamente hablando.

Durante mi etapa universitaria (2013 hasta el momento, 2023) he tenido ciertos momentos puntuales en los que he sentido un salto cuantitativo a nivel profesional: El primero fue en el segundo cuatrimestre de segundo de carrera, cuando las cosas se pusieron tensas con Control II e Informática Industrial. Vaya sudores. El segundo probablemente fue con el fallecimiento de mi madre durante mi ERASMUS+ en Irlanda. Duros y oscuros momentos, alejado de mis seres queridos, que afronté con la mayor entereza posible con la ayuda de compañeros que conocí allí, apoyo de familiares y amigos y cuando mi padre y mi hermana me vinieron a visitar, pero sobre todo con la regla de las tres C: Cabeza, Corazón y Coj****. Ya me entendéis. El tercer momento llega en segundo de máster, durante mi querido ERASMUS+ en Finlandia, donde compagino una estancia preciosa en Tampere (visitando Laponia, Rusia (nunca olvidaré cuando cogimos un piso tan barato en Moscú, *i.e.* 7 euros la noche, que había chinches en la ropa al día siguiente), Estonia, Letonia, etc) y un pre-inicio de doctorado. Me equivoqué al empezar tan pronto con la beca de doctorado FPI, "queriendo cobrar" cuanto antes, en vez de terminar tranquilamente el TFM y plantear el doctorado, pero eso no lo sabría hasta tiempo después.

Fue en la tesis cuando empezaron realmente los quebraderos de cabeza. Continuamente altibajos, mala planificación por mi parte (y no tan mi parte ...), momentos puntuales donde me equivoqué rotundamente al querer soldar una estructura compleja para nuestro vehículo eléctrico sin ninguna ayuda, no estudiar PyTorch tras el congreso WAF 2018 tras la sugerencia de mi tutor, no enfocarme en técnica individual hasta bien entrado el doctorado, no querer hacer nada hasta que no tuviese la teoría perfectamente asimilada, tener demasiado respeto a la Inteligencia Artificial y escurrir el bulto de mi tesis en un compañero mientras yo me dedicaba a integrar y corregir los *bugs* del grupo que para mí *era lo fácil*. Mal. Todo mal. Pero todo cambió tras mi segunda estancia de doctorado, en Estados Unidos, cuando tras llorar por no entender el camino a seguir (probablemente el mayor reto de un doctorado), nadie que me ayudara, decidí crear mi

propio camino, con paciencia y fé, práctica y error, todo ello compaginado con lectura de artículos, para mejorar mi confianza y autoestima y así afrontar con el mayor estándar de calidad posible el tiempo que me quedaba de doctorado. Gracias a todos mis errores, desventuras y discusiones, a día de hoy, excepto momentos inevitables, me encuentro con muchísima más capacidad para atacar, diseccionar y gestionar prácticamente cualquier problema, consultar documentación y organizarme, aunque esta última sigue siendo mi tarea pendiente. En ese sentido, me gustaría recalcar una frase recientemente dicha (Julio, 2023) por parte de Petar Veličković, uno de los mayores expertos actuales en *Graph Neural Networks* a nivel mundial, resumiendo lo que representa terminar un doctorado:

"A successful PhD is not something just that makes you a very deep expert in a particular area, but it also makes you a master adapter"

Desde hace ya varios, mi primera publicación del año en Instagram viene seguida de la frase "Trabaja duro en silencio y deja que tu éxito haga todo el ruido". Filosofía Kaizen, mejora y aprendizaje continuo, para así cada día entender el mundo un poquito mejor. Si toda la dedicación y estudio que he depositado en este trabajo sirven para algo en el futuro, sé que todo el esfuerzo habrá merecido la pena.

Después de este particular monólogo, a lo cual soy muy propenso y de lo cual mis amigos y compañeros no cesan en su empeño de recordádmelo, debo, como no puede ser de otra manera, dar paso a los agradecimientos.

En primer lugar, me gustaría agradecer a mis profesores del grupo RobeSafe, especialmente a mis tutores Luis Miguel Bergasa Pascual y Rafael Barea Navarro (siempre recordaré el abrigo que me prestaste cuando fuimos a Nueva Zelanda en 2019 porque me había dejado el mío en el aeropuerto), por ofrecerme estar en el grupo (así como aguantarme) durante todos estos años e intentar que tuviésemos el mejor *experimental setup* y *roadmap* en el laboratorio, aunque no fuese siempre sencillo. Especialmente me gustaría resaltar de nuevo la figura de Luis Miguel, a quien con mucho cariño considero mi padre académico, por confiar en mí en su momento, sus múltiples consejos sobre la vida y el trabajo, y haber lidiado con mi ambición y frustración a partes iguales como un gran capitán que ha sabido guiar una humilde embarcación para que creciera personal y profesionalmente con el paso inexorable del tiempo. Sin lugar a dudas considero realmente interesante la temática propuesta en esta tesis doctoral, predicción de movimiento en el contexto de vehículo inteligente, ya que entra en el plano filosófico sobre cómo razonar el futuro de la escena de tráfico para tener una mayor seguridad y comfort durante la conducción. Es bonito ver como durante el doctorado tu mente cambia y te fijas en tu día a día (en este caso, fundamentalmente a la hora de conducir) en todo lo que intentas reproducir durante tu investigación. Habrá que seguir esta tendencia muy de cerca en los próximos años, porque personalmente considero que sus aplicaciones son fantásticas.

A mis tutores en las estancias de doctorado, Christoph Stiller y Eduardo Molinos en el Karslruhe Institute of Technology (KIT, Alemania) y Wei Zhan y Masayoshi Tomizuka

en la University of California, Berkeley (UCB, Estados Unidos). Se suele decir que unas veces se gana y otras se aprende, y yo en estas estancias quizás aprendí demasiado, porque vaya tela ... No obstante, me guardo momentos muy bonitos (admirar las secuoyas gigantes de Yosemite, visitar más solo que la una la zona de Baden-Wurtemberg (la Selva Negra del Age of Empires!), hacer mi primera escalada en roca, las milanesas que le quitaba (cariñosamente) a los argentinos en Berkeley durante mis incursiones nocturnas a la nevera, comer guisantes con jamón junto al río con la luz tenue del atardecer con una tarjeta de crédito porque se me había olvidado el tenedor al visitar Heidelberg, etc.) y buenos amigos, como Su Shaoshu o Frank Bieder, con los que aún guardo un cierto contacto.

A mis compañeros, mejor dicho, amigos, de laboratorio, especialmente Javier Araluce, Rodrigo, Felipe (chavalín), Santiago, Miguel Antunes, Miguel Eduardo, antiguos compañeros como Javier del Egido, Óscar, Alejandro, Eduardo, Roberto y Pablo Alcantarilla, y a nuevos compañeros del grupo como Fabio, Navil y Pablo. Gracias de corazón por estar ahí, por vuestras charlas sobre tecnología, empleos, el camino correcto a seguir y la vida en general.

Especial mención vuelvo a hacer a Miguel Eduardo y mi compañero Marcos Conde, cuyo apoyo intenso ayudó a centrar mi camino en técnica y escritura. Sois dos pedazo de máquinas. Muchísimas gracias por todo lo que aprendí a vuestro lado y os deseo lo mejor en vuestro futuro profesional y personal.

A mi querido profesor Ángel Álvarez, por sus valiosos consejos para afrontar mi carrera profesional y mi vida en general de la mejor forma posible. Eres muy grande.

A mis grandes amigos de la universidad con los que sigo teniendo un contacto bastante estrecho y les quiero un montón, especialmente a Rocío, Juan Carlos, Esther, Sergio, Antonio, Pablo, Rubén y Adrián Rocandio. Una alegría cuando me junto con ellos siempre y compartimos recuerdos y objetivos futuros, tanto personales como profesionales. Aún me acuerdo de cuando empezamos con la carrera y como el paso inexorable del tiempo nos moldea a conveniencia. Os deseo lo mejor.

A mis buenos amigos Samuel y Adrián, con quien gran parte de mi vida he compartido. Con especial cariño guardo las interminables charlas sobre la vida y el futuro después de entrenar en Karate, de comer, de cenar, en el coche, siempre quejándonos de la hora que marcaba el reloj al final de tan extenuantes conversaciones.

A mi familia, uno de los pilares de mi vida. A mis abuelos Gerardo, Petra y Juan Pablo, que están en el cielo, y a mi querida abuela Juli, con la que tantas porras con chocolate he comido de pequeño y no tan pequeño, siendo la huelga semanal de dos humildes euros mi mayor tesoro hace no tantos años. A mi padre Juan Antonio y a mi madre Petra, que en paz descanse, les debo todo lo que soy y es por ello por lo que les estaré siempre agradecido. Querido padre, gracias por ser tan Genaro, arisco y pesado. Siempre has sido mi ejemplo a seguir, aunque cuando tenga 42 años me sigas regañando por subir con las

zapatillas puestas a la habitación o no cerrar la puerta porque entran moscas. Querida madre, no se muere quien se va, sólo se muere el que se olvida, y tú nunca caerás en el olvido. A mi querida hermana-calili-*chessmaster* Silvia, con quien tantas regañinas he tenido, pero el cariño que nos tenemos las supera a todas. A mi perrita Nuka (*a.k.a.* Dragón, ChupaChups cuando le cortamos el pelo o Nuki-Nuki), cuyos paseos matutinos son probablemente el ingrediente secreto para la elaboración de este documento, dando rienda suelta a mi cabeza para imaginar nuevas propuestas mientras miraba el cielo azul.

A mi querido *experimental setup* que me ha acompañado durante toda mi vida académica: Silla de madera de la cocina, ratón de Hello Kitty "tomado prestado" de mi hermana, mi querido portátil táctil, disco duro portátil con fundita de cartón y goma, y la mochila negra que me lleva acompañando en mis aventuras desde Irlanda. Sois la base de todo mi trabajo y habéis recorrido medio mundo, compañeros (menos la silla, claro)!

Al resto de la familia, amigos, compañeros, entrenadores y profesores, gracias por todo.

Y, por último, la persona más importante de mi vida ahora mismo. Mi querida Marta, la persona más maravillosa y buena que conozco. Hemos compartido risas, lloros, besos y abrazos. Nunca me cansaré de repetirte lo suave que tienes la piel tras darte un beso en la mejilla y después hacerte de rabiar. Espero que esta situación esté dentro de un bucle *while* cuya condición sea *True*.

"Te quiero más que ayer, pero menos que mañana. Hoy, y siempre ..."

Mi querido lector, disculpa mi monólogo (te lo avisé) de agradecimientos, es mi forma de ser y la cual tengo por bandera, aunque creo que ha quedado bonito. Podría decir mil y un anécdotas más de mi doctorado, pero como diría Aragorn, hijo de Arathorn, heredero de Isildur y legítimo Rey de Gondor, enfrente de la mismísima Puerta Negra de Mordor: *Hoy no es ese día.*

Vamos a la lectura importante, que empiece el *Rock and Roll* !!

Resumen

La conducción autónoma es considerada uno de los más grandes retos tecnológicos de la actualidad. Cuando los coches autónomos conquisten nuestras carreteras, los accidentes se reducirán notablemente, hasta casi desaparecer, ya que la tecnología estará testada y no incumplirá las normas de conducción, entre otros beneficios sociales y económicos.

Uno de los aspectos más críticos a la hora de desarrollar un vehículo autónomo es percibir y entender la escena que le rodea. Esta tarea debe ser tan precisa y eficiente como sea posible para posteriormente predecir el futuro de esta misma y ayudar a la toma de decisiones. De esta forma, las acciones tomadas por el vehículo garantizarán tanto la seguridad del vehículo en sí mismo y sus ocupantes, como la de los obstáculos circundantes, tales como viandantes, otros vehículos o infraestructura de la carretera.

En ese sentido, esta tesis doctoral se centra en el estudio y desarrollo de distintas técnicas predictivas para el entendimiento de la escena en el contexto de la conducción autónoma. Durante la tesis, se observa una incorporación progresiva de técnicas de aprendizaje profundo en los distintos algoritmos propuestos para mejorar el razonamiento sobre qué está ocurriendo en el escenario de tráfico, así como para modelar las complejas interacciones entre la información social (distintos participantes o agentes del escenario, tales como vehículos, ciclistas o peatones) y física (es decir, la información geométrica, semántica y topológica del mapa de alta definición) presente en la escena.

La capa de percepción de un vehículo autónomo se divide modularmente en tres etapas: Detección, Seguimiento (*Tracking*), y Predicción. Para iniciar el estudio de las etapas de seguimiento y predicción, se propone un algoritmo de *Multi-Object Tracking* basado en técnicas clásicas de estimación de movimiento y asociación validado en el dataset KITTI, el cual obtiene métricas del estado del arte. Por otra parte, se propone el uso de un filtro inteligente basado en información contextual de mapa, cuyo objetivo es monitorizar los agentes más relevantes de la escena en el tiempo, representando estos agentes filtrados la entrada preliminar para realizar predicciones unimodales basadas en un modelo cinemático. Para validar esta propuesta de filtro inteligente se usa CARLA (*CAR Learning to Act*), uno de los simuladores hiperrealistas para conducción autónoma más prometedores en la actualidad, comprobando cómo al usar información contextual de mapa se puede reducir notablemente el tiempo de inferencia de un algoritmo de *tracking* y predic-

ción basados en métodos físicos, prestando atención a los agentes realmente relevantes del escenario de tráfico.

Tras observar las limitaciones de un modelo de predicción basado en cinemática para la predicción a largo plazo de un agente, los distintos algoritmos de la tesis se centran en el módulo de predicción, usando los datasets Argoverse 1 y Argoverse 2, donde se asume que los agentes proporcionados en cada escenario de tráfico ya están monitorizados durante un cierto número de observaciones.

En primer lugar, se introduce un modelo basado en redes neuronales recurrentes (particularmente redes LSTM, *Long-Short Term Memory*) y mecanismo de atención para codificar las trayectorias pasadas de los agentes, y una representación simplificada del mapa en forma de posiciones finales potenciales en la carretera para calcular las trayectorias futuras unimodales, todo envuelto en un marco GAN (*Generative Adversarial Network*), obteniendo métricas similares al estado del arte en el caso unimodal.

Una vez validado el modelo anterior en Argoverse 1, se proponen distintos modelos base (sólo social, incorporando mapa, y una mejora final basada en *Transformer encoder*, redes convolucionales 1D y mecanismo de atención cruzada para la fusión de características) precisos y eficientes basados en el modelo de predicción anterior, introduciendo dos nuevos conceptos. Por un lado, el uso de redes neuronales gráficas (particularmente GCN, *Graph Convolutional Network*) para codificar de una forma potente las interacciones de los agentes. Por otro lado, se propone el preprocesamiento de trayectorias preliminares a partir de un mapa con un método heurístico. Gracias a estas entradas y una arquitectura más potente de codificación, los modelos base serán capaces de predecir distintas trayectorias futuras multimodales, es decir, cubriendo distintos posibles futuros para el agente de interés. Los modelos base propuestos obtienen métricas de regresión del estado del arte tanto en el caso multimodal como unimodal manteniendo un claro compromiso de eficiencia con respecto a otras propuestas.

El modelo final de la tesis, inspirado en los modelos anteriores y validado en el más reciente dataset para algoritmos de predicción en conducción autónoma (Argoverse 2), introduce varias mejoras para entender mejor el escenario de tráfico y decodificar la información de una forma precisa y eficiente. Se propone incorporar información topológica y semántica de los carriles futuros preliminares con el método heurístico antes mencionado, codificación de mapa basada en aprendizaje profundo con redes GCN, ciclo de fusión de características físicas y sociales, estimación de posiciones finales en la carretera y agregación de su entorno circundante con aprendizaje profundo y finalmente módulo de refinado para mejorar la calidad de las predicciones multimodales finales de un modo elegante y eficiente. Comparado con el estado del arte, nuestro método logra métricas de predicción a la par con los métodos mejor posicionados en el Leaderboard de Argoverse 2, reduciendo de forma notable el número de parámetros y operaciones de coma flotante por segundo.

Por último, el modelo final de la tesis ha sido validado en simulación en distintas aplicaciones de conducción autónoma. En primer lugar, se integra el modelo para proporcionar predicciones a un algoritmo de toma de decisiones basado en aprendizaje por refuerzo en el simulador SMARTS (*Scalable Multi-Agent Reinforcement Learning Training School*), observando en los estudios como el vehículo es capaz de tomar mejores decisiones si conoce el comportamiento futuro de la escena y no solo el estado actual o pasado de esta misma. En segundo lugar, se ha realizado un estudio de adaptación de dominio exitoso en el simulador hiperrealista CARLA en distintos escenarios desafiantes donde el entendimiento de la escena y predicción del entorno son muy necesarios, como una autopista o rotonda con gran densidad de tráfico o la aparición de un usuario vulnerable de la carretera de forma repentina. En ese sentido, el modelo de predicción ha sido integrado junto con el resto de capas de la arquitectura de navegación autónoma del grupo de investigación donde se desarrolla la tesis como paso previo a su implementación en un vehículo autónomo real.

Palabras clave: Conducción Autónoma, Predicción de Movimiento, Aprendizaje Profundo, Entendimiento de la Escena, Eficiencia, Simulación.

Abstract

Autonomous driving is considered one of the greatest technological challenges of today. When autonomous cars take over our roads, accidents will be significantly reduced, almost disappearing, as the technology will be tested and will not violate driving regulations, among other social and economic benefits.

One of the most critical aspects in developing an autonomous vehicle is perceiving and understanding the surrounding scene. This task must be as accurate and efficient as possible to predict the future of the scene and assist in decision-making. In this way, the actions taken by the vehicle will ensure the safety of the vehicle itself and its occupants, as well as that of surrounding obstacles, such as pedestrians, other vehicles, or road infrastructure.

In this context, this doctoral thesis focuses on the study and development of different predictive techniques for scene understanding in the context of autonomous driving. Throughout the thesis, there is a progressive incorporation of Deep Learning techniques into the proposed algorithms to improve reasoning about what is happening in the traffic scenario, as well as modeling the complex interactions between social information (different participants or agents in the scene, such as vehicles, cyclists, or pedestrians) and physical information (geometric, semantic, and topological information from the high-definition map) present in the scene.

The perception layer of an autonomous vehicle is modularly divided into three stages: Detection, Tracking, and Prediction. To start studying the tracking and prediction stages, a Multi-Object Tracking algorithm based on classical motion estimation and association techniques is proposed and validated on the KITTI dataset, which has state-of-the-art metrics. Furthermore, the use of an intelligent filter based on contextual map information is proposed, aiming to monitor the most relevant agents in the scene over time. These filtered agents serve as the preliminary input for making uni-modal predictions based on a kinematic model. In order to validate our proposal including the map-based filter we make use of CARLA (CAR Learning to Act), one of the most promising hyper-realistic simulators for autonomous driving. We demonstrate how using contextual map information can significantly reduce the inference time for physics-based tracking and prediction algorithms by focusing on the truly relevant agents in the traffic scenario.

After observing the limitations of a kinematics-based prediction model for long-term agent prediction, the different algorithms in the thesis focus on the prediction module using the Argoverse 1 and Argoverse 2 datasets. These datasets assume that the agents provided in each traffic scenario have already been monitored for a certain number of observations.

Firstly, a model based on recurrent neural networks (particularly LSTM, Long-Short Term Memory, networks) and an attention mechanism is introduced to encode the past trajectories of agents. It also uses a simplified representation of the map in the form of potential final positions on the road to calculate uni-modal future trajectories. These components are wrapped in a Generative Adversarial Network (GAN) framework, achieving metrics similar to the state-of-the-art in the uni-modal case.

Once the previous model is validated on Argoverse 1, different precise and efficient baseline models are proposed for the prediction module. These baselines (only social, including map and a final improvement based on Transformer encoders, 1D-Convolutional Neural Networks, and cross-attention mechanism for feature fusion) introduce two main concepts. First, we make use of Graph Neural Networks (particularly Graph Convolutional Networks, GCNs) to encode the interactions between agents. Second, we preprocess preliminary trajectories from the map using a heuristic method. These models predict different multi-modal future trajectories, covering various possible futures for the agent of interest. The proposed base models achieve state-of-the-art regression metrics in both multi-modal and uni-modal cases while maintaining a clear efficiency compromise compared to other proposals.

The final model of the thesis, inspired by the previous models and validated on the most recent dataset for autonomous driving prediction algorithms (Argoverse 2), incorporates several improvements to better understand the traffic scenario and decode information accurately and efficiently. It proposes to incorporate topological and semantic information of the preliminary future lanes using the aforementioned heuristic method. It uses map encoding based on Deep Learning with Graph Convolutional Networks, a fusion cycle of physical and social features, Deep Learning estimation of goal points and aggregation of their surrounding environment, and a refinement module to further improve temporal consistency of the final multi-modal predictions in an elegant and efficient manner. Compared to the state-of-the-art, our method achieves prediction metrics on par with the top-ranked methods in the Argoverse 2 Leaderboard while significantly reducing the number of parameters and floating-point operations per second.

Lastly, the final model of this thesis has been validated in simulation in various autonomous driving applications. Firstly, the model is integrated to provide predictions to a Reinforcement Learning-based decision-making algorithm in the SMARTS (Scalable Multi-Agent Reinforcement Learning Training School) simulator, observing in the studies how the vehicle can make better decisions if it knows the future behavior of the scene, not

just the current or past state of it. Secondly, a successful domain adaptation study has been conducted in the hyper-realistic CARLA simulator in different challenging scenarios where scene understanding and environment prediction are highly necessary, such as a highway or roundabout with high traffic density or the sudden appearance of a vulnerable road user. In this regard, the prediction model has been integrated alongside the rest of the layers of the autonomous navigation architecture of the research group where the thesis is being developed, as a preliminary step towards its implementation in a real autonomous vehicle.

Keywords: Autonomous Driving, Motion Prediction, Deep Learning, Scene Understanding, Efficiency, Simulation.

Contents

List of Figures

List of Tables

List of Algorithms

List of Acronyms

ACC	Adaptive Cruise Control.
AD	Autonomous Driving.
AD-PerDevKit	Autonomous Driving Perception Development Kit.
ADAM	ADaptive Moment Estimation.
ADAS	Advanced Driver Assistance System.
ADE	Average Displacement Error.
ADS	Autonomous Driving Stack.
AI	Artificial Intelligence.
AMOTA	Average Multi-Object Tracking Accuracy.
AMOTP	Average Multi-Object Tracking Precision.
API	Application Programming Interface.
BAB	Best Augmented Baseline.
BEV	Bird's Eye View.
BMB	Best Map Baseline.
BSB	Best Social Baseline.
CA	Constant Acceleration.
CARLA	CAr Learning to Act simulator.
CCA	Constant Curvature and Acceleration.
cGAN	conditional Generative Adversarial Network.
CMP	Conditional Motion Prediction.
CNN	Convolutional Neural Network.
CSAA	Constant Steering Angle and Acceleration.
CSAV	Constant Steering Angle and Velocity.
CTRA	Constant Turn Rate and Acceleration.
CTRV	Constant Turn Rate and Velocity.
CUDA	Compute Unified Device Architecture.
CV	Constant Velocity.

DAMOT	Detection and Multiple-Object Tracking.
DL	Deep Learning.
DM	Decision-Making.
FC	Fully Connected.
FDE	Final Displacement Error.
FLOP	FLoating-point Operations per second.
FN	False Negative.
FP	False Positive.
GAN	Generative Adversarial Network.
GCN	Graph Convolutional Network.
GNN	Graph Neural Network.
GPU	Graphics Processing Unit.
GRU	Gated Recurrent Unit.
GT	Ground-Truth.
HA	Hungarian Algorithm.
HardM	Hard-Mining.
HD map	High-Definition map.
IDS	IDentity Switches.
IOU	Intersection Over Union.
ITS	Intelligent Transportation Systems.
KF	Kalman Filter.
LiDAR	Light Detection And Range.
LR	Learning Rate.
LSTM	Long Short-Term Memory.
MDP	Markov Decission Process.
MHCA	Multi-Head Cross-Attention.
MHSA	Multi-Head Self-Attention.
minADE	minimum Average Displacement Error.
minFDE	minimum Final Displacement Error.
ML	Machine Learning.
MLP	Multilayer Perceptron.

MOT	Multi-Object Tracking.
MOTA	Multi-Object Tracking Accuracy.
MOTP	Multi-Object Tracking Precision.
MP	Motion Prediction.
MSE	Mean Squared Error.
NHTSA	National Highway Traffic Safety Administration.
NLL	Negative Log Likelihood.
PMP	Passive Motion Prediction.
PPO	Proximal Policy Optimization.
RADAR	RAdio Detection and Ranging.
RANSAC	RANdom SAmple Consensus.
ReLU	Rectifier Linear Unit.
RL	Reinforcement Learning.
RNN	Recurrent Neural Network.
ROS	Robot Operating System.
RVIZ	ROS VIsualiZator.
SMARTS	Scalable Multi-Agent Reinforcement Learning Training School.
SORT	Simple Online and Realtime Tracking.
SOTA	State-of-the-Art.
SUMO	Simulation of Urban MObility.
TempDec	Temporal Decoder.
VRU	Vulnerable Road User.
WTA	Winner-Takes-All.

Chapter 1

Introduction

Aaay, el oro, la fama, el poder.
Todo lo tuvo el hombre
que en su día se autoproclamó
el rey de los piratas, ¡GOLD ROGER!
Mas sus últimas palabras
no fueron muy afortunadas:
"¿¡MI TESORO!? Lo dejé todo allí,
¡Buscadlo si queréis!,
¡Ojalá se le atragante al rufián que lo encuentre!

Opening 1 de One Piece: "We are"
Autor original: Hiroshi Kitadani

1.1. Motivation

Autonomous Driving (AD) have held the attention of technology enthusiasts and futurists for some time as is evidenced by the continuous research and development of this topic in Intelligent Transportation Systems (ITS) over the past decades, being one of the emerging technologies of the *Fourth Industrial Revolution*, and particularly of the Industry 4.0.

The concept Fourth Industrial Revolution or Industry 4.0 was first introduced by Klaus Schwab, CEO (Chief Executive Officer) of the World Economic Forum, in a 2015 article in Foreign Affairs (American magazine of international relations and United States foreign policy). A technological revolution can be defined as a period in which one or more technologies are replaced by other kinds of technologies in a short amount of time. Hence, it is an era of accelerated technological progress featured by Researching, Development and Innovation whose rapid application and diffusion cause an abrupt change in society. In particular, the Fourth Industrial Revolution conceptualizes rapid change to industries, technology, processes and societal patterns in the 21st century due to increasing interconnectivity and smart automation. This industrial revolution focuses on operational efficiency, being the following four themes which summarize it:

- **Decentralized decisions**: Ability of cyber physical systems to make decisions on their own and to perform their tasks as autonomously as possible.
- **Information transparency**: Provide operators with comprehensive information to make decisions. Inter-connectivity allows operators to gather large amounts of information and data from all points in the manufacturing process in order to identify key areas or aspects that can benefit from improvement to enhance functionality.
- **Technical assistance**: Ability to assist humans with unsafe or difficult tasks and technological facility of systems to help humans in problem-solving and DM.
- **Interconnection**: Ability of machines, sensors, devices and people to communicate and conect with each other via the Internet of Things (IoT) or the Internet of People (IoP).

Based on the aforementioned principles, this revolution is expected to be marked by breakthroughs in emerging technologies in fields such as nanotechnology, quantum computing, 3D printing, Internet of Things (IoT), fifth-generation wireless technologies (5G), Robotics, Computer Vision (CV), Artificial Intelligence (AI) or the scope of this doctoral thesis, Autonomous Driving Stacks (ADSs). The sum of all these advances are resulting in machines that can potentially see, hear and what is more important, think, moving more deftly than humans.

An ADS, driverless car or autonomous car, is a vehicle than can sense its surrounding and moving safely with little or even no human intervention. These ADSs must combine a variety of sensors to understand the traffic scenario, like RAdio Detection and Ranging (RADAR), LiDAR, cameras, Inertial Measurement Unit (IMU), wheel odometry, GNSS (Global Navigation Satellite System) or ultrasonic sensors, in order to detect, track and predict (which is the main purpose of this thesis) the most relevant obstacles around the ego-vehicle. Then, advanced control and planning systems process this sensory information in combination with a predefined global route to calculate the corresponding control commands to drive the vehicle throughout the environment, ensuring a safe driving.

The dream of seeing fleets of ADSs efficiently delivering goods and people to their destination has fueled billions of dollars and captured consumer's imaginations in investment in recent years. Nevertheless, according to the *Autonomous driving's future: Convenient and connected* report, published by the global management consulting firm McKinsey & Company in January 2023, even after some setbacks have pushed out timelines for AD launches and delayed customer adoption, the transportation community still broadly agrees that AD has the potential to transform consumer behaviour, transportation and society at large. AD is considered as one of the solutions to the aforementioned problems and one of the greatest challenges of the automotive industry today.

The World Health Organization (WHO) has indicated that the global population is increasingly concentrated in cities, which has significant implications for public health.

The trend of urbanization has been observed for several decades, with people migrating from rural to urban centers in search of better opportunities and improved living conditions. As a result, cities are becoming more crowded, and the WHO predicts that by the year 2050, nearly 70 % of the world population will reside in urban areas.

This concentration of people in cities poses both challenges and opportunities for public health. On the positive side, cities offer access to better healthcare facilities, educational institutions, and employment opportunities. Urban areas also tend to have improved sanitation systems and infrastructure, which can contribute to better overall health outcomes. However, the rapid growth of cities can strain existing resources and lead to overcrowding, inadequate housing, and increased pollution levels, all of which can have adverse effects on public health.

Aware of this problem, the European Commision (EU) has set several objectives and statistics to improve transport mobility in the future. These objectives and statistics are part of the EU broader vision for a sustainable, efficient, and interconnected transport system to create a seamless, sustainable, and integrated transport system across member states:

- **Sustainable Transport**: The European Commission aims to promote sustainable modes of transport, such as railways, public transport, cycling, and walking, to reduce greenhouse gas emissions, congestion, and air pollution. The target is to achieve a 60 % reduction in transport emissions by 2050 compared to 1990 levels.
- **Infrastructure Investment**: The EU has committed to investing in modern and efficient transport infrastructure, including the Trans-European Transport Network (TEN-T) and the Connecting Europe Facility (CEF). These investments aim to improve connectivity, remove bottlenecks, and enhance multi-modal transport options across the EU.
- **Road Safety**: The European Commission has prioritized improving road safety to reduce the number of accidents, injuries, and fatalities. The objective was to reduce road fatalities by 50 % by 2030 compared to 2020 levels. This includes implementing measures such as stricter vehicle safety standards, promoting safe driving behaviors, and improving road infrastructure.
- **Digitalization and Innovation**: The EU aims to harness digital technologies and innovation to improve transport efficiency, reliability, and user experience. This includes initiatives such as ITSs, the use of big data for planning and optimization, and the development of Connected and Autonomous Vehicles (CAVs) to enhance mobility.
- **Freight Transport Efficiency**: The European Commission aims to improve the efficiency and sustainability of freight transport through measures such as promoting

inter-modal transport, increasing the use of clean and energy-efficient vehicles, and implementing logistics optimization strategies. The objective is to reduce external costs, including congestion, noise, and emissions, associated with freight transport.

In that sense, the existence of reliable and economically affordable ADSs are expected to create a huge impact on society affecting social, demographic, environmental and economic aspects. It can produce substantial value for the automotive industry, drivers and society, making driving safer, more convenient and more enjoyable. In other words, the hours on the road previously spent by manual driving could be used to work, watch a funny movie or even to video call a friend. For employees with long commutes, AD might shorten the workday, increasing worker productivity. Since workers, specially those related to digital jobs or related fields, may perform their jobs from an ADS, they could more easily move further away from the office, which, in turn, could attract more people to suburbs and rural areas. Besides this, it is estimated to cause a reduction in road deaths, reduce fuel consumption and harmful emission associated and improve traffic flow, as well as an improvement in the overall driver comfort and mobility in groups with impaired faculties, such as disable or elderly people, providing them with mobility options that go beyond car-sharing services or public transportation. Other industrial applications of autonomous vehicles are agriculture, retail, manufacturing, commercial and freight transport or mining.

1.2. Historical Context

ADSs have become a challenge for automation and technology companies, which has derived in an intense competition. Though today companies such as Mercedes, Ford or Tesla are racing to build ADSs for a radically changing consumer world, the research and development of autonomous robots is not new.

In 1500, centuries before the invention of the automobile, Leonardo da Vinci designed a cart that could move without being pulled or pushed. In 1868, Robert Whitehead invented a torpedo that could propel itself underwater in order to be a game-changer for naval fleets all over the world. In terms of robotic solutions for intelligent mobility, the study was started in the 1920s, being the concept of Autonomous Car defined in Futurama, an exhibit at the 1939 New York Wolrd's Fair. General Motors created the exhibit to display its vision of what the world would look like in 20 years, including an automated highway system that would guide ADS. By 1958, General Motors made this concept a reality (at least as a proof of concept) being the car's front end embedded with sensors to detect the current flowing through a wire embedded in the road. The first semi-automated car was developed in 1977 by Japan's Tsukuba Mechanical Engineering Laboratory. The vehicle reached speeds up to 30 km/h with the support of an elevated rail.

Figure 1.1: Stanley, 2005 DARPA Grand Challenge winner
Source: *Stanford university*

Nevertheless, the first truly autonomous cars appeared in the 1980s with Carnegie Mellon University's Navlab and ALV projects funded by the USA company DARPA (Defense Advanced Research Projects Agency) in 1984 and EUREKA Prometheus project (1987) developed by Mercedes-Benz and Bundeswehr University Munich's. By 1985, the ALV project had shown self-driving speeds on two-lane roads of 31 km/h with obstacle avoidance added in 1986 and off-road driving in day and night conditions by 1987. Furthermore, from the 1960s through the second DARPA Grand Challenge in 2005 (212 km off-road course near the California-Nevada state line, surpassed by all but one of the 23 finalists), automated vehicle research in the United States was primarily funded by DARPA, the US Army and US Navy, yielding rapid advances in terms of speed, car control, sensor systems and driving competence in more complex conditions. This caused a boost in the development of autonomous prototypes by companies and research organizations, most of them from the United States. Figure 1.1 shows Stanley, the 2005 DARPA Gran Challenge winner, from Stanford university.

Even though self-driving cars have not yet displaced conventional cars, there can be found several examples of how it has become a hot topic for powerful companies such as Delphi Automotive Systems, Audi, BMW, Tesla, Mercedes-Benz or Waymo. In 2005 Delphi broke the Navlab's record achievement (driving 4,584 km while remaining 98 % of the time autonomously) by piloting an Audi, improved with Delphi technology, over 5,472 km through 15 states while remaining in self-driving mode 99 % of the time. Moreover, in 2005 the USA states of Michigan, Virginia, California, Florida, Nevada and the capital, Washington D.C., allowed the testing of automated cars on public roads.

In 2017, Audi stated that its A8 car prototype would be automated at speeds up to 60 km/h by using its perception system named "Audi AI". Also, in 2017 Waymo (self-driving

technology development company subsidiary of Alphabet Inc) started a limited trial of a self-driving taxi service in Phoenix, Arizona.

Figure 1.2 shows the total number of autonomous test miles and miles per disengagement in California (Dec 2019 - Nov 2020) by some of the most important AD technology development companies around the world. The concept disengagement is quite useful to assess the quality of an ADS, defined as the deactivation of the autonomous mode when a failure of the autonomous technology is detected or when a safe operation requires that the autonomous vehicle test driver disengages the autonomous mode, resulting in control being seized by the human driver. As observed, Waymo and Cruise were, by far, the companies with the highest number of miles per disengagement, indicating the superiority and stability of their ADS. Furthermore, we can conclude from Figure 1.2 that most AD companies are from the United States of America (specially from the state of California) and China, being United States clearly the most developed country in this field.

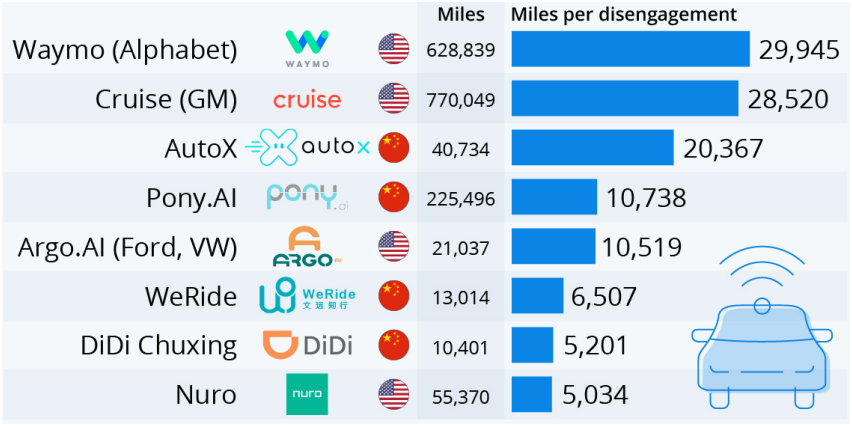

Figure 1.2: Number of autonomous test miles and miles per disengagement (Dec 2019 - Nov 2020)
Source: *DMV California, via The Last Driver License Holder*

At the moment of writing this thesis (2023), most vehicles on the road are considered to be semi-autonomous due to presence of Advanced Driver Assistance Systems (ADASs) that include assisted parking, lane departure warning, driver monitoring, emergency break or Adaptive Cruise Control (ACC), among others. Regarding this, the Society of Automotive Engineers (SAE) published the concept of autonomy levels in 2014, as part of its *Taxonomy and Definitions for Terms Related to On-Road Motor Vehicle Automated Driving Systems* [1] report. Figure 1.3 illustrates the six levels of autonomy (the higher the level, the more autonomous the car is), where it can be appreciated that Level Zero means *No Automation*, being the acceleration, braking and steering controlled by a human driver at all times, and Level Five represents Full Automation, where there is a full-time automation of all driving tasks on any road, under any conditions, whether there is a human on board or not.

According to a 2021 McKinsey consumer survey, growing demand for AD systems could create billions of dollars in revenue. Based on a consumer interest in AD features and commercial solutions available on the market today, ADAS and AD could generate

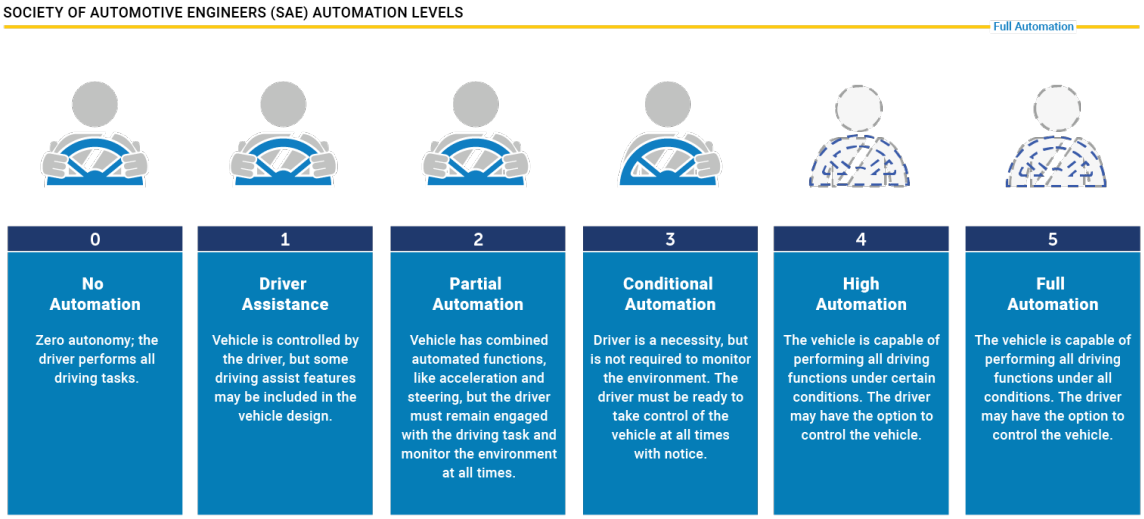

Figure 1.3: Society of Automotive Engineers (SAE) automation levels
Source: *NHTSA (National Highway Traffic Safety Administration)*

between \$300 and \$400 billions in the passenger car market by 2035. Figure 1.4 illustrates an interesting study reporting the revenues of ADAS and AD from Level 1 (Driver Assistance) to Level 4 (High Automation). As expected, Level 5 is excluded from this study due to the huge difficulties the automotive companies would have to face to adapt their systems under totally different environmental conditions.

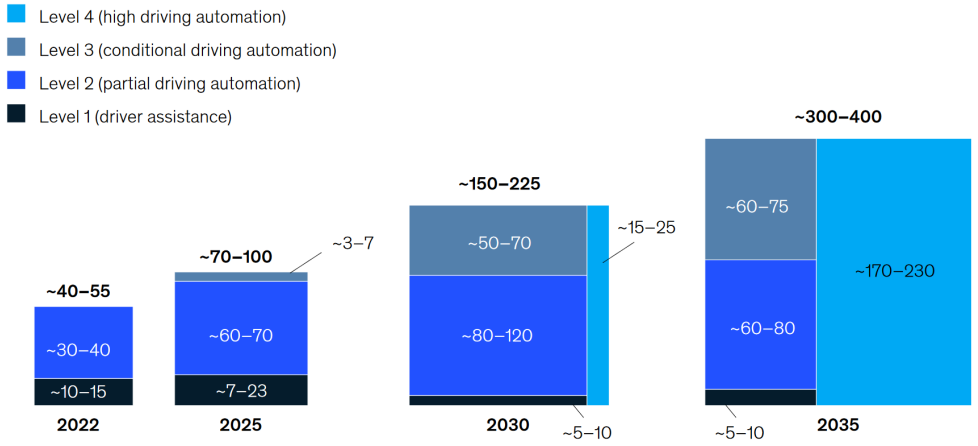

Figure 1.4: Advanced Driver Assistance systems (ADAS) and Autonomous Driving (AD) revenues in \$ billion
Source: *McKinsey Center for Future Mobility*

So far this Chapter has focused on a commercial analysis of the ITS field. The remaining content of this Chapter focuses on the technical study of an ADS, problem statement and objectives of this thesis.

1.3. Autonomous Driving Stack

To sum up what commented above, increasing the level of autonomous navigation in mobile robots (from agriculture to public and private transport) are expected to create tangible business benefits to those users and companies employing them. However, designing an ADS does not seem to be an easy task. In the SOTA we can distinguish two main kind of software architectures: End-to-End and modular. Note that in this thesis we focus on the software components of the ADS, not on the hardware tasks of the vehicle.

Figure 1.5 illustrates the entire AD architecture starting from sensing to longitudinal (throttle/brake) and lateral (steering angle) control of the vehicle, which are the commanded signals that feed the low-level electronic system that moves the vehicle and that is known as the Drive-By-Wire system [2]. End-to-End are considered black-box models, where a single neural network performs the whole driving task (throttle/steering/brake) from raw sensor data, in such a way the error be may vanished since intermediate representations are jointly optimized, but these are not very interpretable. On the other hand, modular architectures (considered as glass models as counterpart to End-to-End approaches) separate the driving task into individually programmed or trained modules. This solution is more interpretable, since the know-how of a research group or company is easily transferred, they allow parallel development, being the standard solution in industrial research, but the error is propagated, where intermediate representations can led to sub-optimal performance. For example, incorrect object detection can lead to low-quality tracking and MP.

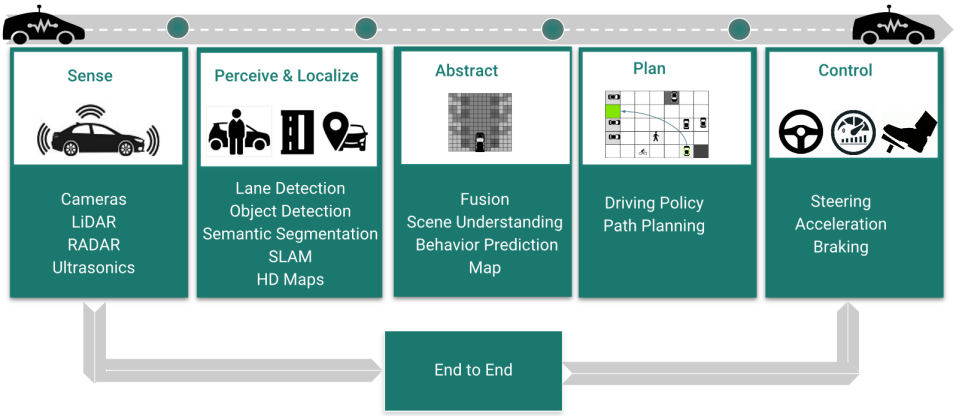

Figure 1.5: Autonomous Driving Stack (ADS) modular vs end-to-end pipeline
Source: *Vrunet: Multi-task learning model for intent prediction of vulnerable road users* [3]

Considering the RobeSafe (Robotics and eSafety) research group and the main projects (Techs4AgeCar, AIVATAR) where this thesis has been developed, we integrate our algorithms in a software modular approach. An example of this modular approach is shown in Figure 1.6. Despite the fact in literature some authors disagree on the specific software architecture of an ADS, specially the motion prediction module, which is usually classified as a perception algorithm but sometimes is included as part of the planning or DM

layers, we can hierarchically break down (from raw data to the driving task) a standard AD architecture into the following software layers:

- **Localization layer**: Positions the vehicle on a map with real-time and centimetric accuracy approach. The main source of information is a robust differential-GNSS, though IMUs, wheel odometry and even cameras.

- **Perception layer**: Understands the environment around the ego-vehicle thanks to the information collected by the sensors. If defined as multi-stage, the perception layer first detects the most relevant obstacles, then tracks them over time and predicts their trajectories. In that sense, the perception layer represents one of the most important modules of an ADS, responsible of analyzing the online information, also referred as the traffic situation, through the use of a global perception system which involves different on-board sensors as: LiDAR, Inertial Measurement Unit (IMU), RADAR, Differential-Global Navigation Satellite System (D-GNSS), Wheel odometers or Cameras. Additionally, HD map information is frequently used in the MP tasks by most SOTA algorithms.

- **Mapping layer**: Responsible for creating a topological, semantic and geographical modeling of the environment through which the vehicle drives, being the HD map graph the most common source of information.

- **Planning layer**: This layer is comprised of three components: route, behaviour and trajectory planner. The route planner computes the most optimal (in terms of distance, time and so forth and so on) global route from some predefined start and goal. It uses the localization and mapping output. On the other hand, the behaviour planner, also referred as DM layer by some authors, performs high-level DM of driving behaviours such as lane changes or progress through intersections, mostly focused on the previously computed global route and current localization. It can be seen as an atomization of the global route in different behaviors to reach the goal. Finally, the trajectory planner, also known as local planner, generates a time schedule for how to follow a path given constraints such as position, velocity and acceleration in order to meet the previously decided behaviour and taking into account the prediction from the perception layer, avoiding obstacles in optimal direction and speed conditions.

- **Control layer**: Once the local plan is calculated, the control layer is responsible for generating the commands that are sent to the actuators. It receives as input some waypoints from the trajectory planner and most authors perform spline interpolations and a velocity profile that ensures a smooth and continuous trajectory.

Note that, regarding the perception layer, most authors [4]

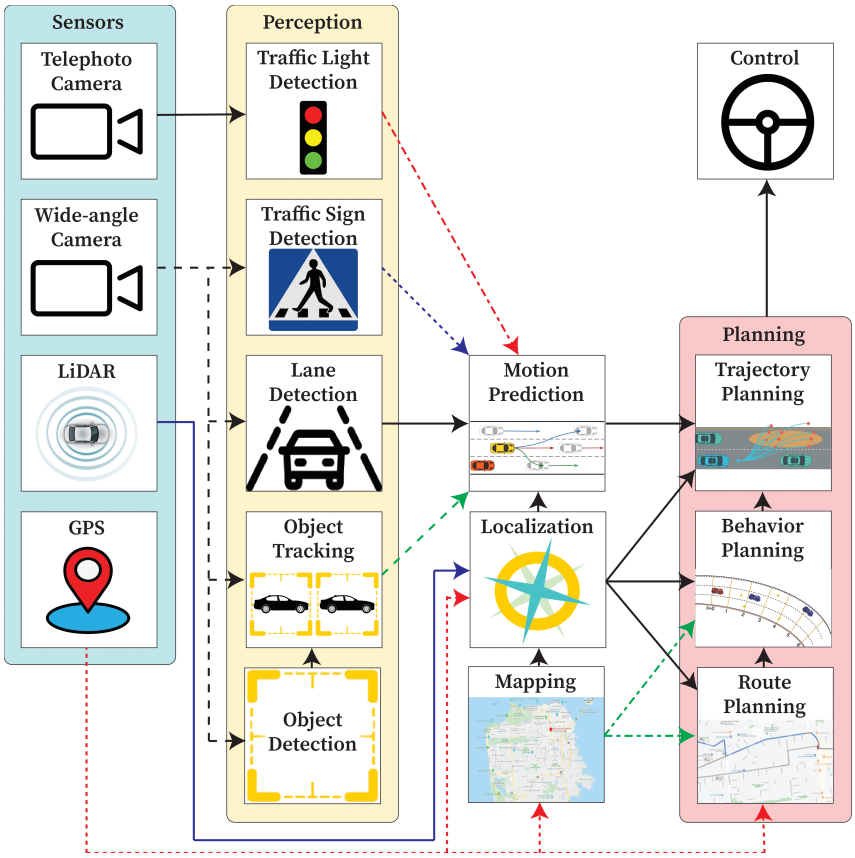

Figure 1.6: Autonomous Driving Stack (ADS) modular pipeline
Source: *Pylot: A modular platform for exploring latency-accuracy trade-offs in autonomous vehicles* [5]

1.4. Problem statement

As commented in previous sections, in order to operate efficiently and safely in highly dynamic, complex and interactive driving scenarios, ADS need to smartly reason like human beings via predicting future motions of surrounding traffic participants during navigation. Nevertheless, achieving accurate and robust MP is one of the most difficult challenges to achieve full-autonomy, since it is equivalent to a bridge between the former stages of the perception layer, where the scene is understood detecting and tracking static and dynamic objects of the environment, and the planning and control layer, where the future trajectory of the ego-vehicle is computed and the driving commands are sent to the physical layer (e.g. Drive-by-Wire [2]). Here are some of the most important challenges:

- **Heterogeneity of traffic participants**: Traffic participants (specially those which are dynamic) can be roughly classified as cyclists, pedestrians or other vehicles. The prediction model should be capable of differentiating the motion patterns of heterogeneous traffic participants, in such a way fine-grained classification (detection module) is quite beneficial to include additional metadata along with the past observations.

- **Complexity of road structure**: Road structures are highly diverse and complex, specially in highways and urban areas, which noticeably affect the motion behaviours of traffic participants.

- **Variable number of interactive agents**: The prediction model must deal with a number of associated traffic participants within a certain area that can vary from time to time, such as intersections or roundabouts. Then, while driving, a comprehensive representation of the scene must be able to accommodate an arbitrary number of involved traffic participants.

- **Multi-modality of driving behaviours**: In real-world, despite we know the behaviour our vehicle will carry out, the motion patterns of other traffic participants can be considered inherently multi-modal since there is usually more than one reasonable option for a driver to choose, specially in intersections, when the number of lanes increases or even in the same lane with different velocity profiles (constant velocity, sudden break, sudden acceleration). In that sense, a robust and reliable MP model is expected to be human-like and capture different plausible motion modalities where an agent can travel in the prediction horizon.

- **Complex interpendencies among traffic participants and road infrastructure**: Agent-Agent, Agent-Road and Road-Road interpendencies are of great importance for MP and interaction modeling, even more taking into account the complexity of road structures and heterogeneity of traffic participants aforementioned. As expected, an agent future trajectory will be affected not only by its own past trajectory and driving objectives (given by the behaviour planner) but also by other surrounding agents past trajectories, traffic rules and physical constraints.

- **Low latency and Real-Time responsiveness**: ADSs require quick responses to changing road conditions and the behavior of other road users. Then, the MP model should have low latency, meaning it can process input data and generate predictions rapidly, ideally in milliseconds. Nevertheless, the frequency can vary depending on the use case and system requirements, but typically predictions should be updated multiple times per second (*e.g.* 5 Hz, 10 Hz, or higher) to keep pace with the rapidly changing environment.

- **Synchronization with other system components**: The prediction frequency should be aligned with other critical components in the autonomous driving system, such as perception, planning, and control modules. Consistent and synchronized updates between these components are essential to maintain the overall system stability and safety.

1.5. Contributions of this Thesis

The main scope of this thesis is to develop novel and efficient interaction-aware Deep Learning (DL) based MP models in the field of AD, focusing on long-term (from 3 to 6 s) prediction horizon and AD, where traffic participants can range from trucks to pedestrians. The main inputs will be the physical (map) information and historical states (that may include agent position, velocity, orientation, object type and category) of traffic participants in BEV, assuming these objects have been previously tracked by our ego-vehicle (also referred as the autonomous car).

The validation of these methods will be done using a single target agent (either the model has considered multiple or a single agent in the loss function), as proposed by some of the most important prediction datasets in the literature, like Argoverse 1 [6] and Argoverse 2 [7], at the moment of writing this thesis. In this work, the solutions to the aforementioned challenges will be discussed and investigated progressively.

We summarise the contributions of this doctoral thesis in the following points:

- **Contribution 1**: SmartMOT, a simple-yet-accurate combination of traditional techniques is proposed for state estimation and data association respectively, in order to solve the tracking-by-detection paradigm. Moreover, we incorporate HD map semantic, geometric and topological information, in addition to the ego-vehicle status, to enhance the efficiency and reliability of the MOT system and subsequent uni-modal predictions (Chapter 4).

- **Contribution 2**: An Attention-based GAN prediction model that can successfully predict plausible uni-modal future trajectories in the context of vehicle prediction (Argoverse 1 dataset), taking into account not only the past trajectory of the agents (encoded by Long Short-Term Memory (LSTM) networks and attention mechanisms) but also the HD map information to compute a set of acceptable target points representing the physical constraints for our problem (Chapter 5).

- **Contribution 3**: Three efficient (social, map and augmented) baselines for multi-modal MP in the Argoverse 1 dataset built upon the previous model proposed in Chapter 5 removing the adversarial framework. In this case, we integrate GNNs to compute complex interactions among the different agents and a heuristic-based method to calculate some preliminary future centerlines for the vehicles as an enhanced interpretable representation of the map information with respect to the acceptable target points aforementioned (Chapter 6).

- **Contribution 4**: A multi-modal multi-agent MP model in the Argoverse 2 dataset, built upon the augmented efficient baseline, which incorporates topological and semantic information of preliminary future lanes using the aforementioned heuristic

method, map encoding based on DL with GNN, a cycle of physical and social feature fusion, DL-based estimation of final positions on the road, aggregation of the surrounding environment, and finally, a refinement module to enhance the quality of the final multi-modal predictions in an elegant and efficient manner. Compared to the state of the art, our method achieves prediction metrics up-to-pair with to the top-performing methods on the Argoverse 2 Leaderboard while significantly reducing the number of parameters and floating-point operations per second (Chapter 7).

- **Contribution 5**: The final model of the thesis, only considering social information, is successfully validated in two interesting applications, such as DM in the SMARTS simulator and domain adaptation studies in the hyper-realistic CARLA simulator, involving other vehicle layers as a preliminary step towards implementation in a real autonomous vehicle (Chapter 8).

Note that additional qualitative results, such as videos or how to run the proposed models, may be found in the corresponding links provided in each chapter to our open-source solutions.

1.6. Structure of this Thesis

The organization of this document has been done as follows:

- **Chapter 2** reviews the contextual factors, a MP methods classification according to the context encoding or representation approaches and SOTA databases and simulators to validate the algorithms.
- **Chapter 3** presents a technical background, mostly focused on physics-based methods and DL mechanisms to deal with temporal sequences and interactions, to deeply understand the proposed methods.
- **Chapter 4** addresses our integration between single-yet-powerful MOT and HD map information as a preliminary stage before computing uni-modal predictions.
- **Chapter 5** illustrates our GAN-based proposal, the first DL-based vehicle MP method of this thesis, considering both physical context, computing acceptable target points from the driveable area around the target agent, and social context, computing the past trajectory as a temporal sequence via recurrent networks and social interactions with attention mechanism.
- **Chapter 6** presents our efficient baselines, where high-level and well-structured physical context is structured in the form of centerlines, Graph Convolutional Network (GCN)-based approaches are employed to model more complex agent-agent interactions, and transformer encoders and cross-attention are employed for powerful-yet-efficient context encoding and multi-modal decoding.

- **Chapter 7** illustrates the final model of the thesis, which takes into account agent-agent, agent-map, map-agent and map-map interactions, using a novel scene representation with heuristic proposals, graph-based encoding, DL-based goal areas proposals and motion refinement.
- **Chapter 8** addresses the integration and validation of the final model of the thesis in a hyper-realistic simulator with upstream and downstream modules to contribute the entire pipeline and closed-loop for AD.
- **Chapter 9** summarizes the thesis and provides some promising directions for future work in the areas of MP and validation.

Chapter 2

Related Works

Llegaré a ser el mejor, El mejor que habrá jamás.
Mi causa es ser su entrenador, Tras poderlos capturar.
Viajaré a cualquier lugar, Llegaré a cualquier rincón
Y al fin podré desentrañar el poder de su interior.
¡Pokémon! Hazte con todos (solos tú y yo),
Es mi destino, mi misión
¡Pokémon! Tú eres mi amigo fiel,
Nos debemos defender.

Opening 1 de Pokémon: "Gotta catch 'em all!"
Autor original: Jason Paige

2.1. Introduction

One of the crucial tasks that ADSs must face during navigation, specially in arbitrarily complex urban scenarios, is to predict the behaviour of dynamic obstacles [6], [8]. In a similar way to humans that pay more attention to nearby obstacles and upcoming turns than considering the obstacles far away, the perception layer of an ADS must focus more on the salient regions of the scene, particularly on the more relevant dynamic agents to predict their future behaviour before conducting a maneuver, such as lane changing or accelerating.

Before proceeding with the study of the different methods of the SOTA of MP in the field of AD, one important thing to note is that this thesis is focused on non-conditional motion prediction, also referred as Passive Motion Prediction (PMP), where the prediction of surrounding agents is not influenced by the future decisions of the ego-vehicle or even other agents, referred as Conditional Motion Prediction (CMP) in the literature. Most existing works [9]–[14] focus on a passive prediction scheme, where the future states of a particular agent are predicted given its past information, other surrounding agents information and interactions as well as the physical context. Then, downstream planning modules, specially the behaviour planning module (also referred as DM layer, as stated

in Section 1.3) and the ego-vehicle (our vehicle) future actions are computed according to the predicted trajectories in a passive manner, that is, without modifying the output of the prediction model, and the global route previously calculated.

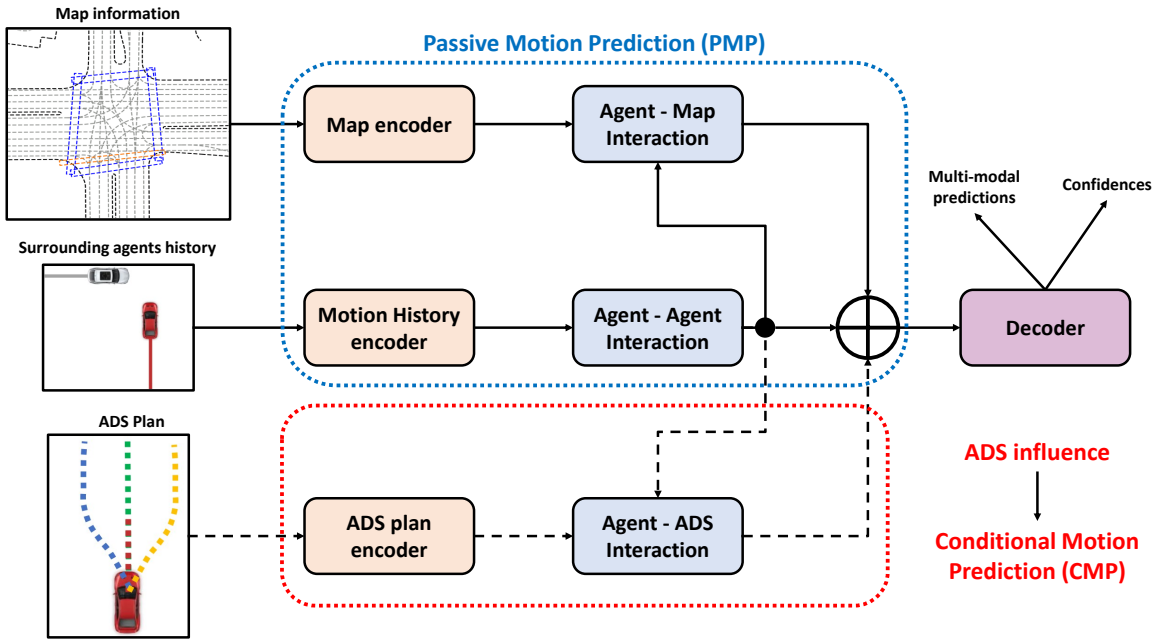

Figure 2.1: Example of a Conditional Motion Prediction (CMP) pipeline. We **highlight** the influence of the ADS in the prediction of surrounding agents.

Nevertheless, to ensure safety under various predicted trajectories of the surrounding agents, our ADS must overly conservative with inefficient maneuvers, specifically in arbitrarily complex traffic scenarios, because PMP models ignore the fact that the future states of an agent can influence the future actions of other agents, what is the most realistic situation. Figure 2.1 shows the differences between these two approaches. To this end, researchers recently started to explore a more coherent interactive prediction and planning framework which relies on predicting the surrounding agents future trajectories conditioned on the ego-vehicle future actions [15] [16] [17], as a preliminary state to implement a fully-interaction graph where the future states of all agents (either autonomous prototypes or human-driven) influence in the decision of all agents.

Once the differences between CMP and PMP have been illustrated, we proceed with the problem formulation, main contextual factors and classification of prediction methods.

2.2. Problem Formulation of Motion Prediction

Given a sequence of past trajectories $a_P = [a_{-obs'_{len}+1}, a_{-obs'_{len}+2}, ..., a_0]$ for an agent, we aim to predict its future steps $a_F = [a_1, a_2, ..., a_{pred_{len}}]$ up to a fixed time step $pred_{len}$. Running in a specific traffic scenario, each agent will interact with static HD maps m and the other dynamic actors, meeting the corresponding traffic and social rules. Therefore,

the probabilistic distribution that we want to capture is $p(a_F|m, a_P, a_P^O)$, where a_P^O denotes the other agents observed states.

The output of most existing methods is a weighted set of trajectories $A_F = \{a_F^k\}_{k\in[0,K-1]} = \{(a_1^k, a_2^k, ..., a_{pred_{len}}^k)\}_{k\in[0,K-1]}$ for each agent, where K represents the number of modes or plausible future directions, due to the inherent uncertainty associated to the prediction problem. Note that the set is weighted since each mode will have an associated confidence or probability of occurrence, where the sum of all mode probabilities must be equal to 1. This weighted set of trajectories for each agent will be used by downstream decision modules. On top of that, TNT (Target-driven trajectory prediction) [18] is one of the first methods that introduces specific preliminary future positions in the problem formulation, also referred as goals, being TNT [18]-like methods distribution approximated as:

$$\sum_{\tau\in T(m,a_P,a_P^O)} p(\tau|m, a_P, a_P^O)p(a_F|\tau, m, a_P, a_P^O) \tag{2.1}$$

where $T(m, a_P, a_P^O)$ is the space of candidate goals depending on the driving context and τ a specific goal.

However, the map space m is large, and the goal space $T(m, a_P, a_P^O)$ requires careful design. In that sense, some methods expect to accurately predict the actor motion by extracting good features. For example, LaneGCN [14] tries to approximate $p(a_F|m, a_P, a_P^O)$ by modeling $p(a_F|M_{a_0}, a_P, a_P^O)$, where M_{a_0} is a *local* map feature that is related to the actor state a_0 at final observed step $t = 0$.

To extract M_{a_0}, they use a_0 as an anchor to retrieve its surrounding map elements and aggregate their features. In that sense, not only the local map information is important, but also the goal area maps information is of great importance for accurate trajectory prediction. So, the probability can be reconstructed as:

$$\sum_{\tau} p(\tau|M_{a_0}, a_P, a_P^O)p(M_\tau|m, \tau)p(a_F|M_\tau, M_{a_0}, a_P, a_P^O) \tag{2.2}$$

Then, in this work we aim to progressively include preliminary heuristic information, as well as predict possible goals τ based on agents motion histories and driving context to retrieve the map elements in goal areas explicitly and aggregate their map features as M_τ to meet the requirements of the problem formulation.

2.3. Contextual Factors and Classification of Motion Prediction methods

This section studies the contextual factors (inputs) and classification of MP in the field of AD according to its encoding method of the different inputs and output types. Figure 2.2 summarizes the main inputs and outputs of these methods.

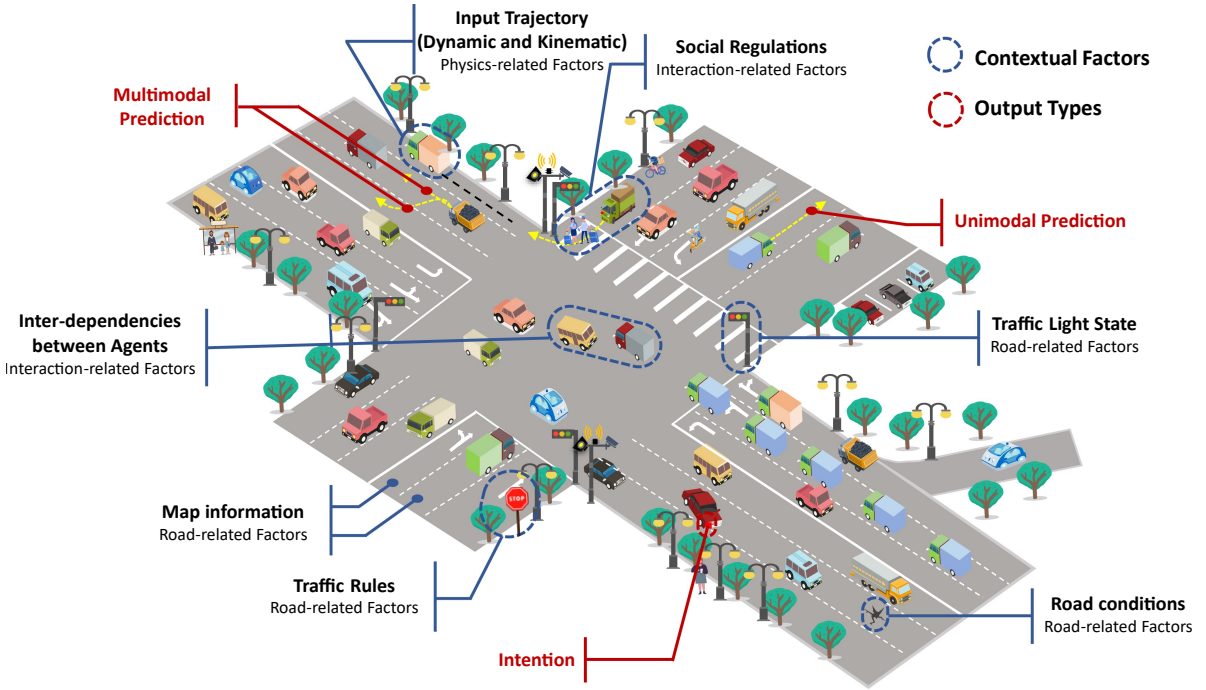

Figure 2.2: Contextual factors and output types in Vehicle MP
Source: *A survey on trajectory-prediction methods for autonomous driving* [19]

In order to model the future states of surrounding agents, MP models must pay attention to the current environment, where some contextual factors can be clearly identified:

- **Physics-related factors** refer to the kinematic and dynamic variables of the agents, specifically to their spatio-temporal variables (such as position, velocity, acceleration, object type or mass) as well as past behaviours.
- **Interaction-related factors** include the inter-dependencies and social regulations between agents maneuvers. It is important to consider that traffic agents can be either non-relevant pedestrians on the sidewalk as well as an extremely relevant truck in front of the ego-vehicle.
- **Road-related factors** include the corresponding traffic rules (lane type, traffic signals, stops, etc.) as well as the modeling of the map (usually HD map), including its topological, semantic and geometrical information.

On the other hand, regarding the output types, MP methods need to provide the future trajectories of traffic participants. Nevertheless, these methods can provide these future

trajectories in different ways, even though these outputs can be unified as a single output, depending on the application:

- **Uni-modal prediction**: In the uni-modal case, the prediction method only returns a single future trajectory, without taking into account other possible behaviours.
- **Multi-modal prediction**: Models that generate a multi-modal prediction compute multiple K future trajectories (also referred as modes in the literature) with the probability of each future trajectory. The higher the mode probability (also referred as score), the more probable a particular future trajectory should be. Instead of providing a single trajectory, these models would generate a range of probable trajectories, considering different driving styles, intentions, and uncertainties. Multi-modal prediction can enable ADS to anticipate and respond to a wider range of possible scenarios, enhancing safety and adaptability. This output type is specially useful for fast-changing and highly interactive situations where multiple options are available. One important thing to note is that multi-modal methods must be designed in order to not only reason in terms of different maneuvers (keep straight, turn right, lane change, etc.) but also different velocity profiles (constant velocity, acceleration, sudden break, etc.) regarding the same maneuver. This type of prediction will be the final objective throughout this thesis.
- **Intention**: Also referred as maneuver in the literature, the intention can be part of the final output or just be an intermediate step in the method. MP methods usually produce maneuver intention (*i.e.* a discrete space of actions, such as turn left, turn right, sudden acceleration, emergency break, and so forth and so on) to assist in the subsequent prediction. In the literature, the maneuver or behaviour is usually returned by a behavioural planner (DM) module, while the specific future trajectory is usually returned by a MP algorithm to compute the specific future steps of the agents.

As we will study throughout this section, most prediction methods focus on the multi-modal output with an associated probability for each mode, since this is the most realistic way to imitate the human brain during navigation. First of all, there are plenty of problems during navigation, since there is a high uncertainty of traffic behavior and a large number of different situations. That means that one cannot use a discrete number of situations and a discrete number of car movements. Second, the main tasks of ADS, like ensuring safe and efficient operations and anticipating a multitude of possible behaviors of traffic actors in its surroundings, provide a large need in knowing the position of all vehicles beforehand. Multi-modal means that we have multiple predictions for each timeframe.

Figure 2.3 illustrates an interesting traffic scenario processed by one of our algorithms. The **target agent** is getting close to an intersection, where several future maneuvers are plausible. In both cases (uni-modal and multi-modal), the model must reason the future

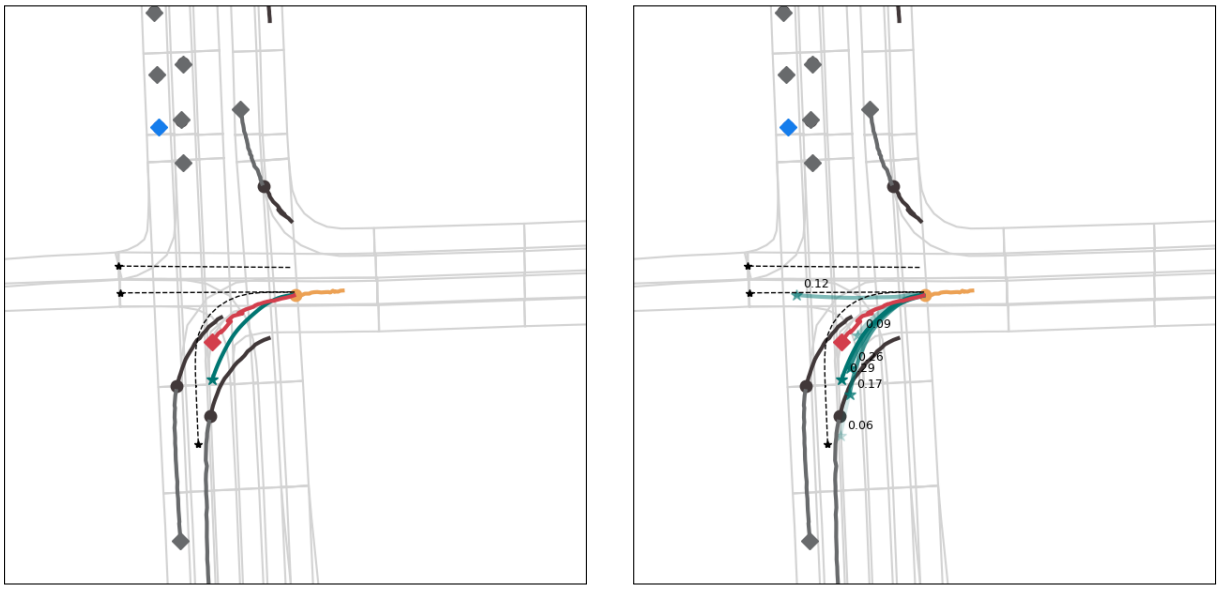

(a) Uni-modal prediction

(b) Multi-modal prediction

Figure 2.3: Modeling uni-modality vs multi-modality of future 3-second agent trajectories with one of our algorithms; We represent: our vehicle (**ego**), the **target agent**, and **other agents**. We can also see the **ground-truth** trajectory of the target agent, our **multi-modal predictions** (with the corresponding confidences) for the target agent and **plausible centerlines**, also for the target agent in this algorithm. Circles represent last observations and diamonds last future positions.

trajectory of the target agent based on its past observations, interactions with other agents and physical context. On the left (2.3a) illustrates the uni-modal case, where a single trajectory is predicted. On the right (2.3b), multiple trajectories (or modes) with associated probabilities are predicted, with most modes turning left and one mode keeping straight since in similar situations the agent could also perform this behaviour with a similar context. As stated above, the main point of having this multi-modality is to compute different plausible options with an associated confidence. Note that lots of SOTA algorithms study the problem of multi-modal predictions since similar past trajectories (*e.g.* a vehicle stopped in front of an intersection) can produce totally different future trajectories (*e.g.* turn left, turn right or keep straight).

After defining the contextual factors and output types, a classification of the prediction methods according to different modeling approaches is illustrated. Over the last two decades, MP can be divided into four parts in chronological order: Physics-based, classic Machine Learning (ML)-based, RL-based and DL-based, as shown in Figure 2.4. The remaining content of this section, based on the study performed by [19], illustrates the main algorithms used in this thesis, especially focusing on DL since in this work we focus on predictive techniques for scene understanding based on deep models.

2.3.1. Physics-based Motion Prediction

Physics-based methods are the first and simplest methods used by researchers. Although the accuracy of these methods is relatively low, more and more models use the

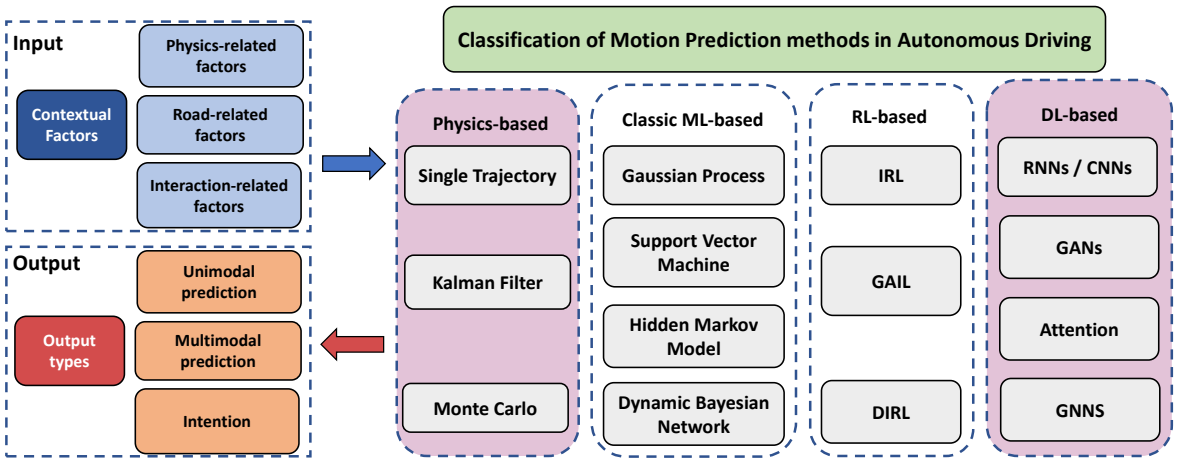

Figure 2.4: Contextual factors and output types in Vehicle Motion Prediction. We **highlight** the main algorithms used in this thesis: Physics-based and Deep Learning based.

idea of physics-based models to improve the accuracy. Physics-based methods have more accurate results when the movement of vehicles can be accurately described by kinematics or dynamics models, but the physical model of the traffic participants is constantly changing, such that most of these methods are only suitable for short-term prediction (no more than 1s). Dynamics models can be quite complex, including many inherent parameters and introducing an extra computation burden, in such a way that researchers prefer simple dynamic methods for motion prediction. In terms of vehicle MP, the bicycle model is usually employed to model the vehicle physics, driven by the front wheels [20], [21]. In the literature three main types of physics-based models are distinguished, where the main different is the way in which the uncertainty is handled: Single Trajectory, KF-based and Monte Carlo-based.

2.3.1.1. Single-Trajectory

One of the most straightforward methods to predict an agent trajectory is to directly apply the agent current state to the physic model. In order to increase the accuracy and stability of the estimation, the vehicles are mostly assumed to comply with motion models that describe their dynamic behavior. In the past, numerous single-trajectory motion models have been proposed for this task [21]–[23]. A first systematization can be achieved by defining different levels of complexity. At the lower end of such a scale, linear motion models are situated. These models assume a Constant Velocity (CV) or a Constant Acceleration (CA). Their major advantage is the linearity of the state transition equation which allows an optimal propagation of the state probability distribution. On the other hand, these models assume straight motions and are thus not able to take rotations (especially the yaw rate) into account.

A second level of complexity can be defined by taking rotations around the z-axis into account. The resulting models are sometimes referred to as curvilinear models. They can

be further divided by the state variables which are assumed to be constant. The most simple model of this level is the CTRV model. By defining the derivative of the velocity as the constant variable, the Constant Turn Rate and Acceleration (CTRA) model can be derived. Both CTRV and CTRA assume that there is no correlation between the velocity v and the yaw rate ω. As a consequence, disturbed yaw rate measurements can change the yaw angle of the vehicle even if it is not moving. In order to avoid this problem, the correlation between v and ω can be modeled by using the steering angle Φ (angle between the axis of motion and the direction of the front wheels) as constant variable and derive the yaw rate from v and Φ. The resulting model is called Constant Steering Angle and Velocity (CSAV). Again, the velocity can be assumed to change linearly, which leads to the Constant Curvature and Acceleration (CCA) model.

From a geometrical point of view, nearly all curvilinear models are assuming that the vehicle is moving on a circular trajectory (either with a constant velocity or acceleration). The only exception is the CTRA model, which models a linear variation of the curvature and thus assumes that the vehicle is following a clothoid.

On the other hand, single trajectory methods are not able to consider the road-related factors and the uncertainty of the current state is unreliable for long-term prediction in such a way these single trajectory models should only be used for estimating uni-modal trajectories of the surrounding agents in the short-term. We further study the state transition equations of physics-based models in Chapter 3 since they will be used in the algorithms proposed in this thesis as preliminary proposals for the DL models.

2.3.1.2. Kalman Filter

Kalman Filter (KF)-based methods aim to solve one of drawbacks of physics-based models. In real-world, the states of agents are not perfectly known since they present an associated noise. These methods model the uncertainty of the current agent state and its physic model by means of a Normal (Gaussian) distribution. Compared to the single trajectory methods, the main advantage is that KF methods consider the uncertainty of the predicted trajectory, specially when using its Extended (EKF) or Unscented (UKF) versions where non-linearities are modeled. As proposed by the original algorithm [24], the prediction and update steps are combined into a loop where the mean value and covariance matrix of the agent state is computed for each future step, calculated as an average trajectory with related uncertainty.

Nevertheless, these KF-based methods use uni-modal Gaussian distributions, which are not enough to represent agents interactions. In that sense, [25] propose an Interactive Multiple Model (IMM) to compute a multi-modal prediction. Moreover, [26] model a set of KFs used to describe physical models of the vehicles and switch between them, defined as Switched Kalman Filter (SKF). [27] propose IMM-KF, a novel Interacting

Multiple Model Kalman Filter which takes interaction-related factors (social regulation, inter-dependencies) into consideration, as shown in Figure 2.2.

2.3.1.3. Monte Carlo

In the same way KF methods aimed to solve the associated noise to the physics state of the agent, Monte Carlo method aims to simulate the state distribution approximately since an analytical expression for the predicted state distribution is usually unknown without any assumptions of the linearity or the model's Gaussian nature. This method randomly samples the input variables and applies the physics model to compute potential future trajectories. In order to ensure the plausibility of the future behaviour in the context of AD, the generated future states are usually filtered with a lateral acceleration lower than the actual allowable lateral acceleration [28], though other vehicle physical limitation can also be used such that the input of the model will be more realistic. [29] present a model that identifies a preliminary maneuver and then applies the Monte Carlo method to compute future trajectories by the identified maneuver. Furthermore, [30] first use the Monte Carlo algorithm to predict future trajectories and then utilize MPC (Model Predictive Control) algorithm to refine these preliminary future trajectories.

2.3.2. Deep Learning based Motion Prediction

DL-based methods are by far the most used at this moment in the field of MP in AD to predict the future trajectory of traffic participants, being this thesis focused in these particular methods. Most traditional predictions methods [19], which usually only consider physics-related factors (like the velocity and acceleration of the target vehicle that is going to be predicted) and road-related factors (prediction as close as possible to the road centerline), are only suitable for short-time prediction tasks [19] and simple traffic scenarios.

Recently, MP methods based on DL have become increasingly popular since they are able not only to take into account these above-mentioned factors but also consider interaction-related factors (like agent-agent [31], agent-map [32] and map-map [14]) in such a way the algorithm can adapt to more complex traffic scenarios (intersections, sudden breaks and accelerations, etc.). It must be consider that multi-modal, specially in the field of vehicle motion prediction, does not refer necessarily to different directions (*e.g.* turn to the left, turn to the right, continue forward in an intersection), but it may refer to different predictions in the same direction that model a sudden positive or negative acceleration, so as to imitate a realistic human behaviour in complex situations.

The main DL-based approaches are: Convolutional Neural Networks (CNNs), Recurrent Neural Networks (RNNs), GANs, Attention mechanisms (where the Transformer architecture is included) and GNNs. Figure 2.5 illustrates the main idea of using DL to

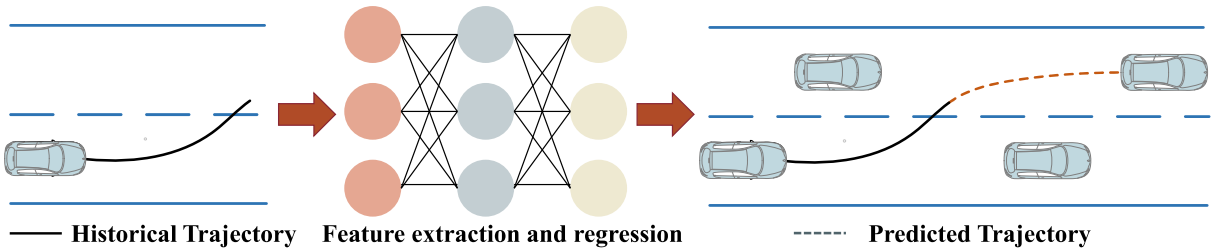

Figure 2.5: Deep Learning methods applied in MP
Source: *A survey on trajectory-prediction methods for autonomous driving* [19]

predict the future trajectories of the agents. Since this thesis is focused on developing efficient and accurate DL-based MP models in the field of AD, the theoretical explanation of the different DL mechanisms used in our pipelines will be further detailed in Chapter 3 along with some physics-based models theory to fully-understand the proposed models.

Table 2.1: Main SOTA DL methods for MP. Main categories are Encoder, Decoder, Output representation and Distribution over future trajectories

Method	**Encoder**			**Decoder**	**Output**	**Trajectory Distribution**
	Motion history	Social info	Map info			
SocialLSTM [33]	LSTM	spatial pooling	–	LSTM	states	samples
SocialGan [31]	LSTM	maxpool	–	LSTM	states	samples
Jean [34]	LSTM	attention	–	LSTM	states	GMM
TNT [18]	polyline	maxpool, attention	polyline	MLP	states	weighted set
LaneGCN [14]	1D-conv	GNN	GNN	MLP	states	weighted set
WIMP [17]	LSTM	GNN+attention	polyline	LSTM	states	GMM
VectorNet [35]	polyline	maxpool, attention	polyline	MLP	states	uni-modal
SceneTransformer [36]	attention	attention	polyline	attention	states	weighted set
HOME [9]	raster	attention	raster	conv	states	heatmap
GOHOME [10]	1D-conv+GRU	GNN	GNN	MLP	states	heatmap
MP3 [37]	raster	conv	raster	conv	cost function	weighted samples
CoverNet [38]	raster	conv	raster	lookup	states	GMM w/ dyn. anch.
DESIRE [39]	GRU	spatial pooling	raster	GRU	states	samples
MFP [15]	GRU	RNNs+attention	raster	GRU	states	samples
MANTRA [40]	GRU	–	raster	GRU	states	samples
PRANK [41]	raster	conv	raster	lookup	states	weighted set
IntentNet [32]	raster	conv	raster	conv	states	uni-modal
Multi-modal [42]	raster	conv	raster	conv	states	weighted set
MultiPath [43]	raster	conv	raster	MLP	states	GMM w/ static anchors
MultiPath++ [11]	LSTM	RNNs+maxpool	polyline	MLP	control poly	GMM
PLOP [44]	LSTM	conv	raster	MLP	state poly	GMM
Trajectron++ [8]	LSTM	RNNs+attention	raster	GRU	controls	GMM
CRAT-PRED [13]	LSTM	GNN+attention	–	MLP	states	weighted set
R2P2 [45]	GRU	–	polyline	GRU	motion	samples
DKM [46]	raster	conv	raster	conv	controls	weighted set
GANet [12]	1D-conv+GRU	GNN	GNN	MLP	states	weighted set

In order to classify DL based MP methods, we can identify different factors (physics, interaction and road) and determine which type of neural network is employed to extract features of the corresponding input. In the literature we mainly distinguish the following inputs and outputs: Motion history (physics-based factors), Social information (interaction-based factors), Map information (road-related factors), how the model returns the output trajectory and its corresponding distribution. Table 2.1 summarizes main SOTA methods, inspired in the classification proposed by [11].

- **Motion history**: Most methods encode the sequence of past observed states using 1D-CNN [14], [34], able to model spatial information, or via a recurrent net [33] (LSTM, Gated Recurrent Unit (GRU)), which are more useful to handle temporal information. Other methods that use a raster version of the whole scenario represent the agent states rendered as a stack of binary mask images depicting agent oriented bounding boxes [9]. On the other hand, other approaches encode the past history of the agents in a similar way to the road components of the scene given a set of vectors or polylines [18], [35] that can model the high-order interactions among all components, or even employing attention to combine features across road elements and agent interactions [36]. In our approaches, we will mainly use LSTM, 1D-CNN and Attention mechanism given the relative displacements of the agents.

- **Social information**: In complex scenarios, motion history encoding of a particular target agent is not sufficient to represent the latent space of the traffic situation, but the algorithm must deal with a dynamic set of neighbouring agents around the target agent. Common techniques are aggregating neighbour motion history with a permutation-invariant set operator: soft attention [36], a combination of soft attention and RNN [11] / GNN [13] or social pooling [31], [33]. Raster based approaches rely on 2D convolutions [43] [37] over the spatial grid to implicitly capture agent interactions in such a way long-term interactions are dependent on the neural network receptive fields. We will make use of Attention-based and GNN-based algorithms in our approaches.

- **Map information**: High-fidelity maps [47] have been widely adopted to provide offline information (also known as physical context) to complement the online information provided by the sensor suite of the vehicle and its corresponding algorithms. Recent learning-based approaches [32], [48], [49], which present the benefit of having probabilistic interpretations of different behaviour hypotheses, require to build a representation to encode the trajectory and map information. Map information is probably the feature with the clearest dichotomy: raster vs vector treatment. The raster approach encodes the world around the particular target agent as a stack of images (generally from a top-down orthographic view, also known as Bird's Eye View). This world encoding may include from agent state history, agent interactions and usually the road configuration, integrated all this different-sources information as a multi-channel image [9], in such a way the user can use an off-the-shelf CNN-based pipeline in order to leverage this powerful information. Nevertheless, this representation has several downsides: constrained field of view, difficulty in modeling long-range interactions and even difficulty in representing continuous physical states due to the inherent world to image (pixel) discretization.

  On the other hand, the polyline approach may describe curves, such as lanes, boundaries, intersections and crosswalks, as piecewise linear segments, which usually rep-

resents a more compact and efficient representation than using CNNs due to the sparse nature of road networks. Some state-of-the-art algorithms not only describe the world around a particular agent as a set-of-polylines [17] [18] in an agent-centric coordinate system, but they also leverage the road network connectivity structure [14] [50] treating road lanes as a set of nodes (waypoints) and edges (connections between waypoints) in a graph neural network so as to include the topological and semantic information of the map. In our case, we will use discrete map information in the form of target goals and high-level well-structured centerlines, as well as road network connectivity structure using GNN-based operations to compute deep physical features.

- **Decoder**: Pioneering works of DL-based MP usually adopt the autoencoder architecture, where the decoder is often represented by a recurrent network (GRU, LSTM, etc., specially designed to handle temporal information) to generate future trajectories in an autoregressive way, or by CNNs [9] [10] or Multilayer Perceptron (MLP) [14] [13] using the non-autoregressive strategy. If the method makes use of an autoregressive strategy the pipeline generates tokens (in this case, positions or relative displacements) in a sequential manner, in such a way the new output is dependent on the previously generated output. On the other hand, MLP [13], CNN [9] or Transformer [36]-based strategies usually follow a non-auto-regressive approach, where from a latent space the whole future trajectory is predicted. Throughout this work, we will make use of the auto-regressive strategy using LSTM networks as well as the decoding from the latent space in the latest proposed algorithm, where we will appreciate that given an enriched encoded representation, it is possible to directly decode from the deep features instead of carrying out the decoding process iteratively.

- **Output**: The most popular model output representation is a sequence of states (absolute positions) or state differences (relative displacements for any dimension considered). The spacetime trajectory may be intrinsically represented as a continous polynomial representation or a sequence of sample points. Other works [9] [10] first predict a heatmap and then decode the corresponding output trajectories after sampling points from the heatmap, whilst [37] [51] learn a cost function evaluator of trajectories that are enumerated heuristically instead of being generated by a learned model. As proposed by most methods, we will represent our output as a sequence of states, being absolute positions when decoding from the encoded latent space or relative displacements when decoding iteratively by means of the auto-regressive approach as aforementioned.

- **Trajectory Distribution**: The choice of output trajectory distributions has several approaches on downstream applications. Regardless the agent to be predicted is described as a (non-)holonomic [52] platform, an intrinsic property of the MP problem

is that the agent may follow one of a diverse set of possible future trajectories, instead of a single future trajectory (uni-modal) [35], which might not be optimal. To address the multi-modal issue, a popular choice to represent a multi-modal prediction are Gaussian Mixture Models (GMMs) due to their compact parameterized form, where mode collapse (associated frequently to GMMs) is addressed through the use of trajectory anchors [43] or training tricks [42]. Other approaches model a discrete distribution via a collection of trajectory samples extracted from a latent space and decoded by the model [45] or over a set of trajectories (fixed a priori or learned). In that sense, at the moment of writing this work, the most used trajectory distribution is a weighted set of trajectories [13], [14], [18], where each set is a trajectory with a discrete number of future steps and an associated confidence indicating the probability of occurrence of the corresponding behaviour. In this work, for those approaches which make use of the multi-modal approach, a weighted set will be used to model the trajectory distribution, where each trajectory is a sequence of discrete states, and each sequence has a certain confidence illustrating the probability of occurrence of that particular behaviour.

2.4. Motion Prediction Datasets

As stated in previous sections, MP (also referred in the literature as Motion Forecasting) addresses the problem of predicting future states (or occupancy maps) for dynamic actors within a local environment. Some examples of relevant actors for autonomous driving include: vehicles (both parked and moving), pedestrians, cyclists, scooters, and pets. Predicted futures generated by a forecasting system are consumed as the primary inputs in motion planning, which conditions trajectory selection on such forecasts. Generating these forecasts presents a complex, multi-modal problem involving many diverse, partially-observed, and socially interacting agents. Considering these requirements, there are several datasets in the literature to train and validate multiple proposals that vary in terms of data size, geographic coverage, sensor modalities, annotations, and limitations. Choosing the most appropriate dataset depends on the specific research goals, target environment, and available resources. Researchers should consider these factors when selecting a dataset for motion forecasting tasks in autonomous driving. Table 2.2 shows an interesting comparison between different SOTA datasets in the field of vehicle MP.

As observed, Yandex is the dataset with the highest number of scenarios, total recorded time and amount of data, but there are very few entries and all of them dated from 2021, so, at the moment of writing this thesis, the research community is not focused in this dataset anymore. On the other hand, Lyft has the highest number of entries, but the number of unique roadways is limited to 10 km and it does not provide a vector map. Interaction is limited to some interesting scenarios, with very few unique tracks and roadways compared to the other datasets. Overall, these datasets have common goals of

Table 2.2: Comparison between different *state-of-the-art* vehicle Motion Prediction datasets. Hyphens "-" indicate that attributes are either not applicable, or not available. † Public leaderboard counts as retrieved on Aug. 27, 2021.
Source: *Argoverse 2: Next generation datasets for self-driving perception and forecasting* [7]

	Argoverse 1 [6]	Interaction [53]	Lyft [54]	Waymo [55]	NuScenes [56]	Yandex [57]	Argoverse 2 [7]
Scenarios	324k	-	170k	104k	41k	600k	250k
Unique Tracks	11.7M	40k	53.4M	7.6M	-	17.4M	13.9M
Average Track Length	2.48 s	19.8 s	1.8 s	7.04 s	-	-	5.16 s
Total Time	320 h	16.5 h	1118 h	574 h	5.5 h	1667 h	763 h
Scenario Duration	5 s	-	25 s	9.1 s	8 s	10 s	11 s
Test Forecast Horizon	3 s	3 s	5 s	8 s	6 s	5 s	6 s
Sampling Rate	10 Hz	10 Hz	10 Hz	10 Hz	2 Hz	5 Hz	10 Hz
Cities	2	6	1	6	2	6	6
Unique Roadways	290 km	2 km	10 km	1750 km	-	-	2220 km
Avg. tracks per scenario	50	-	79	-	75	29	73
Evaluated object categories	1	1	3	3	1	2	5
Multi-agent evaluation	×	✓	✓	✓	×	✓	✓
Mined for Interestingness	✓	×	-	✓	×	×	✓
Vector Map	✓	×	×	✓	✓	×	✓
Download Size	4.8 GB	-	22 GB	1.4 TB	48 GB	120 GB	58 GB
Public Leaderboard Entries†	194	-	935	23	18	3	-

enabling motion prediction and improving the safety and efficiency of ADSs. However, their coverage, data size, features, and limitations vary, which makes it important to consider the specific requirements and use cases when choosing a dataset for research or development purposes.

Regarding this, we conclude the best vehicle MP datasets in the literature are NuScenes, Waymo, Argoverse 1 and Argoverse 2. In that sense, since the DL part of the thesis was started (around 2021) approximately when Argoverse 1 had a lot of interest from the research community, and, on top of that, they recently released Argoverse 2 (the largest MP dataset to date) we finally decided to build our algorithms upon the Argoverse 1 and Argoverse 2 datasets.

2.4.1. Argoverse 1 Motion Forecasting

The Argoverse 1 Motion Forecasting dataset is a widely used dataset in the field of AD for studying and developing algorithms related to MP. It includes HD maps and a detailed map API to get the corresponding rasterized or vector information of the map. This dataset is a curated collection of 324,557 scenarios (particularly, 205942 training samples, 39472 validation samples and 78143 test samples). Data was sampled at 10 Hz, where each sample contains the BEV position (x,y) of all agents in the scene in the past 2s (20 observed points), the local map, and the labels are the 3s (30 predicted points) future positions of one target agent in the scene. For training and validation, full 5-second trajectories are provided, while for testing, only the first 2 seconds trajectories are given.

Table 2.3 shows an estimated distribution of the target agent maneuver in the Argoverse 1 dataset, regarding the most common use cases in urban scenarios, such as going straight, turn and lane change. We can observe how most sequences are focused on keeping the same lane. Nevertheless, most of these *going straight* use cases do not conduct a trivial

Table 2.3: Distribution of the Target Agent Maneuver in the Argoverse 1 Motion Forecasting Dataset
Source: *Improving diversity of multiple trajectory prediction based on map-adaptive lane loss* [58]

Maneuver	Training	Validation
Going straight	191024 (92.75%)	34958 (90.70%)
Left turn	7860 (3.82%)	1880 (4.88%)
Right turn	4757 (2.31%)	1238 (3.21%)
Left lane change	1084 (0.53%)	284 (0.74%)
Right lane change	1217 (0.59%)	184 (0.48%)

constant velocity trajectory, but there are sudden accelerations or breaks, which are quite interesting and challenging.

We have used this dataset to train and validate our algorithms in Chapters 5, 6.

2.4.2. Argoverse 2 Motion Forecasting

Argoverse 2 [7] Motion Forecasting dataset has been used to implement and validate our final MP included in Chapter 7. In the same way than Argoverse 1, Argoverse 2 is a high-quality MP dataset where the real driving scenario are paired with the corresponding local HD map. Nevertheless, while Argoverse 1 provides a substantial amount of labeled data, it may still have limitations in capturing the full diversity of real-world driving scenarios. Built upon the success of Argoverse 1, the Argoverse 2 Motion Forecasting dataset provides an updated set of prediction scenarios collected from a self-driving fleet, improving its previous version by spanning +2000 km over six different cities and the traffic scenarios approximately twice longer and more diverse.

The design decisions [7] to create the Argoverse 2 dataset as a noticeable enhanced version of Argoverse 1 were:

- **Motion forecasting is a safety critical system in a long-tailed domain**: A good dataset must be biased towards diverse, interesting and challenging scenarios containing different types of focal agents. The Argoverse 2 goal is to encourage the development of methods that ensure safety during tail events, rather than to optimize the expected performance on easy miles where even simple models are able to solve the problem.

- **Goldilocks zone of task difficulty**: The number and diversity of methods performing at or near the SOTA continues growing since early 2020 when Argoverse 1 was released, but the performance on the test set (leaderboard) has begun to plateau, also referred in the literature as goldilocks zone.

  In that sense, Argoverse 2 is designed to increase prediction difficulty incrementally, spurring productive focused research for the next few years. These changes are intended to encourage methods that perform well on extended forecast horizons (3 s $\rightarrow$ 6 s), handle multiple types of dynamic objects (1 $\rightarrow$ 5), and ensure safety in

scenarios from the long tail. Future Argoverse releases could continue to increase the problem difficulty by reducing observation windows and increasing forecasting horizons.

- **Usability matters**: Argoverse 1 benefited from a large and active research community in large part due to the simplicity of setup and usage. Existing Argoverse models can be easily ported to run on Argoverse 2. In particular, the Argoverse 2 have prioritized intuitive access to map elements, encouraging methods which use the lane graph as a strong prior. To improve training and generalization, all poses have also been interpolated and resampled at exactly 10 Hz (Argoverse 1 was approximate). In that sense, Argoverse 2 includes fewer, but longer and more complex scenarios. This ensures that total dataset size remains large enough to train complex models but small enough to be easily downloadable and manageable.

2.4.3. Evaluation metrics

Most MP datasets (either in the field of AD or others focused on pedestrian motion prediction) use the same metrics to evaluate the performance of the different proposed algorithms. In this work we focus on the most important ones: minimum Average Displacement Error (minADE) and minimum Final Displacement Error (minFDE) (both in the uni-modal and multi-modal scenario) to evaluate our models with respect to the SOTA both in terms of validation and tests sets.

1. The minimum Average Displacement Error (minADE, also referred as $ADE_{K=N}$) measures the average $\mathcal{L}_2$ distance between the best predicted trajectory and the ground-truth trajectory over all time steps. The best here refers to the trajectory (or mode) that has the minimum average error. It is defined as:

$$minADE = \min_{i=1}^{K=N} \left(\frac{1}{T} \sum_{t=1}^{T} \sqrt{\left(x_{i,t}^{pred} - x_{i,t}^{gt}\right)^2 + \left(y_{i,t}^{pred} - y_{i,t}^{gt}\right)^2} \right)$$

   where $K = N$ is the total number of predictions or modes, T is the number of time steps, $(x_{i,t}^{pred}, y_{i,t}^{pred})$ are the predicted coordinates of vehicle i at time step t, and $(x_{i,t}^{gt}, y_{i,t}^{gt})$ are the ground-truth coordinates of vehicle i at time step t. The minADE metric penalizes the algorithm for the worst average displacement error among all the predictions.

2. The minimum Final Displacement Error (minFDE, also referred as $FDE_{K=N}$) measures the minimum $\mathcal{L}_2$ distance between the final predicted position and the corresponding ground-truth position. The best here refers to the trajectory (or mode) that has the minimum average error. It is defined as:

$$minFDE = \min_{i=1}^{K=N} \sqrt{\left(x_{i,T}^{pred} - x_{i,T}^{gt}\right)^2 + \left(y_{i,T}^{pred} - y_{i,T}^{gt}\right)^2}$$

where $(x_{i,T}^{pred}, y_{i,T}^{pred})$ are the predicted coordinates of vehicle i at the last time step T, and $(x_{i,T}^{gt}, y_{i,T}^{gt})$ are the ground truth coordinates of vehicle i at the last time step T. The minFDE metric penalizes the algorithm for the worst final displacement error among all the predictions.

In this work, except for the GAN-based model (Chapter 5) which is focused on uni-modal prediction, we report results for $K = 1$ (uni-modal case, only the mode with the best confidence is considered) and $K = 6$ as this is the standard multi-modal in the Argoverse 1 and 2 Motion Forecasting datasets in order to compare with other models.

2.5. Comparison of *state-of-the-art* simulators in Autonomous Driving

The last section of this Chapter focuses on justifying the necessity of why a hyper-realistic simulator is required to validate the algorithms instead of only using the graphics and metrics calculated on the corresponding datasets. We aim to integrate the best proposal of the thesis with other upstream and downstream modules developed in our research group (specially the MOT and DM modules) to validate the influence of the prediction step in a holistic way.

In order to validate a whole ADS the system must be tested in countless environments and scenarios, which would escalate the cost and development time exponentially with the physical approach. Considering this, the use of photo-realistic simulation (virtual development and validation testing) and an appropriate design of the driving scenarios are the current keys to build safe and robust AD technology. These simulators have evolved from merely simulating vehicle dynamics to also simulating more complex functionalities. Simulators intended to be used for testing AD technology must have requirements that extend from simulating physical car models to several sensor models, path planning, control and so forth and so on. Some SOTA simulators [59] are as following:

- **CarSim** [60] is a vehicle simulator commonly used by academia and industry. Its newest version supports moving objects and sensors that benefit simulations involving self-driving tecnology and ADAS. These moving objects may be linked to 3D objects with their own embedded animations, such as vehicles, cyclists or pedestrians.
- **PreScan** [61] provides a simulator framework to design self-driving cars and ADAS. It presents PreScan's automatic traffic generator which enables manufacturers to validate their autonomous navigation architectures providing a variety of realistic environments and traffic conditions. This simulator supports Hardware-in-the-Loop (HIL) simulation, quite common for evaluating Electronic Control Units (ECUs) used in real-world applications.

- **CARLA** [62] an open-source autonomous driving simulator implemented as a layer over Unreal Engine 4 (UE4) [63]. This simulation engine provides to CARLA an ecosystem of interoperable plugins, a realistic physics and a state-of-the-art image quality. CARLA is designed as a server-client system so as to support this functionality provided by UE4, where the simulation is rendered and run by the server. The environment is composed of 3D models of static objects, such as buildings, infrastructure or vegetation, as well as dynamic objects like pedestrians, cyclists or vehicles. These objects are designed using low-weight geometric textures and models though maintaining visual realism by making use of variable level of detail and carefully crafting the materials. Moreover, one of the main advantages when using CARLA is the possibility to modify in an easy way the vehicle on-board sensors and their features in order to obtain accurate data, the weather and even the possibility to create realistic traffic scenarios.

- **Gazebo** [64] is an scalable, open-source, flexible and multi-robot 3D simulator. It supports the recreation of both outdoor and indoor environments in which there are two core elements that define the 3D scene, also known as world and model. The world is used to represent the 3D scene, defined in a Simulation Description File (SDF) and a model is basically any 3D object. Gazebo uses Open Dynamic Engine (ODE) as its default physic engine.

- **LGSVL (LG Electronics America R&D Center)** [65] is the most recent simulator for testing autonomous driving technology, focused on multi-robot simulation. It is based on the Unity game engine [66], providing different bridges for message passing between the simulator backbone and the autonomous driving stack. LGSVL provides a PythonAPI to control different environment entitities, such as weather conditions, the position of the adversaries, etc, in a similar way to the CARLA simulator. It also provides Functional Mockup Interface (FMI) so as to integrate vehicle dynamics platform to the external third party dynamics models.

In order to choose the right simulator, there is a set of criteria [59] that may serve as a metric to identify which simulators are most suitable for our purposes. In our case we have selected such as perception (sensors and weather conditions), multi-view geometry, traffic infrastructure, vehicle control, traffic scenario simulation, 3D virtual environment, 2D/3D groundtruth, scalability via a server multi-client architecture and last but not the least, if the simulator is open-source. In Table 2.4, we provide a comparison summary where all five simulators aforementioned are further compared. For further details about this AD comparison, we refer the reader to [59].

In that sense, we identify that CarSim is usually connected to MATLAB/Simulink [67] to simulate simple scenarios, with efficient plot functions and computation, where the user can control the vehicle models from CarSim and build their upper control algorithms in

Table 2.4: Comparison of some *state-of-the-art* simulators for AD. GT stands for Ground-Truth. ✓ and ✗ indicate that the corresponding requirement is supported or not respectively. U = Unknown, TL = Traffic Light, SS = Stop Signal, INT = Intersections, IN = Indoor, OUT = Outdoor, ROS = Robot Operating System. MCA = Multi-Client Architecture. Hyphens "-" indicate that attributes are either not applicable, or not available.

Requirements	CarSim	PreScan	CARLA	Gazebo	LGSVL
Sensor models supported	✓	✓	✓	✓	✓
Different weather conditions	✗	✓	✓	✗	✓
Camera Calibration	✗	✓	✓	✗	✗
Path Planning	✓	✓	✓	✓	✓
Proper vehicle control dynamics	✓	✓	✓	✓	✓
3D Virtual Environment	✓	✓	✓, OUT (Urban)	✓, IN & OUT	✓, OUT (Urban)
Traffic Infrastructure	✓	✓	✓ (including TLs, INTs, SSs, lanes)	✓ (including TLs, INTs, SSs, lanes)	✓
Simulate different dynamic objects:	✓	✓	✓	✗	✓
2D/3D ground-truth	✗	✗	✓	-	✓
Interfaces to other software	✓, with MATLAB	✓, with MATLAB	✓, with ROS, Autoware	✓, with ROS	✓, with Autoware, Apollo, ROS
Scalability via a server MCA	-	-	✓	✓	✓
Open Source	✗	✗	✓	✓	✓
Stability	✓	✓	✓	✓	✓
Portability	✓	✓	✓, Windows & Linux	✓, Windows & Linux	✓, Windows & Linux
Flexible API	✓	-	✓	✓	✓

MATLAB/Simulink to do a co-simulation project, but the realism, the quality of the sensors and the complexity is limited. PreScan presents better capabilities to build realistic environments and simulate different weather conditions, unlike MATLAB and CarSim. Gazebo is quite popular as a robotic simulator, but the effort and time needed to create complex and dynamic scenes does not make it the first choice for testing self-driving technology.

Figure 2.6: CARLA simulator overview

To this end, we have two simulators as our final options: LGSVL and CARLA. At the moment of writing this thesis, they are the most suited simulators for end-to-end testing of unique functionalities offered by autonomous vehicles, such as perception, mapping, vehicle control or localization. Most of their features, summarized in [59] are identical (open-source, traffic generation simulation, portability, 2D/3D groundtruth, flexible API and so forth and so on), with the only difference that LGSVL does not present camera calibration to perform multi-view geometry or Simultaneous Localization and Mapping (SLAM). Regarding this, we decided to use the CARLA simulator since the performance is very similar to LGSVL and the group had previous experience in the use of this simulator.

2.6. Summary

In order to finish this Chapter, we perform a brief comparison between the different methods (Physics-based, Classic ML, RL and DL) in terms of accuracy, prediction horizon, computation cost and applications in the AD field.

Table 2.5: Summary of MP methods features. Short-term and long-term characterize prediction horizons of no more than 1-s and no less than 3-s, respectively.

Methods	Accuracy	Prediction Horizon	Computation Cost	Applications
Physics-based	High in short-term prediction, low in other prediction horizon	Short	Small	Colision risk analysis
Classic Machine Learning-based	Good at recognizing maneuvers but generalization ability is poor	Medium	Medium	Maneuver recognition
Reinforcement Learning-based	Relatively high, prediction methods are relatively few	Long	High	More applied in planning
Deep Learning-based	High in considering some factors	Long	Relatively high	More and more applied in real-world

- **Physics-based methods** are suitable for the movement of vehicles, which can be accurately described by kinematics or dynamics models. Given a suitable physics model, these methods can be applied to a variety of scenarios at small computational cost and in a short time but without training. However, the prediction results based on such models heavily depends on the inputs and the model selection. The inputs are closely related to human or machine drivers, influenced by the driving environment or the interactions with other participants. Therefore, without the capability to describe such factors, physics-based models are limited to short-term prediction and in static scenes. Because of its simplicity and fast response, these methods can be easily used in real applications for ADSs, such as collision risk analysis.
- **Classic ML-based methods**, compared with physics-based methods, are able to consider more factors and its accuracy is relatively high with a longer prediction length at a higher computing cost. Most of these methods are maneuver-based methods, which predicts the trajectory with the maneuver known as a prior. However, vehicle maneuvers of human drivers are usually diverse and vary greatly in different scenarios such that the generalization ability of this approach is poor. In real applications for ADSs, such methods are used in scenarios such as lane change studies, leveraging their advantages in maneuver recognition.
- **RL-based methods** imitate the human DM process and obtain the reward function through learning the expert demonstration to generate the corresponding optimal driving policy. They can continuously evolve through learning and adapt to complex environments and long prediction horizons. Such methods probably generate higher accuracy trajectories than DL methods in a longer time domain. However, most of these methods are typically computationally expensive in their recovery of an expert cost function, require long training times and its training is based on actions and

episodes, in such a way its use in real-world MP applications is not suitable, being RL more applied to trajectory planning, taking its advantages in the DM process.

- **DL-based methods** can perform accurate predictions in a longer time horizon with respect to traditional methods that are only suitable for simple scenes and short-term prediction. By means of powerful neural networks, such as RNNs, CNNs, GANs, Attention mechanisms or GNNs for feature extraction, physics-related, interaction-related and road-related factors are processed as inputs to the model. Furthermore, they can adapt to more complex environments and a longer prediction horizon. DL-based methods require to use a large amount of data for training.

  Besides, with the increase of consideration factors and the increase of the number of network layers, the computing costs and time increases sharply. Such methods can naturally generate multi-modal trajectories, which is consistent with the diversity of vehicles maneuvers. In real applications for ADS, it is necessary to reach a balance between calculation time and model complexity to ensure the real-time performance and safety of ADS. At present, more and more real-world trials use these methods to predict the future trajectory of traffic participants.

As observed in Table 2.5 and discussed in this section summarizing the different MP algorithms, we focus this thesis on DL methods since they are the most suitable methods for long-term prediction with a lower computation cost than RL-based approaches, specially focusing on the ability of extracting and combining the latent spaces of the different inputs by means of SOTA algorithms. Then, they are more suitable to model complex real-world applications, which is the final objective of this thesis.

Furthermore, the validation framework (both in terms of datasets and AD simulator) is defined. In this thesis we choose Argoverse 1 and Argoverse 2 as databases to build our DL-based MP algorithms, since both are extensively used by the research community to build this kind of algorithms, and CARLA to validate the prediction methods in a holistic way (that is, integrated with other layers such as DM or control) in a hyper-realistic AD simulator as a preliminary stage before implementing it in a real-world platform.

Chapter 3

Theoretical Background

Desde que el mundo cambió,
estamos mucho más unidos
con los Digimon,
luchamos juntos contra el mal.
Algo extraño pasaba,
Digievolucionaban, en tamaño y color,
¡Ellos son los Digimon!.

Opening 1 de Digimon: "Butterfly"
Autor original: Kōji Wada

3.1. Introduction

As commented in previous Chapters, the MP algorithms covered by this thesis range from tracking multiple objects and subsequent prediction with physics-based methods to the most recent SOTA techniques to compute the deep traffic context and then decode multi-modal predictions with associated confidences, assuming the physical information is given and surrounding participants have been multi-tracked beforehand. Throughout this Chapter, an in-depth theoretical study will be made of those algorithms, neural networks or heuristics that form the foundations of this work in order to address the proposed methods in future chapters.

First of all, we will start with the mathematical formulation of the methods to perform physics-based Multi-Object Tracking, such as the well-known Kalman Filter (KF) algorithm [24] for agent state estimation and the Hungarian Algorithm (HA) [68] for the association of detections and trackers, which represents the preliminary stage before carrying out the subsequent physics-based uni-modal prediction. On top of that, since several single-trajectory models (CTRV, CTRA) are used to compute the most plausible centerlines in the Argoverse 1 [6] and Argoverse 2 [7] datasets, we will review the state transition equations to properly understand the constraints for each model. Furthermore, the principal DL techniques (*e.g.* 1D-CNN, LSTM, GAN, Attention mechanisms or GCN)

and training losses used in this work to encode and decode the aimed multi-modal predictions will be stated, first a general mathematical formulation and applications, and then, how the corresponding technique is used in the MP field.

3.2. Physics-based algorithms

As stated in Chapter 2, in terms of MP, initially researchers rely on physics-based methods, which are basic and straightforward. These methods may not offer high accuracy, but many models use the underlying idea of physics-based models to improve their accuracy. Physics-based approaches yield better results when the movement of vehicles is described by kinematics or dynamics models accurately. Nevertheless, the physical model of traffic participants is constantly evolving, so most physics-based models are only applicable for short-term predictions of no more than one second. In this Section we will study the mathematical formulation of the physics-based prediction algorithms, as well as the data association problem regarding the Multi-Object Tracking (MOT) stage, that are directly related to our algorithm proposed in Chapter 4.

3.2.1. Kalman Filter under the hood

The Kalman Filter (KF) [24] is a recursive algorithm used for estimating the state of a dynamic system in the presence of noise. It is widely used in various fields such as engineering, control systems, and robotics. The algorithm works by combining a prediction of the system state based on a mathematical model with measurements (updates) from sensors to improve the accuracy of the state estimation, as shown in Figure 3.1. The KF is a powerful algorithm for state estimation, and it has many variations and extensions that can handle various types of systems and measurements. The filter can be applied to non-linear systems using the Extended Kalman Filter (EKF) or the Unscented Kalman Filter (UKF), and it can handle multiple models using the multiple model KF. The filter can also be used for smoothing, which involves estimating the state of the system based on past and future measurements.

In its most simple version, the KF assumes that the system can be described using a set of linear equations, where the state of the system can be represented by a vector $\mathbf{x}_k$, and the measurements can be represented by a vector $\mathbf{z}_k$. The KF also assumes that the noise in the system follows a Gaussian distribution.

The state estimation process is performed in two steps: the prediction step and the update step. In the prediction step, the current state of the system is predicted based on the previous state and a mathematical model of the system. In the update step, the predicted state is corrected based on a measurement from the sensors.

The prediction step can be represented using the following equations:

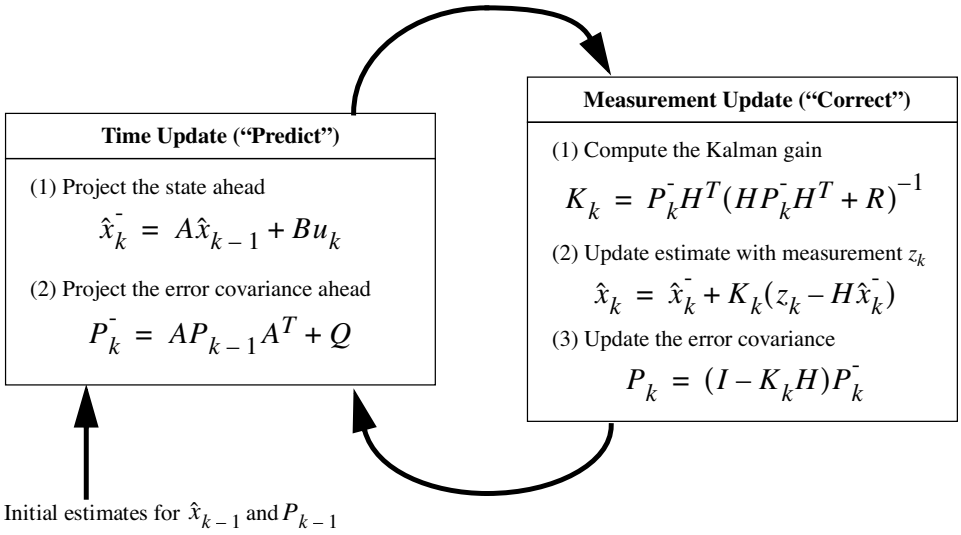

Figure 3.1: Overview of the KF Predict-Update cycle. The KF keeps track of the estimated state of the system and the variance or uncertainty of the estimate. The estimate is updated using a state transition model and measurements.
Source: *An introduction to the kalman filter* [69]

$$\begin{aligned} \hat{x}_k^- &= A\hat{x}_{k-1} + Bu_k \\ P_k^- &= AP_{k-1}A^T + Q \end{aligned} \tag{3.1}$$

where $\hat{x}_k^-$ is the predicted state of the system at time k, $\hat{x}_{k-1}$ is the estimated state of the system at time $k-1$, A is the state transition matrix, B is the control-input matrix, u_k is the control input at time k, P_k^- is the predicted error covariance matrix, and Q is the process noise covariance matrix. Note that the state transition, control-input and process noise covariance matrix values do not depend on the time-step time k.

On the other hand, the update step can be represented using the following equations:

$$\begin{aligned} K_k &= P_k^- H_k^T (HP_k^- H^T + R)^{-1} \\ \hat{x}_k &= \hat{x}_k^- + K_k(z_k - H_k\hat{x}_k^-) \\ P_k &= (I - K_k H)P_k^- \end{aligned} \tag{3.2}$$

where K_k is the KF gain, H is the measurement matrix, R_k is the measurement noise covariance matrix and I the identity matrix of the corresponding dimension. The KF gain determines the relative weight given to the predicted state and the measurement, and is adjusted based on the measurement noise covariance matrix. The measurement matrix relates the measurements to the state variables, and is used to convert the measurements into the same units as the state variables.

3.2.2. Hungarian algorithm formulation

The Hungarian Algorithm (HA) [68], also known as the Kuhn-Munkres algorithm, is an efficient algorithm for solving the assignment problem in combinatorial optimization. An example to illustrate the HA solution for an assignment problem involves finding the optimal assignment of n workers to n jobs, given the cost of assigning each worker to each job.

The HA works by iteratively finding a set of independent zero-cost assignments, which correspond to a perfect matching in a bipartite graph. These assignments are then used to reduce the problem size and find a new set of independent zero-cost assignments, until all workers are assigned to jobs.

This algorithm has a time complexity of $O(n^3)$, which makes it one of the most efficient algorithms for solving the assignment problem. In this algorithm, the cost matrix C is assumed to be an $n \times n$ matrix, where each element $C_{i,j}$ represents the cost of assigning worker i to job j. The matrix M represents the matching, where each element $M_{i,j}$ is 1 if worker i is assigned to job j, and 0 otherwise.

Algorithm 3.1: The Hungarian algorithm for solving the minimum cost perfect matching problem

Input : A cost matrix C of size $n \times n$
Output: A minimum cost perfect matching

Initialize the label vectors $u_i = \min_{j \in 1,\dots,n} C_{i,j}$ and $v_j = 0$ for all i, j; Initialize the empty matching M; **while** $|M| < n$ **do**
  Choose an unmatched row i; Initialize the set $T = i$ and the predecessor vector $P = \emptyset$; **while** *true* **do**
    Let S be the set of columns j such that $i \in T$ and $C_{i,j} = u_i + v_j$; If $|S| > 0$, choose any column j in S; **else**
      Choose a column j such that $v_j = \min_{k \in 1,\dots,n} v_k$ and let S be the set of rows i such that $j \in M$ or $C_{i,j} = u_i + v_j$; Increment each u_i for $i \in T$ by $\delta = \min_{i \in T, j \in S}(u_i + v_j - C_{i,j})$; Decrement each v_j for $j \in S$ by δ; **for** *each row* $i \in T$ *and each column* $j \in S$ **do**
        if $C_{i,j} = u_i + v_j$ **then**
          Add the edge (i, j) to the alternating tree represented by M and P; **if** j *is unmatched* **then**
            Augment M along the alternating tree to create a larger matching; **return** the updated matching M;
          end
          else
            Add j to T and continue the while loop;
          end
        end
      end
    end
  end
end

As observed in Algorithm 3.1, the HA iteratively finds an uncovered zero in the cost matrix C and adds it to the matching M, while also adjusting the cost matrix to ensure that all rows and columns are covered by the matching. This is done by finding the minimum

uncovered cost in each row and subtracting it from all uncovered costs in the row, and finding the minimum cost in each uncovered column and adding it to all uncovered costs in the column. Once all rows and columns are covered, the algorithm returns the final matching M.

In conclusion, the HA is a powerful optimization algorithm that solves the assignment problem in polynomial time. The algorithm has a wide range of applications and can be easily adapted to handle various constraints and objectives. The algorithm is also guaranteed to find the optimal solution to the assignment problem, which makes it a valuable tool in many practical settings.

3.2.3. State Transition Equations of Single-Trajectory Models

As illustrated in Chapter 2, Single-Trajectory prediction methods are used in the field of motion estimation and control, to predict the future state of an object based on its current state and motion. In these methods, the agents are mostly assumed to comply with motion models that describe their dynamic behavior in such a way these are not able to consider the road-related factors and the uncertainty of the current state is unreliable for long-term prediction. Then, these models should only be used for estimating uni-modal trajectories of the surrounding agents in the short-term (no more than 1-s).

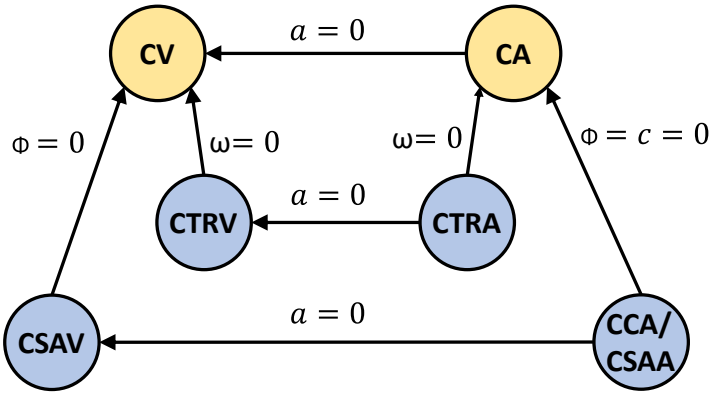

Figure 3.2: Overview of Single Trajectory prediction methods. Every sophisticated model can be transformed into a simpler one by setting one state veriable to zero. a, ϕ, c, ω represent the agent acceleration, steering angle, curvature and yaw rate (angular velocity) respectively
Source: *Comparison and evaluation of advanced motion models for vehicle tracking* [70]

Several single-trajectory prediction models have been proposed in the literature, as illustrated in Figure 3.2:

- Constant Velocity (CV) model assumes that the object moves at a constant velocity and its future position can be predicted by simply extrapolating its current velocity vector. This model is simple and computationally efficient, but it may not accurately capture the object motion if it changes its velocity.

- Constant Acceleration (CA) model is an extension of the CV model, assuming that the object can also change its acceleration in a linear manner. This model can provide more accurate predictions of the object future position and velocity, but it may not be suitable for objects with more complex motion patterns.
- Constant Turn Rate and Velocity (CTRV) model assumes that the object moves in a circular trajectory with a constant turn rate and velocity magnitude. This model is useful for predicting the motion of objects such as drones or missiles, but it may not accurately represent the motion of objects with more complex trajectories.
- Constant Turn Rate and Acceleration (CTRA) model is an extension of the CTRV model, allowing the object to change its acceleration while maintaining a constant turn rate. This model is often used in applications such as autonomous driving or aircraft navigation, where objects can accelerate or decelerate.
- Constant Steering Angle and Velocity (CSAV) model assumes that the object moves along a straight line with a constant speed and acceleration vector. This model can be useful for predicting the motion of objects such as trains or boats.
- Constant Curvature and Acceleration (CCA) model assumes that the object moves along a constant heading angle and can change its acceleration in a linear manner, also referred in the literature as Constant Steering Angle and Acceleration (CSAA) if the steering angle is used as a state variable instead of the curvature. From an algorithmic point of view, however, both names refer to the same model, which can be useful for predicting the motion of objects such as bicycles or motorcycles.

It can be observed how a sophisticated model can be transformed into a simpler one by setting one state variable to zero. For example, CTRA is transformed to CTRV if the agent acceleration a is set to zero. Similarly, CTRA is transformed to CA if the angular velocity ω is set to 0. In this Section we particularly focus on the prediction equations and differences of the most commonly used single-trajectory prediction methods in the field of AD: CTRV and CTRA.

3.2.3.1. Constant Turn Rate Velocity (CTRV)

The Constant Turn Rate and Velocity (CTRV) model is a mathematical model used in the field of autonomous navigation to predict the future motion of a moving object. The model assumes that the agent moves along a smooth, continuous path, *i.e.* the velocity and turn rate remain constant throughout the prediction interval.

With this model we are able to describe and predict the motion of the object using a set of differential equations that relate the rate of change of the agent state to its current state and any external inputs. It uses as main variables the current position, velocity, heading angle, and turn rate, and propagating them forward in time.

The prediction equations for the CTRV model are described as follows:

$$\begin{aligned} x_{k+1} &= x_k + \frac{v_k}{\omega_k}\left[\sin(\psi_k + \omega_k \Delta t) - \sin(\psi_k)\right] \\ y_{k+1} &= y_k + \frac{v_k}{\omega_k}\left[\cos(\psi_k) - \cos(\psi_k + \omega_k \Delta t)\right] \\ v_{k+1} &= v_k \\ \psi_{k+1} &= \psi_k + \omega_k \Delta t \\ \omega_{k+1} &= \omega_k \end{aligned} \tag{3.3}$$

where x_k and y_k are the coordinates of the agent position, v_k is the velocity magnitude, ψ_k is the heading angle (in radians), ω_k is the turn rate (in radians per second) and Δt is the time step size at timestep k respectively.

The first two equations predict the agent position at the next time step, based on its current position, velocity, heading angle, and turn rate. The third and fifth equations predict that the velocity and turn rate will remain constant. The fourth equation predicts the object heading angle at the next time step, based on its current heading angle and turn rate.

3.2.3.2. Constant Turn Rate Acceleration (CTRA)

The Constant Turn Rate and Acceleration (CTRA) model is an extension of the Constant Turn Rate and Velocity (CTRV) model, allowing the agent to change its acceleration while maintaining a constant turn rate.

The motion of the CTRA agent is modeled using the following set of equations:

$$\begin{aligned} x_{k+1} &= x_k + \frac{v_k}{\omega_k}\left[\sin(\theta_k + \omega_k \Delta t) - \sin(\theta_k)\right] \\ y_{k+1} &= y_k - \frac{v_k}{\omega_k}\left[\cos(\theta_k + \omega_k \Delta t) - \cos(\theta_k)\right] \\ \theta_{k+1} &= \theta_k + \omega_k \Delta t \\ v_{k+1} &= v_k + a_k \Delta t \\ \omega_{k+1} &= \omega_k \end{aligned} \tag{3.4}$$

where the variables are the same than the CTRV but at this point including the heading angle θ_k and agent acceleration a_k at timestep k.

The first two equations describe the agent position updates based on its current position, velocity, heading angle, turn rate, and the time step. The third equation describes the agent heading angle update based on its current heading angle and turn rate. The fourth equation describes the agent velocity update based on its current velocity and

acceleration. The last equation assumes that the agent turn rate remains constant over time.

As observed, the prediction equations for the CTRV model are based on the kinematic equations for circular motion, where the object position, velocity, and heading angle change in a continuous and smooth manner. In contrast, the prediction equations for the CTRA model include an additional term for the object acceleration, which allows for more accurate predictions of the object future motion when it can accelerate or decelerate.

In terms of implementation, the CTRA model requires more computational resources due to the additional term for acceleration, which increases the complexity of the equations. This can make the CTRV model more computationally efficient and faster to calculate in real-time applications.

3.3. Deep Learning algorithms

In this section the mathematical formulation of the DL layers employed in this thesis is covered. In particular, these are the 1D-CNN, LSTM, cGAN, Attention mechanism and GCN layers. We briefly introduce each layer, as well as the corresponding mathematical formulation to enhance the comprehension of the learning-based methods proposed in future Chapters.

3.3.1. Convolutional Neural Networks (CNNs)

CNNs are commonly used for image and signal processing tasks. The type of CNN architecture used depends on the nature of the input data. Here are the differences among the three main types of CNNs:

- **1D Convolutional Neural Networks (1D-CNNs)** are used for processing sequential data such as time series data, speech signals or text data. The input is a one-dimensional sequence of data, such as a time series of sensor readings. 1D-CNNs typically have fewer parameters and are computationally efficient compared to 2D- and 3D-CNNs.
- **2D Convolutional Neural Networks (2D-CNNs)** are used for processing 2D images. The input is a two-dimensional image represented as a matrix of pixels. The convolutional layers in a 2D-CNN apply filters that slide over the image to extract local features. The output of each convolutional layer is a set of 2D feature maps. 2D-CNNs are widely used for image classification, object detection, and image segmentation.
- **3D Convolutional Neural Networks (3D-CNNs)** are used for processing 3D volumetric data such as CT scans, MRI images, and video data. The input is a three-

dimensional volume represented as a sequence of 2D images. The convolutional layers in a 3D-CNN apply filters that slide over the 3D volume to extract local features. The output of each convolutional layer is a set of 3D feature maps. 3D-CNNs are used for tasks such as medical image analysis, video classification, 3D object detection and action recognition.

As we will see in further Chapters, in this work we focus on 1D-CNNs. The basic building blocks of a 1D CNN are convolutional layers, which learn local patterns in the input data by applying a set of filters to it, as illustrated in Figure 3.3. Each filter slides over the input sequence and performs a dot product operation at each position to generate a feature map. These feature maps capture the presence of certain patterns at different positions in the input sequence.

The architecture of a 1D-CNN typically consists of several convolutional layers, followed by one or more fully connected layers for classification or regression. The output of each convolutional layer is fed into the next layer, with optional pooling layers in between to reduce the spatial dimension of the feature maps, which are finally flattened before the final layer. The output of the network is obtained by passing the output of the last fully connected layer through a suitable activation function, such as softmax for classification or linear for regression.

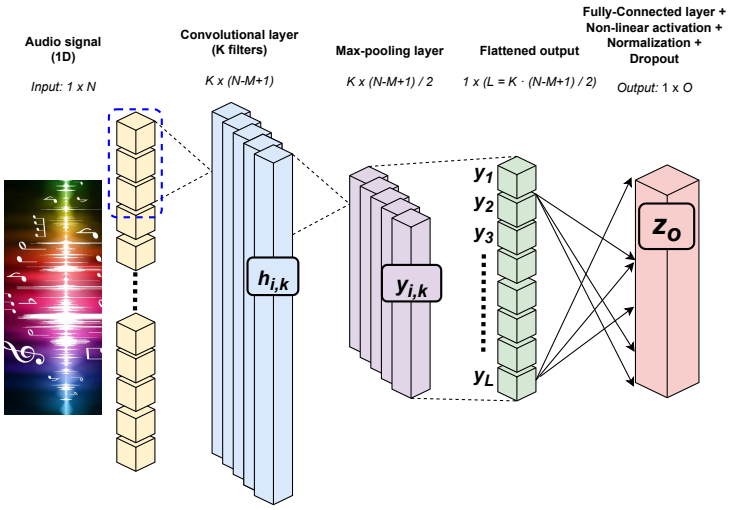

Figure 3.3: Example of a Convolutional Neural Network (CNN) architecture to process 1D-input signals

Let x be a 1-dimensional input sequence of length N, represented as a vector $x = [x_1, x_2, ..., x_N]$. Let K be a set of filters of length M, represented as a vector $k = [k_1, k_2, ..., k_M]$. We can apply the filter k to the input sequence x by computing a convolution operation:

$$(k * x)_i = \sum_{j=1}^{M} k_j x_{i+j-M} \tag{3.5}$$

where $*$ denotes the convolution operation, and i ranges from M to N. This operation produces a new sequence of length $N - M + 1$, representing the local features extracted from the input sequence x by the filter k.

To extract different types of features, we apply K filters in each convolutional layers in the network. Then, each layer applies a set of filters, and produces a set of feature maps. The feature maps can be computed as:

$$h_{i,k} = f(\sum_{k=1}^{M} W_{j,k} x_{i+k-M} + b_j) \tag{3.6}$$

where h is the feature map at position i and filter k, W is the weight matrix of the k-th filter, b is the bias term for the k-th filter, and f is an activation function (such as ReLU or sigmoid). Note that in Figure 3.3 a bench of $K = 4$ filters is applied in the convolutional layer.

After each convolutional layer, we typically apply a pooling layer to reduce the dimensionality of the features and increase the translation invariance of the network. The most common pooling operation is max pooling, which selects the maximum value within a window of size p:

$$y_{i,k} = \max_{j=0}^{p-1} h_{i+k,j} \tag{3.7}$$

where y is the output of the pooling layer at position i and filter k. After this operation, feature dimensionality is normally halved ($L = (N - M + 1)/2$), as observed in Figure 3.3. Once we have the corresponding features maps after the max pooling operation, we typically take the output of the pooling layer and flatten into a vector of L, and fed into a set of fully connected layers, with optional dropout regularization and batch normalization

Finally, we can use one or more fully connected layers to perform the final classification or regression task. The output of the pooling layer is flattened into a vector of length O, and fed into a set of fully connected layers, with optional dropout regularization and batch normalization:

$$z_o = f(\sum_{o=1}^{O} W_{l,o} y_l + b_o) \tag{3.8}$$

where z_o is the o-th element of the output vector with length O, W is the weight matrix, y is the flattened output of the pooling layer with length L, b is the bias term, and f is an activation function.

We make use of the 1D-CNN mechanism in Chapters 6 and 7, studying its effect in our algorithms, leveraging its wider receptive field compared with a MLP to reduce the influence of noisy input data.

3.3.2. Recurrent Neural Networks (RNNs)

Recurrent Neural Networks (RNNs) are a type of neural network that are designed to process sequential data, where the order of the input matters, usually assuming the presence of discrete timestep. They are widely used in a variety of applications such as natural language processing, speech recognition, image captioning, and time series prediction.

The general theory of RNNs is that they have a feedback loop in their architecture that allows information to be passed from one time step to the next, thereby enabling the network to capture dependencies between the inputs at different time steps. The input at each time step is fed into the network along with the output from the previous time step, and the network uses this information to generate a new output.

There are several types of RNNs, including the basic RNN, the GRU, and the Long Short-Term Memory (LSTM) [71]. The basic RNN is the simplest form of RNN, where the output at each time step is a function of the input at that time step and the output from the previous time step. However, it suffers from the vanishing gradient problem, where the gradients become exponentially small as they propagate through time, making it difficult to learn long-term dependencies.

The GRU is a variation of the basic RNN that uses gating mechanisms to control the flow of information through the network. It has fewer parameters than the LSTM and can be faster to train, but it may not perform as well as the LSTM on tasks that require more complex temporal dependencies.

3.3.2.1. Long Short-Term Memory (LSTM)

LSTM networks were introduced to address the vanishing gradient problem in standard RNNs. They achieve this by using a memory cell to store information over long periods of time, and three gating mechanisms to control the flow of information through the network. Figure 3.4 provides a detailed overview of the LSTM cell structure, illustrating the workflow from the previous cell output and input at time $t-1$ in order to compute the current cell state and hidden state at time t.

The three gates are called the input gate, forget gate, and output gate, and they are responsible for deciding which information to store in the memory cell, which information to forget, and which information to output, respectively.

The equations for the input, forget, and output gates are as follows:

- **Input gate**: $i_k = \sigma(W_i R_i \cdot [h_{k-1}, x_k] + b_i)$
- **Forget gate**: $f_k = \sigma(W_f R_f * [h_{k-1}, x_k] + b_f)$
- **Output gate**: $o_k = \sigma(W_o R_o * [h_{k-1}, x_k] + b_o)$

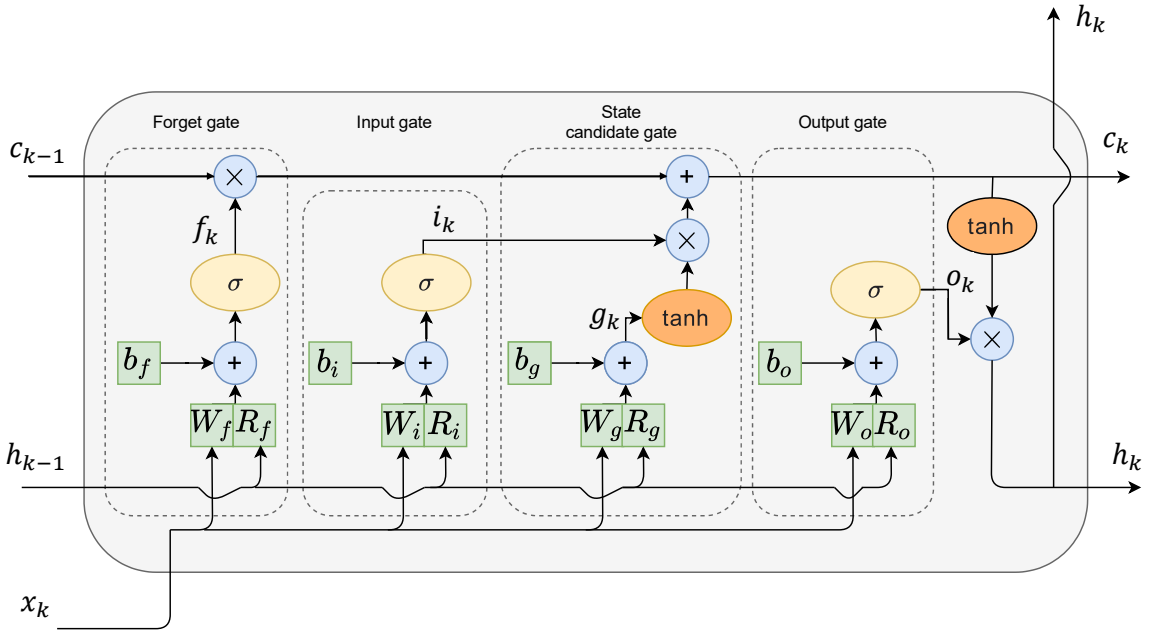

Figure 3.4: Overview of the LSTM cell structure

where x_k is the input at the current timestep k, h_{k-1} is the hidden state from the previous timestep, i_k is the input gate activation, f_k is the forget gate activation, and o_k is the output gate activation for the current timestep k respectively. On the other hand, $W_i R_i$, $W_f R_f$, and $W_o R_o$ are weight matrices (where the component W denotes the weights associated with the input signals x and R denotes the so-called recursive weights, associated with the hidden state of the cell from the previous timestep), and b_i, b_f, and b_o are bias vectors.

Moreover, the memory cell is updated based on the input, forget, and output gates, as well as a new candidate value that is computed based on the current input and hidden state. The equations for the memory cell and candidate value are as follows:

$$\begin{aligned} C_k &= f_k \cdot C_{k-1} + i_k \cdot \tilde{C}_k \\ \tilde{C}_k &= \tanh(W_g R_g \cdot [h_{k-1}, x_k] + b_g) \end{aligned} \tag{3.9}$$

where $\tilde{C}_k$ is the candidate value, C_t is the new memory cell value, and C_{k-1} is the previous memory cell value.

Finally, the hidden state at time t is computed based on the output gate and the new memory cell value, using the following equation:

$$h_k = o_k \cdot \tanh(C_k) \tag{3.10}$$

This equation scales the memory cell value by the output gate activation, then applies a hyperbolic tangent function to obtain the new hidden state.

In summary, LSTMs use a memory cell and three gating mechanisms to learn long-term dependencies in sequential data. The input, forget, and output gates control the flow of information through the network, while the memory cell stores information over time. The equations for LSTMs involve computing the input, forget, and output gate activations, the candidate value, the new memory cell value, and the new hidden state.

We make use of the LSTM network in Chapters 5 and 6 due to its powerful ability to represent as a high-dimensional space the past/future trajectories of the agents, though, as it will be seen in Section 3.3.4 of this Chapter, for the final proposal of the thesis we employ transformer-based modules since they are more powerful than LSTM and easier to train.

3.3.3. Generative Adversarial Networks (GANs)

A discriminative model is a type of machine learning model that learns the relationship between the input features and the target output directly. The goal of a discriminative model is to learn a decision boundary that separates different classes in the input data. In other words, discriminative models focus on learning the conditional probability distribution of the target variable given the input features.

Discriminative models are often used in supervised learning tasks, such as classification and regression, where the goal is to predict a target variable based on a set of input features. Common examples of discriminative models include logistic regression, support vector machines, and neural networks.

Unlike generative models, which learn the joint probability distribution of the input and target variables, discriminative models do not model the probability distribution of the input data explicitly. Instead, they focus on learning a mapping function that directly maps the input features to the target output.

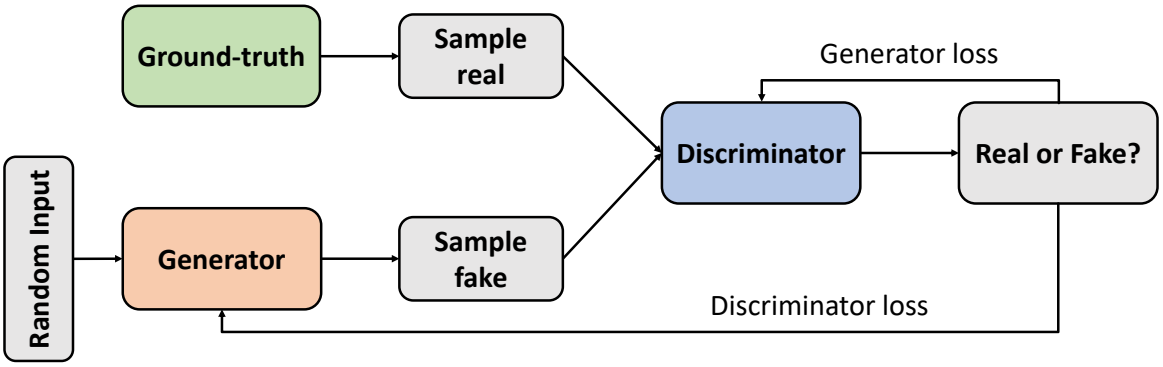

Figure 3.5: Overview of a GAN structure

In 2014, a breakthrough paper introduced Generative Adversarial Networks (GANs) [72], a clever new way to leverage the power of discriminative models to get good generative models. At their heart, GANs rely on the idea that a data generator is good if we cannot tell fake data apart from real data. In statistics, this is called a two-sample test, a test to answer the question whether datasets $X = \{x_1, \ldots, x_n\}$ and $X' = \{x'_1, \ldots, x'_n\}$ were drawn from the same distribution. This allows to improve the data generator until it generates something that resembles the real data. At the very least, it needs to fool the classifier even if our classifier is a state of the art deep neural network. GANs are a powerful technique for generating realistic samples that are similar to some training data. As observed in Figure 3.5, a GAN consists of two neural networks, a generator network and a discriminator network. The generator and discriminator networks are trained in a two-player game, where the generator tries to produce samples that fool the discriminator, and the discriminator tries to correctly classify between real and generated data. The objective function for a GAN is a min-max game between the generator and discriminator, and can be optimized using gradient descent or some other optimization algorithm. Some common applications where GANs are widely used are generating realistic images, videos, audio, data augmentation or style transfer.

The generator network takes as input a random noise vector, and generates a sample that is meant to mimic real data. The discriminator network takes as input a sample, and tries to distinguish between real data and generated data. The two networks are trained in a two-player game, where the generator tries to produce samples that fool the discriminator, and the discriminator tries to correctly classify between real and generated data.

The objective function for a GAN can be formulated as a min-max game between the generator and discriminator. The generator tries to minimize the probability that the discriminator correctly classifies the generated samples as fake, while the discriminator tries to maximize the probability that it correctly classifies the real and generated samples.

The objective function for a GAN can be written as:

$$\begin{aligned} \min_{\theta_G} \max_{\theta_D} V(D, G) &= \mathbb{E}_{x \sim p_{data}(x)}[\log D(x)] + \mathbb{E}_{z \sim p_z(z)}[\log(1 - D(G(z)))] \\ &= \mathbb{E}_{x \sim p_{data}(x)}[\log D(x)] + \mathbb{E}_{z \sim p_z(z)}[\log(1 - D(G(z; \theta_G)))] \end{aligned} \tag{3.11}$$

where θ_G and θ_D are the parameters of the generator and discriminator networks, respectively, x is a real sample from the training data distribution p_{data}, z is a noise vector sampled from a prior distribution p_z, and $G(z; \theta_G)$ is the generated sample from the generator network.

The first term of the objective function represents the expected log-probability of the discriminator correctly classifying a real sample as real. The second term represents the

expected log-probability of the discriminator correctly classifying a generated sample as fake.

During training, the generator network is updated to minimize the objective function with respect to θ_G, while the discriminator network is updated to maximize the objective function with respect to θ_D. This can be done using gradient descent or some other optimization algorithm.

There are some well-known types of GANs, such as:

- **Deep Convolutional GANs (DCGANs)**: These are GANs that use CNNs in the generator and discriminator networks. DCGANs are commonly used for image generation and have been shown to produce high-quality, realistic images.
- **Wasserstein GANs (WGANs)**: These are GANs that use the Wasserstein distance instead of the traditional Kullback-Leibler (KL) divergence or Jensen-Shannon (JS) divergence for measuring the difference between the real and generated distributions. WGANs have been shown to produce more stable training and generate higher-quality samples.
- **CycleGANs**: These are GANs that are designed for image-to-image translation tasks, where the goal is to transform an image from one domain to another. CycleGANs use two generators and two discriminators to learn the mapping between the two domains.

Nevertheless, in this work we focus on a particular type of GAN, known as conditional Generative Adversarial Network (cGAN), where the generator is conditioned on some additional information, allowing for more specific generation of data.

3.3.3.1. GAN vs cGAN

The main difference between the original Generative Adversarial Network (GAN) and conditional Generative Adversarial Network (cGAN) is that the original GAN generates samples without any control over the generated output, whereas the cGAN generates samples conditioned on some additional information.

In the original GAN, the generator network takes as input a random noise vector, and generates a sample that is meant to mimic real data. The discriminator network takes as input a sample, and tries to distinguish between real data and generated data. The goal of the original GAN is to train the generator network to generate samples that are indistinguishable from real data.

In contrast, a cGAN is a GAN that is conditioned on some additional information, such as class labels or image annotations. The generator network in a cGAN takes as input both a random noise vector and a condition vector, and generates a sample that is

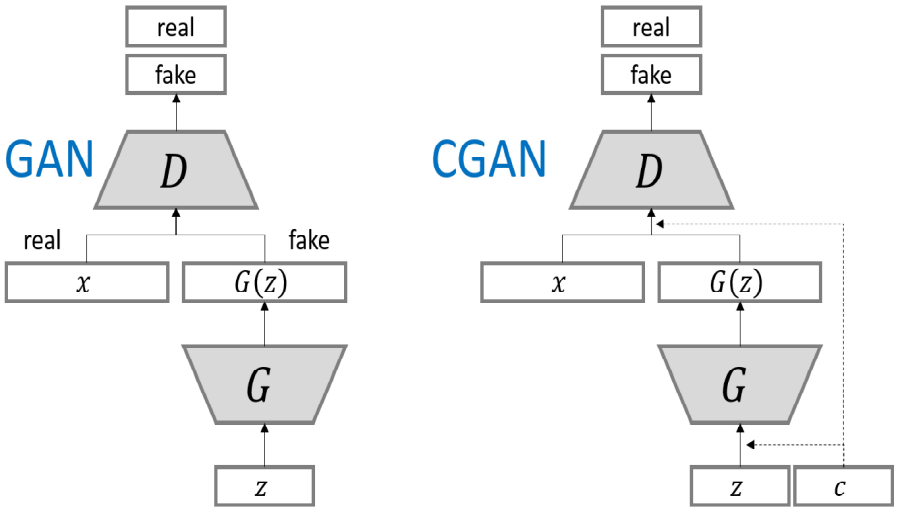

Figure 3.6: Comparison between the original GAN and cGAN
Source: *Logan: Generating logos with a generative adversarial neural network conditioned on color* [73]

conditioned on the additional information. The discriminator network also takes as input both the sample and the condition vector, and tries to distinguish between real data and generated data based on the condition. Figure 3.6 illustrates the differences between both architectures.

The cGAN can be used for a variety of applications, such as image-to-image translation, where the additional information is an input image that is translated to a different output image. For example, a cGAN can be trained to convert grayscale images to color images, or to transform images of one type of object to another type of object.

The training process for a GAN is similar to that of the original GAN, but the loss function for the generator and discriminator networks are modified to include the condition vector. Specifically, the loss function for the generator network includes a term that measures how well the generated samples match the condition vector, in addition to the term that measures how well the generated samples fool the discriminator. Similarly, the loss function for the discriminator network includes a term that measures how well the discriminator can identify the condition vector, in addition to the term that measures how well it can distinguish between real and generated data.

We make use a cGAN-based approach in Chapter 5 to compute plausible uni-modal predictions, where the input to the generative model (as we will see, represented by a LSTM network) is a noise vector z sampled from a multi-variate normal distribution and the physical and social represent the conditions to the model.

3.3.4. Attention Mechanism

The attention mechanism [74] is a computational method used in DL models to help the model focus on the most important parts of the input data. It is commonly used in Natural Language Processing (NLP), speech recognition, and computer vision. In terms of MP, the attention mechanism is usually employed to model interaction among entities (either social or physical) to compute the most important features once the corresponding encoders have previously computed a deep description of the scene, *i.e.* attention is commonly employed to extract relevant information from high-dimensional vectors (*e.g.* 64 or 128).

The basic idea of attention is to compute a set of weights that indicate the relative importance of different parts of the input. These weights are then used to compute a weighted sum of the input, which is used as the output of the attention mechanism. The attention mechanism can be formulated mathematically using the following equations:

- First, we compute a set of *keys*, *values*, and a *query* vector, which are used to compute the attention weights:

$$\begin{aligned} K &= k_1, k_2, ..., k_n \\ V &= v_1, v_2, ..., v_n \\ Q &= q_1, q_2, ..., q_d \end{aligned} \tag{3.12}$$

  where n is the number of elements in the input, and d is the dimension of the query vector.

- Next, we compute the attention weights using a function that compares the query vector to each of the keys:

$$a_i = \text{softmax}(q^T k_i) \tag{3.13}$$

  where a_i is the attention weight for the i-th element of the input.

- Finally, we compute the output of the attention mechanism as a weighted sum of the values:

$$o = \sum_{i=1}^{n} a_i v_i \tag{3.14}$$

3.3.4.1. Positional Encoding

In the attention mechanism, positional encoding is used to incorporate the order of the input sequence into the model. Positional encoding involves adding a fixed-length vector

to the input embeddings that encodes the position of each element in the sequence. It has shown to be an effective way of incorporating sequential information into transformer-based in applications such machine translation, language modeling, sentiment analysis or the present case, MP in the field of AD, where the order the sequence plays a fundamental role.

The mathematical formulation of positional encoding is as follows:

$$\mathrm{PE}_{(pos,2i)} = \sin\left(\frac{pos}{10000^{2i/d}}\right) \tag{3.15}$$

$$\mathrm{PE}_{(pos,2i+1)} = \cos\left(\frac{pos}{10000^{2i/d}}\right) \tag{3.16}$$

where pos is the position of the element in the sequence, i is the index of the dimension, and d is the dimension of the input embeddings. The positional encoding vectors are added to the input embeddings before they are passed through the self-attention mechanism.

The choice of the hyperparameters used in the positional encoding formulation, such as the use of the sine and cosine functions and the value of 10000, is arbitrary but has been shown to work well in practice. The positional encoding vectors add a sinusoidal pattern to the input embeddings that allows the model to distinguish between elements at different positions in the sequence.

3.3.4.2. Multi-Head Attention

Multi-head attention is a type of attention mechanism used in DL models, particularly in transformer-based architectures. This Multi-Head concept allows the model where it is integrated to attend to multiple parts of the input at once, which is really useful for capturing complex relationships between different parts of the input. It involves splitting the input into multiple heads and computing separate attention scores for each head, which are then combined to produce the final output. It can be formulated mathematically using the following equations:

- First, we split the keys, values, and query vectors into multiple *heads*, each of which has its own set of learned weight matrices:

$$\begin{aligned} K_i &= k_{i,1}, k_{i,2}, ..., k_{i,n} \\ V_i &= v_{i,1}, v_{i,2}, ..., v_{i,n} \\ Q_i &= q_{i,1}, q_{i,2}, ..., q_{i,d} \end{aligned} \tag{3.17}$$

  where i is the index of the head.

- Next, we compute the attention weights and outputs for each head separately, using the same equations as in the basic attention mechanism:

$$a_{i,j} = \text{softmax}(Q_i^T K_{i,j}) \tag{3.18}$$

$$o_i = \sum_{j=1}^{n} a_{i,j} V_{i,j} \tag{3.19}$$

  where in this case i represents the head index and j the corresponding element of the input, being o_i the whole output of the i-th head.

- Finally, we concatenate the outputs from all the heads and multiply them by a learned weight matrix W_O to produce the final output:

$$\text{MultiHead}(Q, K, V) = \text{Concat}(o_1, \ldots, o_H) W_O \tag{3.20}$$

  where H is the number of attention heads.

3.3.4.3. Self-Attention vs Cross-Attention

Both self-attention and cross-attention are usually employed by means of several heads, that is, Multi-Head Self-Attention (MHSA) and Multi-Head Cross-Attention (MHCA). Self-attention operates on a single sequence, while cross-attention operates on two sequences.

Self-attention is a type of attention mechanism used in deep learning models, particularly in transformer-based architectures, that allows the model to attend to different parts of the input sequence to compute a representation of each input element.

In self-attention, the input sequence (same source of information) is transformed into three different vectors: the query vector, the key vector, and the value vector. These vectors are then used to compute the attention score for each element of the input sequence with respect to every other element in the sequence. The attention scores are used to weight the value vectors, which are then combined to produce the final output.

The mathematical formulation of self-attention is as follows:

$$\text{Self-Attention}(X_1) = \text{softmax}\left(\frac{Q_1 K_1^T}{\sqrt{d_k}}\right) V_1 \tag{3.21}$$

where X_1 is the input sequence, Q, K, and V are the query, key, and value vectors, respectively, and d_k is the dimension of the key vectors. Subindex *1* indicates that the query, key and value come from the same source of information. The softmax function is applied row-wise to the matrix $\frac{QK^T}{\sqrt{d_k}}$, resulting in an attention matrix that has the same

dimensions as X. The attention matrix is then used to weight the value vectors V, which are combined to produce the final output.

The query, key, and value vectors are obtained through linear transformations of the input embeddings. The exact way in which these transformations are carried out can vary depending on the specific architecture, but in general they involve matrix multiplications with learnable weight matrices.

Self-attention has been shown to be a powerful mechanism for capturing long-range dependencies in sequential data, and it has been used successfully in a variety of natural language processing tasks, including machine translation, language modeling, and sentiment analysis.

On the other hand, in cross-attention, there are two sources of information, where one of the input sequences serves as the query sequence, while the other sequence serves as the key-value sequence. The query sequence is transformed into a query vector, while the key-value sequence is transformed into key and value vectors. The query vector is then used to compute the attention score for each element in the query sequence with respect to every element in the key-value sequence. The attention scores are used to weight the value vectors, which are then combined to produce the final output. Cross-attention is commonly used in machine translation models, where one of the input sequence is the source language and the other sequence is the target language.

The mathematical formulation of cross-attention is as follows:

$$\text{Cross-Attention}(X_1, X_2) = \text{softmax}\left(\frac{Q_1 K_2^T}{\sqrt{d_k}}\right) V_2 \tag{3.22}$$

where X_1 and X_2 are the input sequences which must have the same dimensionality, Q_1 is the query vector that comes from the first source of information, and K_2 and V_2 are key and value vectors that come from the second source of information respectively. As stated before, d_k is the dimension of the key vectors. The softmax function is applied row-wise to the matrix $\frac{QK^T}{\sqrt{d_k}}$, resulting in an attention matrix that has the same dimensions as the query sequence. The attention matrix is then used to weight the value vectors, which are combined to produce the final output.

To summarize the differences between both types of attention, in self-attention, the query, key, and value vectors are all derived from the same input sequence, while in cross-attention, the key-value sequence provides the key and value vectors. Self-attention is used to capture relationships between elements within a sequence, while cross-attention is used to capture relationships between elements in different sequences. Both types of attention can be appreciated as part of the Transformer architecture (Figure 3.7) proposed in [74].

3.3.4.4. Transformer

The Transformer model wraps-up previous attention mechanisms into a single and elegant architecture which allows the model to weigh the importance of different parts of the input sequence when computing a representation of each element in the sequence. Introduced in 2017 [74], it has become the absolute standard for Natural language Processing (NLP) tasks such as language modeling, question answering or machine translation. Figure 3.7 depicts the Transformer architecture proposed in the original paper.

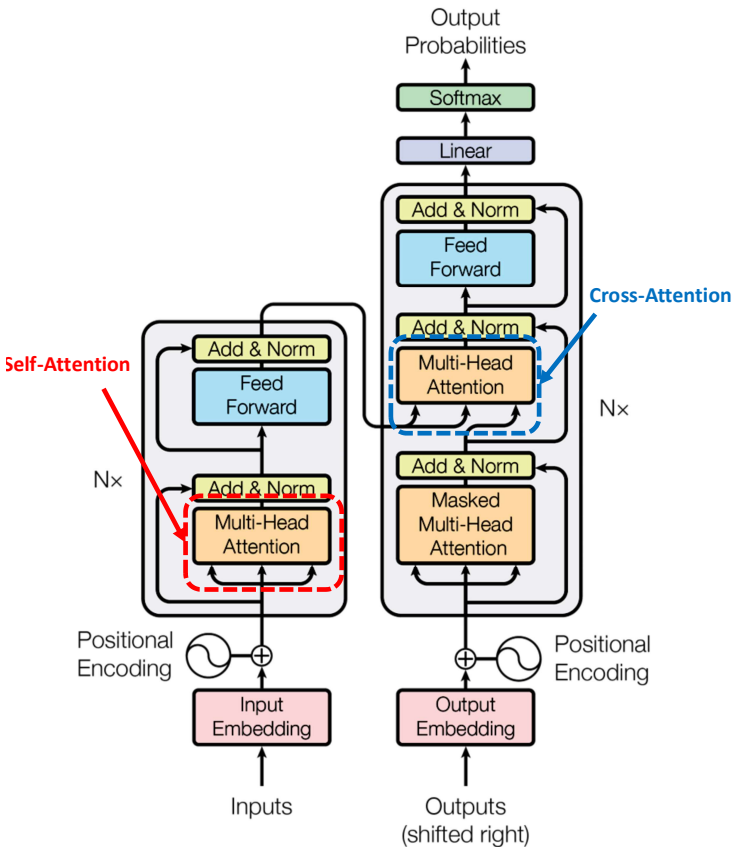

Figure 3.7: Overview of the Transformer architecture
Source: *Attention Is All You Need* [74]

The Transformer architecture consists of an encoder and a decoder. The encoder takes as input a sequence of embeddings, such as word embeddings or character embeddings, and produces a sequence of hidden states that capture the information in the input sequence. The decoder takes as input the encoder hidden states and produces a sequence of output embeddings that represent the output sequence.

The encoder consists of multiple layers, each of which contains two sub-layers: a self-attention sub-layer and a feedforward sub-layer. In the self-attention sub-layer, the model computes a representation of each element in the input sequence by attending to all the other elements in the sequence. The feedforward sub-layer applies a pointwise fully connected layer to each position in the sequence independently and identically.

The decoder also consists of multiple layers, each of which contains three sub-layers: a self-attention sub-layer, a cross-attention sub-layer, and a feedforward sub-layer. In the self-attention sub-layer, the model attends to the previously generated output embeddings to compute the next output embedding. In the cross-attention sub-layer, the model attends to the encoder hidden states to incorporate information from the input sequence. The feedforward sub-layer applies a pointwise fully connected layer to each position in the sequence independently and identically.

The Transformer architecture uses residual connections and layer normalization to facilitate training of deep neural networks. Residual connections allow information to flow directly from one layer to another, bypassing the intermediate layers, which can help prevent the vanishing gradient problem. Layer normalization normalizes the input to each sub-layer to have zero mean and unit variance, which can help stabilize the training process. Finally, the original architecture proposes a fully-connected layer and softmax operation to compute the probability distribution over the target vocabulary that determines the words with the highest probability.

Overall, the Transformer architecture has achieved SOTA results on a wide range of natural language processing tasks, and its success has led to the development of a variety of transformer-based architectures. As we will see in future sections, Transformers have several advantages over recurrent networks (such as LSTM) to encode and decode information with temporal dependencies. Here are some key advantages of transformers:

- **Attention mechanism**: Transformers employ the attention mechanism (both self and cross, if the Transformer decoder is used) that allows them to capture relationships between elements in a sequence more effectively. This mechanism enables the model to focus on relevant elements (or agents, in the field of MP) and assign different weights to different words during the encoding and decoding processes. LSTM networks, on the other hand, rely on recurrent connections that propagate information sequentially, which may not capture long-range dependencies as effectively as self-attention.

- **Parallel Computation**: Transformers are highly parallelizable, meaning that they can process inputs in parallel, which accelerates training and inference. In contrast, LSTM networks are inherently sequential in nature, as the recurrent connections require information from previous time steps to be processed before moving on to the next step. This sequential nature limits the parallelizability of LSTM networks and can result in slower training and inference times.

- **Long-term Dependency**: Transformers are specifically designed to capture long-term dependencies in sequences. The self-attention mechanism allows the model to consider all positions in the input sequence when making predictions, enabling it to capture dependencies over long distances. LSTM networks, although capable of cap-

turing short-term dependencies, can struggle with capturing long-term dependencies due to the vanishing or exploding gradient problem.

- **Transfer Learning**: Transformers have shown to be highly effective for transfer learning tasks. Pretrained transformer models, such as BERT (Bidirectional Encoder Representations from Transformers), have been trained on large-scale datasets and can be fine-tuned for specific downstream tasks with relatively small amounts of task-specific data. LSTM networks typically require more task-specific data to achieve good performance, as they don't benefit from the same level of transfer learning capabilities as transformers.
- **Handling Variable-length Inputs**: Transformers can handle variable-length inputs more easily than LSTM networks. Since transformers process the entire input sequence in parallel, they do not rely on fixed-length input vectors like LSTM networks. This flexibility is particularly advantageous for tasks with variable-length inputs, such as the present work, where a traffic scenario may have an undetermined number of agents around the ego-vehicle.

While transformers have these advantages, it is important to note that LSTM networks are still extensively used by the research community. They have been widely used and well-studied in various applications, especially in tasks where sequential information is critical. The choice between transformers and LSTM networks depends on the specific requirements of the task at hand. The attention mechanisms (including self-attention, cross-attention and transformer encoder) will be a key component of this thesis in the proposed learning-based models (Chapters 5, 6 and specially 7).

3.3.5. Graphs

A graph is a type of data structure that contains nodes and edges. A node can be a person, place, or thing, and the edges define the relationship between nodes. The edges can be directed and undirected based on directional dependencies.

Graphs are excellent in dealing with complex problems with relationships and interactions. They are used in pattern recognition, social networks analysis, recommendation systems, and semantic analysis. Creating graph-based solutions is a whole new field that offers rich insights into complex and interlinked datasets.

Nevertheless, Graph-based data structures have drawbacks, and researchers must understand them before developing graph-based solutions.

- **A graph exists in non-euclidean space**. It does not exist in 2D or 3D space, which makes it harder to interpret the data. To visualize the structure in 2D space, various dimensionality reduction tools must be used.

- **Graphs are dynamic**, *i.e.* they do not have a fixed form. There can be two visually different graphs, but they might have similar adjacency matrix representations. It makes it difficult for us to analyze data using traditional statistical tools.

- **Large size and dimensionality** will increase the graph complexity for human interpretations. The dense structure with multiple nodes and thousands of edges is harder to understand and extract insights.

3.3.5.1. Graph Neural Networks (GNNs)

Graph Neural Networks (GNNs) are a class of neural networks that operate on graphs, which are collections of nodes and edges. A typical graph is represented by a set of node features, represented by a matrix $X \in \mathbb{R}^{N \times D}$, where N is the number of nodes, and D is the number of features associated with each node. Each node is also connected to other nodes via edges, which are represented by an adjacency matrix $A \in 0, 1^{N \times N}$, where $A_{ij} = 1$ if there is an edge between nodes i and j, and 0 otherwise, as observed in Figure 3.8.

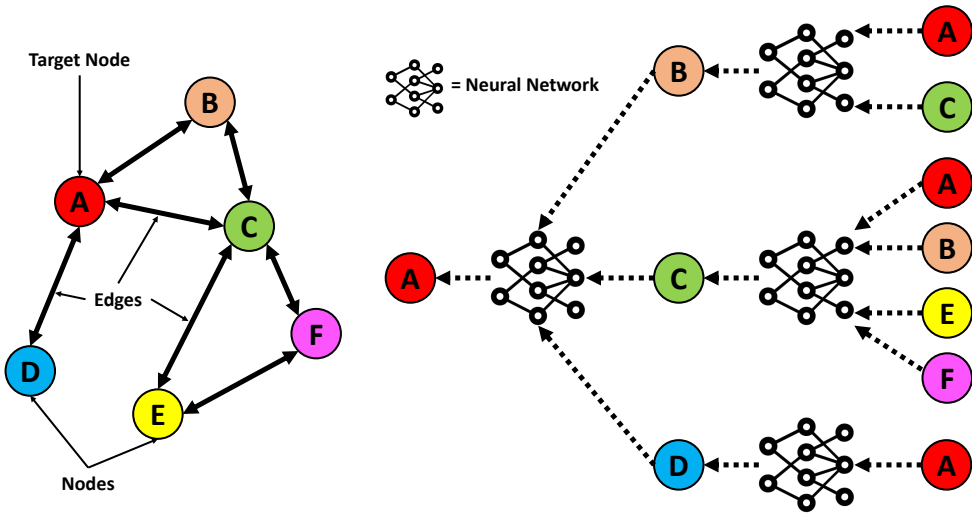

Figure 3.8: Overview of a GNN. On the left, it can be observed the input graph of N agents (in this particular case six agents for simplicity) where **A** represents the target node over which the influence of neighbouring nodes is going to be calculated. On the right, the latent space of the neighbours is measured as a preliminary stage before aggregating their information to the target node.

The basic idea behind GNNs is to iteratively update the node representations using information from the graph neighborhood. Specifically, at each iteration, each node aggregates information from its neighbors, and the resulting aggregated representation is used to update the node own representation. This process is typically repeated for multiple iterations until convergence.

One common way to implement this idea is to use the following update rule:

$$h_i^{(l+1)} = f(h_i^{(l)}, \sum_j A_{ij} h_j^{(l)}) \tag{3.23}$$

where $h_i^{(l)}$ is the representation of node i at iteration l, f is a non-linear activation function, and $\sum_j A_{ij} h_j^{(l)}$ is the sum of the representations of the neighbours of node i at iteration l (as stated above, j represents the neighbour node).

By stacking multiple layers of such updates, a GNN can learn increasingly complex representations of the graph.

There are several types of neural networks, such as:

- **Graph Auto-Encoder Networks**, which learn graph representation using an encoder and attempt to reconstruct input graphs using a decoder. They are commonly used in link prediction as Auto-Encoders and are good at dealing with class balance.
- **Recurrent Graph Neural Networks(RGNNs)** are able to learn the best diffusion pattern, and they can handle multi-relational graphs where a single node has multiple relations. They are commonly used in generating text, machine translation, speech recognition or generating image descriptions.
- **Gated Graph Neural Networks (GGNNs)** improve Recurrent Graph Neural Networks by adding a node, edge, and time gates on long-term dependencies, being the common uses similar to RGNNs.

Nevertheless, in this work we focus on a particular type of GNN, that is, Graph Convolutional Networks (GCNs), which are the most common type of GNN used in the field of MP for AD.

3.3.5.2. Graph Convolutional Networks (GCNs)

The majority of GNNs are Graph Convolutional Networks (GCNs), which are a specific type of GNN that use convolutional operations to aggregate information from the graph neighborhood. GCNs were introduced when CNN failed to achieve optimal results due to the arbitrary size of the graph and complex structure. The basic idea behind GCNs is to treat the graph as a signal and use convolutional operations to extract features by inspecting neighboring nodes. GCNs aggregate node vectors, pass the result to the dense layer, and apply non-linearity using the activation function.

The major difference between GCN and CNN is that it is developed to work on non-euclidean data structures where the order of nodes and edges can vary, as it can be appreciated in Figure 3.9. In the 2D convolution operation, each pixel in an image is taken as a node where neighbours are determined by the filter size. The 2D convolution takes the weighted average of pixel values of the red node along with its neighbors. The

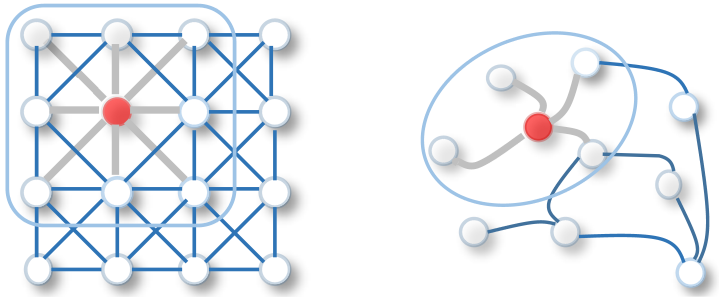

Figure 3.9: Overview of the sliding kernel of a 2D-CNN vs GCN
Source: *A comprehensive survey on graph neural networks* [75]

neighbours of a node are ordered and have a fixed size. On the other hand, to get a hidden representation of a given node red, one simple solution of the graph convolutional operation is to take the average value of the node features of the red node along with its neighbors. Different from image data, the neighbors of a node are unordered and variable in size.

The convolution in GCN is the same as a convolution in CNNs. It multiplies neurons with weights (filters) to learn from data features. A convolutional operation on a graph is defined as:

$$H^{(l+1)} = \sigma(D^{-\frac{1}{2}}AD^{-\frac{1}{2}}H^{(l)}W^{(l)}) \tag{3.24}$$

where $H^{(l)}$ is the matrix of node representations at iteration l, $W^{(l)}$ is the weight matrix of the l-th layer, A is the adjacency matrix of the graph, D is the degree matrix of the graph, and σ is a non-linear activation function. Note that in the mathematical field of algebraic graph theory, the degree matrix of an undirected graph is a diagonal matrix which contains information about the degree of each vertex, that is, the number of edges attached to each vertex

The operation $D^{-\frac{1}{2}}AD^{-\frac{1}{2}}$ is a normalization step that scales the adjacency matrix by the inverse square root of the degree matrix. This normalization ensures that nodes with different degrees have similar influence in the convolutional operation. By stacking multiple layers of such convolutions, a GCN can learn increasingly complex features of the graph.

3.3.6. Training

Training is the process of iterating through a dataset to make the network learn the optimal mapping (combination of weights) from input to desired output in the data samples. In each iteration, a forward pass through the network is performed, computing the output of each layer until the end. This produces the output response of the network,

which is then compared to a desired output through a defined Loss function ($\mathcal{L}$). This function estimates the output error, which is back-propagated through the network to update its weights with the aim of minimizing the error.

Regarding the supervised training paradigm, backpropagation [76] is an algorithm used for training artificial neural networks to update the weights and biases of the neurons in the multi-layer network based on the error between the predicted output and the actual output.

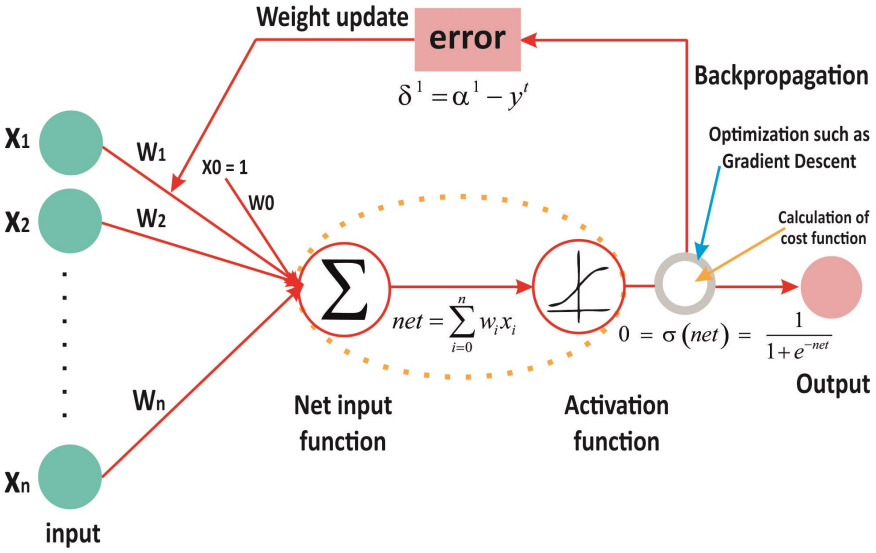

Figure 3.10: Gradient Descent and Backpropagation
Source: *Backpropagation: The basic theory* [76]

The backpropagation (Figure 3.10) algorithm consists of two phases: the forward pass and the backward pass. During the forward pass, the input is fed into the network and propagated through the layers to obtain the predicted output. During the backward pass, the error between the predicted output and the actual output is computed and used to update the weights and biases of the neurons in the network. This algorithm is based on the chain rule of calculus, which allows the gradient of the loss function with respect to each weight and bias to be computed recursively from the output layer to the input layer of the network. The gradient descent algorithm is then used to update the weights and biases in the direction of the negative gradient of the loss function. In that sense, the main losses used in this work are described throughout the remaining content of this Chapter.

3.3.6.1. Optimizer and learning rate

There are several optimizers commonly used for training deep neural networks in the literature, such as Stochastic Gradient Descent (SGD) [77], Adagrad [78], Root Mean Square Propagation (RMSprop) [79] or Adadelta [80]. In this work we use one of the most extended, the ADaptive Moment Estimation (ADAM) [81] optimizer. It is a popular

optimization algorithm used in deep learning, particularly for training neural networks. It is an adaptive learning rate optimization algorithm that is well suited for large datasets and high-dimensional parameter spaces.

The basic idea behind ADAM is to compute adaptive learning rates for each parameter based on estimates of the first and second moments of the gradients. The algorithm computes a moving average of the gradients and their squared values, and uses these estimates to update the parameters with a learning rate that adapts to the local curvature of the loss function. The algorithm also includes bias-correction terms to ensure that the estimates are unbiased, especially in the early stages of training when the estimates are highly uncertain.

The update rule for ADAM can be expressed mathematically as follows:

$$\begin{aligned} m_t &= \beta_1 m_{t-1} + (1-\beta_1) g_t \\ v_t &= \beta_2 v_{t-1} + (1-\beta_2) g_t^2 \\ \hat{m}_t &= \frac{m_t}{1-\beta_1^t} \\ \hat{v}t &= \frac{v_t}{1-\beta_2^t} \\ \theta t + 1 &= \theta_t - \frac{\alpha}{\sqrt{\hat{v}_t} + \epsilon} \hat{m}_t \end{aligned} \tag{3.25}$$

where θ_t is the parameter vector at time step t, g_t is the gradient vector, m_t and v_t are the first and second moment estimates at time step t, $\hat{m}_t$ and $\hat{v}_t$ are the bias-corrected moment estimates, α is the learning rate, β_1 and β_2 are the decay rates for the moment estimates, and ϵ is a small constant to prevent division by zero.

The algorithm starts with initializing m_0 and v_0 as zero vectors, and θ_0 as the initial parameter vector. At each iteration, the gradient vector g_t is computed using a batch of training data, and the moment estimates m_t and v_t are updated according to the first two lines of the update rule. The bias-corrected moment estimates $\hat{m}_t$ and $\hat{v}_t$ are then computed using the next two lines of the update rule. Finally, the parameter vector θ_t is updated using the last line of the update rule.

The hyperparameters α, β_1, β_2, and ϵ can be tuned to optimize performance on a particular dataset and neural network architecture.

On the other hand, the learning rate is a key hyperparameter in the optimization process of machine learning algorithms, including optimizer updates like the ADAM optimizer. The learning rate controls the step size taken in the direction of the negative gradient during each iteration of the optimization process.

If the learning rate is too small, the optimization process will be slow and may get stuck in local minima. On the other hand, if the learning rate is too large, the optimization process may overshoot the minimum and oscillate back and forth, or even diverge.

In the context of the ADAM optimizer, the learning rate is used to adjust the size of the update step taken in the direction of the estimated gradient. The update step is multiplied by the learning rate, which determines the size of the step. A larger learning rate will result in larger update steps, and a smaller learning rate will result in smaller update steps.

In practice, the learning rate is usually set through a process called hyperparameter tuning, where different values of the learning rate are tried on a validation set to find the optimal value that results in the best performance of the model on the test set.

One common technique to adjust the learning rate during training is called learning rate scheduling. This involves decreasing the learning rate over time, often according to a predetermined schedule or based on the performance of the model on a validation set. This technique can help improve the convergence and stability of the optimization process, particularly in the later stages of training when the model is close to the optimal solution.

Overall, the learning rate plays a crucial role in the optimization process of machine learning algorithms, including optimizer updates like the ADAM optimizer. Selecting an appropriate learning rate is important for achieving fast and stable convergence to the optimal solution.

In this thesis, we will use the ADAM optimizer and learning rate scheduler in Chapters 5, 6 and 7. Particularly, in terms of the learning rate scheduler, we will make use of the well-established *ReduceLROnPlateau*, which reduces the learning rate when a certain metric of interest (in our case, minADE) has stopped improving for a pre-defined *patience* (*i.e.* number of epochs over the dataset).

3.3.6.2. Losses

In this Section we explore the different losses that will be employed in order to train the DL-based MP algorithms in Chapter 5, 6 and 7.

3.3.6.2.1. Regression losses A regression loss is a type of loss function used in regression problems to measure the difference between the predicted and true values of a continuous variable. In other words, it is a way to quantify how well a machine learning model is able to predict numerical values based on input data.

In regression problems, the goal is to learn a function that maps input features to output values. A regression loss is used to train the model by penalizing the difference between the predicted and true output values. The loss function is typically minimized

during training, so that the model learns to make more accurate predictions. There are several types of regression loss functions, such as the Quantile loss, Log-Cosh or Mean Absolute Error (MAE). In this work we mainly focus on the Mean Squared Error (MSE) and SmoothL1 losses, also known as the Huber loss.

Mean Square Error (MSE) loss The Mean Squared Error (MSE) loss is a commonly used loss function in regression problems. It measures the average squared difference between the predicted and true values of a continuous variable. The MSE loss is given by:

$$MSE(y, \hat{y}) = \frac{1}{n}\sum_{i=1}^{n}(y_i - \hat{y}_i)^2 \tag{3.26}$$

where y_i is the true value of the i-th data point, $\hat{y}_i$ is the predicted value, and n is the number of data points.

The MSE loss penalizes large errors more strongly than small errors, since it uses the square of the difference between the predicted and true values. This makes it sensitive to outliers and can lead to overfitting if the data contains extreme values.

The MSE loss is used in many regression problems, such as linear regression or polynomial regression. It is often used as a performance metric to evaluate the performance of the model predictions.

SmoothL1 loss The SmoothL1 loss, also known as Huber loss, is a loss function used in regression problems to measure the difference between the predicted and true values of a continuous variable. It is a variant of the L1 loss that is less sensitive to outliers and has a smooth gradient near zero.

The SmoothL1 loss function can be defined as follows:

$$L(y, \hat{y}) = \begin{cases} \frac{1}{2}(y - \hat{y})^2 & \text{if } |y - \hat{y}| < 1 \\ |y - \hat{y}| - \frac{1}{2} & \text{otherwise} \end{cases} \tag{3.27}$$

where y is the true value, $\hat{y}$ is the predicted value, $|y - \hat{y}|$ corresponds to the L_1 loss (absolute error or distance) and $\frac{1}{2}(y - \hat{y})^2$ corresponds to the L_2 loss (Euclidean error or distance).

The SmoothL1 loss function behaves like the L1 loss for small errors and like the $\mathcal{L}_2$ (*a.k.a.* Euclidean distance) loss for large errors. Specifically, for errors smaller than 1, it uses the squared difference between the predicted and true values ($\mathcal{L}_2$), which has a smooth gradient. For larger errors, it uses the absolute difference ($\mathcal{L}_1$), which is less sensitive to outliers than the squared difference.

The SmoothL1 loss is used in regression problems when the data contains outliers or when the model needs to be less sensitive to large errors. It is commonly used in object detection and localization tasks, where the predicted bounding boxes can be highly sensitive to small changes in the input data.

3.3.6.2.2. Softmax loss The softmax loss, also known as the cross-entropy loss, is a commonly used loss function in classification problems. It measures the difference between the predicted probability distribution and the true probability distribution of a categorical variable. The softmax loss is given by:

$$CE(y, \hat{y}) = -\frac{1}{n} \sum_{i=1}^{n} \sum_{j=1}^{k} y_{i,j} \log(\hat{y_{i,j}}) \tag{3.28}$$

where $y_{i,j}$ is the true probability of the i-th data point belonging to class j, $\hat{y_{i,j}}$ is the predicted probability, n is the number of data points, and k is the number of classes.

The softmax function is applied to the output of the model to obtain a probability distribution over the classes. The predicted probability of class j is given by:

$$\hat{y_{i,j}} = \frac{e^{z_{i,j}}}{\sum_{l=1}^{k} e^{z_{i,l}}} \tag{3.29}$$

where $z_{i,j}$ is the unnormalized score or logit for class j of the i-th data point.

The softmax loss penalizes the model more heavily for predictions that are far from the true probabilities. It encourages the model to assign higher probabilities to the correct classes and lower probabilities to the incorrect classes.

The softmax loss is used in many classification problems, such as image classification, natural language processing, and speech recognition. It is often used as a performance metric to evaluate the quality of the model predictions.

3.3.6.2.3. Negative Log-Likelihood (NLL) loss The Negative Log Likelihood (NLL) loss is a loss function commonly used in classification problems, particularly in deep learning models that output probabilities for each class. It is a type of Maximum Likelihood Estimation (MLE) loss, which means it attempts to maximize the similarity between the predicted probability distribution and the true probability distribution of the target classes.

The NLL loss function can be defined as follows:

$$L(y_i, \hat{y}_i) = -\log(\hat{y_{i,y_i}}) \tag{3.30}$$

where y_i is the true label of the i-th data point, $\hat{y}_i$ is the predicted probability distribution for that point, and $\hat{y_{i,y_i}}$ is the predicted probability for the true label.

This penalizes the model for assigning low probabilities to the true label, while rewarding it for assigning high probabilities. It is a logarithmic loss function, which means that the penalty for low probabilities increases exponentially as the predicted probability approaches zero.

The Negative Log Likelihood (NLL) loss is used in classification problems because it provides a gradient that can be used to update the model parameters during training, in order to improve the accuracy of the predicted probabilities. It is commonly used in conjunction with softmax activation function, which ensures that the predicted probabilities sum to one across all classes.

Nevertheless, after revisiting the literature when developing the multi-modal prediction paradigm, we realized that most works employed the Winner-Takes-All (WTA) and max-margin (*a.k.a.* Hinge) losses to maximize the similarity between the future trajectories and the ground-truth. A comparison between employing the NLL loss and WTA+Hinge will be further detailed in Chapter 6.

3.3.6.2.4. Winner-Takes-All loss Winner-Takes-All (WTA) loss is a loss function used in clustering problems, particularly in competitive learning models. It is a type of unsupervised learning, which means that it does not require labeled data for training.

The WTA loss function can be defined as follows:

$$L(y_i, f(x_i)) = \begin{cases} 0 & \text{if } y_i = \arg\max_j f_j(x_i) \\ 1 & \text{otherwise} \end{cases} \tag{3.31}$$

where y_i is the true cluster of the i-th data point, $f_j(x_i)$ is the activation of the j-th neuron in the output layer for that point, and $\arg\max_j f_j(x_i)$ is the index of the neuron with the highest activation.

This loss function penalizes the model for assigning a data point to the wrong cluster. It works by forcing each neuron in the output layer to specialize in a particular cluster, such that the neuron with the highest activation for a given point corresponds to the true cluster of that point.

The WTA loss is used in clustering problems because it encourages the model to learn a set of representative clusters that capture the structure of the data, without requiring any prior knowledge of the true labels. It is commonly used in conjunction with competitive learning algorithms, such as self-organizing maps (SOMs), that use local competition between neurons to learn a topology-preserving mapping from the input space to the output space.

3.3.6.2.5. Hinge loss Hinge loss is a loss function used in classification problems, particularly in Support Vector Machines (SVMs). It is a type of max-margin loss, which means it attempts to maximize the margin between the decision boundary and the data points.

The hinge loss function can be defined as follows:

$$L(y_i, f(x_i)) = \max(0, 1 - y_i f(x_i)) \tag{3.32}$$

where y_i is the true label of the i-th data point, $f(x_i)$ is the predicted score for that point, and 1 is a margin hyperparameter that determines the width of the margin.

If $y_i f(x_i) \geq 1$, then the point is correctly classified and the loss is zero. If $y_i f(x_i) < 1$, then the point is misclassified and the loss is proportional to the distance between the predicted score and the correct score. The loss function penalizes misclassifications linearly, with a slope of -1 for negative misclassifications and 0 for positive misclassifications.

The hinge loss is used in SVMs because it encourages the model to find a decision boundary that maximizes the margin between the classes, while still correctly classifying the data points. This results in a more robust and generalizable model.

3.3.6.3. Regularization techniques

Regularization techniques in deep learning are used to prevent overfitting and improve the generalization performance of a model. Overfitting occurs when a model fits the training data too closely and captures noise or irrelevant patterns, resulting in poor performance on new, unseen data. Here are some commonly used regularization techniques in deep learning, which can be combined and tuned to improve the performance of a model on a specific task or dataset:

- $\mathcal{L}_1$ **and** $\mathcal{L}_2$ regularization are two popular regularization techniques that add a penalty term to the loss function during training. L1 regularization adds the sum of the absolute values of the weights to the loss function, while $\mathcal{L}_2$ regularization adds the sum of the squares of the weights. This encourages the model to learn simpler and more generalizable representations by shrinking the weights towards zero.
- **Dropout** is a regularization technique that randomly drops out some units (neurons) in a layer during training. This forces the remaining units to learn more robust and diverse representations that generalize better to new data. Dropout has been shown to be effective in reducing overfitting, particularly in deep neural networks with many layers.
- **Data augmentation** is a technique that artificially increases the size of the training set by generating new examples from existing ones. This can be done by applying transformations such as rotations, translations, flips, or adding noise to the input

data. Data augmentation can help reduce overfitting by increasing the diversity of the training data and improving the generalization performance of the model.

- **Early stopping** is a technique that monitors the performance of the model on a validation set during training and stops the training process when the performance starts to degrade. This prevents the model from overfitting to the training data and allows it to generalize better to new data.

- **Batch normalization** is a technique that normalizes the activations of a layer by subtracting the batch mean and dividing by the batch standard deviation. This helps stabilize the distribution of the activations and reduces the internal covariate shift, which can improve the training process and reduce overfitting.

- **Weight decay** is a technique that adds a penalty term to the loss function during training, similar to $\mathcal{L}_2$ regularization. The penalty term is proportional to the square of the weights, and it encourages the model to learn smaller and simpler weights, which can reduce overfitting.

Moreover, another interesting technique to help the model improve during training is hard-mining. Hard-mining is a technique in DL used to improve the training of a model by focusing on the samples that are most difficult to classify correctly. In terms of vehicle MP, hard-mining is used to improve the accuracy of predictions by focusing on challenging or critical scenarios. It involves selecting and prioritizing difficult or informative examples during the training process to emphasize learning in those areas. It typically involves identifying and emphasizing challenging situations where accurate prediction is crucial. These situations could include complex traffic interactions, sudden maneuvers, or high-risk scenarios. By focusing on these challenging instances, the model can learn to handle them more effectively and improve its overall prediction capabilities.

Assuming a dataset with a wide range of situations is provided (*e.g.* Argoverse 1 and 2 datasets), the process of hard-mining involves several steps:

1. **Training**: The model is trained on the annotated dataset using machine learning techniques. During the training process, the model learns to predict future vehicle motions based on the available input data.

2. **Evaluation and Selection**: After training, we identify in the training dataset the instances where the model performance is suboptimal or where it fails to accurately predict certain behaviors (for example, challenging intersections, sudden accelerations or emergency breaks). These scenarios might include instances where the model fails to predict dangerous maneuvers accurately or struggles with complex interactions.

3. **Sample Selection**: The challenging examples identified in the previous step are selected as hard-mining samples. These samples are then given more weight or importance during subsequent training iterations.

4. **Iterative Training**: The model is retrained using the original dataset, giving more emphasis to the hard-mining samples in the batch (*e.g.* at least 20 % of the samples of the batch must be a random subset of total hard-mining samples). By increasing the exposure to challenging scenarios, the model learns to improve its predictions specifically for those cases.

5. **Iterative Evaluation**: The model performance is evaluated on the validation set, and the hard-mining process is repeated if necessary. This iterative approach allows the model to gradually refine its predictions and adapt to challenging situations more effectively.

As observed, by incorporating hard-mining into the training process, vehicle MP models can focus on challenging scenarios and improve their generalization and performance in unknown scenarios and critical situations respectively.

3.4. Summary

In this Chapter, the mathematical background of various physics-based and DL-based techniques used for MP models is thoroughly examined. The Chapter aims to provide a comprehensive understanding of these methods and their applications in the field of motion prediction.

The Chapter begins by introducing the physics-based techniques, starting with the KF. The Kalman Filter is a recursive algorithm used to estimate the state of a dynamic system by incorporating noisy measurements. Its mathematical foundation, including the state-space model and the prediction and update steps, is discussed in detail. Next, the HA is presented, which is a combinatorial optimization algorithm used for data association in multiple object tracking. The Chapter delves into the mathematical formulation of the Hungarian Algorithm and how it can be applied to motion prediction tasks.

Moving on to the physics-based models, the Chapter explores the CTRV and CTRA models. These models are widely used for trajectory prediction and capture the motion dynamics of objects by considering their position, velocity, and acceleration. The mathematical equations for these models are examined, highlighting how they can be utilized to predict future motion paths.

The Chapter then transitions to DL-based techniques, which have gained significant attention in recent years due to their ability to capture complex patterns and dependencies in data. Several models are discussed in detail, starting with the 1D-CNN. The

mathematical architecture of the 1D-CNN is explained, emphasizing its ability to extract spatial and temporal features from sequential data for motion prediction.

Next, the LSTM model is introduced, which is a type of RNN specifically designed to handle sequence data. The chapter provides an overview of the LSTM architecture, including its memory cell and gate mechanisms, which enable it to capture long-term dependencies and predict future motion accurately.

The chapter then explores GANs and their application in motion prediction. GANs consist of a generator and discriminator network that compete against each other, resulting in the generation of realistic and coherent motion trajectories. The mathematical formulation of GANs and their training process are examined in detail.

Furthermore, the Attention mechanism is examined, which is a component commonly integrated into deep learning models to focus on relevant parts of the input data. The chapter explores the mathematical formulation of the Attention mechanism and its application in motion prediction models, highlighting its ability to assign different weights to different input features based on their relevance.

Then, the GCN is discussed, which is a deep learning model capable of operating on graph-structured data. The chapter explains how GCNs can be used to represent and predict motion patterns in scenarios where objects interact with each other.

Finally, an overview of the training process, including the optimization and back-propagation strategy, the losses covered in this thesis and regularization techniques, are explored.

Chapter 4

SmartMOT: Exploiting the fusion of HD maps and Multi-Object Tracking for Real-Time scene understanding

¡Avanzad, sin temor a la oscuridad!
¡Luchad! ¡Luchad! ¡Luchad jinetes de Théoden!
¡Caerán las lanzas, se quebrarán los escudos,
aún restará la espada!
¡Rojo será el día hasta el meced del sol!
¡Cabalgad! ¡Cabalgad!
¡Cabalgad a la desolación y al fin del mundo!
¡Muerte! ¡Muerte! ¡Muerte! ¡Adelante Eorlingas!

Discurso de Theoden, Rey de Rohan
Batalla de los Campos de Pelennor
El Señor de los Anillos: El Retorno del Rey

4.1. Introduction

In order to achieve a reliable navigation, Autonomous Driving Stacks (ADSs) must perform safe driving behaviours following conventional traffic rules. One of the key concepts when developing safe ADSs is the perception of the environment. Furthermore, the reliability of the DM and local planning modules lies on the performance of the environment detector and its ability to predict future situations. In that sense, a real-time MOT system, which goal is to associate detections (usually in the 3D or BEV space) in a sequence, is essential for AD applications, representing in most cases the preliminary stage before predicting the subsequent future trajectories of these obstacles in the scene, giving the car a valuable reaction time to avoid critical situations or to anticipate its behaviour for the corresponding traffic scenario. The improvements in object detection in the last years have allowed the research community, specially those groups related to AD, to focus on MOT techniques as a preliminary stage before implementing MP, yielding

higher accuracy at the cost of computational complexity, making its use prohibitive in real-time systems.

MOT systems aim to estimate the orientation, location and scale of all the objects in the environment over time. While object detection only captures the information of the environment in a single frame, a tracking system must take temporal information into account, filtering outliers (*a.k.a.* false positives) in consecutive detections and being robust to partial or full occlusions. When travelling throughout a route programmed by the path-planner, the vehicle may detect an undetermined number of unforeseen objects over which the MOT module should consider only the most relevant from a safety point of view (such as pedestrians, cyclists or cars) to predict and monitor their trajectories. Then, the vehicle can use the evolution of the scene over time to infer driving behaviour and motion patters for improved MP.

Most MOT approaches [82], [83] model the state of each obstacle with its 3D position, scale, orientation and their corresponding linear and angular velocity. These approaches introduce an unnecessary complexity and computational cost to the system, since most traffic scenes can be described in terms of 2D position, angular and linear velocity, apart from the orientation and scale of the resulting bounding box, that is, a BEV perspective, as depicted in Figure 4.1.

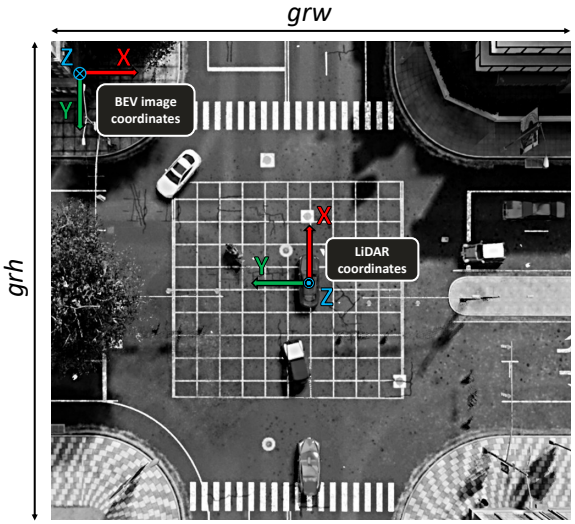

Figure 4.1: LiDAR to BEV coordinates transformation illustrated in the CARLA simulator. *grw* and *grh* stands for the height and width of our real-world grid respectively.

This Chapter summarizes the SmartMOT pipeline and the experimental results obtained with our proposal. The work in this Chapter was partially published in the following conference paper [84]: "SmartMOT: exploiting the fusion of HD maps and multi-object tracking for real-time scene understanding in intelligent vehicles applications", 2021 IEEE Intelligent Vehicles Symposium (IV), p. 710-715. We make the following contributions:

1. We propose SmartMOT, an open-source [1] simple-yet-accurate pipeline to perform real-time MOT and physics-based uni-modal MP.
2. A Monitored Lanes-based Attention Module is proposed to extract monitored lanes around the ego-vehicle (including standard lanes and intersections) and filter non-relevant obstacles. Then, the ego-vehicle will track only those agents that are in the monitored area.
3. We study the MOT in the KITTI MOT dataset and in data captured by our real-world vehicle, as well as the influence of the map monitor to reduce the inference time of the pipeline in the CARLA simulator, with the ultimate goal of achieving real-time uni-modal prediction based on kinematics.

4.2. SmartMOT pipeline

In order to solve the problem of monitoring the relevant objects around the ego-vehicle in an efficient way, we propose SmartMOT [84], a simple-yet-accurate tracking-by-detection pipeline which consists of a combination of traditional techniques such as the KF [24] and HA [68] for state estimation and data association respectively. Moreover, we incorporate HD map information, in addition to the ego-vehicle status, so as to enhance the efficiency and reliability of the tracking system and subsequent predictions, as observed in Figure 4.2.

The SmartMOT pipeline (Figure 4.2) is made up by: (1) 3D object detection module that returns the bounding boxes, (2) Monitored Area to filter non-relevant objects, *e.g.* the Vulnerable Road Users (VRUs) that are inside the sidewalk far away the road or the vehicles that are located in a lane in which lane change is not allowed, (3) Bird's Eye View (BEV) Kalman Filter (KF) that predicts the object state from the current frame and updates the object state based on the detected bounding boxes at current frame, (4) Hungarian Algorithm (HA), which associates the current trackers with new detections, (5) Birth and Death memory that deals with the disappeared trajectories (unmatched trajectories exceeding age_{max} frames) and the newly appeared trajectories (matched trajectories exceeding f_{min} frames) and (6) CTRV model which performs short-term physics-based MP of the updated trackers information using both the linear and angular velocity information. As observed, except for the pre-trained object detector module, our MOT system does not need any training and can be directly used for inference.

4.2.1. 3D Object Detection

The first step our MOT algorithm must carry out is to detect the obstacles in the environment around the ego-vehicle. Since this thesis does not focus on the object detection

[1] https://github.com/Cram3r95/SmartMOT

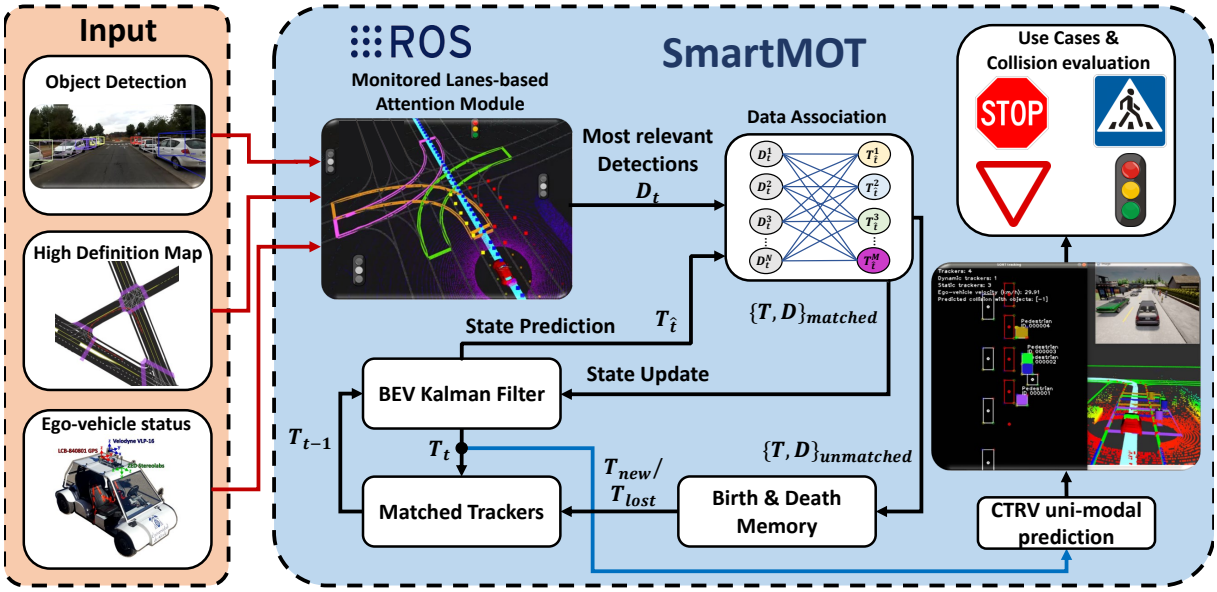

Figure 4.2: SmartMOT pipeline for Multiple-Object Tracking and Short-Term Motion Prediction. It can be observed that we use as inputs the obstacles 360° detected in the environment, the HD map information and ego-vehicle status. Only those agents that are relevant are tracked, predicted and evaluated in the corresponding use cases.

stage of the perception layer, experiments to integrate the object detection and monitored area are conducted in the CARLA assuming ground-truth detection including Gaussian noise in the x,y,z-axis to simulate real-world detections. Then, at a given frame t, the detections provided by the object detection module are given in the following form:

$$D_t = [D_t^1, D_t^2, ..., D_t^N] \tag{4.1}$$

Where N is the number of detected 3D bounding boxes at a given frame and threshold. At this point, instead of using all the 3D information of the object [82], [83], we take its projection on the floor plane (BEV information), to reduce the complexity and computational cost of the tracking stage, specially in those urban scenarios full of vehicles, based on the assumption that the height (z) dimension is not as important as other coordinates (x-axis, y-axis) in a context of self-driving navigation. Detected 3D bounding boxes are referred to the LiDAR coordinate system. A grid is applied to establish a relation between real-world and image dimensions to discretize the possible positions of the detected bounding boxes and decrease the complexity and computational cost of the tracking module.

Conducting MOT in the discrete space BEV using pixels instead of 3D real-world units using meters offers several advantages in certain applications and scenarios. Some of these advantages include:

- **Computational Efficiency**: Representing the 3D scene in the BEV space using pixels allows for faster and more efficient processing, with reduced memory requirements. Working with pixels reduces the complexity of computations compared to

using real-world units, as it involves simple 2D operations rather than more complex 3D calculations which often involve larger floating-point values, particularly in terms of the KF update/predict transitions or 3D-Intersection Over Union (IOU) as metric in the affinity matrix of the Hungarian Algorithm (HA).

- **Simplified Data Representation**: In the BEV space, the environment is represented as a 2D image, which can be easily handled by standard computer vision techniques. This simplification makes it easier to implement and integrate MOT algorithms with existing image processing pipelines.
- **Sensor Independence**: The BEV representation is sensor agnostic, meaning it can be easily adapted to work with various sensor types, such as LiDAR (present case) but also camera or RADAR, without the need for sensor-specific calibration or transformations.
- **Occlusion Handling**: In the BEV, occlusions between objects can be more straightforward to handle. Occluded objects may still be partially visible in the image, and tracking algorithms can take advantage of this partial information to maintain better tracking continuity.
- **Top-Down Contextual Information**: By observing the scene from a top-down perspective, the algorithm can gain a holistic view of the environment and utilize higher-level contextual information, such as road layout, lanes, and traffic rules, which can aid in improving tracking accuracy.
- **Object Shape Normalization**: When objects are projected onto the BEV, they are often represented by simple shapes (*e.g.* rectangles) rather than complex 3D shapes. This simplification can facilitate object association and matching across frames (as proposed in the present Chapter).

Nevertheless, despite these advantages, it is essential to note that using pixels in the BEV space may introduce limitations. For instance, the resolution and accuracy of the tracking might be constrained by the pixel grid size. In that sense, our grid is featured by a rectangle, whose center is located at the LiDAR position on the vehicle, where grw and grh represent the width and height of the grid in LiDAR coordinates m (meters) respectively, as depicted in Figure 4.1. Then, each detection in Equation 4.2 is represented as the tuple:

$$D_t^i = [x_m, y_m, w_m, l_m, \theta, type, score] \tag{4.2}$$

Where x_m, y_m correspond to the object centroid in LiDAR coordinates (m), w_m and l_m correspond to the width and length of the object respectively (m), θ its orientation angle around the LiDAR z-axis, object type and detection confidence. Figure 4.1 illustrates the

transformation from the source coordinate system (LiDAR), measured in m and placed at the ego-vehicle, to the target coordinate system (BEV), measured in px (pixels) and placed on the top-left corner of the grid, which is the most common way to work with images in computer vision. In other words, we deal with the MOT problem from the BEV image perspective, in order to adapt MOT algorithms originally designed for computer vision purposes.

Equations 4.3 and 4.4 show the transformation matrix between both coordinate systems, including both the rotation and the translation ($\frac{grw}{2}$ and $\frac{grh}{2}$), where a $LiDAR_{point} = [x_m, y_m, z_m, 1]^T$ is given as the column vector in homogeneous coordinates.

$$T = \begin{bmatrix} 0 & -1 & 0 & \frac{grw}{2} \\ -1 & 0 & 0 & \frac{grh}{2} \\ 0 & 0 & -1 & 0 \\ 0 & 0 & 0 & 1 \end{bmatrix} \tag{4.3}$$

$$BEVV_{point} = T \cdot LiDAR_{point} \tag{4.4}$$

At this point, each detection is represented by the tuple shown in Equation 4.2, but now x_m, y_m represent the obstacle centroid in BEV image perspective. Furthermore, the resolution of the BEV image can be modified, in such a way the image width in pixels is given to the algorithm and the image height is calculated according to the aspect ratio of the real world with respect to the width of the image in pixels. Finally, to convert a point from real-word units (m) to image units (pixels, px), we apply the corresponding scale factor to each coordinate:

$$\begin{bmatrix} x_{px} \\ y_{pc} \end{bmatrix} = \begin{bmatrix} \frac{gpw}{grw} & 0 \\ 0 & \frac{gph}{grh} \end{bmatrix} \begin{bmatrix} x_m \\ y_m \end{bmatrix} \tag{4.5}$$

However, it is very common to have different scales for x and y-axis since it is more interesting to have a further view in the x LiDAR axis rather than a large side sweep in terms of y LiDAR axis. Considering this hypothesis, the right way to obtain the width and length of the BEV LiDAR bounding box in *pixels* is to obtain the corners of the rotated bounding box in pixels and then compute the $\mathcal{L}_2$ distance among the corresponding corners to obtain the width and length in *pixels*. Nevertheless, the object detector provides the rotation angle of the obstacle (featured as θ) according to its own coordinate system and not around the ego-vehicle coordinate system. Regarding this constraint, to calculate the dimensions of the bounding box in pixels, three steps must be followed:

- First, we assume a horizontal bounding box ($\theta = 0$) at the BEV image coordinate system origin, where $c_{1,m}$ corresponds to the top-left corner ($c_{2,m}$, $c_{3,m}$ and $c_{4,m}$ are placed clockwise).

$$
\begin{aligned}
c_{1,m} &= (x_m - \frac{l_m}{2}, y_m - \frac{w_m}{2}) \\
c_{2,m} &= (x_m - \frac{l_m}{2}, y_m + \frac{w_m}{2}) \\
c_{3,m} &= (x_m + \frac{l_m}{2}, y_m - \frac{w_m}{2}) \\
c_{4,m} &= (x_m + \frac{l_m}{2}, y_m + \frac{w_m}{2})
\end{aligned}
\tag{4.6}
$$

- Second, each corner point is converted from real-world units (m) to image units (px) using Equation 4.5.
- Then, the $\mathcal{L}_2$ distance is applied between $c_{1,m}$ and $c_{2,m}$ to obtain the width in pixels, in the same way that the $\mathcal{L}_2$ distance is applied between $c_{1,m}$ and $c_{4,m}$ to obtain the length in pixels.

$$
w_{px} = \sqrt{(c1_{px,x} - c2_{px,x})^2 + (c1_{px,y} - c2_{px,y})^2} \tag{4.7}
$$

$$
l_{px} = \sqrt{(c4_{px,x} - c2_{px,x})^2 + (c4_{px,y} - c2_{px,y})^2} \tag{4.8}
$$

- Finally, the detection tuple that will feed the tracking algorithm remains as follows, where all variables are expressed in px:

$$
D_{t,i} = [x_{px}, y_{px}, w_{px}, l_{px}, \theta, type, score] \tag{4.9}
$$

4.2.2. Monitored Lanes-based Attention Module

ADSs need to locate itself in the environment to know what is happening around in order to make decisions and execute a correct navigation like a human driver would. When we talk about localization, the first thing we need is a map where to be located and, particularly for AD, a HD map that contains not only a general geometric description of the scene, but also the topological information of the lanes (lanes type, boundaries constraints, etc.) as well as the semantic information of the road.

A HD map is usually a text file describing the real-world features related to the road map and its location within a 2D/3D space, and can do things that other sensors cannot [85]: First, they have an *infinite range* and, therefore, can *see* even into occluded areas. Second, HD maps will never fail due to environmental conditions. Lastly, HD maps contain highly refined data. This information can be used by different modules of an ADS (including localization, vehicle control, path planning, perception and system management) drastically reducing the computational load and complexity in comparison to other

more complex methods, providing robustness and reliability to the system. Regarding this, in terms of mapping information, we may distinguish three main categories:

- **Topological information** provides the connectivity between geometry features. Particularly in the field of AD, this is usually the network of roads. This kind of information can allow vehicles to traverse the most energy-efficient route, based on traffic speed, road grade or distance, as well as ensure that ADSs obey traffic regulation orders, such as one-way streets or the corresponding regulatory elements (pedestrian crossing, traffic light, stop signal, etc.).
- **Geometric information** provides the geometry or shape of other environmental features that can be static (permanent obstruction, such as buildings, bridges or tunnels), temporary (exist for only a limited amount of time, like traffic cones, parked vehicles or temporary road works) and dynamic features (moving people, objects or vehicles). Most of these features are incorporated by means of perception systems, specially in terms of dynamic features, in order to include that information in the HD map for successful motion planning and prediction.
- **Semantic information** returns the *meaning* of aforementioned features, such as road speed limit, road classification, lane information or even the relational information among the different lanes, *i.e.* how lanes work together, different types of lanes, where vehicles must stop and where vehicles can and cannot turn.

As illustrated, providing rich physical contextual information allows ADSs to make informed decisions in different driving scenarios. In this thesis, we particularly make use of the OpenDrive [86] HD map format, which has been mainly used for two different purposes, as shown in Figure 4.3:

- **Global Path Planning**, which uses a specific path planner where inputs are the HD map information and the ego-vehicle current location to retrieve an optimal (usually optimized based on the traveled distance) global route towards an specific goal.
- **Map monitoring**, responsible for monitoring the most relevant static and dynamic map elements around the ego-vehicle at each time-step, such as standard lanes (current, back), intersection lanes (merge, split and cross) and regulatory elements (e.g. give way, stop, pedestrian crossing, traffic light).

In particular, given a pre-defined global route, in this thesis we focus our interest on designing a map monitor module, responsible for retrieving the most relevant lanes around the ego-vehicle to enhance real-time perception and scene understanding requirements.

4.2.2.1. Map Monitor

In a similar way to humans that pay more attention to close obstacles, people walking towards them or upcoming turns rather than considering the presence of building or people

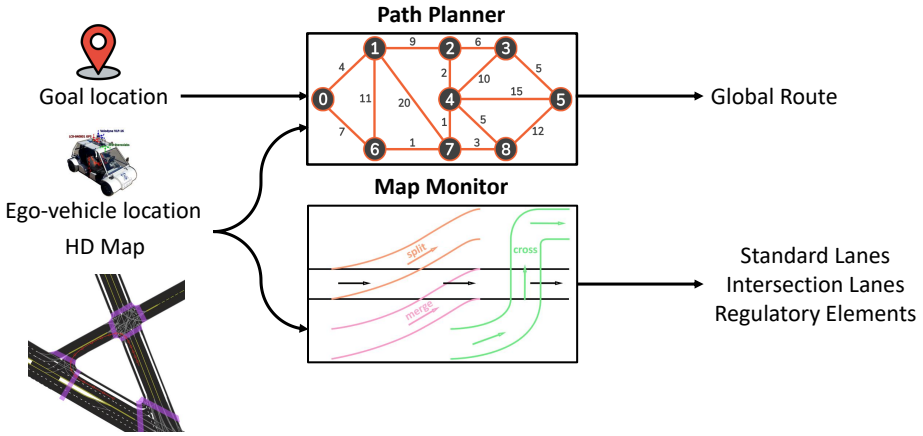

Figure 4.3: Main uses of HD map: Path Planning and Map Monitoring

far away, the perception layer of a self-driving car must be modelled to focus more on the salient regions of the scene [87] and the more relevant agents to predict the future behaviour of each traffic participant. In that sense, HD maps have been widely adopted to provide offline (also known as context) information to complement the online information provided by the sensor suite of the vehicle and its corresponding algorithms.

Recent learning-based approaches [88] [43] [35] [32], which present the benefit of having probabilistic interpretations of different behaviour hypotheses, require to build a representation to encode the trajectory and map information. [88] assumes that detections around the vehicle are provided and focuses its work on behaviour prediction by encoding entity interactions with ConvNets. Intentnet [32] proposes to jointly detect traffic participants (mostly focused on vehicles) and predict their trajectories using raw LiDAR pointcloud and rendered HD map information. PRECOG [16] aims to capture the future stochasiticity by flow-based generative models. Furthermore, MultiPath [43] uses ConvNets as encoder and adopts pre-defined trajectory anchors to regress multiple possible future trajectories.

As observed, recent DL-based techniques use relatively complicated filters to predict, in an accurate way, the spatial features of the obstacles in the scene, increasing the complexity and computational cost of the system. On the other hand, traditional methods for behaviour prediction are rule-based, where multiple behaviour hypothesis are generated based on constraints from the road maps. As stated above, road maps present some clear advantages over other perception sensors. Then, HD maps can be an additional sensor that cannot fail unless the road infrastructure changes, providing meaningful, accurate and useful information in real-time operation.

Regarding this, we design a Map Monitor in charge of monitoring the surrounding area of the vehicle. The inputs of the Map Monitor are the information provided by

the Map Parser module (in charge of getting the information of the map from the HD map file and transform it into custom classes that can be used by other modules like Planning or Perception) and the waypoint route previously obtained by the path planner. The main goal of the Map Monitor is to only monitor the most relevant map elements around the ego-vehicle given the route provided by the global planner (or a new route if the local planer decides to recalculate the route). This Map Monitor was published (where I am a co-author) in the following conference paper [89]: "HD maps: Exploiting OpenDRIVE potential for Path Planning and Map Monitoring", 2022 IEEE Intelligent Vehicles Symposium (IV), p. 1211-1217.

First, the path planner returns the route that is divided in segments separated by a given distance and calculates in which segment of the route the ego-vehicle is found, activating a flag in such a way the Map Monitor can start operating. Otherwise, in case the ego-vehicle cannot be located inside the route, the Map Monitor is deactivated. Secondly, a monitor callback is called periodically every time the ego-vehicle status (position, velocity, orientation, etc.) is received, as observed in Figure 4.2. This callback evaluates, if the Map Monitor module is active, calculates the monitored elements frontwards and backwards for a given distance which is proportional to the ego-vehicle velocity given a braking distance linear model that establishes a linear regression between two arrays of velocity and braking distance data. Nevertheless, we make use of a threshold distance to still monitor the environment if the ego-vehicle is stopped.

The monitored elements are:

- **Standard Lanes**: Current, back and the corresponding left and right lanes. Current lane is monitored from current position to a dynamic distance depending on the velocity of the ego-vehicle. Back lane is monitored from current position to back a proportional distance of the dynamic current lane obtained distance. Left and right lanes are monitored the same distance that current and back only if the lane marking from the HD map data allows the lane change.

- **Intersection Lanes**: Other lanes that intersect the current monitored lane are checked. Intersection lanes can have different roles: split (1 lane splits into 2 or more), merge (2 or more lanes merge into 1) and cross (a lane crosses a part of the current lane). To calculate the intersection lanes, each lane of every junction (junctions are areas where more than 2 roads meet) in the current lane is evaluated. The polygon of each lane is calculated and evaluated if is inside the polygon of the current lane. It is important to consider that roundabouts are considered as a set of multiple junctions.

- **Regulatory Elements**: The monitored elements are stops, giveaways, traffic lights, speed limits and crosswalks. The regulatory elements are only monitored for the next intersection affecting the route.

An example of our map monitor module in the CARLA simulator [62] using the RVIZ [90] may be observed in Figure 4.4.

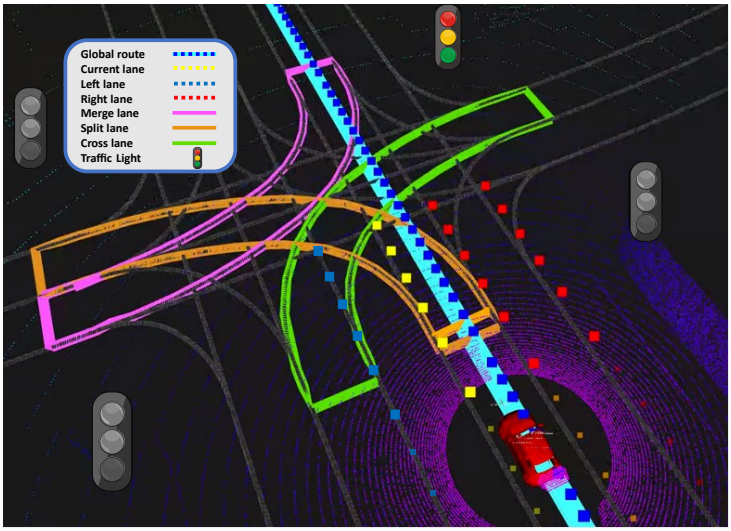

Figure 4.4: Monitored area in the CARLA simulator using the RVIZ tool. It can be appreciated the visualization of the global route, standard lanes, intersection lanes and different traffic lights (regulatory elements). Note that the relevant traffic light is coloured while remaining ones are masked.

As illustrated in Figure 4.2, once the object detections have been provided and the monitored area has been computed, the Monitored Lanes-based Attention Module helps us to increase the efficiency and robustness of the system to avoid tracking and predicting all obstacles in the environment, which would escalate the computational cost especially in arbitrarily complex urban scenario.

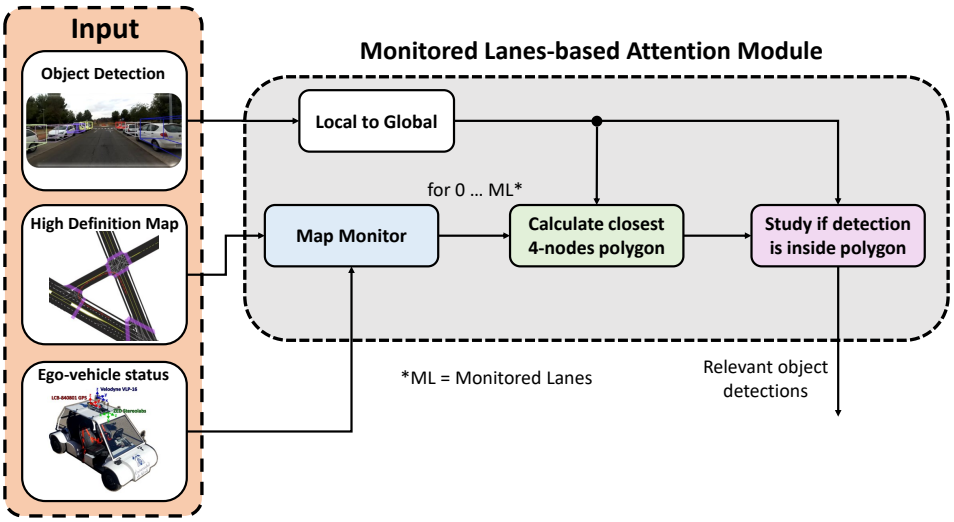

Figure 4.5: Overview of our proposed Monitored Lanes-based Attention module to filter non-relevant object detections. Note that in order to study if a detection is inside a polygon, we make use of the Jordan's Curve Theorem. Moreover, if the object detection is a VRU, the closest polygon is widened towards the sidewalk. Both map, ego-vehicle status and object detection must be in global (map) coordinates.

This attention module is not focused on DL because the main purpose is to filter non-relevant obstacles in an efficient and interpretable way, such as agents driving way

in opposite direction lanes, parked vehicles or pedestrians who are chatting on the sidewalk. The filtering process carried out by our Monitored Lanes-based Attention Module is illustrated in Figure 4.5 and summarized as follows:

Algorithm 4.1: Jordan's Curve theorem to determine if a point is inside a polygon

```
   Data: point, polygon
   Result: isInside
 1 crossings ← 0;
 2 for i from 0 to (polygon.length - 1) do
 3 |   vertex1 ← polygon[i];
 4 |   vertex2 ← polygon[(i + 1) mod polygon.length];
 5 |   if (point.y > min(vertex1.y, vertex2.y)) and (point.y ≤ max(vertex1.y, vertex2.y)) then
 6 |   |   if point.x ≤ max(vertex1.x, vertex2.x) then
 7 |   |   |   if vertex1.y ≠ vertex2.y then
 8 |   |   |   |   xIntersection ← (point.y - vertex1.y) * (vertex2.x - vertex1.x) / (vertex2.y -
   |   |   |   |    vertex1.y) + vertex1.x;
 9 |   |   |   |   if vertex1.x == vertex2.x or point.x ≤ xIntersection then
10 |   |   |   |   |   crossings ← crossings + 1;
11 |   |   |   |   end
12 |   |   |   end
13 |   |   end
14 |   end
15 end
16 isInside ← (crossings % 2 == 1);
17 return isInside;
```

1. We determine the lanes of interest around the vehicle provided by the map monitor, until a given threshold, which will depend on the ego-vehicle velocity. The minimum information will be the current front and back lane information (mandatory for the ACC and Unexpected VRU use cases), as well as left and right lane information, if lane change is available considering the presence of a discontinuous line. Moreover, if an intersection is near the ego-vehicle, other lanes of interest such as merging, splits and intersections are considered (see Figure 4.4), which are specially useful in urban scenarios.

2. In order to consider an agent as relevant, we study the presence of this agent in our monitored lanes. The main idea is to find the closest polygon segment (two nodes on the left, same on the right) to the agent. To do that, we iteratively compute the $\mathcal{L}_2$ distance between the agent position (transformed into global (*a.k.a.* map) coordinates) and the left way nodes (starting from the beginning) of a certain lane. Note that it is irrelevant to take either the left or right way in terms of observing if the detection is inside a polygon made up by four nodes of the lane, such as there exists the same number of nodes for both ways. For example, in the case of an agent located in front of the vehicle, the distance will decrease since the subsequent left way nodes are closer to the agent.

3. Once the new calculated distance is greater than the previous value, that means the closest segment with nodes N_0 and N_1 are found. Taking the same lane indexes

in the right way, we obtain a four-side polygon in which the detection is evaluated using the Jordan's curve theorem [91], as depicted in Algorithm 4.1. In this theorem, the input parameters are a point and a polygon, where, by means of a simple-yet-accurate ray casting algorithm, a loop is used to iterate over the polygon vertices and performs the necessary checks to determine the number of crossings. The Jordan's Curve Theorem states that a point is inside a polygon if the number of crossings from an arbitrary direction is odd. Consequently, in our particular case, if the object detection lies outside the closest polygon segment, the traffic participant is considered as non-relevant.

4. Nevertheless, despite this proposal is coherent for non-holonomic obstacles with more constrained behaviours like cars, vans or trucks, the behaviour of Vulnerable Road Users (VRUs), is usually difficult to predict. Hence, we widen the closest segment area a certain threshold L to the sidewalk so as to track the closest VRUs to the road. Note that according to the ITS society, VRUs are road users not in a car, bus or truck, generally considered to include pedestrians, motorcycle riders, cyclists, children 7-years and under, the elderly and users of mobility devices.

4.2.3. BEV Kalman Filter: State Prediction

Once we have obtained the most relevant BEV detections of the environment, a BEV KF is used to track the objects. To predict the state of object trajectories from the previous frames to the current frame, we approximate objects inter-frame displacement using a constant velocity model, which is independent of other objects in the scene and of the LiDAR motion. Regarding this, the estimation of the measured variables in the following frame are:

$$\begin{aligned} x_{px}(\hat{t}) &= x_{px}(t) + v_x \\ y_{px}(\hat{t}) &= y_{px}(t) + v_y \\ s(\hat{t}) &= s(t) + v_s \\ \theta(\hat{t}) &= \theta(t) + v_\theta \end{aligned} \tag{4.10}$$

Since we formulate the tracking problem over the BEV plane, we remove all variables related to the z-coordinate of the object. On the other hand, since our tracking-by-detection algorithm is inspired by the well-established Simple Online and Realtime Tracking (SORT) [92] tracking algorithm, originally proposed to track pedestrians using videos as input, some additional variables are included in the object state, such as the aspect ratio and the scale of the bounding box, to help in the tracking stage. The aspect ratio can be defined as the relation between the width and the length of the obstacle. Likewise, the scale represents the area of the target bounding box. Then, the state of each

object tracker (usually referred as trajectory tracker in the literature) can be expressed as:

$$T_t^j = [x_{px}, y_{px}, s, r, \theta, x_{px}^{'}, y_{px}^{'}, s^{'}, \theta^{'}] \tag{4.11}$$

Note that the angular velocity $\theta^{'}$ is used in the state space to improve the prediction of the obstacle in later frames. Furthermore, as shown in [92], the aspect ratio of the bounding box is considered to be constant. As observed in Figure 4.2, at every frame t, a tuple $T_t = [T_t^1, T_t^2, ..., T_t^M]$ is returned by the data association module, where each element correspond to an association between a detection and a tracker. Note that M represents the current number of trackers. Then, based on these associations between trackers of the previous frame and current detections, and assuming a 1st-order KF (constant velocity model), the tuple $T_{\hat{t}}$ is calculated, where each element corresponds to the predicted trajectory ($T_{\hat{t}}^j$) in the current frame t expressed as:

$$T_{\hat{t}}^j = [x_{px}(\hat{t}), y_{px}(\hat{t}), s(\hat{t}), r, \theta(\hat{t}), x_{px}^{'}, y_{px}^{'}, s^{'}, \theta^{'}] \tag{4.12}$$

This tuple of predicted trajectories based on the previous frame associations, in addition to the current frame detections, represents the inputs to the data association algorithm at frame t.

4.2.4. Data association

In order to associate the detections D_t and the trackers information after the KF state prediction $T_{\hat{t}}$, the Hungarian Algorithm (HA) is applied. The resulting affinity matrix presents N rows (number of filtered detections after the monitored lanes-based attention module at frame t) and M columns, which correspond to the number of predicted trajectories (*i.e.* the trackers) based on the information of frame $t-1$. Each element of the matrix corresponds to the IOU in the BEV plane between every pair of predicted trajectory and detection.

Then, following the principles stated in the HA stated in Chapter 3.2.2, we solve the bipartite graph matching problem, rejecting the matching if the BEV-IOU metric is lower than a given hyperparameter IoU_{th}, giving rise to a set of matched detections ($D_{matched}$) and predicted trackers ($T_{matched}$) with the same length H (the number of matches), as well as a set of unmatched detections ($D_{unmatched}$), where $P = N - H$ is the number of unmatched detections, and a set of unmatched trajectories ($T_{unmatched}$), where $Q = M - H$ is the number of unmatched trackers.

4.2.5. BEV Kalman Filter - Object State Update

As observed in Figure 4.2, once we have the corresponding sets of matched detections and trajectories, based on the KF prediction-update cycle, we update the state space of each trajectory based on its corresponding matched detection. To do that, we use the weighted average between the matched detection values and the state space of the trajectory tracker, according to [24].

On the other hand, in the same way that [82], we appreciate that this state update does not work properly for obstacle orientation. The reason is simple: Unless the object detector is based on sensor fusion and vision information is included, the object detector cannot distinguish if the obstacle is rotated 0 or π, $\frac{\pi}{2}$ and $\frac{3\pi}{2}$, and so on, around its z-axis. That is, the orientation may differ by π in two consecutive frames. Then, if no orientation correction is applied, the Kalman Filter associated to the tracker can get easily confused, since it tries to adapts itself to the new orientation value rotating the object by π in following frames, giving rise to a low BEV-IoU between new detections and predicted trajectories.

In that sense, regarding the assumption that obstacles must move smoothly and its orientation cannot be modified by π in one frame (0.1 s assuming a frequency of 10 Hz), when this happens the orientation of the corresponding matched detection or matched tracker can be considered wrong. To solve this problem, the detection module only considers angle from 0 to π (that is, if an angle exceeds π, it is substracted to the provided angle). Moreover, if the difference of orientation between a given matched detection and its corresponding matched trajectory is greater than $\frac{\pi}{2}$, as stated before, either the orientation of the detection or the orientation of the tracker is wrong. Finally, we add π to the orientation of the tracker with the aim to be consistent with the matched detection.

4.2.6. Deletion and Creation of Track Identities

When obstacles leave and enter the aforementioned monitored lanes, unique identities must be destroyed or created accordingly. In most tracking algorithms it is known as the Birth and Death Memory, which is based on the set of unmatched trackers and detections provided by the data association algorithm, where the unmatched trackers represent potential objects leaving the monitored area, in the same way that unmatched detections represent potential objects entering in the area of interest.

In order to avoid tracking of false positives or non-relevant obstacles, a new tracker is not created until the unmatched detection has been continuously detected in the next f_{min} frames. Then, the tracker is initialized with the features of the detected bounding box, and the associated velocities set to zero. Note that, as stated in [92], since the velocity associated to the measured variables is unobserved at this moment (*i.e.* tracker initialization), the covariance initializes the value of the velocities (in the present work,

velocity of the x_{px}, y_{px} centroid, scale s and rotation angle θ) with large values, reflecting their uncertainty.

To avoid removing true positives trajectories from the scene, they are not terminated unless they are not detected during consecutive a_{max} frames. This assumption prevents an unbounded growth in the number of localization errors and trackers due to predictions over long duration where the object detector does not provide any correction. Note that since this work does not consider object re-identification for simplicity, an object should leaves the scene and then reappears, according to the SORT algorithm, if it is initialized with a new tracker under a new identity. As shown in Figure 4.2, the inputs to the Matched Trackers module are the updated matched trajectories from the BEV KF and a set of created and deleted trackers, which jointly represent the input trajectories for the prediction step in the following frame.

4.2.7. CTRV uni-modal prediction

The last stage of our SmartMOT pipeline is a physics-based MP model to predict the future behaviour of the agents in the short-term. In particular, we make use of the previously studied CTRV model. Once the tracker information (position, velocity and orientation) has been retrieved in real-world coordinates (instead of BEV image coordinates), we are able to differentiate between static and dynamic agents. Then, given the ego-vehicle status and dynamic agents short-term prediction, we analyze the risk of collision or carry out the state of the current behaviour (ACC, Pedestrian Crossing, Give way, and so forth and so on) in such a way SmartMOT can send the corresponding signal to the DM layer.

4.3. Experimental results

We validate our proposed tracking algorithm (SmartMOT) using the KITTI MOT benchmark [93] in a quantitative and qualitative way, as well as using some LiDAR recorded data from our campus to observe some qualitative results and a comparison of inference frequency using an edge-computing device and standard Personal Computer (PC) desktop. Finally, we study some interesting scenarios in the CARLA simulator where map information is included in order to appreciate how the inference time of the MOT may be drastically reduced when the system pays attention to the most relevant agents around the ADS according to the current traffic scenario.

4.3.1. Dataset

In order to evaluate our proposed MOT system pipeline, we carry out the evaluation in the KITTI MOT benchmark [93] based on the method proposed by [82]. This is

composed of 29 testing and 21 training/validation video sequences, where each sequence is provided with RGB images (left and right camera of the stereo pair), LiDAR point-cloud and the corresponding calibration file. Since KITTI does not provide any annotation (*i.e.*, the ground-truth) for the testing split, we decided to evaluate our system in the training/validation split. Moreover, although KITTI distinguish among eight different classes for the object type, our work focus on the car subset, since it is the class that contains the most number of instances over the whole benchmark.

4.3.2. Multi-Object Tracking metrics

Mainstream metrics applied to MOT systems are extracted from CLEAR MOT metrics [94], such as Multi-Object Tracking Accuracy (MOTA) and Multi-Object Tracking Precision (MOTP). These metrics provide a comprehensive assessment of tracking performance by considering aspects such as accuracy, precision, and overall performance. Now, the main metrics are described:

4.3.2.1. Multi-Object Tracking Accuracy (MOTA)

The Multi-Object Tracking Accuracy (MOTA) metric is commonly used to evaluate the performance of multi-object tracking algorithms. It measures the overall tracking accuracy by considering the False Positives (FPs), False Negatives (FNs), and IDentity Switches (IDS) in the tracking results. The formula for calculating Multi-Object Tracking Accuracy (MOTA) is given as:

$$MOTA = 1 - \frac{\text{FN} + \text{FP} + \text{IDS}}{\text{GT}} \tag{4.13}$$

where:

- **FN (False Negatives)** represents the number of ground-truth objects that were not correctly detected by the tracking algorithm.
- **FP (False Positives)** represents the number of false detections made by the tracking algorithm.
- **IDS (Identity Switches)** represents the number of times the algorithm incorrectly switches the identity of a tracked object.
- **GT (Ground-Truth)** represents the total number of ground-truth objects in the video sequence.

A higher MOTA value indicates better tracking accuracy, with a perfect tracking result yielding MOTA = 1.

4.3.2.2. Multi-Object Tracking Precision (MOTP)

The Multi-Object Tracking Precision (MOTP) metric is used to assess the localization accuracy of a MOT algorithm. It measures the average precision of the tracked object positions by considering the distance between the predicted locations and their corresponding ground truth locations. The formula for calculating Multi-Object Tracking Precision (MOTP) is given as:

$$MOTP = \frac{\sum_{i=1}^{N} d_i}{N} \tag{4.14}$$

where:

- N represents the total number of matched object pairs between the predicted and ground truth locations.
- d_i represents the $\mathcal{L}_2$ between the predicted location and the ground-truth location for the i-th matched object pair.

The MOTP metric ranges between 0 and 1, with a higher value indicating better localization accuracy. A perfect tracking result with exact object positions would yield MOTP $= 1$.

4.3.2.3. Integral metrics: AMOTA and AMOTP

Previous MOT metrics analyze the MOT system performance at a given threshold, not taking into account the confidence provided by the object detector and possibly misunderstanding the capability of the method. That means they do not take into account the full spectrum of precision and accuracy over different thresholds. Moreover, as discussed by AB3DMOT [82], KITTI 2DMOT evaluates the performance MOT by means of aforementioned traditional CLEAR MOT metrics, where the detected 3D bounding box onto the image plane. As expected, this does not demonstrate the full strength of 3D Detection and Multiple-Object Tracking (DAMOT).

In that sense, AB3DMOT [95] recently presented a 3D extension of the KITTI 2DMOT evaluation, known as KITTI-3DMOT, which introduces two new integral MOT metrics to solve the problem of evaluating the MOTA and MOTP of the system across all detection thresholds, known as Average Multi-Object Tracking Accuracy (AMOTA) and Average Multi-Object Tracking Precision (AMOTP), as shown in Equation 4.15:

$$AMOTA = \frac{1}{L} \sum_{\{\frac{1}{L}, \frac{2}{L}, \ldots, 1\}} (1 - \frac{FP + FN + IDS}{num_{gt}}) \tag{4.15}$$

Where L is the number of different recall values. Note that IDS, FPs and FNs are modified according to the results of each threshold value. Likewise, AMOTP can be

estimated by integrating the MOTP metric across all recall values. We will use these integral metrics, in addition to the aforementioned CLEAR MOT metrics, to demonstrate the effectiveness of our tracking pipeline. Note that, since both AMOTA and AMOTP metrics are the integral of the corresponding metrics over different detection thresholds, as expected, the follow the same principle: the higher, the better. Note that in our proposed method (BEV based), in order to compare our results with other SOTA approaches in the 3D space using the aforementioned KITTI-3DMOT tool, we simply retrieve z-information (centroid, bounding box height) from the object detection stage.

4.3.3. Comparison with the State-of-the-Art

We compare our proposed SmartMOT pipeline (PointPillars as 3D object detector [96], BEV KF as data estimator and HA as data association algorithm excluding the map monitoring and filtering process in this case), against modern open-sourced 3D MOT systems such as mmMOT [97], FANTrack [98] and Monocular3D [99] using the proposed KITTI-3DMOT. Results are observed in Table 4.1, where we achieve results that are up-to-pair with other SOTA tracking methods. Note that these results were obtained with default values of the hyperparameters in the tracking stage ($age_{max} = 1$, $min_{hits} = 1$, $IoU_{thr} = 0.1$).

Table 4.1: Comparative of Multi-Object Tracking pipelines using the KITTI-3DMOT evaluation tool in the validation set (car class). We bold the best results in **black** and the second best in **blue** for each metric.

Method	AMOTA [%] ↑	AMOTP [%] ↑	MOTA [%] ↑	MOTP [%] ↑	IDS ↓
mmMOT [97]	33.08	72.45	74.07	**78.16**	**10**
FANTrack [98]	**40.03**	**75.01**	**74.30**	75.24	35
Monocular 3D [99]	31.37	64.29	62.38	68.26	**1**
Ours (SmartMOT [84] (tracking only))	**39.90**	**79.31**	**94.20**	**82.06**	150

For a deeper information of these hyperparameters, we refer the reader to the next section. Note that in terms of the 3D object detection stage (Section 4.2.1), we set the size of the real-world grid *grw* (width)=50m (25m to the left/right, respectively) and *grh* (height)=140m (70m to the bottom/top, respectively), considering the ego-vehicle is in the center of the grid, as depicted in Figure 4.1. On the other hand, since the MOT is performed in the BEV image space in *pixels*, in order to compute the corresponding equivalences, we set *gph* (grid width in *px*) = 1000, in such a way $gpw \approx 358$ *px*. Note that the size of the grid both in m and *px* is empiric and can be manually adjusted.

4.3.3.1. Ablation study

Once we decide to implement a specific tracking-by-detection configuration, we carry out an ablation study to analyze the influence of maximum age, minimum number of hits

and minimum threshold in the data association cost matrix to achieve the best tracking results. The main hyperparameters are:

- age_{max}: Maximum number of frames for a tracker to be associated again to a certain detection.
- min_{hits}: Minimum number of consecutive frames in which a tentative tracker must be associated to a detection to be considered as an actual tracker.
- IoU_{thr}: Threshold to match a predicted trajectory and a detection in the data association module.

Table 4.2 shows an ablation study by modifying these hyperparameters (age_{max}, min_{hits} and IoU_{thr} respectively), where we follow the principles stated by AB3DMOT [95]. In terms of maximum age, the baseline is 1 (*i.e.* if a tracker disappears more than one frame, it is deleted from the set of trajectories), and it is changed to 2 and 3. Moreover, the number of minimum hits is 1 by default, and studied in the case of 3 and 5 minimum hits to consider a detection as a tracker. Finally, the authors in AB3DMOT [82] [95] change the minimum IOU to consider a possible association among detections and trackers in the affinity matrix from 0.01 to 0.1 and 0.25. Note that these ones represent minimum values, and then the HA will optimize the combinations to have the highest IOU in every case. Even though typical numbers for IOU are 0.25, 0.5 and 0.7 in 2D object detection or tracking, since our evaluation is conducted in the 3D space, the risk of occlusions is noticeable decreased in such a way there will not be many associations associated to a particular tracker and vice-versa.

In our particular case, with an IoU_{thr} of 0.01 we get quite similar results in terms of MOTA and MOTP as in the 0.1 case, decreasing from 150 to 54 the number of identity switches. This is coherent since if the HA is able to observe more possible combinations, once it computes the optimal one, it will have a better chance of being the real identifier, although the inference time increases. On the other hand, increasing min_{hits} allows us to reduce the identity switching noticeably, overcoming one of the main drawbacks associated to the motion metric proposed by SORT. Moreover, modifying the maximum age to consider a tracker has left the scene barely modifies the studied metrics. As illustrated in Table 4.2, our final configuration achieves an impressive number of 2 IDS and quite acceptable CLEAR and integral metrics, which are key as a preliminary stage to predict the short-term for each trajectory in the MP stage.

Finally, our final system configuration is as following: We use PointPillars [96] as object detector, trained over 1,187,840 training steps using the KITTI benchmark database, the BEV KF formulated in the previous section, an $IoU_{th} = 0.1$ as the threshold to associate a detection with a tracker in the data association module, and $min_{hits} = 3$, $age_{max} = 1$ values for the birth and death module respectively.

Table 4.2: Ablation study of the final tracking stage configuration of SmartMOT using the KITTI-3DMOT evaluation tool in the validation set (car class). We bold the best results in **black** and the second best in **blue** for each metric.

age_{max}	min_{hits}	IoU_{thr}	AMOTA [%] ↑	AMOTP [%] ↑	MOTA [%] ↑	MOTP [%] ↑	IDS ↓
1	1	0.1	**39.90**	79.31	94.20	82.06	150
1	1	0.01	39.84	70.96	95.13	81.84	54
1	1	0.25	39.37	**79.35**	89.10	82.42	176
1	**3**	**0.1**	**39.54**	**71.24**	**91.38**	**83.23**	**2**
1	5	0.1	39.26	71.36	88.84	**83.68**	3
2	1	0.1	39.49	79.24	94.91	81.48	154
3	1	0.1	39.50	79.15	**95.16**	81.15	152

4.3.4. Qualitative results

In this subsection we may appreciate some qualitative results using SmartMOT in the KITTI MOT benchmark in data captured by our real-world prototype and in the CARLA simulator. It is important to note that the map monitor and filtering process is only included in simulation.

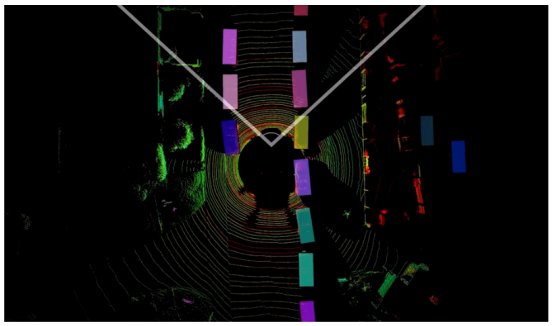

(a) BEV LiDAR perspective, t

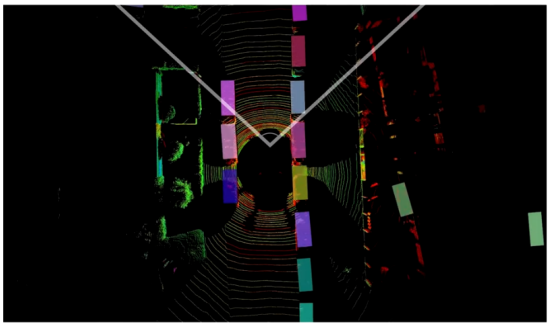

(b) BEV LiDAR perspective, $t + 20$

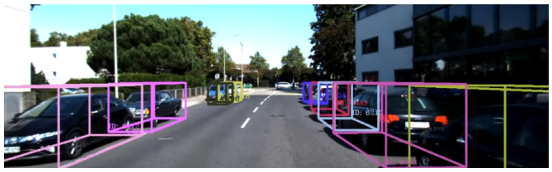

(c) Left RGB camera perspective, t

(d) Left RGB camera perspective, $t + 20$

Figure 4.6: SmartMOT in the KITTI MOT validation dataset without map monitoring. Velodyne HDL-64 is used as raw data. It can be appreciated two perspectives ((a) (b) BEV LiDAR and (c) (d) Left RGB camera) in frame t (left column) and $t + 20$ (right column).

Figure 4.6 illustrates the tracked agents in a standard urban scenario of the KITTI MOT dataset in frames t and $t + 20$ respectively, where the Velodyne HDL-64 is used as raw data for the object detector. It may be observed how the corresponding agents are correctly estimated, compensating their position with the ego-motion. Moreover, as aforementioned, SmartMOT operates in the BEV plane, in such a way we assume the dimensions, in particular the z-coordinate of the agents, are the same for the detection and the tracker.

On the other hand, in terms of our real-world prototype, we focus on implementing a 360°real-time and power-efficient SmartMOT pipeline in an efficient way. Perception systems in AD must process a huge amount of information coming from at least one sensor in order to understand the environment. However, the physical space occupied by the processing units in the vehicle or their power consumption are metrics to be deeply analyzed, even more if these processing units will be integrated in an electric vehicle, where the state of the batteries is crucial.

Regarding this, the SOTA approach is to use powerful but power-efficient AI embedded systems as computation devices for autonomous machines, since they present a remarkable ratio between performance and power consumption in a reduced-size hardware. In terms of the advantage of using neural networks in Graphics Processing Unit (GPU), these embedded systems present a powerful GPU unit as well as fast storages based on Solid State Disks (SSDs) and a large Random Access Memory (RAM) memory size. At the time of writing this paper (2023), the best ratio of performance vs power consumption and size is represented by the NVIDIA Jetson embedded computing boards. NVIDIA Jetson is the world's leading AI computing platform for GPU-accelerated parallel processing in mobile embedded systems. These kits allow to implement SOTA frameworks and libraries to conduct accelerated computing, such as Compute Unified Device Architecture (CUDA), cuDNN or TensorRT (Tensor RealTime).

Table 4.3: Comparative of inference frequency of SmartMOT between the NVIDIA Jetson AGX Xavier and our PC desktop (Intel Core i7-9700, 16GB RAM) with CUDA-based NVIDIA GeForce RTX 1080 Ti 11GB VRAM.

Stage	Frequency AGX ↑ Xavier (Hz)	Frequency PC ↑ desktop (Hz)	Ratio
Detection	7.3	**41.7**	5.7x
Tracking	15	**101.9**	6.7x

In this particular work we make use of the NVIDIA Jetson AGX Xavier, one of the most powerful AI embedded system specially designed for ADSs. Table 4.3 shows a comparative between the embedded system and our PC frequency in the inference stage, where the detection stage (PointPillars) is reduced by almost 6 times and the tracking by almost 7 times. Nervertheless, although the detection and tracking frequencies are on the border to be considered real-time according to the requirements of the perception systems for ADSs (at least 10 Hz), the embedded system consumes 30 W whilst only the 1080 Ti GPU consumes 250 W at full power respectively.

Considering that the embedded system computation power is reduced by 6.2 times (average between the detection and tracking frequency ratios) but only the GPU (not considering the whole PC desktop) presents a power consumption 8.3 higher, it makes the NVIDIA Jetson AGX Xavier a better suitable option for large scale-deployment in

the AD field rather than using heavy desktop graphic cards. Distributing several sensor processing across multiple embedded systems for parallelization will result in lower power consumption than using conventional GPUs in future AD prototypes.

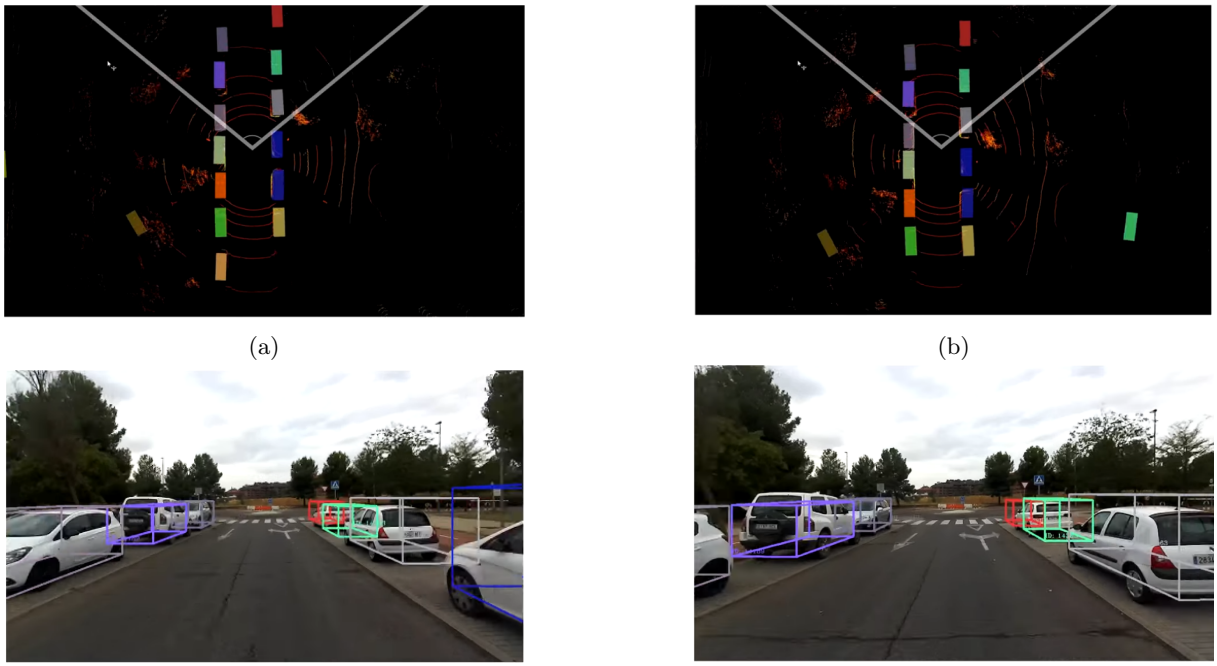

(a) (b)

(c) (d)

Figure 4.7: SmartMOT in our campus with our real-world vehicle without map monitoring. Velodyne VLP-16 is used as raw sensor data. It can be appreciated two perspectives ((a) (b) BEV LiDAR and (c) (d) Left RGB camera) in frame t (left column) and $t + 20$ (right column).

Qualitative results of running our SmartMOT pipeline in our own vehicle, equipped with a VLP-16 LiDAR instead of the HDL-64 shown in KITTI, are illustrated in Figure 4.7. It can be appreciated that although the obtained results are slightly worse than with the KITTI dataset (equipped with a HDL-64 sensor), we obtain quite promising results, validating the pipeline studied in this work both in terms of accuracy and real-time operation.

Finally, we illustrate some qualitative results in CARLA with and without the Monitored Lanes-based Attention Module to study the average inference time in several scenarios. Note that this attention module was not applied neither in the KITTI dataset (since HD map information is not provided here) nor in our campus with the real-world vehicle of our research group since map information was not available at the moment of conducting the different experiments.

One of the best advantages of CARLA is the possibility to create ad-hoc urban layouts by means of an OpenSCENARIO [100] script definition where town, vehicles, climate conditions and also driving behaviours are defined, helpful to validate AD algorithms (specially those focused on the perception layer) under different traffic and weather conditions.

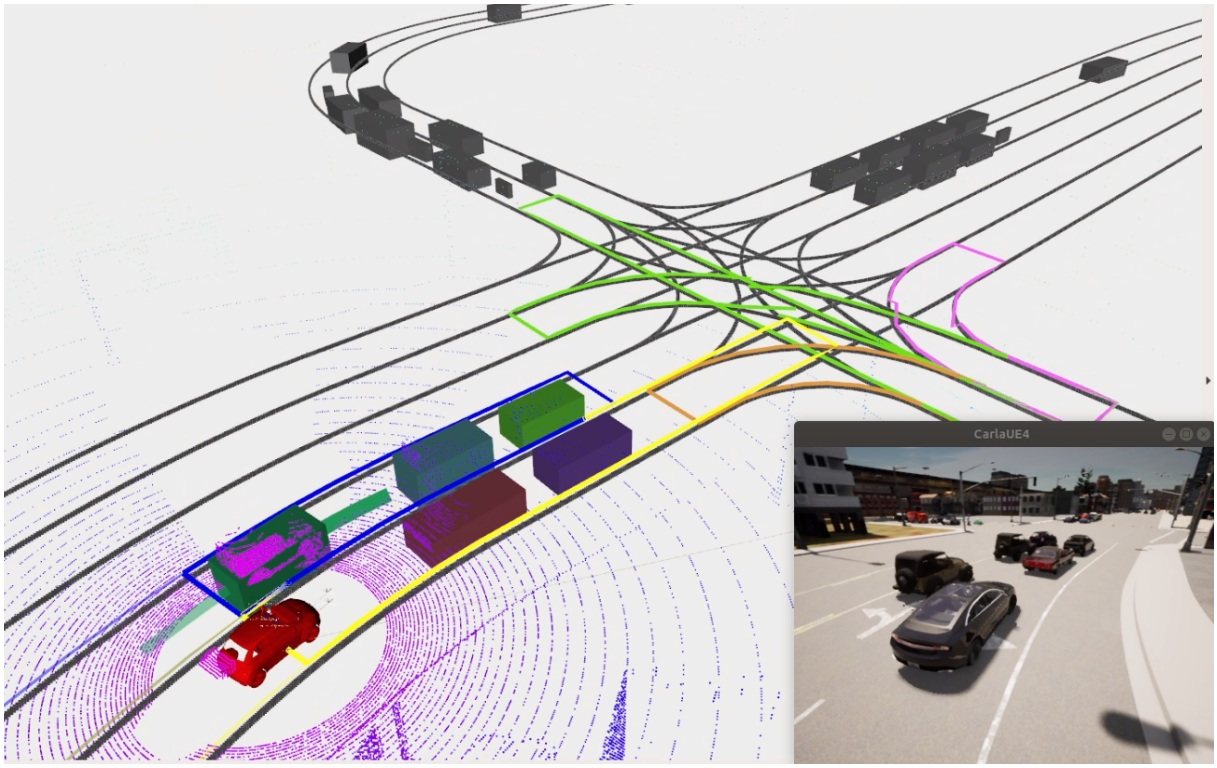

(a) Traffic scenario at frame t

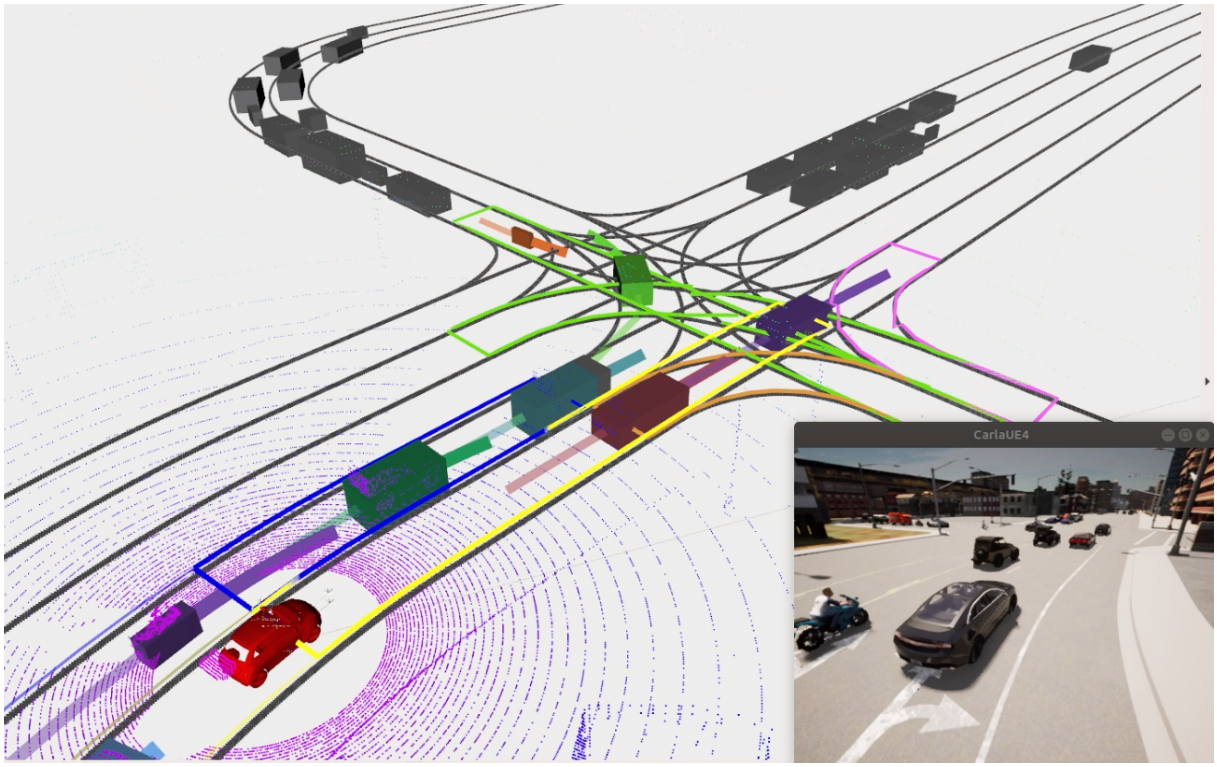

(b) Traffic scenario at frame $t + 40$

Figure 4.8: Simulation use case processed by SmartMOT (tracking + map monitor filtering + CTRV prediction in the CARLA simulator). As observed, only the most relevant objects are tracked (*i.e.* those which are in the monitored area and may be relevant in the short-term for the ego-vehicle).

In this particular case, we design different complex 4-ways intersection in the Town03, where different lanes of interest are monitored (*i.e.* current, left, merge, split and intersection). Note that we chose intersections since the number of agents and relevant lanes are noticeable higher than other traffic situations. For simplicity, in order to appreciate the full strength of SmartMOT when applying our proposed Monitored Lanes-based Attention Module, we take the detection Ground-Truth (GT) of the simulator until a given threshold (in this case, $150m$), in order to avoid the error propagated from the detection stage in real-world scenarios. Additional qualitative results may be found in SmartMOT [2].

As an example, Figure 4.8 illustrates how only the agents which current positions are within the monitored area are considered as relevant detections (*i.e.* agents which are on the left or right lane where a lane change maneuver is possible, agents which are within an intersection lane where there is an explicit risk of collision, etc.), noticeable reducing the average inference time throughout the route since there are way less agents to be tracked. In particular, after running the model several times in the different intersections with an average number of 30 traffic agents (located 360°around the ego-vehicle) we report an average inference time of the tracking stage of 27 ms when the map monitor module is not used. This inference time makes sense since it represents a frequency of 37Hz, whilst in Table 4.3 we illustrated a frequency of 101.9Hz with fewer detected obstacles (Figure 4.7). On the other hand, considering the same experimental setup (*i.e.* same traffic scenario, number of agents and platform, in our case a PC desktop (Intel Core i7-9700, 16GB RAM) with CUDA-based NVIDIA GeForce RTX 1080 Ti 11GB VRAM), when our Monitored Lanes-based Attention module is used in the SmartMOT pipeline, we are able to reduce the inference time of the overall pipeline from 27ms to an average time of 8ms (around 6 agents are considered in the monitored area), that is, about a third of the original inference time when all objects in the environment (including relevant and non-relevant) were tracked.

In conclusions, with this experimental setup, it takes approximately 1ms to perform state estimation, data association and physics-based. The higher the number of trackers, the longer the inference time of SmartMOT since calculations are not parallelized, so our filtering process helps the overall model to avoid unnecessary calculations which will not be relevant for the ego-vehicle at least in the short-term.

4.4. Summary

In this Chapter we propose SmartMOT, an open-source simple-yet-powerful pipeline that fuses the concepts of tracking-by-detection and HD map information to design a real-time and power-efficient MOT and uni-modal MP pipeline used to track and predict

[2] https://github.com/Cram3r95/SmartMOT

the future trajectories of only the most relevant obstacles around the ego-vehicle, incorporating a Monitored Lanes-based Attention Module to the pipeline, improving the way in which the vehicles are considered as relevant.

Then, experimental results focus on validating the tracking stage (without including map monitoring) in the KITTI dataset where the Velodyne HDL-64 is used, performing an ablation study to choose the final hyperparameters of the proposal. This proposal is also validated using data captured from our LiDAR using a Velodyne VLP-16, obtaining successful qualitative results since we do not have GT in this case. On top of that, we run the pipeline in a PC desktop and the Jetson NVIDIA AGX Xavier mounted in our real-world vehicle, concluding that even though the PC desktop presents a higher inference frequency, the higher ratio compared to the power consumption saved when using the edge computing device is lower. In that sense, in spite the fact that its integration is more difficult due to the distribution of several sensor processing across multiple embedded systems for parallelization, multiple edge-computing devices will be a preferred option rather than using heavy PC desktops and GPU in future AD prototypes.

Finally, the Chapter illustrates some results in CARLA, including map monitor information, where it can be clearly appreciated how tracking the most relevant agents of the scene (*i.e.* those which are included in the monitored area) can drastically reduce the inference time, making it suitable for real-time classic MOT and uni-modal MP operation, where no learning-based methods are required to reason what is happening in the traffic scenario, both in terms of physical and social information.

Chapter 5

Exploring GAN for Vehicle Motion Prediction

El mundo no es todo alegría y color,
es un lugar terrible y por muy duro que seas
es capaz de arrodillarte a golpes
y tenerte sometido a golpes permanentemente
si no se lo impides.
Ni tú ni yo ni nadie golpea mas fuerte que la vida.
Pero no importa lo fuerte que golpeas,
sino lo fuerte que pueden golpearte
hay que soportar sin dejar de avanzar.
¡Así es como se gana!

Discurso de Rocky a su hijo
Rocky Balboa

5.1. Introduction

Traditional methods for MP in the field of AD are based on physical kinematic constraints and road map information with handcrafted rules. Though these approaches are sufficient in many simple situations (*i.e.* vehicles moving in constant velocity or straightforward intersections), they fail to capture the rich behavior strategies and interaction in complex scenarios, in such a way they are only suitable for simple prediction scenes and short-time prediction tasks [19]. In that sense, recently DL-based methods have dominated this task and they usually follow an encoder-decoder paradigm. For example, even though an agent is not within the monitored area and can presumably be classified as non-relevant (as proposed in Chapter 4), in terms of learning based methods the model may find a pattern to identify complex interactions and determine that this agent is essential for the long-term prediction of the traffic scenario, and therefore, for taking the most optimal action in terms of local planning and Decision-Making (DM).

The main challenge in the MP is that human driver behaviour can neither be modeled and consequently nor predicted properly, specially in negotiating situations [101] [34] with many participants where considering agent-environment/agent-agent interactions [87] plays a determinant role. Then, resulting trajectories may not be necessarily feasible, not covering the full spectrum of possible trajectories that a vehicle can take. In that sense, a more natural way of capturing the feasible directions [102] is to first compute a set of intermediate target points from a distribution of acceptable positions.

Prior knowledge on MP in pedestrian datasets like ETH [103] or UCY [104] usually focuses on deep methods such as LSTMs [71] and GANs [72]. SocialLSTM [33] proposes an LSTM-based model that can jointly predict the paths of all agents in the scene taking into account the common sense rules and social conventions using a social-pooling module. SocialGAN [31] enhances SocialLSTM with a generative adversarial framework, introducing a variety loss that encourage the network to cover the space of plausible paths and proposing a novel global social pooling vector that encodes the subtle cues for all agents involved in the scene. SoPhie [87] considers not only the path history of all agents but also the physical context information (captured by a top-view static image, computing salient regions of the scene), combining physical and social attention mechanisms in order to help the model knows what to extract and where to focus. Goal-GAN [102] predicts the most likely goal points of the agent in the scene, estimating a set of trajectories towards these potential future goals using both physical and social context, as proposed by [87]. As observed, since these previous methods are focused on pedestrians MP datasets, in such a way no HD map information (considering topological, semantic and geometric information) is available, only basic driveable areas in a city, such as the sidewalks.

On the other hand, in the context of vehicle prediction [6], [56], prior physical information takes more importance regarding the risk at certain velocities in urban / highway environments in order to perform safe navigation. As stated in Chapter 2.3.2, HD maps have been widely adopted to provide a preliminary raw physical context and then apply data-driven approaches. Recent learning-based approaches [32], [88], which present the benefit of having probabilistic interpretations of different behaviour hypotheses, require to build a representation to encode the trajectory and map information. [88] assumes that detections around the vehicle are provided and focuses its work on behaviour prediction by encoding entity interactions with CNNs. Intentnet [32] proposes to jointly detect traffic participants (mostly focused on vehicles) and predict their trajectories using raw LiDAR pointcloud and rendered HD map information. PRECOG [16] aims to capture the future stochasiticity by flow-based generative models. Furthermore, MultiPath [43] uses CNNs as encoder and adopts pre-defined trajectory anchors to regress multiple possible future trajectories. Nevertheless, most of these approaches make use of 2D-CNNs to analize the top-view map information of the traffic scenario, which is usually very slow computationally and non-interpretable.

Furthermore, in a similar way to humans that pay more attention to close obstacles, people walking towards them or upcoming turns rather than considering the presence of people or building far away, the perception layer of an ADS car must be modelled to focus more on the more relevant features of the scene, specially considering the traffic agents. Social Attention is a mechanism that allows selective interactions within relevant agents. SoPhie [87] computes a different context vector for each agent, in such a way other agents features are sorted in terms of their relative distance to the agent of interest. Then, a soft attention mechanism is used to compute a context feature vector, which represents the social context. Nevertheless, a fixed size ($N_{\max}$ agents) list that considers the context of all agents is sensitive to small variations [34] of other agents positions. In that sense, SocialWays [105] presents a hand-crafted relative geometric feature to produce a set of normalized weights, in such a way the context vector represents a convex sum of other feature vectors (context of each agent) that is invariant to the ordering.

However, these attention mechanisms were not designed to model complex interactions, taking into account that more complex interactions than simple distances and angles should be produced in the context of vehicle forecasting to account for specific behaviours such as following or yielding no more than angles and distances due to the inherent problem of pedestrian prediction. In that sense, GRIP [106] proposes a graph representation of vehicle neighbours, but takes into account just those local interactions with vehicles that are closer to the target agent than a threshold distance d.

Moreover, [107] use a dot product attention module, inspired from the well-established attention mechanism proposed by [74] for sentence translation. This mechanism allows joint forecast of every vehicle in the observed scenes without spatial limitations. It accounts for long range interactions within a varying number of vehicles and does not require the ordering of the vehicles tracks it takes as input. [107] combines this dot product with a spatio-temporal graph representation to take into account temporal and spatial dependencies of the agents, such as their absolute/relative positions and time step movements. In our case, similarly to [34], we make use of a multi-head extension of this dot attention mechanism, where each agent is embedded by means LSTMs before computing the dot product attention in order to produce social interactions, allowing a varying number of vehicles and not required a particular order of the agents in the traffic scenario.

In this Chapter we explore the influence of attention mechanisms in generative models, in particular based on GAN [72], to carry out the task of uni-modal MP. Our model considers both physical context, computing acceptable target points from the driveable area around the target agent, and social context, encoded by a LSTM-based Social Feature Extractor and a Multi-Head Self-Attention (MHSA) module. Regarding this, the input of our generator is the concatenation of the scene understanding around the target agent vehicle and the corresponding multi-variate noise vector associated to generative models, in order to compute the trajectories using a LSTM decoder. In this context, the discrim-

inator is applied in order to force the generator model to produce more realistic samples (*i.e.* trajectories), hence, to improve the performance. The work in this Chapter was partially published in the following conference paper [108]: "Exploring Attention GAN for Vehicle Motion Prediction", 2022 IEEE 25th International Conference on Intelligent Transportation Systems (ITSC), p. 4011-4016.

Figure 5.1 illustrates the overall pipeline. We make the following contributions:

1. We study the influence of the adversarial training in uni-modal vehicle MP compared to other proposals.
2. A kinematic-based interpretable way to obtain preliminary target points from the driveable area is proposed.
3. We study the influence of the class balance in the dataset during training, particularly focusing on straight and curved target agent trajectories.
4. Finally, we provide an open-source [1] framework for MP.

5.2. Attention-based GAN

In this work, we aim to develop a model [108] that can successfully predict plausible future trajectories in the context of vehicle MP, taking into account not only the past trajectory of the corresponding target agent but also the HD map information to compute a set of acceptable target points representing the physical constraints for our problem.

When vehicles drive through a traffic scenario, they usually aim to reach partial goals, depending on their predefined navigation route and scene context (both physical and social), until they finally arrive at their final destination. Formally, given a certain goal, vehicles must face different traffic rules and other agents along their way to reach their final destination. Regarding this, our model computes both the social context and acceptable target points for the corresponding agent given its past trajectory and then generates plausible trajectories towards the estimated goals. Our model consists of three main blocks:

- **Target Points Encoder**: Compute the latent space of some random points extracted from the driveable area. These random points are calculated in advance by combining HD map information and dynamic features of the target agent (speed and orientation) to generate these acceptable goal points (in frame $pred_{len}$) in the driveable area.
- **Social Attention Module**: Computes the agents dynamic features recursively by means a LSTM unit and capture complex social interactions among agents by means of the Multi-Head Self-Attention (MHSA) mechanism.

[1] https://github.com/Cram3r95/mapfe4mp

- **GAN module**: Given the target points and highlighted social features, this module generates plausible and realistic trajectories using a LSTM-based decoder, which represents the generator. Discriminator is applied to enhance the performance of the generator by forcing it to compute more realistic predictions.

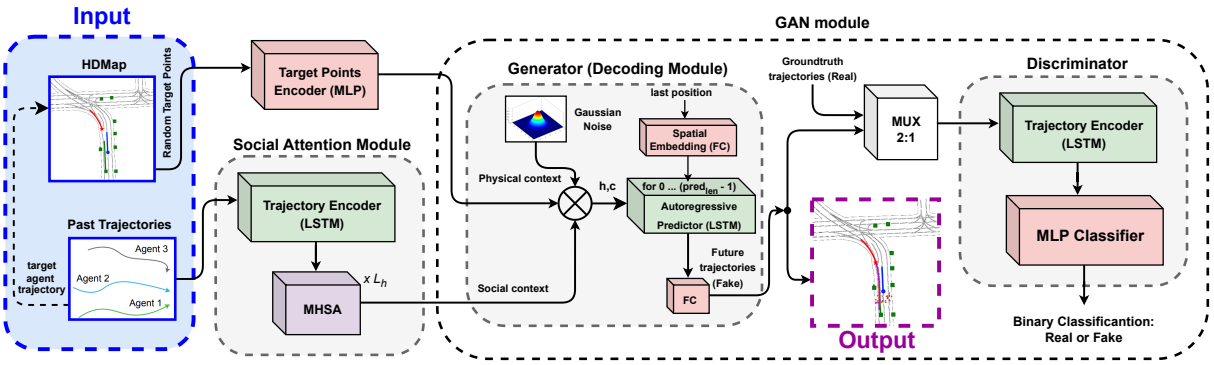

Figure 5.1: Overview of our Attention-based GAN model

Figure 5.1 illustrates an overview of our model. Next, we describe the different blocks of our model.

5.2.1. Target Points Extraction

Multiple approaches have tried to predict realistic trajectories by means of learning physically feasible areas as heatmaps or probability distributions of the agent future location [9], [87], [102]. These approaches require either a top-view RGB BEV image of the scene, or a HD map with exhaustive topological, geometric and semantic information (commonly codified as channels). This information is usually encoded using a CNN and fed into the model together with the social agent information [35], [87], [102].

In our model, we propose to estimate the range of motion (360°) using a minimal HD map representation that only includes the feasible area $\mathcal{F}$ (*i.e.* a 1-channel BEV map image with the driveable area of the traffic scenario in white), which can be discretized as a subset of R randomly sampled points $\{p_0, p_1 ... p_R\}$ from such area in the map (easy to extract from a binarized image) considering the orientation and velocity in the last observation frame for target the agent. This step can be considered as pre-processing of the HD map, therefore the model never sees the HD map image nor the whole graph of nodes.

Figure 5.2 summarizes step-by-step the whole process.

- First, we calculate the driveable area (white area in Figure 5.2) around the vehicle considering a hand-defined d threshold.
- Then, we consider the dynamic features of the agent of interest in the last observation frame obs_{len} to compute acceptable target points in local coordinates. As we

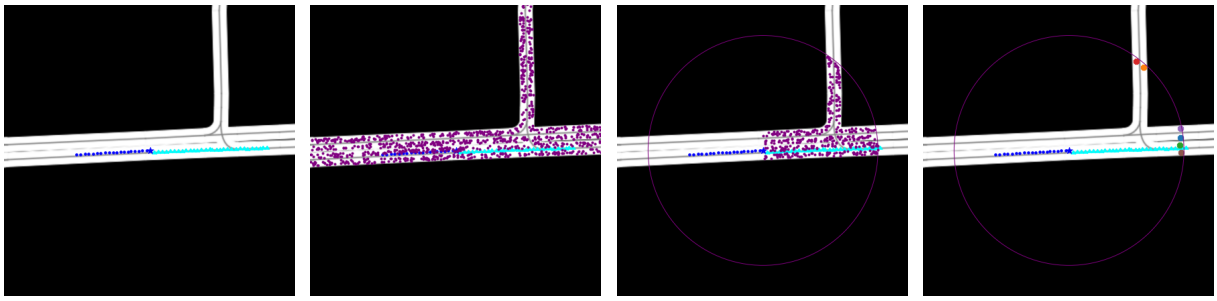

(a) (b) (c) (d)

Figure 5.2: Target Points Estimation from the Feasible area process: (a): Agent Past Trajectory (**past observations** and **ground-truth**), (b) Feasible area discretization (**random points** in the driveable area), (c) Non-holonomic-based dynamic filter (both angle and velocity), (d) K-means clustering to get the final proposals

will detail in future sections, the Argoverse 1 Motion Forecasting dataset focuses on estimating the future prediction of a particular target agent. On top of that, the aforementioned dynamic features (orientation and velocity) are not provided, in such a way they must be calculated. Since the trajectory data are noisy with tracking errors, as expected from a real-world dataset, simply interpolating the coordinates between consecutive time steps, assuming constant frequency, results in noisy estimation. Then, in order to estimate the orientation and velocity of the target agent in the last observation frame obs_{len}, we compute a vector for each feature given:

$$\begin{aligned} \theta_i &= \arctan\left(\frac{y_i - y_{i-1}}{x_i - x_{i-1}}\right) \\ v_i &= \frac{X_i - X_{i-1}}{t_i - t_{i-1}} \end{aligned} \tag{5.1}$$

where X_i represents the 2D position of the agent at each observed frame i as state above.

- Once both vectors are computed, we obtain a smooth estimation as proposed by [109] of the heading angle (orientation) and velocity by assigning less importance (higher forgetting factor) to the first observations, in such a way the immediate ones are the key states to determine the current spatio-temporal variables of the agent, as depicted in Equation 5.2 (which applies to both the velocity and orientation vector):

$$\hat{\psi}_{obs_{len}} = \frac{(\hat{\psi}_\theta, \hat{\psi}_v)_{obs_{len}} = \sum_{t=0}^{obs_{len}} \lambda^{obs_{len}-t}\psi_t}{obs_{len}} \tag{5.2}$$

where obs_{len} is the number of observed frames, ψ_t is the estimated orientation/velocity at the t_i frame and $\lambda \in (0, 1)$ is the forgetting factor. After estimating the velocity and orientation in the last observation frame, we calculate the range of motion around the target agent as a circle with radius: $H * \psi_v$ where ψ_v is the estimated velocity

using Equation 5.2 and $H = 3$ is the time horizon of 3s. After that, we randomly sample R points $r \in \mathcal{F}$ in this range considering a constant velocity model during the prediction horizon and the estimated orientation, assuming non-holonomic constraints [52], which are inherent of standard road vehicles, that is, the car has three degrees of freedom, its position in two axes and its orientation, and must follow a smooth trajectory in a short-mid term prediction.

- Finally, we estimate k target points (one per mode required in the future prediction) using the well-known K-means [110] clustering algorithm. This clustering method aims to partition N observations into K clusters in which each observation belongs to the cluster with the nearest mean (cluster centers or cluster centroid), serving as a prototype of the cluster. In this particular model, we focus on uni-modal prediction, that is, the model must reason the most plausible future trajectory based on the agents past observations, attention-based social interaction and target points as physical context.

As observed, this representation not only reunites information about the feasible area around the agent, but also represents potential target points [102] (*i.e.* potential destinations or end-of-trajectory points for the agents). Moreover, this information is *"cheap"* and *interpretable*, therefore, we do not need further exhaustive annotations from the HD map in comparison with other methods like HOME [9], which gets as input a 45-channel encoded map [9].

After these target points are obtained, we compute the deep features by means of a standard MLP, which will be concatenated to the social context and Gaussian vector to generate more realistic trajectories, as observed in Figure 5.1.

5.2.2. Social Attention Module

Multiple methods [13], [14] consider only the agents that are observable at $t{=}0$, handling those that are not observed over the full sequence spectrum (observation length = obs_{len} + prediction length = $pred_{len}$) by concatenating a binary flag b_i^t that indicates if the agent is padded or not.

In our case, we consider the N_{agents} that have information over the full history horizon (*e.g.* $5s = 2s(observationtime) + 3s(predictionstime)$ for Argoverse 1) as relevant agents, reducing the number to be considered in complex traffic scenarios. Nevertheless, instead of using the past obs_{len} observations in map (global) coordinates for each agent marked as relevant, we transform to local (relative) coordinates by substracting the last observation of the target agent (considered as the origin of the scene) to the past trajectory of an agent to make the model translation-invariant given the local coordinates of the scene. Then, using absolute 2D-BEV (xy plane) local coordinates, the input for the agent n is a series of relative displacements:

$$\Delta\nu_n^t = \nu_n^t - \nu_n^{t-1} \tag{5.3}$$

Where ν_n^t represents the state vector (in this case, xy position of the agent i at timestamp t).

Unlike other methods, we do not limit nor fix the number of agents per sequence. Given the relative displacements of all different agents, we model their past motion history by means of a single LSTM (Trajectory Encoder in Figure 5.1), which is used to compute the temporal information of each agent in the sequence:

$$out, h_{out}, c_{out} = LSTM(\Delta\nu^{obs_{len}}, h_{in}, c_{in}) \tag{5.4}$$

This LSTM-based encoder shares the weights for all vehicles in the batch. The input hidden and cell vectors (h_{in}, c_{in}) are initialized with a tensor of zeros. $\Delta\nu^{obs_{len}}$ represents the relative displacements vector over the past observations. Then, we consider the hidden vector h_{out} as the latent past information of the relevant $n-th$ in the traffic scenario.

After computing the social information for each agent, we aim to learn complex social interactions, where each agent of the scene should pay attention to specific features around it, while being invariant to their number and ordering. Since we want to avoid a fixed size ($N_{\max}$ agents) list of agents, which would be sensitive to small variants in the agent positions, we make use of the well-established Multi-Head Self-Attention (MHSA) mechanism [74] (particularly, the scaled dot-product variant, as proposed by [34]), which is applied to the matrix made up by the concatenation of the hidden state vector of all relevant agents in the traffic scenario.

The MHSA mechanism allows vehicle interactions while keeping independence from their number and ordering. The computations made by each attention head is represented in Figure 5.3.

Each agent should pay attention to specific features from a selection of the other agents. This is made with four steps: pulling together specific features, identifying these feature collections, enquiring among identifiers, and gathering the results.

In the MHSA mechanism, each head produces a different selection of features using a linear projection of the input tensor resulting in the value tensor V. In order to identify these features, a key tensor K is associated to each value. Then, each agent must select which other agents to pay attention to. For that purpose, a query Q is produced to find a selection of keys. As aforementioned, we make use of the scaled-dot product version of the MHSA mechanism, where the match score between a key and a query is their dot product, it is scaled with the square root of the key dimension $\sqrt{d_k}$ and normalized with a softmax operation. This produces an attention matrix that contains coefficients close to 1 for matching queries and keys and close to 0 otherwise.

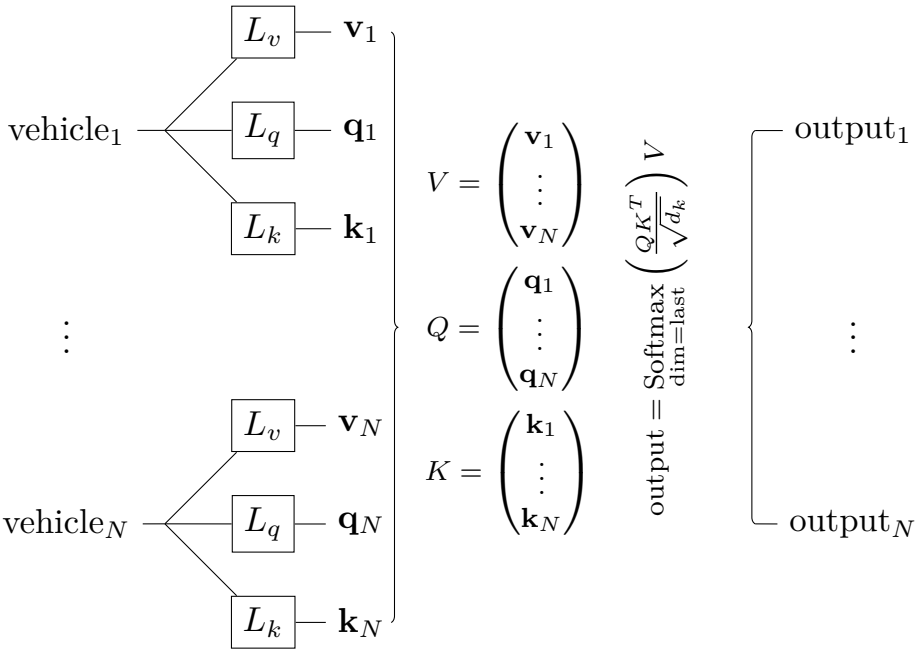

Figure 5.3: Single attention head computations. L_q, L_v, L_k are matrix multiplications of the input vectors. Note that in this case N stands for N_{agents}.

Regarding this, the attention matrix is square of size N_{agents}, where each coefficient (i, j) is the attention coefficient of vehicle i on vehicle j. Hence, this matrix is used to gather the values from V. Thus, the self-attention computation for each head can be expressed as following:

$$\text{output} = \underbrace{\underset{\text{dim=last}}{\text{softmax}}\left(\frac{QK^T}{\sqrt{d_k}}\right)}_{\text{attention matrix}} V \tag{5.5}$$

Finally, the social attention matrix $SATT$ is computed as the combination of L_h different attention heads in a single matrix:

$$SATT = (head_1 || \ldots || head_{L_h}) W_{\text{o}} + \begin{pmatrix} b_{\text{o}} \\ \vdots \\ b_{\text{o}} \end{pmatrix}. \tag{5.6}$$

Where each row of the matrix $SATT$ (output of the Social Attention Module, after the LSTM and MHSA mechanisms) represents the interaction-aware feature of the *n-th* agent with its surroundings agents, considering the temporal information under the hood, being W_{o} / b_{o} the corresponding weight and bias of the layer that merges the different attention heads.

As this model has been developed upon the Argoverse 1 Motion Forecasting benchmark, we only consider the row of the social matrix that takes into account the interactions of the target agent with its surrounding obstacles.

5.2.3. GAN module

To capture the stochastic nature of motion prediction, state-of-the-art methods leverage the power of generative models, such as Variational Autoencoders (VAEs) and Generative Adversarial Network (GAN). In our work we use an adversarial framework in order to train our trajectory generator, responsible for generating physically and realistic feasible trajectories. In a GAN, the Generator (which after being trained will be the inference network) and Discriminator networks compete in a two-player min-max game [72], as observed in Equation 5.7. While the generator aims at producing feasible trajectories, the discriminator learns to differentiate between fake and real samples, in other words, ground-truth (which are feasible by definition) and inferred trajectories, in such a way the tasks of the discriminator is to enhance the performance of the generator by forcing it to compute more realistic predictions, more and more similar to the ground-truth trajectory. As a result, the generator should be able to produce outputs which the discriminator cannot discriminate clearly, indicating that the output is realistic.

$$\min_{Gen}\max_{Dis} V(Dis, Gen) = E_{X\sim p_{data}(X)}[\log Dis(X, Y)] + E_{z\sim p_z(z)}[\log(1 - Dis(X, Gen(X, z)))], \tag{5.7}$$

In the present case, the generator is represented by a LSTM-based decoder ($LSTM_{gen}$) and the discriminator by a LSTM-based encoder + MLP classifier ($LSTM_{dis}$) so as to estimate the temporally dependent future states. Similar to the cGAN proposed by [87], the input to our generator is a concatenation of a noise vector z sampled from a multi-variate normal distribution, being the physical context (goal points in relative coordinates in the last observation frame, $C_{Ph(i)}^{t_{obs}}$) and social context (interactions among agents, $C_{So(i)}^{1:t_{obs}}$) its conditions. Then, the generated future trajectory ($pred_{len}$ steps) for a particular agent is modelled as Equation 5.8:

$$\hat{Y}_i^{t_{obs}:t_{pred}} = LSTM_{gen}\left(C_{Ph(i)}^{t_{obs}}; C_{So(i)}^{1:t_{obs}}; z\right) \tag{5.8}$$

On the other hand, the input trajectory $T_i^{t_{obs}:t_{pred}}$ to the discriminator is a randomly chosen future trajectory sample either from the predicted trajectory computed by the generator or the ground-truth for the corresponding agent up to $t = t_{obs} + t_{pred}$ frame, *i.e.* $T_i^{t_{obs}:t_{pred}} \sim p(\hat{Y}_i^{t_{obs}:t_{pred}}, Y_i^{t_{obs}:t_{pred}})$, as illustrated in Figure 5.1 with the MUX block.

$$\hat{L}_i^{t_{obs}:t_{pred}} = LSTM_{dis}(T_i^{t_{obs}:t_{pred}}) \tag{5.9}$$

After encoding this trajectory, an MLP module and softmax operation returns a label $\hat{L}_i^{t_{obs}:t_{pred}}$ for the chosen trajectory indicating whether the trajectory is ground-truth (real) $Y_i^{t_{obs}:t_{pred}}$ or predicted (fake) $\hat{Y}_i^{t_{obs}:t_{pred}}$, being the labels 0 and 1 for fake and real trajectories respectively. Equation 5.9 summarizes the discriminator working principles.

5.2.4. Losses

To train our GAN-based model, we use the following losses:

$$\begin{aligned} W^* = \underset{W}{\operatorname{argmin}} \quad & \mathbb{E}_{i,\tau}[\lambda_{gan}\mathcal{L}_{GAN}\left(\hat{L}_i^{t_{obs}:t_{pred}}, L_i^{t_{obs}:t_{pred}}\right) + \\ & \lambda_{ADE}\mathcal{L}_{ADE}(\hat{Y}_i^{t_{obs}:t_{pred}}, Y_i^{t_{obs}:t_{pred}}) + \\ & \lambda_{FDE}\mathcal{L}_{FDE}(\hat{Y}_i^{t_{obs}+t_{pred}}, Y_i^{t_{obs}+t_{pred}})], \end{aligned} \tag{5.10}$$

where W is the collection of weights of all networks used in our model and the different λ represent the corresponding regularizers between these losses. As stated in Equation 5.7, $\mathcal{L}_{GAN}$ represents the min-max game where the generator tries to minimize the function while the discriminator tries to maximize it. $\mathcal{L}_{ADE}$ loss function is commonly used to compute the average error between the predicted trajectories and the corresponding ground-truth. Moreover, we add $\mathcal{L}_{FDE}$ loss function to explicitly optimize the distribution towards the final real point computing its $\mathcal{L}_2$ error.

5.3. Experimental Results

5.3.1. Dataset

We evaluate this model on the well-established and public available Argoverse 1 Motion Forecasting dataset [6], including the training, validation and testing subsets from its official website [111].

As stated in Chapter 2, it consists of 205942 training samples, 39472 validation samples and 78143 test samples. Each sample has a length of 5s, with an observation window of 2s and a prediction window of 3s, including the corresponding labels of the agents ($AGENT$, as the target agent, AV, the vehicle that captures the scene and $OTHER$, representing the remaining relevant obstacles) and a global map from the cities of Pittsburgh and Miami. The sampling frequency is 10Hz. The main goal here is to predict the 3s future position of the target agent in the scene, which is supposed to be the vehicle that faces the most challenging traffic scenarios.

5.3.2. Metrics

Previous works [34], [43], [87] report the minADE (minADE$_K$), which averages the $\mathcal{L}_2$ distances between the ground-truth and predicted trajectory across all timesteps, and minFDE (FDE$_K$), which computes the $\mathcal{L}_2$ distance between the final points of the ground-truth and the predicted final position, taking the best K trajectory sample of each agent compared to the ground-truth. In this model, since we do not focus on multi-modal prediction but on the predicting the most plausible uni-modal trajectory, we use $K = 1$ (uni-modal case).

5.3.3. Implementation details

All local test were conducted in a PC desktop (AMD Ryzen 9 5900X, 32GB RAM with CUDA-based NVIDIA GeForce RTX 3090 24GB VRAM, Ubuntu 18.04).

Regarding the ablation study, we train the different models for 150 epochs using the ADAM optimizer with learning rate 0.001 and default parameters, linear Learning Rate (LR) scheduler with factor 0.5 decay on plateaus (every 5K iterations) and batch size 128. The loss function is weighted by setting λ_{gan}=1.4, λ_{ade}=1 and λ_{fde}=1.5, giving more importance to the adversarial loss and the final displacement error.

Similar to [87], the LSTM encoder (attention block) encodes trajectories using a single layer MLP with an embedding dimension of 16. We set all LSTM units to have 32 hidden dimensions.

In order to calculate the proposed target points we consider the same prediction horizon $pred_{len} = 30 \longleftrightarrow 3s$ to estimate the distance travelled assuming a CV model. The number of target points is set also to 32 in order to compute the physical context, which are then clustered by means of the KMeans algorithm into 6 plausible target points. The top-view image, illustrating the driveable area in white and off-road in black, covers the map information $50m$ around the target agent in the last observation frame (t=obs_{len}), which is then transformed into a 600x600 px 1D-binarized image. We estimate this distance around the agent from a preliminary statistical study. Since Argoverse 1 is mainly focused on urban scenarios or low-speed highways, most target agents future trajectories (3s) do not travelled, in average, more than $45m$.

To make our model more robust to scene orientation, we augment the training data adding some white noise ($\mu = 0, \sigma = 0.25$, [m]) to the observation data, rotating the scene and also dropping and replacing (with their last frame) some observations of the past trajectory in order to make the trained model general enough so as to perform well on the unseen traffic scenarios in the split test that includes different scene geometries such as left/right turning or emergency braking.

5.3.4. Statistical study of the GAN baseline in validation

In terms of validation, we conduct a preliminary statistical analysis for Average Displacement Error (ADE) and Final Displacement Error (FDE) metrics, distinguishing the performance between straight and curved trajectories for our baseline model, *i.e.* without considering target goals as physical information. To this end, we make use of the Argoverse 1 validation set that consists of 31,000 samples.

We classify a trajectory as straight or curve estimating a 1^{st} degree polynomial trajectory by means the RANdom SAmple Consensus (RANSAC) algorithm with the highest number of inliers (tolerance t set to $2m$, max trials=30, min samples=60 % total observations). Then, if the current target whole trajectory presents 20 % or more consecutive points further than t with respect to the closest point of the fitted trajectory, the whole traffic scenario is labelled as curve.

Regarding this, the Argoverse 1 validation dataset has 23,012 and 7,988 straight and curved trajectories respectively given the aforementioned RANSAC-based classification.

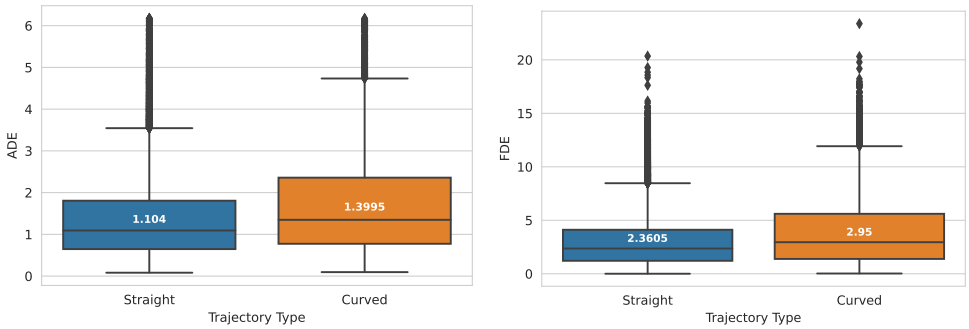

Figure 5.4: Statistical distribution on the Argoverse 1 validation set of regression metrics in straight and curved trajectories. We show the boxplots for ADE and FDE metrics. We distinguish between straight and curved trajectories. We highlight the median (Q2) in each boxplot.

Figure 5.4 illustrates the boxplots for ADE and FDE metrics. As stated before, our method, as most methods, struggles with curved trajectories, the overall ADE and FDE is "always" better for the straight trajectory cases. The median provides a robust estimator of our trajectories error. Note that we detected multiple outliers in our analysis, these are due to the uni-modal nature of the model, unable to consider multiple possible hypotheses (multi-modal).

Regarding this, we design our dataloader to sample in each iteration of the training process a specific proportion (*i.e.* class balance) of straight and curved trajectories (regarding the whole trajectory of the target agent). We do this to focus in the training process in non-linear prediction, which represents one the key challenges in vehicle MP.

5.3.5. Comparative with the State-of-the-Art

In this section, we perform an ablation study and compare our method performance against SOTA methods on the Argoverse 1 Motion Forecasting benchmark test set. Table 5.1 illustrates the comparison with some Argoverse baseline methods. Our GAN baseline is represented by the system pipeline illustrated in Figure 5.1, that is, Attention-based GAN with LSTM as encoder-decoder, without target points extractor and class balance.

Table 5.1: Ablation study of our GAN-based uni-modal (K=1) pipeline, and comparison with other relevant methods on Argoverse 1 Motion Forecasting test set. We can see the improvement using Target points (TP) and Class balance (CB). Our methods are indicated with †. Prediction metrics (minADE, minFDE) are reported in meters. We bold the best results in **black** and the second best in **blue** for each metric.

Model	minADE ↓	minFDE ↓
Constant Velocity [6]	3.53	7.89
Argoverse Baseline (NN) [6]	3.45	7.88
Argoverse Baseline (LSTM) [6]	2.96	6.81
TPNet [112]	2.33	5.29
TPNet-map [112]	2.33	4.71
Jean (1st) [6], [34]	**1.74**	**4.24**
† GAN Baseline (*)	1.98	4.47
† GAN Baseline + TP	1.78	4.13
† GAN Baseline + CB	1.82	4.32
† GAN Baseline + TP + CB	**1.73**	**4.07**

It may be appreciated how our GAN baseline (only-social) obtains better results than the baselines [6] proposed by Argoverse 1. The reason is simple: Even in traffic scenarios where the target agent conducts a straight trajectory, it may perform sudden braking or acceleration, since, given the complexity of the dataset. Then, simple learning-based or physics-based prediction methods are not enough to encode the complexity of the dataset. TPNet [112] improves upon previous baselines (particularly when including map information). Jean (1st) [34] is the winner of the CVPR 2019 Argoverse Challenge, which produces joint forecasts for all vehicles on a road scene as sequences of multi-modal probability density functions of their positions, including the centerlines of the surrounding lanes. We conduct an ablation study to observe the influence of incorporating target points and class balance to our baseline. As expected, by explicitly defining in an interpretable way the locations an agent is likely to be at a fixed prediction horizon for a given input trajectory and scene geometry, we are able to improve our baseline. Additionally, since non-linear trajectories are more challenging than standard straight trajectories, we also observe how enforcing the class balance (straight, curve) during training is able to improve performance, obtaining results that up-to-pair with other SOTA methods.

5.3.6. Qualitative results

Figure 5.5 illustrates some qualitative results, all of them considering uni-modal prediction towards the pre-computed target points, meeting the physical and social constraints in the scenes. It can be clearly appreciated that a naive CTRV model could not generalize in these situations, where the vehicle can describe a curved future trajectory given a predominant straight input trajectory and vice-versa. First, second and third rows show feasible predicted trajectories in challenging scenarios, including straight and curved trajectories.

On the other hand, the fourth row shows interesting challenging scenarios in which our current approach is not able to properly reason due to the lack of reasoning and multi-modality (producing a set of K-trajectories towards the set of target points) is revealed, being situations in which predicting accurately the end-point is difficult, and the FDE is extremely high. Particularly, left image shows how we compute an uni-modal prediction in the wrong direction of a split, even though target points are extracted very close to the ground-truth end point. Center image shows an extreme difficult situation, where the input trajectory is almost in the same place (probably the target agent was stopped in front a traffic light) whilst the ground-truth future trajectory is clearly an acceleration since the last observation frame. Finally, right image shows a deceleration because of the ahead obstacle whilst our model is not able to properly reason the presence of this obstacle in order to meet common sense safety constraints.

5.4. Summary

Forecasting the future trajectories of surrounding actors in the scene is mandatory to achieve a safe planning, and thus, a crucial part of the AD stack. In this Chapter we explore a GAN-based LSTM with MHSA for uni-modal vehicle MP using the Argoverse 1 Motion Forecasting Benchmark. Our model considers both the deep physical and social context of the scene to predict the most plausible trajectory using a generative model, and achieves competitive results in comparison to other SOTA methods regarding the uni-modal prediction scenario.

Given the aforementioned results, we realize that this uni-modal method lacks capacity to model complex traffic scenarios where several future actions are plausible (both in terms of directions or velocity profiles). Then, the future steps, which will be covered in further Chapters, are an enhanced social attention and interaction, high-level and well-structured physical context, specially focusing on the HD map vector features, in order to produce feasible and realistic multi-modal trajectories.

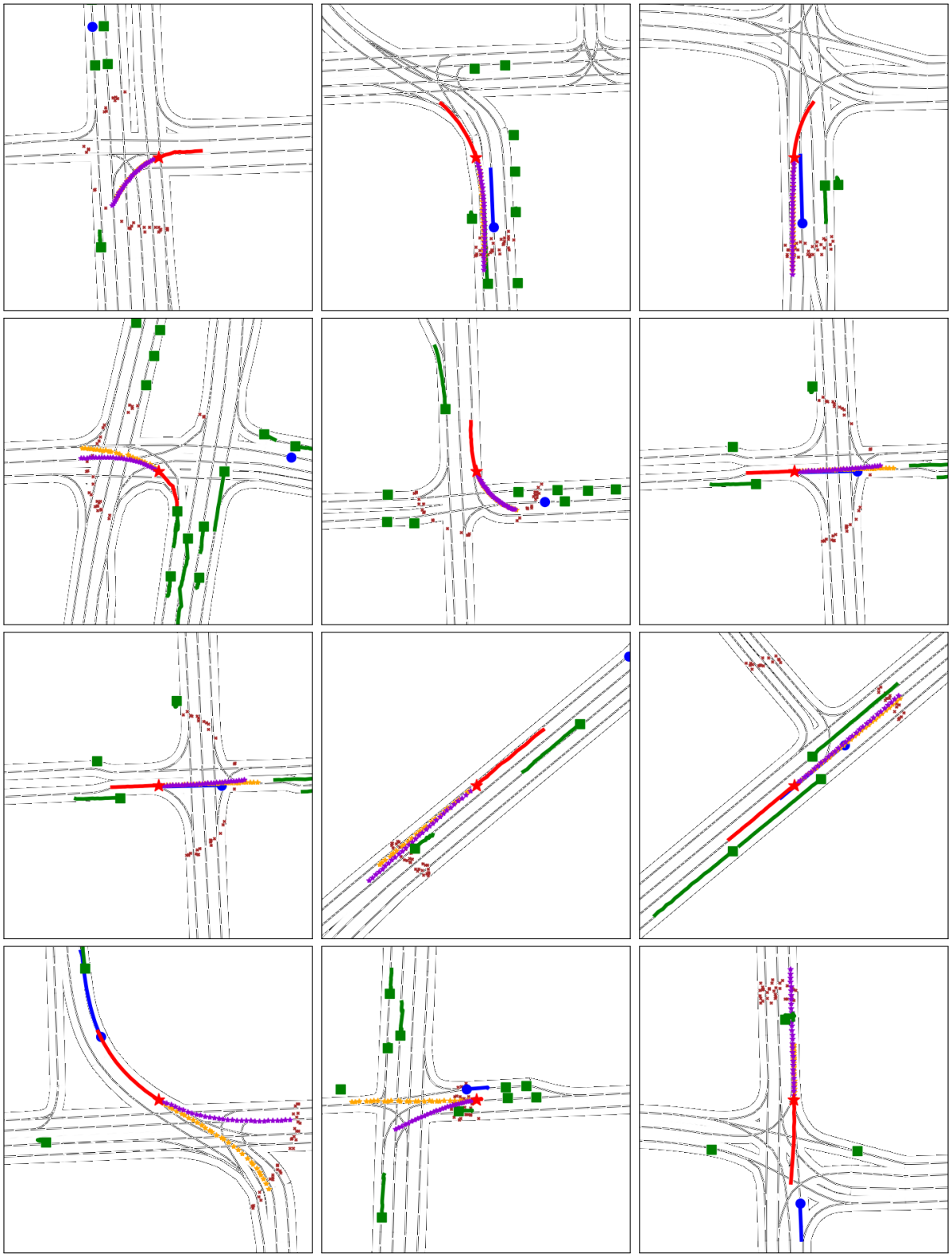

Figure 5.5: Qualitative Results using our Attention-based GAN best model (including target points extraction and class balance). The legend is as follows: our vehicle (**ego**), the target **agent**, and **other agents**. We can also see the **real** trajectory, the **prediction** and potential **goal-points**. Markers (starts and squares) represent the last observations for each agent.

Chapter 6

Efficient Baselines for Multi-modal Motion Prediction in Autonomous Driving

La fuerza de tus convicciones
determina tu éxito,
no el número de tus seguidores.

Reamus Lupin
Harry Potter y Las Reliquias de la Muerte, Parte 2

6.1. Introduction

As observed in the previous Chapter, our GAN-based model (more specifically the generator) was able to compute the deep context regarding the agents past observations, attention-based social interaction and target points as physical context, but the prediction was limited to the uni-modal case. In other words, the GAN-based model is able to reason more complex interactions and future behaviours than SmartMOT (physics-based prediction), but it lacks one of the main features of a DL-based MP model as a preliminary stage before the local planning or DM layers: Multi-modality.

On top of that, at this point of the thesis the literature was re-visited and despite GANs-based approaches [31], [87], [102], [108] provide certain control since they are focused on more simple methods framed in an adversarial training, most competitive approaches on MP benchmarks in the field of AD, such as Argoverse [6], NuScenes [56] or Waymo [55], do not use adversarial training as the first choice due to several reasons:

- **Limited interpretability and explainability**: GANs often lack interpretability and explainability. The internal workings of a GAN can be challenging to understand and explain to humans, which is a crucial requirement in safety-critical applications

like AD. Moreover, explainability is essential for building trust and understanding the DM process of the system. GANs typically prioritize generating realistic samples over providing explicit explanations for the predictions.

- **Data requirements and availability**: GANs typically require large amounts of data for training, specially in those scenarios where the input can be quite similar (the target agent is approaching to an intersection) but the output is totally different (in terms of future directions or velocity profiles). Acquiring such datasets for MP in AD can be challenging, as it requires accurately annotated and diverse real-world motion data. On the other hand, users can also opt for synthetic data generation to complement data obtained from the real world, but generating high-quality synthetic data that adequately represents the complexity of real-world driving scenarios is difficult. In contrast, other approaches like GNNs can be trained with readily available trajectory data, making them more practical and accessible in this context.
- **Focus on generation rather than prediction**: GANs are primarily designed for data generation tasks, where the objective is to generate new samples that resemble the training data distribution, as illustrated in Chapter 3. Nevertheless, in MP for AD, the goal is to accurately predict future trajectories based on current observations and historical data, where GANs may not inherently prioritize predictive accuracy, as they are not explicitly optimized for this task.

In this Chapter, following the same principles as recent SOTA methods, we aim to achieve competitive results that ensure reliable predictions, yet, using light-weight multi-modal prediction models that take as input the past trajectories of each agent, and integrate prior-knowledge about the map easily.

In that sense, throughout this Chapter we develop several multi-modal efficient MP models (social, map and augmented baselines) focused on the use of Graph Neural Networks (GNNs) and Attention mechanism as an alternative to the uni-modal GAN proposed in Chapter 5. The work in this Chapter was partially published in the following conference paper [113]: "Efficient Context-Aware Graph Transformer for Vehicle Motion Prediction", 2023 IEEE 26th International Conference on Intelligent Transportation Systems (ITSC). Additionally, the following paper: "Efficient Baselines for Motion Prediction in Autonomous Driving" has been sent for review (January 2023) to the IEEE Transactions on Intelligent Transportation Systems journal.

The main contributions of this Chapter are as following:

1. We identify a key problem in the size of motion prediction models, with implications in real-time inference and edge-device deployment.
2. Several open-source [1] efficient baselines (social, map and augmented) for vehicle MP are proposed, based on RNNs, GNNs and Attention mechanisms. Moreover, these

[1] https://github.com/Cram3r95/mapfe4mp

methods do not explicitly rely on an exhaustive analysis of the context HD map (either vectorized or rasterized), but on prior map information obtained in a simple heuristic-based preprocessing step, that serves as a guide in the prediction.

3. Our proposals use noticeable fewer parameters and operations (FLoating-point Operations per seconds (FLOPs)) than other SOTA models to achieve competitive performance on Argoverse 1 [6] with lower computational cost.

6.2. Efficient Baselines

Considering the trade-off between curated input data and complexity, we aim to achieve competitive performance in the MP using powerful DL techniques in terms of prediction metrics (minADE, minFDE), including attention mechanisms and GNNs, while reducing the number of parameters of operations with respect to other SOTA methods. In particular, we propose three baselines: social, map and augmented baseline.

It is important to note that both the social and map baseline refer to the same pipeline (Figure 6.1). The only inputs for the social baseline are the agent past trajectories and their corresponding interactions. On the other hand, for the map baseline, we propose an extension with respect to our previous target points proposals presented in Chapter 5 where, based on a simple-yet-powerful map pre-processing algorithm where the corresponding agent trajectory is initially filtered, the feasible area with which the agent can interact is computed. On the other hand, the augmented baseline (Figure 6.4) can be considered an improved version of the map baseline, where we focus on an enhanced encoding of the physical and social interaction, as well as its corresponding interaction.

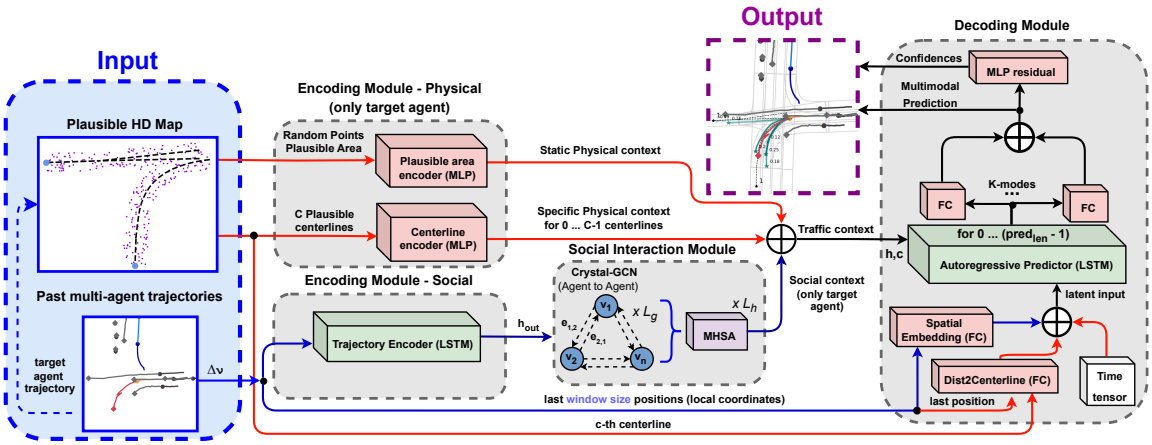

Figure 6.1: Overview of our Social and Map Efficient Baselines
(**Blue links** and **Red links** represent **Social** and **Map** information respectively).

Even though topological, semantic and geometric information are involved while computing the feasible physical information for the target agent, we only retrieve the geometric information of the feasible area proposals in an efficient and elegant way, both in the map

baseline and in the augmented baseline. Therefore, the map-based models do not require full-annotated (including, topological, geometric and semantic) HD map information as input or even rasterized BEV representations of the scene to compute the physical context.

Figure 6.1 illustrates an overview of the **social** and **map** baselines. We distinguish three main blocks:

- **Encoding Module**, which uses plausible HD map information (specific centerlines and driveable area around) and agents past trajectories to compute the motion and physical latent features.
- **Social Interaction module**, which calculates the interaction among the different agents and returns the most relevant social features.
- **Decoding Module**, responsible for calculating the multi-modal prediction by means of an auto-regressive strategy concatenating low-level map features and social features as a baseline, as well as iterating over the different latent centerlines for specific physical information per mode.

6.2.1. Social Baseline

Our social baseline is inspired in the architecture proposed by [13]. It uses as input the past trajectories of the most relevant obstacles as relative displacements to feed a LSTM-based Trajectory Encoder, as performed in Chapter 5. Then, node aggregation (each agent takes information from surrounding agents and vice-versa) is computed by means of several GNN layers, in particular Crystal-Graph Convolutional Network (GCN) layers [13], [114], and MHSA [74] to obtain the most relevant agent-agent interactions. Finally, we decode this latent information using an auto-regressive strategy where the output at the *i-th* step depends on the previous one for each mode respectively in the Decoding Module. The following sections provide in-depth description of the aforementioned modules.

6.2.1.1. Encoding Module - Social

In a similar way to the GAN-based model proposed in Chapter 5, in these efficient baselines we only consider the agents that have information over the full history horizon ($obs_{len} + pred_{len}$), reducing the number of agents to be considered in complex traffic scenarios. Nevertheless, instead of only substracting the origin of the scene (last position of the target agent) to make the model translation-invariant, we also rotate the whole coordinate system, *i.e.* the coordinate system is now centered on the target agent at $t = 0$, and we use the orientation from the target location in the same timestamp as the positive x-axis. Note that this representation will benefit the model to have a common representation to enhance the generalization of the model and prevent over-fitting. Once

the scene has been translated and rotated, instead of using absolute 2D-BEV (xy plane) local coordinates, the input for the agent i is a series of relative displacements.

Then, as stated in Chapter 5, we do not limit nor fix the number of agents per sequence, and a single LSTM-based Trajectory Encoder computes the deep features of the agents motion history. Finally, in order to feed the agent-agent interaction module (Social Attention Module in Figure 6.1), we take the output hidden vector (h_{out}).

6.2.1.2. Social Interaction Module

After encoding the past history of each vehicle in the traffic scenario, we compute the agent-agent interactions to obtain the most relevant social information of the scene. To this end, we make use of several GNNs layers and MHSA to model complex agent-agent interactions as an enhanced version with respect to the GAN approach proposed in Chapter 5. The main advantages of using GNNs for social interactions are as following:

- **Representation of spatial dependencies**: As stated in Chapter 3, GNNs are well-suited for capturing complex spatial relationships and dependencies among agents in a scene. In AD, understanding the interactions among different entities such as vehicles, pedestrians, and cyclists is crucial for accurate MP. Then, GNNs can effectively model these spatial dependencies by leveraging the graph structure of the scene, where objects are represented as nodes (v) and edges (e) capture their relationships, as illustrated in Figures 6.1.
- **Temporal modeling**: GNNs can naturally incorporate temporal information (processed in advance) by propagating messages across the graph structure over multiple time steps. This allows the model to capture the historical context and dependencies in the motion of objects. By considering past trajectories and interactions, GNNs can make more informed predictions about future motion.
- **Explainability and interpretability**: GNNs provide inherent interpretability by encoding the reasoning process within the graph structure. This interpretability is particularly important in safety-critical applications like AD, where the DM module (*i.e.* the next stage after the prediction module) needs to be explainable to humans.

In this particular case, we construct an interaction graph using Crystal-GCN layers [13], [114], originally developed for the prediction of material properties, allowing to efficiently leverage edge features.

Before creating the interaction mechanism, we split the temporal information in the corresponding scenes, taking into account that each traffic scenario may have a different number of agents. The interaction mechanism is defined in [13] as a bidirectional fully-connected graph, where the initial node features $v_i^{(0)}$ for the *i-th* agent in the graph are represented by the latent temporal information for each vehicle $h_{i,out}$ computed by

the motion history encoder. On the other hand, the edge from node k to node l is represented as the vector distance ($e_{k,l}$) between the position ν of both agents at t = obs_{len} in local coordinates, as stated in Equation 6.1. Note that the origin of the traffic scenario ($x = 0, y = 0$) is represented by the position of the target agent at t = obs_{len}:

$$e_{k,l} = \nu_k^{obs_{len}} - \nu_l^{obs_{len}} = \mathcal{L}_2(\nu_k^{obs_{len}}, \nu_l^{obs_{len}}) \tag{6.1}$$

Then, given the interaction graph, represented by a set of nodes (v = agent latent state) and edges (e = vector distance between last observations), the Crystal-GCN, proposed by [114], is defined as:

$$v_i^{(g+1)} = v_i^{(g)} + \sum_{j=0:j\neq i}^{N} \sigma\left(z_{i,j}^{(g)} W_{\mathrm{f}}^{(g)} + b_{\mathrm{f}}^{(g)}\right) \odot \mu\left(z_{i,j}^{(g)} W_{\mathrm{s}}^{(g)} + b_{\mathrm{s}}^{(g)}\right) \tag{6.2}$$

This operator, in contrast to many other graph convolution operators [14], [50], allows the incorporation of edge features in order to update the node features based on the distance among vehicles (the closer a vehicle is, the more is going to affect to a particular node). As stated by [13], we use L_g GNN layers ($g \in 0, \ldots, L_g$ denotes the corresponding Crystal-GCN layer) with Rectifier Linear Unit (ReLU) and batch normalization as non-linearities between the layers. σ and μ are the sigmoid and softplus activation functions respectively and $\odot$ denotes element-wise multiplication.

Moreover, $z_{i,j}^{(g)} = (v_i^{(g)} || v_j^{(g)} || e_{i,j})$ corresponds to the concatenation of two node features in the g_{th} GCN layer and the corresponding edge feature (distance between agents), N represents the total number of agents in the scene and W and b the weights and bias of the corresponding layers respectively.

After the interaction graph, each updated node feature $v_i^{(L_g)}$ contains information about the temporal and social context of the agent i. Nevertheless, depending on their current position and past trajectory, an agent may require to pay attention to specific social information. To model this, we make use of a scaled dot-product MHSA, which is applied to the updated node feature matrix $V^{(L_g)}$ that contains the node features $v_i^{(L_g)}$ as rows. Then, each head $h \in 1, \ldots, L_h$ is applied to the updated node feature matrix after the GCN layers as following:

$$\mathrm{head}_h = \mathrm{softmax}\left(\frac{V_{Q_h}^{(L_g)} V_{K_h}^{(L_g)T}}{\sqrt{d}}\right) V_{V_h}^{(L_g)}. \tag{6.3}$$

where $V_{Q_h}^{(L_g)}$ (Query), $V_{K_h}^{(L_g)}$ (Key) and $V_{V_h}^{(L_g)}$ (Value) represent the h_{th} head linear projections of the updated node feature matrix $V^{(L_g)}$ and d is the normalization factor corresponding to the embedding size of each head. The result of the softmax weights multiplied by the node feature matrix $V_{V_h}^{(L_g)}$ (Value) is often referred as the attention weight matrix, representing in this particular case pairwise dependencies among vehicles.

Finally, as stated in Chapter 5, the social attention matrix $SATT$ is computed as the combination of L_h different attention heads in a single matrix. As in the present Chapter our proposals are focused on the Argoverse 1 Motion Forecasting dataset, we only consider the row of the social matrix corresponding to the target agent for every traffic scenario.

6.2.2. Map Baseline

As aforementioned, we extend our social baseline using minimal HD map information (*i.e.* the map baselines includes both the past trajectories and map information), from which we discretize the plausible area $\mathcal{P}$ of the target agent as a subset of r randomly sampled points $\{p_0, p_1 ... p_r\}$ (low-level features) around the plausible centerlines (high-level and well-structured features) considering the velocity and acceleration of the corresponding agent in the last observation frame, as observed in Figure 6.2. As stated in Section 5.2, this is a map pre-processing step, therefore the model never sees the HD map (either vectorized or rasterized) image nor the whole graph of nodes.

6.2.2.1. Centerlines proposals and Plausible area

In a similar way to the target points computed in our GAN-based model, we want to compute the heuristic proposals for each agent. Nevertheless, instead of limiting the map baseline to some discrete target points, now we aim to compute the most plausible future centerlines (that is, the center of the lane) as a connection of nodes (waypoints). Considering lane connectivity, multiple approaches have tried to predict realistic trajectories by means of learning physically feasible areas as heatmaps or probability distributions of the agent future location [9], [87], [102]. [14] represents the map as a set of lanes and their connectivity (predecessor, successor, right neighbour, left neighbour), taking into account all lanes whose distance from the target agent is smaller than 100 m as the input, regardless the orientation or the velocity of the vehicle.

On the other hand, [115] encodes static elements such as crosswalks, lane, road boundaries and intersections that are included in a local map 150m x 100m centered in the corresponding vehicle as a multi-channel image. These approaches require either a top-view RGB BEV image of the scene, or a HD map with exhaustive topological, geometric and semantic information (commonly codified as channels). This information is usually encoded using a CNN and fed into the model together with the social agent's information [35], [87], [102].

As observed, when trying to utilize HD map information, specially in terms of lane proposals, most SOTA methods utilize this physical to enhance the latent information to decode the future trajectories, but heavy computation or raw data features are required.

Effectively and efficiently exploiting HD maps is a must for MP models to produce accurate and plausible trajectories in real-time applications, specifically in the field of

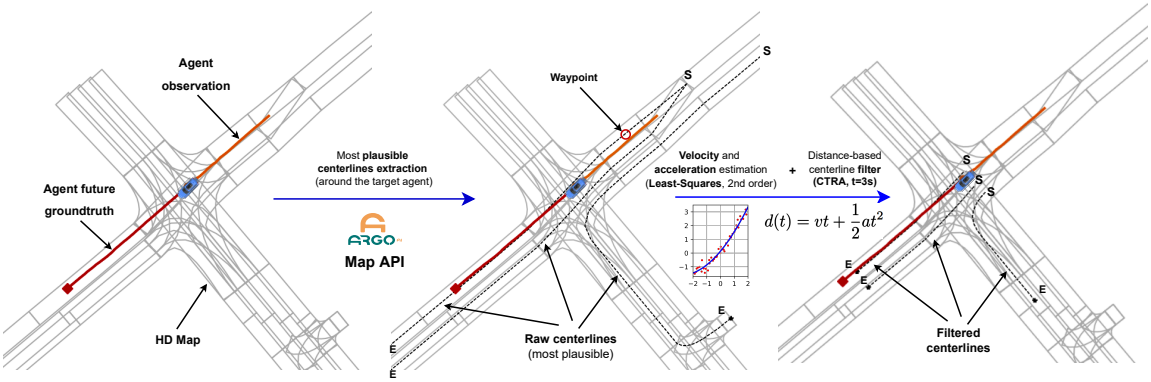

Figure 6.2: Plausible centerlines estimation. Left: General view of the scene, only considering the target agent (**observation (2s)** and **future ground-truth (3s)**) and HD map around its last observation (position of the **blue** vehicle). Center: **Raw Centerlines** proposed by the Argoverse Map Application Programming Interface (API) (maximum number of centerlines C set to 3). Right: We filter the input observation by means of Least-Squares (2^{nd}-order) algorithm to estimate the velocity and acceleration of the agent. Then, the distance considering a CTRA model and a prediction horizon of 3 s are used to obtain the end-points **E** of the final proposals **Filtered centerlines**. Start-points **S** are the closest centerlines waypoints to the agent in the last observation frame.

AD, providing specific map information to each agent based on its kinematic state and geometric HD map information. In that sense, we propose to obtain the most plausible C lane candidates by means of some heuristic functions proposed by the Argoverse 1 Motion Forecasting dataset Map API [6], [17]. By doing so, we will choose the closest centerlines to the last observation data of the target agent, which will represent its most representative future trajectories, as an enhanced and high-structured version of interpretable prior map information compared to the target points calculated in Chapter 5.

On the other hand, as depicted in the dataset used to train this model (Argoverse 1), vehicles are the only evaluated object category as the target agent. Then, considering a vehicle as a rigid structure with non-holonomic [52] features (no abrupt motion changes between consecutive timestamps) and the road driving task is usually described as anisotropic [116] (most relevant features are found in a specific direction, in this case the lanes ahead). In other words, the agent should follow a smooth trajectory in a short-mid term prediction.

The heuristic process to obtain these centerlines is summarized as follows:

1. Trajectory data presents noise associated to the real-world data capturing the exact position of the previously tracked vehices in real-world scenarios. Regarding this, we filter the agent trajectory as a polynomial curve fitting problem by means of the Least Squares (2^{nd}-order) per axis and Savitzky-Golais [117] algorithms to obtain a smooth representation of the position vector.

2. By doing so, and assuming the agent is moving with a constant acceleration, we are able to calculate the subsequent derivatives (velocity and acceleration) of the target agent in $t_{obs_{len}}$. Then, a vector of obs_{len} - 1 and obs_{len} - 2 length is computed to

estimate the velocity and acceleration respectively as $V_i = \frac{X_i - X_{i-1}}{t_i - t_{i-1}}$ and $A_i = \frac{V_i - V_{i-1}}{t_i - t_{i-1}}$, where $X_i = [x_i, y_i]$ represents the 2D position of the agent at each observed frame i.

3. In order to compute the velocity, acceleration and yaw angle in the last observation frame, we compute a weighted mean by assigning less importance (weight) to the first positions of the corresponding vector and higher importance to the latter states, in such a way immediate past observations are the key states to determine the current spatio-temporal variables of the agent, as depicted in Equation 5.2.

4. We compute the future travelled distance by means of the well-known CA model:

$$d(t) = x_0 + vt + \frac{1}{2}at^2 \tag{6.4}$$

where t corresponds to the prediction horizon $pred_{len}$, x_0 is equal to 0 since we want to determine the travelled distance from the current position and v and a are the velocity and acceleration in the last observation frame previously calculated. Note that we assume that this is a CTRA model, instead of only CA in a specific direction, since the orientation is implicit in the lane boundaries. That's why it does not make sense to involve the orientation at frame $t = 0$ in the travelled distance calculation.

5. Get all lane candidates within a bubble, given the agent last observation and Manhattan distance.

6. Expand the bubble until at least 1 lane is found.

7. Once some preliminary proposals are found, we employ the Depth First Search (DFS) algorithm to get all successor and predecessor candidates, merging the past and future candidates and removing the overlapping ones.

8. Then, we process these raw candidates so as to use them as plausible physical information. Given these raw lanes, we aim to limit the number of centerlines to a fixed number C. First, given the previously computed smoothed trajectory, we compute the closest centerlines to our current position since they will represent the most realistic future lanes in the traffic scenario. Second, we evaluate the above-mentioned travelled distance along the raw centerlines. We determine the end-point index p of the $c-th$ centerline as the waypoint (each discrete node of the centerline) where the accumulated distance (considering the $\mathcal{L}_2$ distance between each waypoint) is greater or equal than the above-computed $d(obs_{len})$:

$$p \quad : \quad d(obs_{len}) \leq \sum_{p=start_{point}}^{centerline_{length}} \mathcal{L}_2(w(p+1), w(p)) \tag{6.5}$$

9. Finally, in order to have the same points (particularly, the number of points matches the prediction horizon $pred_{len}$) per centerline, we interpolate them using a 1^{st}-spline

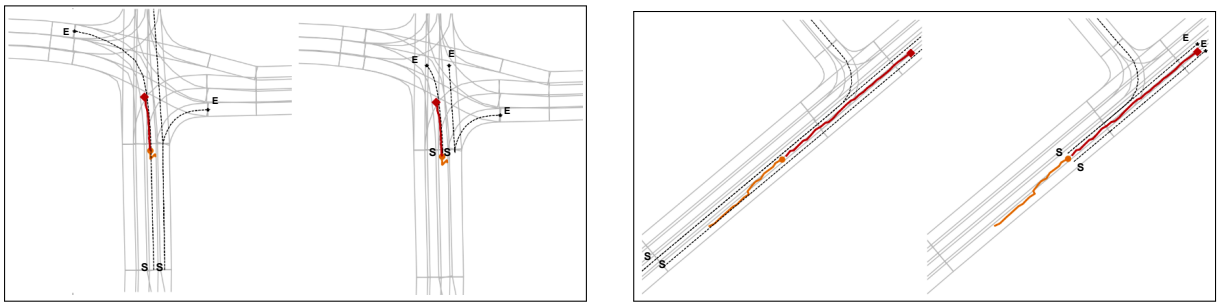

(a) (b)

Figure 6.3: Some challenging examples of our preprocessing step to obtain relevant map features. In both scenarios (a) and (b), the target agent (**observation (2s)** and **future ground-truth (3s)**) presents a noticeable noisy past trajectory and the provided raw **centerlines** do not consider the current kinematic state of the vehicle. (a) The agent is stopped (maybe due to an stop, pedestrian crossing or red traffic light use case). We estimate a minimum travelled distance of 25m in these situations to determine the centerline end-points **E**. (b) In this scenario, we can observe how the raw centerlines consider way more distance (both ahead and behind) than required. Our kinematic-based filter is able to minimize these proposals in an interpretable way to serve as prior information to the MP model

order, considering as start point the last agent observation and as end or goal point the aforementioned travelled distance along the corresponding centerline.

10. Note that if the number of proposed centerlines is lower than a pre-defined number C, a virtual centerline is created and padded with zeros.

Figure 6.2 summarizes this HD map filtering process, where we are able to estimate the preliminary centerlines proposals as a simplified version of the HD map. Moreover, Figure 6.3 illustrates how after our filtering process the end-points of the plausible centerlines are noticeable closer to the ground-truth prediction at the final timestep.

In addition to these high-level and well-structured map information, we apply point location perturbations to all plausible centerlines under a $\mathcal{N}(\mu, \sigma)$ [m] distribution [118] in order to discretize the plausible area $\mathcal{P}$ as a subset of r randomly sampled points $\{p_0, p_1 ... p_r\}$ around the plausible centerlines. We make use of a normal distribution $\mathcal{N}$ to calculate these random points. The main objective of calculating these low-level features is to have a common term for all plausible centerlines for the target agent, which will change in each iteration of the training process (in similar way to the target points proposed in Chapter 5), as an additional regularization term in a similar way that data augmentation is applied to the past trajectories.

6.2.2.2. Encoding Module - Physical

In order to calculate the latent map information, we employ a plausible area and centerline encoder (Figure 6.1) to process the low-level and high-level map features respectively. Each of these encoders is represented by an MLP. First, we flat the information along the points dimension, alternating the x-axis and y-axis information. Then, the corresponding MLP (three layers, with batch normalization, interspered ReLUs and dropout in the first

layer) transforms the interpretable absolute coordinates around the origin ($x = 0, y = 0$) into representative latent physical information. The static physical context (output from the plausible area encoder) will serve as a common latent representation for the different K modes, whilst the specific physical context will illustrate specific map information for each mode.

6.2.3. Augmented Baseline

Once the social and map baseline encoders are stated, we design an augmented baseline as an enhanced version upon the map baseline while keeping its structure as simple and efficient as possible, particularly improving the physical and social encoders by means of a combination of MLP/CNN, MHSA block and normalization. Moreover, the information fusion is performed using a Multi-Head Cross-Attention (MHCA) block since both feature vectors come from different sources of information. We illustrate this augmented baseline in Figure 6.4.

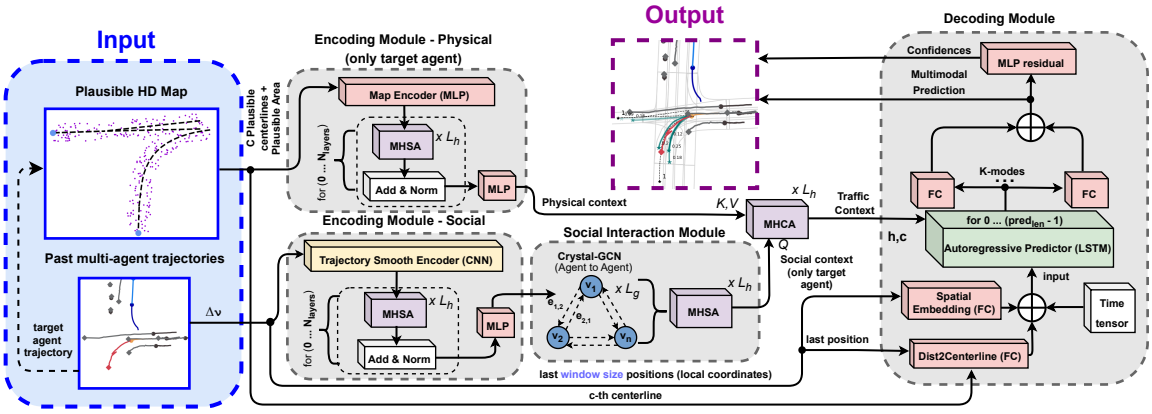

Figure 6.4: Augmented baseline with attention-based encoders and information fusion via cross-attention. Note that in this case we do not specifically differentiate between map and social information links since the augmented baseline uses both sources of information.

In terms of the physical encoder, instead of computing separately the latent space of the plausible area and the plausible centerlines (high-level features), in this case we concatenate the centerlines and the plausible area as following. More specifically, we generate T local perturbations for each waypoint of the centerline (*i.e.* a local area around the corresponding waypoint. In that sense, the map input which is received by the Map Encoder (see Figure 6.4) receives a 3D matrix of (C x $pred_{len}$ x $2 \cdot (T+1)$), where C is the number of centerlines in the traffic scenario, $pred_{len}$ the number of points per centerline that matches the prediction horizon, $2 \cdot (T + 1)$ the xy features of the corresponding waypoint and associated perturbations.

Once the map input has been pre-preprocessed, we first use an MLP-based Centerline encoder with a ReLU as non-linear layer to transform the input matrix into deep features, obtaining a matrix of size (C x $pred_{len}$ x h_{dim}), where h_{dim} represents the length of the

hidden vector. However, to predict the future trajectory, the separate feature of each vector is insufficient. For example, even if two road segments in the first half have the same structure, the difference in the last half can result in a total difference in geometric meaning. Therefore, we make use of a combination of MHSA, residual connection and layer normalization (also referred in the literature as "Add & Norm" block). This combination will be repeated N_{layers}, as illustrated in Figure 6.4, to encode the overall set of physical features per agent as a single vector. Finally, we adopt an MLP with a ReLU non-linear layer to aggregate the features of vectors within a traffic scenario. Now, we have a 2D matrix (B x h_{dim}), where B represents the number of traffic scenarios in the batch and h_{dim} the length of hidden features that summarizes the plausible future physical information for the target agent.

For agents, we use similar techniques to encode and aggregate the information. In particular, we use a CNN-based Trajectory Smooth Encoder block to encode each agent trajectory. Then, just like roads, even two agents have the same movement in the first half of their trajectory, the differences in the last half of trajectories can lead to a totally different future trajectory. Therefore, as aforementioned, we use a combination of MHSA, residual connection and layer normalization, to encode the overall features of a past trajectory in the observed time period and form a single feature vector for each agent. Finally, an MLP-based aggregator is used to construct a single feature vector for each trajectory.

One aspect worth mentioning is the trajectory encoder. While trajectory data are, unlike roads (well-structured) usually non-smooth, as expected from real-world datasets. Then, while we make use of MLP to compute the deep physical features, we use a 1D-CNN based motion encoder due to its wider receptive field compared with an MLP in such a way the convolutional encoder can smooth the trajectories and reduce the influence of noisy input trajectories.

The Social Interaction Module is the same than previous social and map baseline, where the Crystal-GCN and MHSA layers focus on modelling complex interactions among the relevant agents in the scene. Finally, as states in preonly consider the row of the social matrix corresponding to the target agent for every traffic scenario.

At this point, we have the Physical context and Social context (only target agent), as shown in Figure 6.4. Then, instead of concatenating the information, we make use of the MHCA mechanism to focus on the interaction between the features features that summarizes the social and physical information of the scene respectively. As illustrated in Chapter 3, in cross-attention there are two sources of information where one of the input sequences serves as the query (Q) sequence, while the other sequence serves as the key,value (K, V) sequence. Since in the present case we want to obtain the most representative social features according to the corresponding physical features, we set the social feature vector as Q and the physical feature vector as K, V. Then, the output

sequence has dimension and length of Q, though in our cases both the social and physical vector have the same length of hidden features h_{dim}.

6.2.4. Decoding module

The decoding module is the third component of our baselines (social, map and augmented), as observed in Figures 6.1 and 6.4. The decoding module consists of an LSTM network, which recursively estimate the relative displacements for the future timesteps, in the same way we studied the past relative displacements in the Motion History encoder.

Regarding the social baseline, the model uses the social context computed by the Social Interaction Module, only paying attention to the target agent row. Then, only the social context corresponds to the entire traffic context of the scenario, representing the input hidden vector h of the auto-regressive LSTM predictor.

In terms of the map baseline, for a mode k, we identify the traffic context as the concatenation of the social context, static physical context and specific physical context as stated in Section 6.2.2.2, which will serve as input hidden vector of the LSTM decoder. On the other hand, for the augmented baseline, the input hidden vector is identified as the most representative social features once the MHCA mechanism has computed the attention matrix between social and physical context.

For all our baselines, the initial cell vector c of the LSTM-based decoder is initialized with a vector of zeros of the same dimension than the input hidden vector.

Regarding the LSTM input, in the social baseline it is represented by the encoded past n (we refer this as the window size) relative displacements of the target agent after a spatial embedding (Fully Connected (FC) layer). In terms of the map and augmented baselines, we concatenate the encoded $\mathcal{L}_2$ between the current target agent position in local coordinates (which is updated in each prediction step) and the current centerline to the encoded past displacements. Note that for the map-based baselines, in addition to traffic context that serves as the input hidden vector for the LSTM-based predictor, we incorporate a different centerline c per mode k to enhance the variability of the multi-modal prediction (note that if $k > c$, *i.e.* the mode index in higher than the centerline index, the corresponding centerline is repeated). Furthermore, we also concatenate a time tensor which represents the current scalar timestep value t to help the predictor understand the time order of the input matrix, as shown in Figures 6.1 and 6.4.

The output size of the LSTM-based predictor is common to the different baselines, which will be processed by a standard FC layer (one per mode) to obtain the multi-modal relative prediction at the timestep t. Moreover, as aforementioned, we do not compute as input to the auto-regressive decoder the latent space based on the relative displacement of the target agent at t=obs_{len}, but we compute the n past relative displacements. Then, once we calculate a new multi-modal prediction, we shift the initial past observation data

in such a way we introduce our last-computed relative displacement at the end of the vector, removing the first element of the buffer. We refer this technique as temporal decoder, where a window of size n is analyzed by the auto-regressive decoder in contrast to other techniques [31], [87], [102] where only the last relative position is considered.

Finally, after transforming the decoder output to local coordinates by aggregating all relative predictions per mode, and from local to global coordinates (sum the origin of the traffic scenario and counter-rotate the scene according to the original pre-preprocessing step), we obtain our multi-modal predictions $\hat{Y} \in \mathbb{R}^{K \times pred_{len} \times data_{dim}}$, where K represents the number of modes, $pred_{len}$ represents the prediction horizon and $data_{dim}$ represents the data dimensionality, in this case xy, predictions from the BEV perspective. Once the multi-modal predictions are computed, they are concatenated and processed by a residual MLP and sotfmax operation to obtain the confidences (all confidences must sum 1), the higher a mode's confidence, the more likely it is to be close to the ground-truth of the traffic scenario.

6.2.5. Losses

We use the standard Negative Log Likelihood (NLL) loss to train our baselines in order to compare the ground-truth points $Y \in \mathbb{R}^{pred_{len} \times data_{dim}} = \{(x_0, y_0)...(x_{pred_{len}}, y_{pred_{len}})\}$ with our multi-modal predictions ($\hat{Y} \in \mathbb{R}^{k \times pred_{len} \times data_{dim}}$), given K modalities (hypotheses) $p = \{(\hat{x}_0^1, \hat{y}_0^1)...(\hat{x}_{pred_{len}}^K, \hat{y}_{pred_{len}}^k)\}$, with their corresponding confidences $c = \{c_1...c_K\}$ using Equation 6.6:

$$\text{NLL} = -\log \sum_K e^{\log c^K - \frac{1}{2}\sum_{t=0}^{pred_{len}} (\hat{x}_t^K - x_t)^2 + (\hat{y}_t^K - y_t)^2} \tag{6.6}$$

Similar to [34], we assume the ground-truth points to be modeled by a mixture of multi-dimensional independent normal distributions over time (predictions with unit covariance). Minimizing the NLL loss maximizes the likelihood of the data for the forecast. Nevertheless, the NLL loss tends to overfit most predictions in a similar direction.

As stated above, in the MP task, specially in the AD field, we must build a model that not only reasons multi-modal predictions in terms of different maneuvers (keep straight, turn right, lane change, etc.) but also different velocity profiles (constant velocity, acceleration, etc.) regarding the same maneuver. For this reason, after the baseline models have been trained, as stated by [58], we add as regularization the Hinge (also referred in the literature as max-margin) and Winner-Takes-All (WTA) [14], [58] losses to improve the confidences and regressions respectively.

Algorithm 6.1 illustrates how we compute the max-margin and WTA losses. First, we determine the closest mode k^* to the ground-truth using the $\mathcal{L}_2$ distance, only considering the end-points. Then, WTA loss is computed using Smooth $\mathcal{L}_1$ distance taking into

account in this case the whole prediction horizon between the best mode and ground-truth prediction. Finally, we apply the max-margin loss regarding the confidence of the best mode and a margin (ϵ).

Algorithm 6.1: Additional regularization: Hinge and WTA losses computation

input: ground-truth trajectory ($Y \in \mathbb{R}^{pred_{len} \times data_{dim}}$) and output trajectories ($\hat{Y} \in \mathbb{R}^{K \times pred_{len} \times data_{dim}}$), where K, $pred_{len}$, and $data_{dim}$ denote the number of modes, prediction horizon, and data dimensionality for the target agent.

output: classification loss $\mathcal{L}_{Hinge}$ and regression loss $\mathcal{L}_{WTA}$

for k *in* $\{1, 2, \ldots, K\}$ **do**
  $d^m_{wta} \leftarrow \mathcal{L}_2$ between $\hat{Y}^m_{pred_{len}}$ and $Y_{pred_{len}}$;
end
$k^* = \arg\min_k d^k_{wta}$;
$\mathcal{L}_{reg,WTA} \leftarrow$ Smooth $\mathcal{L}_1$ loss between $\hat{Y}^{k^*}$ and Y;
$\mathcal{L}_{class,Hinge} = \frac{1}{(K-1)} \sum_{k=1 \setminus k \neq k^*}^{K} \max(0, c_k + \epsilon - c_{k^*})$;
return $\mathcal{L}_{WTA}$, $\mathcal{L}_{Hinge}$;

Therefore, our final loss function for the social, map and augmented baselines is as following:

$$\mathcal{L} = \lambda_{NLL}\mathcal{L}_{NLL} + \lambda_{Hinge}\mathcal{L}_{Hinge} + \lambda_{WTA}\mathcal{L}_{WTA} \tag{6.7}$$

6.3. Experimental Results

As we state in previous Sections, our main goal is to achieve competitive results while being efficient in terms of model complexity, particularly considering FLoating-point Operations per seconds (FLOPs) and model parameters, in order to enable these models for real-time operation. For this reason, we have proposed light-weight models, whose main input is the history of past trajectories of the agents, complemented by interpretable map-based features.

6.3.1. Implementation details

To validate these efficient baselines (social, map and augmented baseline), we use the Argoverse 1 Motion Forecasting dataset. In terms of evaluation metrics, we evaluate the performance of our models using the standard metrics minADE and minFDE. Unlike the GAN-based model, the output of the models in this Chapter is multi-modal, then we generate K outputs (*a.k.a.* modes) per prediction step.

We report results for $K = 1$ (uni-modal case, only the mode with the best confidence is considered) and $K = 6$, as this is the standard in the Argoverse 1 in order to compare with other models.

We train our models to convergence using a single NVIDIA RTX 3090, and validate our results on the official Argoverse 1 validation set [6]. We use ADAM optimizer with

learning rate 0.001 and default parameters, batch size 128 and linear LR scheduler with factor 0.5 decay on plateaus (every 5K iterations) and batch size 128.

We rotate the whole scene regarding the orientation in the last observation frame of the target agent to align this agent with the positive x-axis.

By default, all MLP, FC, LSTM encoder/decoder, GCN and attention layers have a latent dimension of 128. We consider T=2 local perturbations ($\mathcal{N}(0, 0.1)$ [m]) for each waypoint of the corresponding centerline, representing local areas around the waypoints, in both the map and augmented baselines. In terms of the Trajectory Encoder (social), both the hidden state and cell state are initialized with a vector of zeros of the same length. We set the number of Crystal-GCN layers $L_g = 2$ and the number of attention heads $L_h = 4$ for all our attention-based mechanisms in the different baselines. Furthermore, regarding the augmented baseline, the number of layers for each encoder (*i.e.* combination of attention, residual connection and layer normalization) is set to 2.

In terms of the auto-regressive predictor, the Spatial Embedding and Dist2Centerline are two FC layers that encode the past data and distance to the specific centerline using a window size n of 20. We set the number of plausible centerlines (C) as 3, which cover most cases (if less than 3 plausible centerlines are available, we add padded centerlines as vector of zeros). The time tensor is a single scalar that represents the current timestep, in such a way the LSTM input is *(2 × window size) + 1 = 41*.

The regression head is represented by K=*6* FC layers which compute the output hidden state returned by the LSTM to the final output relative displacements (dim = 2, xy). Multi-modal predictions are processed by an MLP residual of sizes 60, 60 and 6 with interspersed ReLU activations in order to obtain the corresponding confidences.

In terms of data augmentation, we make use of (i) Dropout and swapping random points from the past trajectory, (ii) point location perturbations under a $\mathcal{N}(0, 0.2)$ [m] noise distribution [118]. Furthermore, in a similar way to the class balance conducted in Chapter 5, we want to focus on training with hard samples to improve the model generalization under difficult scenarios. Nevertheless, after further study, we realize that the baselines heavily failed not only in complex intersections where different directions are possible, but also in traffic scenarios (particularly highways) with sudden acceleration changes, such as emergency breaks or accelerating after a pedestrian crossing or red traffic light scenarios. In that sense, as stated in Chapter 3, we apply the well-established hard-mining technique to improve the model generalization under difficult scenarios. To perform this technique, once a given baseline is trained, we iteratively find the most difficult scenes in terms of minADE in the training dataset. Then, we mine those scenes such that the corresponding baseline performs poorly, and increase their proportion in the batch during training. In our particular case, when hard-mining is applied, we fill the 10 % of the batch with random mined cases.

Finally, if only NLL is applied, we set $\lambda_{NLL} = 1$, whilst if additional regularization with WTA and Hinge losses is applied, $\lambda_{NLL} = 1$, $\lambda_{Hinge} = 0.1$ and $\lambda_{WTA} = 0.65$ initially, and can be adjusted during training (especially $\lambda_{WTA} = 1$).

6.3.2. Comparative with the state-of-the-art

We analyze several ablation studies in the validation set, and prove the benefits of our approaches for vehicle MP. Table 6.1 and Table 6.2 illustrate our ablation study regarding our social, map/augmented baselines respectively (note that map and augmented baselines are included in the same table since both methods include social and map information). In that sense, the best social model will be used as baseline for the map baseline, and the map baseline best configuration will be used as inspiration to conduct the ablation study for the augmented baseline, which represents the most advanced method proposed in this Chapter. Finally, after conducting the corresponding ablation studies, we compare the best experimental setups with other SOTA approaches in the Argoverse 1 test set.

6.3.2.1. Ablation studies

Regarding the social baseline, we compare it with other SOTA models [13], [14], [17] without map information or with the corresponding module disabled. Our baseline social (LSTM-128, GNN with L_g=2, MHSA with L_h=4, without temporal decoder and trained with NLL, as illustrated in Table 6.1), presents a number of 351K parameters and 0.87 / 1.63 for minADE and minFDE (K=6) respectively.

Table 6.1: Ablation Study for map-free MP on the Argoverse 1 validation set. Our methods are indicated with †, whilst out best method without additional regularization techniques is marked as Best Social Baseline (BSB). Prediction metrics (minADE, minFDE) are reported in meters. We bold the best results in **black** and the second best in **blue** for each metric.

Method	Number of Parameters ↓	$K=1$		$K=6$	
		minADE ↓	minFDE ↓	minADE ↓	minFDE ↓
TPCN [118]	-	**1.42**	**3.08**	0.82	**1.32**
LaneGCN [14] (w/o map)	$\approx 1M$	1.58	3.61	**0.79**	**1.29**
WIMP [17] (w/o map)	$> 20M$	1.61	5.05	0.86	1.39
CRAT-Pred (LSTM + GNN + Residual head) [13]	449K	1.44	3.17	0.86	1.47
CRAT-Pred (LSTM + GNN + MHSA + Residual head) [13]	515K	**1.41**	**3.10**	0.85	1.44
† LSTM-128 + GNN + MHSA (Baseline social)	351K	1.82	3.72	0.87	1.63
† LSTM-64 + GNN + MHSA	**97K**	1.83	3.74	0.89	1.62
† LSTM-128 + GNN + MHSA + Residual head	552K	2.02	4.16	1.02	1.95
† LSTM-128 (Temporal Decoder (TempDec)) + GNN + MHSA	365K	1.81	4.04	0.83	1.57
† LSTM-64 (TempDec) + GNN + MHSA (Best Social Baseline (BSB))	**105K**	1.79	4.01	0.81	1.56
† BSB + Hard-Mining (HardM) (10 %)	**105K**	1.76	3.97	0.80	1.53
† BSB + HardM (10 %) *w/* Hinge + WTA losses	**105K**	1.62	3.57	**0.76**	1.43

We perform the following ablation studies in Table 6.1:

1. Reduce hidden dimension (including LSTM, GNN and MHSA modules) from 128 to 64.
2. Substitute the auto-regressive LSTM-based predictor with residual head (directly decode from the latent space with MLP).

3. Replace only last encoded position (standard auto-regressive decoder input) with last n (window size) encoded positions (temporal decoder).

We observe how the results are quite similar with hidden dimension = 64, decreasing the number of parameters by 72.4 %. Surprisingly, linear residual, standard in most MP models, presents worse results with a much higher number of parameters, since most works use it in a non-auto-regressive way where predictions are directly decoded from the latent space. On the other hand, using temporal decoder instead of only the last position as LSTM input achieves better results with a slightly higher number of parameters. Then, since in this thesis we focus on the trade-off between lightness and accuracy, we conclude our Best Social Baseline (BSB), as a preliminary stage before studying the map and augmented baselines, presents the following modifications: social hidden dim = 64 and temporal decoder. Hard-mining and additional losses (Hinge and WTA) applied to the Best Social Baseline (BSB) achieve best social results.

On the other hand, to integrate the map features (Table 6.2) we start from the BSM without hard-mining and with the initial loss (NLL), in order to check how implementing these additional regularization terms at the end help all proposed models to generalize better (social, map and augmented). We perform the following ablations:

1. Compute the most plausible centerline (also referred as oracle in the literature) (C=1) provided by the Argoverse API.
2. Consider the most plausible C=3 centerlines.
3. Replace Centerline encoder (MLP-based) with 1D-CNN, as proposed by [34].
4. Explicitly iterate over all centerlines (one centerline per mode. If $m > c$, the corresponding centerline is repeated) as specific deep physical context instead of decoding from a common latent space.
5. Add low-level features (Random points from the plausible area, encoded by an MLP) as a common static deep physical context for each iteration.
6. Add an additional component to the LSTM input given the concatenation of the time tensor and the vector distance between the last position (in local coordinates) and the corresponding centerline.

It can be observed that, since the map and augmented baselines have essentially the same information with a different encoding branch, we include the ablation studied related to the augmented baseline in Table 6.2, given the best configuration of the map baseline as base model. Additional regularization terms (hard-mining and Hinge/WTA losses) will be applied to both the best map baseline and best augmented baseline to check generalization.

Table 6.2: Ablation Study for map-based motion forecasting on the Argoverse 1 validation set. Our methods are indicated with †. Prediction metrics (minADE, minFDE) are reported in meters. We bold the best results in **black** and the second best in **blue** for each metric.

Method	Number of Parameters ↓	$K=1$		$K=6$	
		minADE ↓	minFDE ↓	minADE ↓	minFDE ↓
† Our Map-free Baseline (Best Social Baseline (BSB), No Hard-mining, Loss = NLL)	**105K**	1.79	4.01	0.81	1.56
LaneGCN [14]	3.7M	**1.35**	**2.97**	**0.71**	**1.08**
WIMP [17] (w/o map, NLL loss)	$> 25M$	**1.41**	6.38	1.07	1.61
WIMP [17] (w/o map, WTA loss)	$> 25M$	1.45	3.19	0.75	**1.14**
† BSB + C=1 (oracle)	**277K**	1.62	3.56	0.79	1.42
† BSB + C=3	307K	1.60	3.53	0.77	1.36
† BSB + C=3 (1D-CNN)	432K	1.63	3.59	0.78	1.39
† BSB + C=3 loop	326K	1.62	3.41	0.76	1.40
† BSB + C=3 loop + Feasible area	458K	1.62	3.40	0.75	1.36
† BSB + C=3 loop + Feasible area + Dist2Centerline (Best Map Baseline (BMB))	459K	1.61	3.40	0.75	1.32
† BMB + Attention Encoders	587K	1.52	3.24	0.74	1.28
† Best Map Baseline (BMB) + Attention Encoders + MHCA (Best Augmented Baseline (BAB))	552K	1.48	3.16	0.73	1.21
† BMB + HardM (10 %)	459K	1.55	3.31	0.74	1.36
† BMB + HardM (10 %) *w/* Loss Hinge + WTA	459K	1.46	3.22	0.73	1.28
† BAB + HardM (10 %)	552K	1.45	3.12	**0.72**	1.17
† Best Augmented Baseline (BAB) + HardM (10 %) *w/* Loss Hinge + WTA	552K	**1.41**	**3.06**	**0.72**	**1.14**

As expected, introducing map features increases the number of parameters in exchange of a noticeable metrics decrement, specially in terms of minFDE ($K = 6$) since this information provides the model with better scene understanding. Even though in most situations the oracle (Argoverse 1 refer this as the most plausible C=1 centerline provided by its API) will be the most probable future lane, considering C=3 centerlines allows the model to compute a more diverse set of predictions. On the other hand, replacing a standard MLP (Plausible centerline encoder in Figure 6.1) with 1D-CNN encoder noticeable increases the number of parameters achieving slightly worse metrics, according to this experimental setup.

Previous experiments have decoded future relative displacements from a common latent space. Next ablation studies focus on iterating (loop in Table 6.2) over different information per node. Nevertheless, since we considering at most C=3 centerlines, and multi-modal prediction is focused on K=6 in Argoverse 1, if the mode index m is higher than the centerline index c, the latent centerline information is repeated. We observe that providing specific latent information for the LSTM-based predictor and corresponding FC also allows the model to compute a more diverse set of predictions.

Moreover, we include some random points from the plausible area (low-level features, particularly T=2) as a deep static physical context which is common to all iterations over the different centerlines and an additional vector distance between the last position in local coordinates to the corresponding centerline, achieving our best results without additional regularization terms (hard-mining and Hinge / WTA losses). We define this last configuration as Best Map Baseline (BMB) in Table 6.2, with 459K parameters and 0.75 / 1.39 for minADE/minFDE (K=6) respectively.

Finally, given BMB, *i.e.* hidden dimension = 64, C=3, static information from the plausible area (T=2 local perturbations associated to each waypoint of the corresponding centerline), specific centerline per mode and temporal decoder n (window size) = 20, we conduct two additional experiments to obtain the final configuration of the augmented baseline:

1. Replace MLP-based social and map encoders with attention-based encoders.
2. Substitute social and map features concatenation with MHCA.

As expected, replacing the map and social encoders (MLP-based, see Figure 6.1) with a combination of 1D-CNN/MLP, MHSA, residual connections and layer normalization, reduces the metrics both in terms of uni-modal and multi-modal prediction. Moreover, we are able to reduce the number of parameters and error metrics at the same time when implementing MHCA instead of concatenating the social and map features. The reason is simple: When concatenating, the actual input hidden dimension of the LSTM-based predictor is $2x$ the hidden dimension of the social/map features vector. However, when using MHCA, as illustrated in Chapter 3, the dimension of the output is the same than the vector length of the query. Then, while the use of the attention mechanism provides the model a more complex way to pay attention to the most relevant features (so, increasing the number of parameters and operations *w.r.t.* a simple concatenation), it actually reduces the complexity of the overall model since the input hidden dimension to the LSTM-based decoder is reduced by half compared to the experiments where both feature vectors were concatenated.

After both ablation studies (map-free and map-based architectures), our models (social, map and augmented baselines) achieve regression metrics (minADE and minFDE with both K=1 and 6) up-to-pair with other SOTA models with a noticeable lower number of parameters, specially in the ablation study for map-based MP models, demonstrating how focusing on the most important future lanes and random points around (high-level and low-level physical features), given an CA-based estimation of the travelled distance as shown in Section 6.2.2.1, drastically decreases the network complexity obtaining similar results in terms of accuracy. This representation not only gathers information about the feasible area around the agent, but also represents potential goal points [102] (*i.e.* potential destinations or end-of-trajectory points for the agents). Moreover, this information is *"cheap"* and interpretable, therefore, we do not need further exhaustive annotations from the HD map in comparison with other methods like HOME, which gets as input a 45-channel encoded map [9].

6.3.2.2. Argoverse 1 Motion Forecasting benchmark and Efficiency discussion

In terms of the test set, at the moment of writing this thesis (2023), the Argoverse 1 Motion Forecasting Benchmark [6] has over 290 submitted methods. However, the top approaches achieve, in our opinion, essentially the same performance. In order to do a fair comparison, we analyze the *state-of-the-art* performance in this benchmark, we show the results in Table 6.3. Given the standard deviations (in meters) of the most important regression metrics (minADE and minFDE, both in the uni-modal and multi-modal case), we conclude that there are no significant performance differences for the top-25 models. In

Table 6.3: Results on the Argoverse 1 Motion Forecasting Leaderboard. We borrow some numbers from [6], [9], [10]. We specify the map info for each model: Raster, GNN or polyline, as stated in Table 2.1. We indicate the error difference of our best method *w.r.t.* top-25 SOTA methods, in centimeters. Our predictions differ *w.r.t.* top-25 SOTA only 6cm and 10cm for the uni-modal and multi-modal minADE metric respectively, yet our model is much more efficient. We bold the best results in **black** and the second best in **blue** for each metric. Our methods are indicated with †. TP = Target Points, CB = Class Balance.

Model	Map info	K=1		K=6	
		minADE ↓	minFDE ↓	minADE ↓	minFDE ↓
Constant Velocity [6]	-	3.53	7.89		
Argoverse Baseline (Nearest Neighbour) [6]	-	3.45	7.88	1.71	3.29
Argoverse Baseline (LSTM) [6]	Polyline	2.96	6.81	2.34	5.44
TPNet-map-mm [112]	Raster	2.23	4.70	1.61	3.70
Challenge Winner: uulm-mrm (2nd) [6]	Polyline	1.90	4.19	0.94	1.55
Challenge Winner: Jean (1st) [6], [34]	Polyline	1.74	4.24	0.98	1.42
TNT [18]	GNN	1.77	3.91	0.94	1.54
mmTransformer [119]	Polyline	1.77	4.00	0.84	1.33
HOME [9]	Raster	1.72	3.73	0.92	1.36
LaneConv [120]	Raster	1.71	3.78	0.87	1.36
LaneGCN [14]	GNN	1.70	3.77	0.87	1.36
LaneRCNN [50]	GNN	1.70	3.70	0.90	1.45
GOHOME [10]	GNN	1.69	3.65	0.94	1.45
† Attention-based GAN [108], including CB and TP	Polyline	1.73	4.07	-	-
SOTA (top-10) [10], [11], [118], [119]		**1.57**±0.06	**3.44**±0.15	**0.79**±0.02	**1.17**±0.04
SOTA (top-25) [10], [11], [118], [119]		**1.63**±0.08	**3.59**±0.20	**0.81**±0.03	**1.22**±0.06
† BSB, including HardM and losses	-	1.89	4.19	1.26	2.67
† BMB, including HardM and losses	Polyline	1.72	3.89	0.96	1.63
† BAB, including HardM and losses	Polyline	1.71 (8cm)	3.75 (26cm)	0.91 (10cm)	1.49 (27cm)

fact, as stated in Chapter 2, Argoverse 2 [7] explicitly mentions that there is a *"goldilocks zone"* of task difficulty in the Argoverse 1 test set, since it has begun to plateau.

Regarding the efficiency discussion (also considering the test set), to the best of our knowledge, very few methods reports efficiency-related information [9], [10], [35], [119]. Furthermore, comparing runtimes is difficult, as only a few competitive methods provide code and models. The Argoverse 1 Motion Forecasting benchmark [6] provides insightful metrics about the model performance, mainly related with the predictions error. However, there are no metrics about efficiency (*i.e.* model complexity in terms of parameters or FLoating-point Operations per seconds (FLOPs)). In the AD context, we consider these metrics as important as the error evaluation because, in order to design a reliable ADS, we must produce reliable predictions on time, meaning the inference time (related to model complexity and inputs) is crucial.

SOTA methods already provide predictions with an error lesser than 1 meter in the multi-modal case. In our opinion, an accident will rarely happen because some obstacle predictions are offset by one or half a meter, this uncertainty in prediction can be acceptable in the design of an ADS, but rather because lack of coverage or delayed response time.

Despite its high accuracy and fast inference time, LaneGCN [14] makes use of multiple GNN-based layers that can lead to issues with over-smoothing for map-encoders [121].

Moreover, as mentioned in [35], CNN-based models for processing the HD map information are able to capture social and map interactions, but most of them are computationally too expensive. LaneRCNN [50] adds huge number of hyperparameters to the model, making it quite complex since it proposes to capture agent and map interactions with a local interaction graph per agent, not just a single vector.

Table 6.4: Efficiency comparison of our baselines against SOTA methods. We show the number of parameters for each model, FLOPs, minADE (K=6) in the Argoverse test set, and runtime. Works from [35] and [108] focus on uni-modal predictions (K=1). *N/A* stands for *Not Available*. Time measured on a RTX 2080 Ti (using batch 32). Some numbers are borrowed from [122], [123]. We bold the best results in **black** and the second best in **blue** for each metric. Our methods are indicated with †. TP = Target Points, CB = Class Balance.

Model	# Parameters [M] ↓	FLOPs [G] ↓	minADE [m] ↓	Runtime [ms] ↓
CtsConv [124]	1.08	0.34	1.85	684
R18-k3-c1-r100 [35]	0.25	0.66	2.21	*N/A*
R18-k3-c1-r400 [35]	0.25	10.56	2.16	*N/A*
VectorNet [35]	**0.072**	0.41	1.66	1103
DenseTNT (w/ 100ms opt.) [125]	1.1	0.763	0.88	2644
DenseTNT (w/ goal set pred.) [125]	1.1	0.763	0.85	531
LaneGCN [14]	3.7	1.071	0.87	173
mmTransformer [119]	2.607	0.177	**0.84**	*N/A*
MF-Transformer [126]	2.469	0.408	**0.82**	*N/A*
GOHOME [10]	0.40	0.09	0.94	32
† Attention-based GAN [108], including TP + CB	0.196	**0.018**	1.73	**12**
† BSB, including HardM and losses	**0.105**	**0.007**	1.26	**7**
† BMB, including HardM and losses	0.459	0.047	0.96	31
† BAB, including HardM and losses	0.552	0.038	0.91	16

Similar to image classification, where model efficiency depends on its accuracy and parameters/FLOPs, we use the same criteria to compare models. We show the **efficiency comparison** with other relevant methods in Table 6.4. Some minor operations were not supported, yet, their contributions to the number of FLOPs were residual and ignored. The results for the other methods are consulted from [9] [10] [35] [126]. We calculate FLOPs (assuming the relation: GMACs $\approx 0.5 * \text{GFLOPs}$) and parameters using a third-party library [2].

In order to calculate the FLOPs, we follow the common practice [35] [125] [10] of fixing the number of lanes, in our case limited to $C = 3$. [35] compares its GNN backbone with CNNs of different kernel sizes and map resolution to compute deep map features (decoder operations and parameters are excluded, min), demonstrating how CNN based methods noticeably increase the amount of parameters and operations per second. We do not require CNNs to extract features from the HD map since we use our map-based feature extractor to obtain the feasible area (see Section 6.2.2), assuming anisotropic driving (the most important features are ahead) and non-holonomic constraints, in such a way these features are interpretable in comparison with CNNs high-dimensional outputs. Note that, in all variants (social, map and augmented baselines), the self-attention module is used with a dynamic number of input agents, this typically implies a quadratic growth

[2] https://github.com/facebookresearch/fvcore

in complexity with the number of agents in the scene [74], yet, this only applies to the MHSA layers.

In summary, as observed in Table 6.3 and Table 6.4, even though our baselines do not obtain the best regression metrics (either K=1 or K=6), we achieve up-to-pair with a number parameters and number of operations (FLOPs) several orders of magnitude smaller than other approaches [125] [14], obtaining a good trade-off (specially the map and augmented baselines) between model complexity and accuracy, making it suitable for real-time operation in the field of AD.

Considering our best proposal (augmented baseline) and the top-25 regression metrics, we achieve near SOTA results (just 10 cm, which represents 12.6 %, worse in terms of minADE K=6) while achieving an impressive reduction of parameters and FLOPs. As observed in Table 6.4, if we compare our final model, which includes social information, agents interaction, preliminary road information, attention-based encoders and cross-attention, and the methods with the closest minADE K=6 (LaneGCN [14], HOME [9] and GOHOME [10]), we obtain a reduction of 96 %, 99 % and 48 % respectively in terms of FLOPs. It can be observed how including preliminary road information assuming non-holonomic [52] and anisotropic [116] constraints respectively (that is, we mostly focus on the front driveable area) instead of processing the whole map, as well as computing social interactions via graph convolutional networks, boost our model for further integration edge-computing devices with a minimum accuracy loss acceptable for real-world AD applications.

Moreover, as it is well known in ML, the number of parameters is not always proportional to the inference speed. In that sense, we may observe how our augmented baseline presents more parameters than the map baseline (552K vs 459K), but the number of operations and inference time is reduced. The reason is simple: As stated in Chapter 3, transformers are highly parallelizable, meaning that they can process inputs in parallel, which accelerates training and inference. In contrast, LSTM networks are inherently sequential in nature, as the recurrent connections require information from previous time steps to be processed before moving on to the next step. Then, by means of the attention-based encoders and cross-attention, the augmented baseline has slightly more parameters with a reduced inference time and number of FLOPs.

6.3.3. Qualitative results

We prove our best model (BAB) qualitatively in Figure 6.5. In particular, from left to right, we illustrate:

- A general overview of the traffic scenario, including the relevant objects considered in our models (*i.e.* those agents which are present in the full observation horizon $obs_{len} + pred_{len}$).

- Estimated centerlines (max C=3), including local perturbations around the corresponding waypoints. Note that these centerlines are filtered in such a way the falls exactly below the center of the ego-vehcile (*i.e.* LiDAR frame), and the last centerline waypoint represents the waypoint where the ego-vehicle would travel the corresponding distance calculated by our heuristic algorithm (see Section 6.2.2.1).
- Uni-modal prediction (only for the target agent), that is, the mode with the highest confidence according to our prediction module.
- Multi-modal prediction, where different plausible future behaviours, not only in terms of directions but also considering different velocity profiles, are considered.

As observed, each row represents a challenging scenario. First row illustrates the target agent approaching to an intersection, which will presumably turn left. The preprocessing step model returns three plausible centerlines (turn left and keep straight). Regarding the past information of the agent, social interactions and lanes information, the model correctly predicts most future trajectories (which have the highest confidences) close to the ground-truth even though it predicts one trajectory to keep straight, in such a way both different directions and velocity profiles are appreciated in the same output.

Second row is similar to first row, where the target agent is approaching from the right and the model clearly predicts two plausible directions (keep straight and turn left). Nevertheless, compared to first row, the target agent past trajectory is conducting a simple CV trajectory, so the model reasons that most predictions will just keep straight with different velocity profiles.

Third row illustrates a specially challenging traffic scenario, where the target agent is moving quite slow, probably due to the presence of a regulatory element (*e.g.* red traffic light or pedestrian crossing), since agents behind are also stopped or with low speed. As expected, with a naive physics-based MP model it would be impossible to predict near the ground-truth, which turns right with a high velocity compared to the previous past trajectory. In fact, it can be appreciated in its uni-modal prediction that the mode with the highest confidence assumes the vehicle will move with nearly the same velocity. Then, multi-modal prediction helps us to solve to these situations. It can be clearly observed, as expected, that the further the modes are from the original trajectory, the more uncertain they will be, but they could happen. That is why considering in future steps (*e.g.* local planning, DM, etc.) should take into account not only the trajectories but also their confidences to compute the optimal future action for the ego-vehicle.

Fourth row correctly predicts the turn right with different velocity profiles. Even though the model receives as input different plausible directions (keep straight and turn right), the past trajectory of the target agent is the key (different from second row traffic scenario where the agent was conducting a straight trajectory while approaching to an intersection), since in this case the target agent is clearly performing a curved past

trajectory. Then, the model avoids predicting non-plausible predictions and focus on the different velocity profiles in the right direction.

Finally, fifth row illustrates an interesting scene where the model understands there are no intersections around the vehicle given the preliminary map information. The highest confidence mode, as expected, assumes a CV prediction, whilst emergency breaks or sudden accelerations are also considering with a lower confidence.

6.4. Summary

In this Chapter, we propose several efficient baselines (social, map and augmented), progressively aggregating contextual information from the traffic scenario. First, a powerful pipeline to process only social-based information is illustrated, including GNN to model social interactions. Second, a heuristic based method to provide the model with minimal map priors which do not rely on heavily annotated HD maps and are interpretable in comparison with CNNs high-dimensional outputs. This preliminary map information, made up by high-level and well-structure features (centerlines) and low-level features (local perturbations around centerlines waypoints), is processed by standard MLP-based encoders. This physical information is concatenated to the social information regarding the target agent. Third, our proposed augmented baseline makes use of powerful yet efficient attention-based encoders to compute richer environment features, in addition to replace social/map features concatenation with MHCA to obtain the most representative social features.

As observed in the quantitative and qualitative results, our baselines are faster, have fewer parameters and FLOPs with minimal loss of accuracy. We achieve SOTA performance results on the Argoverse 1 Motion Forecasting Benchmark while having a low computational cost compared to other proposals.

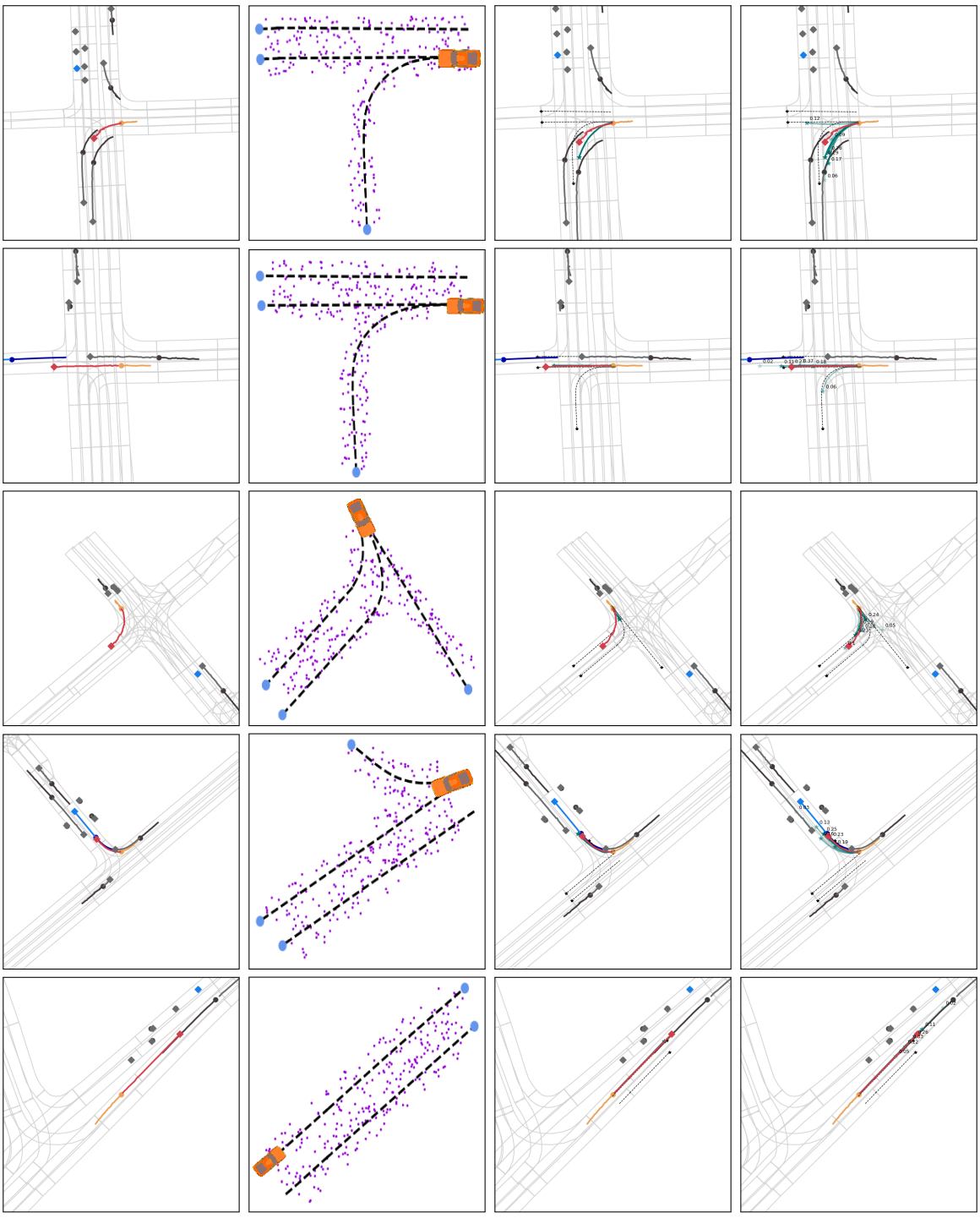

General view | Plausible HD map | K=1 prediction | K=6 predictions

Figure 6.5: Qualitative Results on challenging scenarios in the Argoverse 1 validation set using our best model. We represent: our vehicle (**ego**), the **target agent**, and other agents. We can also see the **ground-truth** trajectory of the target agent, our **multi-modal predictions** (with the corresponding confidences) and **plausible centerlines**. Circles represent last observations and diamonds last future positions. As we can see the plausible HD map serves as a good guidance to our model, which can predict reasonable trajectories in presence of multiple agents and challenging scenarios. We show, from left to right, a general view of the traffic scenario (including social and map information), our calculated plausible HD map, uni-modal prediction (best mode in terms of confidence) and multi-modal prediction ($K = 6$), including confidences (the higher, the most probable)

Chapter 7

Improving Multi-Agent Motion Prediction with Heuristic Proposals and Motion Refinement

Solo sé que no sé nada.

Sócrates
Diálogos de Platón

7.1. Introduction

This Chapter shows the last and most advanced MP algorithm proposed in this thesis. Based on our previously stated augmented baseline [113], we aim to get an efficient model that consider more information about the agents, HD map topological and semantic information (in addition to the previously stated geometric features) and contextual interactions. Note that obtaining and fusing this information (*e.g.* actor-to-actor, map-to-actor) is a research topic by itself [11], [14], [50] and a core part in the ADS pipeline. Here we identify a bottleneck for efficient real-time applications [84], [127], as usually, more (complex) data-inputs implies higher model complexity and inference time [35].

Regarding this, we propose a model to achieve accurate MP, yet, using light-weight transformer-based models for social encoding, GNNs for social-map context interaction, enhanced heuristic map proposals and motion refinement, reducing notably the complexity of our model with respect to previous methods such as GANet [12] to avoid these possible constraints. The work in this Chapter was partially published in the following conference paper [128]: "Improving Multi-Agent Motion Prediction With Heuristic Goals and Motion Refinement", 2023 IEEE/CVF Conference on Computer Vision and Pattern Recognition (CVPR), p. 5322-5331.

The main contributions of this Chapter are as following:

1. We present a Multi-modal Multi-Agent SOTA MP method on the Argoverse 2 Motion Forecasting Benchmark, one of the most recent and challenging vehicle MP datasets.

2. Our model uses transformer encoder to encode past trajectories and heuristic lane proposals, GNN for HD map graph encoding, actor-map fusion cycle, deep goal areas estimation and a motion refinement module to further improve temporal consistency.

3. In comparison to previous methods that rely only on past trajectories and HD map, we additionally use information about the agents (*e.g.* type of agent) and the scene geometry (*e.g.* lane distribution and possible goal points). Note that the proposed method is trained and validated with different types of agents (*e.g.* cars, pedestrians, motorcyclists or vans) as specified in the dataset.

4. Our method reduces in millions of parameters previous methods in Argoverse 2 such as GANet [12], and improves over LaneGCN [14]. It is important to note that, even though we take the most interesting concepts and conclusions from previous baselines proposed in Chapter 5 and Chapter 6, for simplicity we do not adapt and validate these models in Argoverse 2 since the experimental setup (raw data, data extractor, preprocessing, metadata and so forth and so on) is noticeably different *w.r.t.* the Argoverse 1 provided functions.

5. Finally, we provide an open-source [1] framework for MP.

7.2. Our proposal

The MP based on DL throughout this thesis have trained and validating in the Argoverse 1 Motion Forecasting dataset, which only considers one evaluated target category, that is, the target agent is always a vehicle (car, truck or van). Nevertheless, traffic scenarios may include VRUs, such as pedestrians, cyclists, motorcyclists, where the estimating the future behaviour of these vulnerable agents presents additional challenges compared to predicting the behaviour of aforementioned vehicles. Here are some key differences:

- **Size and visibility**: VRUs are smaller and less visible than vehicles, especially in adverse weather conditions or low-light situations. This reduced visibility can make it harder for sensors to detect and track them accurately. On the other hand, vehicles, being larger and equipped with various sensors, are generally easier to detect and track in most driving conditions.

- **Agility and maneuverability**: VRUs are more agile and maneuverable compared to vehicles. They can change lanes quickly, weave through traffic, and make sudden turns, making their behavior less predictable. Conversely, while some vehicles are

[1] https://github.com/Cram3r95/argo2goalmp

also agile, their size and weight typically limit their maneuverability, making their behavior more predictable in certain situations.

- **Road position and behavior**: Cyclists and motorcyclists often use different parts of the road than vehicles. For example, cyclists may ride close to the curb or in designated bike lanes, while motorcyclists may filter between lanes in traffic jams. Predicting their behavior requires understanding their specific road position and tendencies. Moreover, pedestrians are mostly found in pedestrian crossings and on the sidewalk from the ego-vehicle perspective. On the contrary, vehicles usually follow lanes and adhere to traffic rules, making their behavior more constrained and predictable within their designated lanes.
- **Human factors and vulnerability**: VRUs are exposed and more vulnerable to accidents than occupants in vehicles. Predicting their behavior involves considering human factors, such as their emotions, intentions, and safety concerns. On the other hand, vehicles are designed with safety features to protect occupants in the event of an accident. Predicting their behavior can focus more on the compliance with traffic rules and adherence to road conditions.
- **Data availability and model training**: Obtaining reliable and diverse data on VRU behavior can be challenging due to their smaller numbers and the complexity of their actions. This may require specialized data collection efforts and models that are specifically trained for these user types. Vehicles: Predicting vehicle behavior often benefits from extensive historical data and larger-scale datasets, making model training relatively more straightforward.

Regarding this, since this thesis is focused on predictive techniques for scene understanding in the field of AD, it is important to consider the aforementioned specific nature of an agent. This information can be included as additional metadata and encoded by the corresponding neural network to better understand the agent behaviour throughout the traffic scenario.

Moreover, training the model with longer prediction horizons enable models to particularly agents motions further into the future, which is quite beneficial for high-speed traffic scenarios, like highways. On the other hand, the average track length and unique roadways kilometers are two of the most important features of a MP dataset in the AD field to build a general prediction model that can cover standard and most edge cases, preventing overfitting.

To address the aforementioned considerations, at this point of the thesis we decided to carry out our experiments in the Argoverse 2 Motion Forecasting dataset instead of Argoverse 1. As illustrated in Section 2.4 and Table 2.2, Argoverse 2 covers a large geographic area (6 cities) and contains a large object taxonomy with 10 unique classes (such as vehicles, motorcyclists, pedestrians, cyclists, buses, etc.) that encompass a broad

range of actors, both static and dynamic. In comparison to the Argoverse 1 Motion Forecasting Dataset, the scenarios in Argoverse 2 are approximately twice as long and more diverse.

Furthermore, Argoverse 2 presents more semantic information regarding the different HD map lanes than Argoverse 1. In Argoverse 1, HD map information only illustrates the connectivity between geometry features (*i.e.* topological information) among the different lanes in a road, where the user can extract some plausible future centerlines (as proposed in previous Chapters) by means the Argoverse 1 API or the neighbours (that is, predecessor, successor, left/right neighbour) given a particular location.

Nevertheless, as stated by [129], only using the geometric information of the lane centerline as input to get latent features of vector map nodes is not enough. The lane centerline can only provide the position and topology (*i.e.* connection) of the lanes, but other elements of the vector map also contain very rich information to understand the scene around the agent. For example, the lane boundary (left way and right way) can provide traffic rule constraint information such as whether it is possible to conduct the lane change behaviour or not (dashed vs solid line, yellow vs white, etc.). When considering such amount of information, specifically in terms of physical context and interactions, most SOTA methods require an overwhelming model complexity which can be inefficient in terms of computation [35], [47], [124]. In our case, we refer these plausible future centerlines with additional metadata (lane boundaries and presence of intersection) as heuristic-based lane proposals, which will be encoded along with past social information.

Figure 7.1 illustrates the overall pipeline. Throughout this Chapter we will explain the different modules of the proposed MP method, which are:

- **Social Encoder**, which uses the agent past trajectories (relative displacements and additional metadata such as the type (*e.g.* car, cyclist, pedestrian) and category, from less to more important) and preprocessed heuristic-based lane proposals to compute social latent features.
- **Map Encoder**, that constructs a lane graph from the HD map and uses a LaneConv operator [14] to extract lane node features.
- **Fusion Cycle**, responsible for fusing social and map latent features by means of the shared info paradigm (actors to lanes, lanes to lanes, lanes to actors and actors to actors).
- **Goal Areas estimation**, responsible for predicting via DL some goals and aggregating their surrounding (area) information to the agents, as well as recomputing agents interaction.
- **Multimodal Decoder**, which uses the latent actors with deep area context to generate reliable multi-modal predictions.

- **Motion Refinement**, in charge of enhancing the quality of future trajectories, taking into account the past trajectories, actors latent features and preliminary predicted trajectories, to further improve temporal consistency.

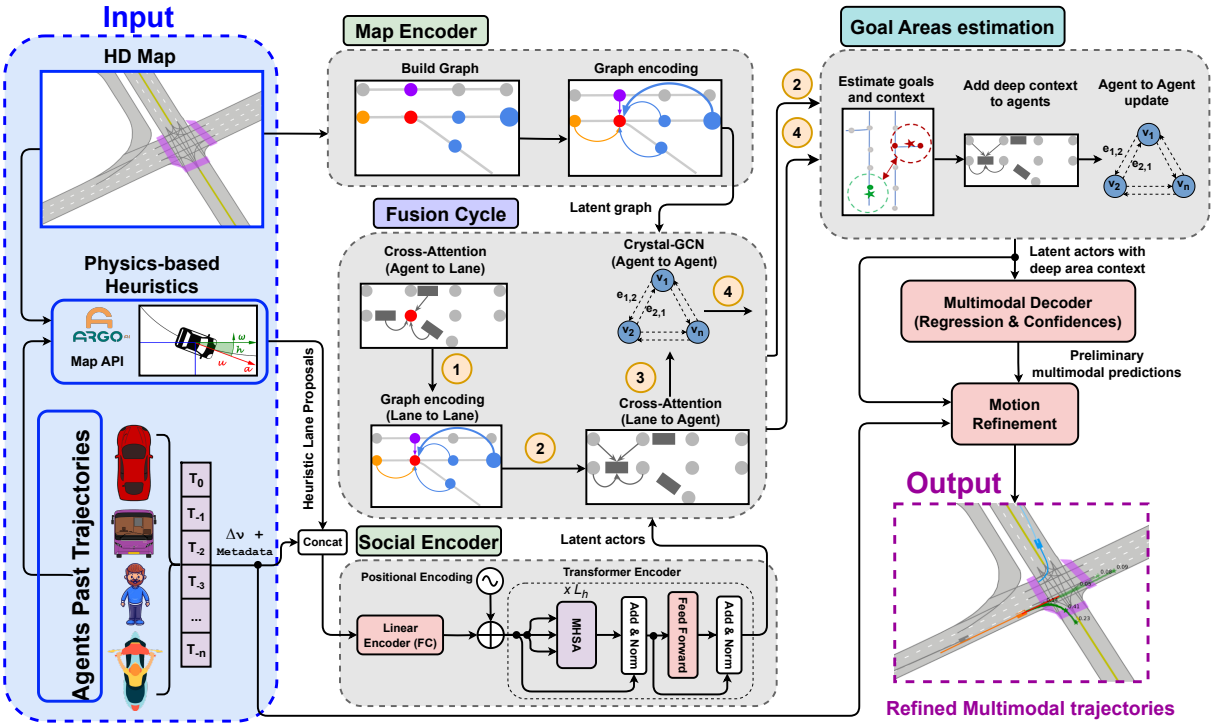

Figure 7.1: Overview of our MP model including Fusion Cycle, Heuristic Proposals and Motion Refinement

7.2.1. Social Encoder

In terms of agent trajectory and preliminary intentions, as observed in Figure 7.1, we integrate additional features related to the type and properties of agents (also referred as metadata in the literature), apart from standard past trajectories. Moreover, we also compute heuristic scene understanding to constrain the model predictions towards the real scene geometry (*e.g.* plausible centerlines and lanes), including lane and boundary topological information or presence of an intersection.

7.2.1.1. Preprocessing of past trajectories and heuristic proposals

The social preprocessing step proposed in this model is slightly different to our previous methods where we only considered those agents that have information over the full history horizon. After revisiting the literature, we realized that all methods in Argoverse 2 consider an agent as relevant even if it was not observed over the whole full sequence spectrum as long as the agent is present in the scene in the last observation frame, *i.e.* $t = 0$. This hypothesis, while being computationally more expensive than our previous

methods (Chapter 5 and Chapter 6), is coherent since even it an agent is occluded for a few timestamps, it can be really relevant to determine the future behaviour of another agent. To this end, as proposed by multiple methods [13], [14], we consider all agents that are observable at *t=0*, handling those agents that are not observed over the full sequence spectrum (observation length = obs_{len} + prediction length = $pred_{len}$) by concatenating a binary flag b_i^t that indicates if the agent is padded or not. Furthermore, we only consider the dynamic agents of the scene (vehicles, pedestrians, motorcyclists, cyclists and buses) and discard unknown or static objects (background, construction or riderless bicycle), since dynamic (which can be stopped or not) are the most relevant for the MP task. Given these final agents, we follow the same principles of translation and rotation invariant, as well as relative displacements, to compute the input past trajectories. It is important to note that this algorithm, unlike our previous methods, is trained to predict the future behaviour of all relevant agents in the scene, even though in the validation set and Argoverse 2 Leaderboard, for fair comparison, we only predict the focal agent (also referred as target agent) in the traffic scenario.

On top of that, we additionally compute and codify the object type (bus, pedestrian, vehicle, cyclist) and agent importance (unscored, scored and focal track) as additional metadata. As described by Argoverse 2, each track is assigned one of the following labels, which dictate scoring behavior in the Argoverse 2 challenges:

1. **Track fragment**: Lower quality track that may only contain a few timestamps of observations.
2. **Unscored track**: Unscored track used for contextual input.
3. **Scored track**: High-quality tracks relevant to the agent.
4. **Focal track**: The primary track of interest in a given scenario (scored in the single-agent prediction challenge of the Argoverse 2 Motion Forecasting Leaderboard).

We can appreciate how, in addition to the attention mechanisms of the model which are responsible of computing the most relevant features, the aforementioned track category serves as a good guidance as preliminary information to refer the importance of a specific agent with respect to another one.

In terms of preliminary intentions, given the map data and API, we propose the use of preliminary plausible area information in a similar way to the heuristic proposals illustrated in Section 6.2.2.1. We follow the same heuristic (filter the agent, calculate the future travelled distance by means a CA model, get all candidates within a bubble, given the agent last observation and Manhattan distance, etc.) to compute the most plausible future centerlines C for the corresponding agent as set of relative displacements with the same length than the prediction horizon $pred_{len}$. It must be considered that in Argoverse 2 the number of categories is modified to 5 (vehicles, pedestrians, motorcyclists, cyclists and

buses) instead of only 1 (vehicle), which is the case of most vehicle MP datasets, including Argoverse 1. So, if the agent is a pedestrian, no centerlines proposals are considered (*i.e.* they are created virtually and padded as stated in previous sections) since we assume that pedestrians are not walking on the road, but on the pedestrian crossings or sidewalks. In future works we will work on integrating specific physical information depending on the object type as preliminary map features. Furthermore, in Argoverse 2, thanks to a more realistic representation of the HD map, we include additional metadata such as lane type (bus, bike, vehicle), presence of intersection (binary flag) or boundaries mark type (dash, solid, yellow), along with the aforementioned centerline relative displacements.

7.2.1.2. Agent trajectories encoding

In terms of social encoding, to capture more complex features for subsequent features fusion and interaction, we initially adopted the social encoder proposed by GANet [12], based on LaneGCN [14], to encode motion history and scene context for its outstanding performance. In this backbone (given the aforementioned social input: translation and rotation invariant with respect to a target agent, and relative displacements), LaneGCN makes use of a network with 3 groups/scales of 1D convolutions 1D CNN to process the trajectory input for its effectiveness in extracting multi-scale features and efficiency in parallel computing. The output is a well-structured feature map, whose element at $t = 0$ is used as the actor feature. The network has 3 groups/scales of 1D convolutions. Then, a Feature Pyramid Network (FPN) [130] to fuse the multi-scale features, and another residual block to obtain the output tensor is applied. Moreover, GANet applies an LSTM network on FPN output features and use two identical parallel networks to enhance the motion history encoding.

Regarding this, we aimed to improve social encoding taking into account that in spite the fact that LSTMs became popular because they could solve the problem of vanishing gradients, they suffer from *short-term memory* due to the vanishing gradient problem, as well as require a lot of resources to get trained and become ready for real-world applications, as discussed in Section 3.3.4.4. In particular, they need high memory-bandwidth because of linear layers present in each cell which the system usually fails to provide for. To solve that, we replace the motion encoder proposed by [12] for a transformer encoder (based on our previous augmented baseline from Chapter 6), which is faster than RNN-based models as all the input is ingested once, decreasing the computational complexity.

On the other hand, even though the heuristic lane proposals represent physical information, they are quite related to preliminary social intentions. Then, as depicted in Figure 7.1, we concatenate the agents past trajectories, additional social metadata (type of agent and relevancy) and heuristic lane proposals (including semantic and topological metadata), which is processed by a linear embedding. Then, positional encoding is added to the output embedding explicitly to retain the information regarding the order

of past trajectories and future preliminar steps. Finally, these latent features feed the transformer encoder, leveraging the self-attention mechanism and positional encoding to learn complex and dynamic patterns from long-term time series data.

7.2.2. Map Encoder

Even though we demonstrate in Chapter 6 how including cheap and interpretable map information represent a good trade-off between model accuracy and computational complexity, more powerful map encoding is required to compute an enriched physical latent space for better scene understanding. To this end, we focus on graph-based methods [50] which construct graph-structured representations from HD maps, which preserve the connectivity of lanes, and therefore the geometry of the scene. VectorNet [35] is one of the first works in this direction, where the authors propose to encode map elements and actor trajectories as polylines and then use a global interactive graph to fuse map and actor features. On the other hand, we find especially related LaneGCN [14], a method that constructs a map node graph and proposes a novel graph convolution. In that sense, we follow the same principles than these well-established baselines by adopting simple form of vectorized map data as our representation of HD maps, where the map data is represented as a set of polylines (lanes) and their connectivity, where each lane contains a centerline (sequence of 2D BEV points), arranged following the lane direction. For any two lanes which are directly reachable, 4 types of connections are given: predecessor, successor, left neighbour and right neighbour.

Moreover, in order to extract deep physical features from the map-graph, we adopt MapNet [14] backbone (*i.e.* Graph encoding in Figure 7.1) to encode the scene context for its outstanding performance. It learns good lane representations which are computationally efficient and preserve map topology. We use a multi-scale LaneConv network to encode the vectorized map data, which is consisted of lane centerlines and their connectivity. We construct a lane node graph from the map data. A lane node is a short lane segment between two consecutive points of the lane centerline, which is represented by the location (the averaged coordinates of its two endpoints) and the shape (the vector between its two endpoints).

While other approaches encode the map as a raster image and apply 2D convolutions to extract features, MapNet consists of two steps:

- Build a lane graph from vectorized map data
- Apply a LaneConv operator to the lane graph to output the map features

Throughout this section, based on the approach proposed by LaneGCN [14], we illustrate how the map-graph is built and encoded by means of GCNs the map encoder (Figure 7.1) is able to compute a very powerful physical latent space.

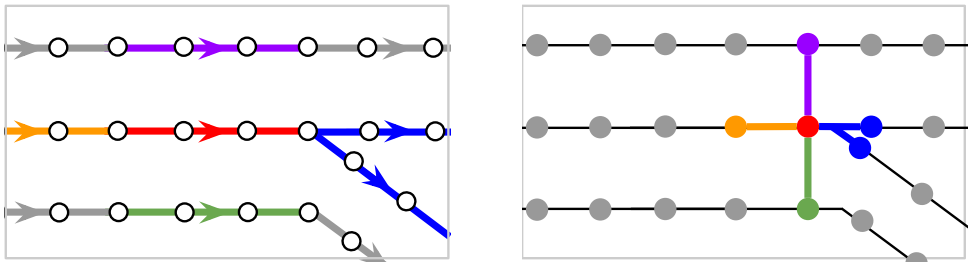

Figure 7.2: Lane graph construction from vectorized map data. We highlighted the most important lanes around the **current lane**: **predecessor**, **successor**, **left neighbour** and **right neighbour**. Source: *Learning lane graph representations for motion forecasting* [14]

7.2.2.1. Build Graph

As observed in Figure 7.2, the map data is represented as a set of lanes and their connectivity. Each lane contains a centerline, *i.e.* a sequence of 2D BEV points, which are arranged following the lane direction. For any two lanes which are directly reachable, 4 types of connections are given: *predecessor*, *successor*, *left neighbour* and *right neighbour*. Given a lane A, its predecessor and successor are the lanes which can directly travel to A and from A respectively. Left and right neighbours refer to the lanes which can be directly reached without violating traffic rules. This simple map format provides essential geometric and semantic information for MP, as vehicles generally plan their routes by reference to lane centerlines and their connectivity.

In order to conduct the Lane Graph construction, we first define a lane node as the straight line segment formed by any two consecutive points (grey circles in Figure 7.2) of the centerline. The location of a lane node is the averaged coordinates of its two end points. Following the connections between lane centerlines, we also derive 4 connectivity types for the lane nodes, *i.e.* **predecessor**, **successor**, **left neighbour** and **right neighbour**. For any lane node A, its predecessor and successor are defined as the neighbouring lane nodes that can travel to A or from A respectively. Note that one can reach the first lane node of a lane l_A from the last lane node of lane l_B if l_B is the predecessor of l_A. Left and right neighbours are defined as the spatially closest lane node measured by ℓ_2 distance on the left and on the right neighbouring lane respectively. We denote the lane nodes with $V \in \mathbb{R}^{N\times 2}$, where N is the number of lane nodes and the i-th row of V is the BEV coordinates of the i-th node. We represent the connectivity with 4 adjacency matrices $\{A_i\}_{i\in\{\text{pre,suc,left,right}\}}$, with $A_i \in \mathbb{R}^{N\times N}$. We denote $A_{i,jk}$, as the element in the j-th row and k-th column of A_i. Then $A_{i,jk} = 1$ if node k is an i-type neighbor of node j.

7.2.2.2. Graph encoding (LaneConv)

A natural operator to handle lane graphs is the graph convolution [131]. The most widely used graph convolution operator [132] is defined as $Y = LXW$, where $X \in \mathbb{R}^{N\times F}$ is the node feature, $W \in \mathbb{R}^{F\times O}$ is the weight matrix, and $Y \in \mathbb{R}^{N\times O}$ is the output. The

graph Laplacian matrix $L \in \mathbb{R}^{N \times N}$ takes the form $L = D^{-1/2}(I + A)D^{-1/2}$, where I, A and D are the identity, adjacency and degree matrices respectively. I and A account for self connection and connections between different nodes. All connections share the same weight W, and the degree matrix D is used to normalize the output. However, this vanilla graph convolution is inefficient in our case due to the following reasons. First, it is not clear what kind of node feature will preserve the information in the lane graphs. Second, a single graph Laplacian can not capture the connection type, *i.e.* losing the directional information carried by the connection type. Third, it is not straightforward to handle long range dependencies within this form of graph convolution. Motivated by these challenges, LaneGCN [14] introduces a novel operator for lane graphs, called *LaneConv*.

7.2.2.2.1. Node Feature Before applying the LaneConv operator, first input features of the lane nodes must be defined. Each lane node corresponds to a straight line segment of a centerline. To encode all the lane node information, we need to take into account both the shape (size and orientation) and the location (the coordinates of the center) of the corresponding line segment. We parameterize the node feature as follows:

$$\mathbf{x}_i = \mathrm{MLP}_{\mathrm{shape}}\left(\mathbf{v}_i^{\mathrm{end}} - \mathbf{v}_i^{\mathrm{start}}\right) + \mathrm{MLP}_{\mathrm{loc}}\left(\mathbf{v}_i\right) \tag{7.1}$$

where MLP indicates a multi-layer perceptron and the two subscripts refer to shape and location, respectively. $\mathbf{v}_i$ is the location of the i-th lane node, *i.e.*, the center between two end points, $\mathbf{v}_i^{\mathrm{start}}$ and $\mathbf{v}_i^{\mathrm{end}}$ are the BEV coordinates of the node i's starting and ending points, and $\mathbf{x}_i$ is the i-th row of the node feature matrix X, denoting the input feature of the i-th lane node.

7.2.2.2.2. LaneConv operator As observed, the node feature above only captures the local information of a line segment. Then, in order to aggregate the topology information of the lane graph at a larger scale, LaneGCN [14] proposes the LaneConv operator as following:

$$Y = XW_0 + \sum_{i \in \{\mathrm{pre,suc,left,right}\}} A_i X W_i \tag{7.2}$$

where A_i and W_i are the adjacency and the weight matrices corresponding to the i-th connection type respectively. Since we order the lane nodes from the start to the end of the lane, A_{suc} and A_{pre} are matrices obtained by shifting the identity matrix one step towards upper right (non-zero superdiagonal) and lower left (non-zero subdiagonal). A_{suc} and A_{pre} can propagate information from the forward and backward neighbours whereas A_{left} and A_{right} allow information to flow from the cross-lane neighbours. It can appreciated that by means of this LaneConv operator, the map encoder encodes more geometric information (such as connection type or direction) that general graph convolution operator.

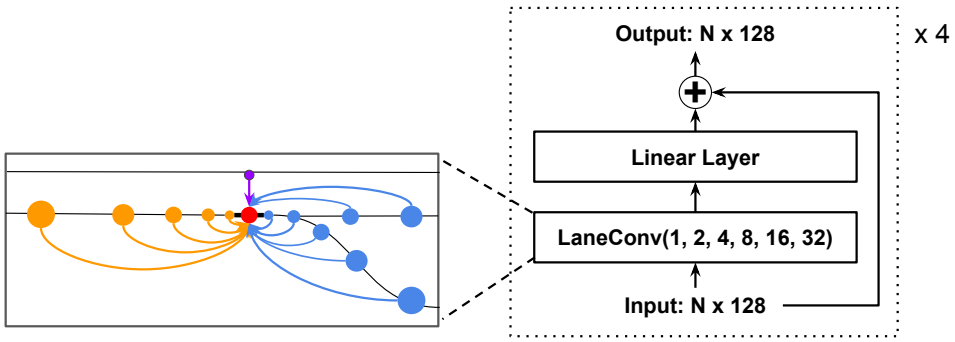

Figure 7.3: LaneGCN architecture. LaneGCN is a stack of 4 multi-scale LaneConv residual blocks, each of which consists of a LaneConv(1,2,4,8,16,32) and a linear layer with a residual connection.
Source: *Learning lane graph representations for motion forecasting* [14]

7.2.2.2.3. Dilated LaneConv Since MP models usually predict the future trajectories of actors with a time horizon of several seconds, actors with high speed could have moved a long distance. Therefore, the model needs to capture the long range dependency along the lane direction for accurate prediction. In regular grid graphs, a dilated convolution operator [133] can effectively capture the long range dependency by enlarging the receptive field. Inspired by this operator, LaneGCN [14] proposes the *dilated LaneConv* operator to achieve a similar goal for irregular graphs.

In particular, the k-dilation LaneConv operator is defined as follows:

$$Y = XW_0 + A^k_{\text{pre}} XW_{\text{pre},k} + A^k_{\text{suc}} XW_{\text{suc},k} \tag{7.3}$$

where A^k_{pre} is the k-th matrix power of A_{pre}. This allows us to directly propagate information along the lane for k steps, with k a hyperparameter. Since A^k_{pre} is highly sparse, one can efficiently compute it using sparse matrix multiplication. Note that the dilated LaneConv is only used for predecessor and successor, as the long range dependency is mostly along the lane direction.

7.2.2.2.4. LaneGCN Based on the dilated LaneConv, LaneGCN [14] proposes a multi-scale LaneConv operator and use it to build the currently their well-established LaneGCN network (Figure 7.3). Combining Equations (7.2) and (7.3) with multiple dilations, we get a multi-scale LaneConv operator with C dilation sizes as follows:

$$Y = XW_0 + \sum_{i \in \{\text{left},\text{right}\}} A_i XW_i + \sum_{c=1}^{C} \left(A^{k_c}_{\text{pre}} XW_{\text{pre},k_c} + A^{k_c}_{\text{suc}} XW_{\text{suc},k_c} \right), \tag{7.4}$$

where k_c is the c-th dilation size. We denote LaneConv$(k_1, \cdots, k_C)$ this multi-scale layer.

7.2.3. Fusion Cycle

Once both the map and social latent features are computed, we obtain a 2D feature matrix X where each row X_i indicates the feature of the i-th actor, and a 2D matrix Y where each row Y_i indicates the feature of the i-th lane node. Then, we make use of the well-established actor-map fusion cycle proposed by [14] (also referred as FusionNet in the literature) that transfers and aggregates features among actors and lane nodes.

The behaviour of an actor strongly depends on its context, *i.e.*, other actors and the map. Although social interactions have been widely explored by previous works (as proposed in our previous baselines from Chapter 6, with a Crystal-GCN network calculating the most relevant social relations among actors), the interactions between the actors and the map, and map conditioned interactions between actors have received much less attention. FusionNet makes use of spatial attention and LaneGCN to capture a complete set of actor-map interactions, as observed in Figure 7.1.

FusionNet makes use of a stack of four fusion modules to capture all information flows between actors and lane nodes, *i.e.*, (1) Actors to Lanes (A2L), (2) Lanes to Lanes (L2L), (3) Lanes to Actors (L2A) and (4) Actors to Actors (A2A). This order is not coincidence. Assuming several agents are on the road and all of them have a web service that shares information providing details about their geographical location (*e.g.* Google Maps):

- First (A2L module), agents introduce their real-time traffic information to lane nodes, such as blockage, presence of an accident, etc. In other words, the HD map information is updated with the traffic information of the agents.
- Then, in L2L module HD map information of a particular node is propagated to immediate neighbours.
- After updating the map information based of message propagation, further agents are updated (L2A module) with the information of surrounding map nodes, which were previously updated by neighboring nodes.
- Finally, A2A module concludes the actor-map fusion cycle handling the interactions between actors and produces the output actor features.

We implement L2L using another LaneGCN, which has the same architecture as the one used in the aforementioned MapNet backbone. Regarding the A2L, L2A and A2A modules, [14] applies a spatial attention layer as defined in Section 3.3.4. Taking the first module (A2L) as en example, given an actor node i, we aggregate the features from its context lane nodes j as follows:

$$\mathbf{y}_i = \mathbf{x}_i W_0 + \sum_j \phi(\text{concat}(\mathbf{x}_i, \Delta_{i,j}, \mathbf{x}_j) W_1) W_2 \tag{7.5}$$

where $\mathbf{x}_i$ represents the feature of the i-th node, W a weight matrix, ϕ the composition of layer normalization and ReLU, and $\Delta_{ij} = \text{MLP}(\mathbf{v}_j - \mathbf{v}_i)$, where $\mathbf{v}$ denotes the node location.

The context nodes are defined to be the lane nodes whose ℓ_2 distance from the actor node i is smaller than a threshold. Each of A2L, L2A and A2A has two residual blocks, which consist of a stack of the proposed attention layer and a linear layer, as well as a residual connection.

Nevertheless, as observed in our model (Figure 7.1), once implemented FusionNet to compute actor-map interactions, we substitute the final module that models Actor to Actor interactions with a Crystal-GCN, inspired in the efficient baselines proposed in Chapter 6.

7.2.4. Goal Areas estimation

So far, the proposed model includes a social encoder to process past trajectories, agents metadata and heuristic lane proposals, map encoder to extract deep physical features from the HD map and an actor-map fusion cycle to perform features interaction. Nevertheless, as stated by GANet [12], since the traveling mode of an actor is highly diverse, the fixed size stride proposed by LaneGCN cannot effectively model distant relevant map features and thus limits the prediction performance.

While most works [14], [32], [34], [43] focus on map encoding and motion history modeling, another family methods [18], [102], [125], which is built on DL goal-based prediction, captures the agent intentions in the future explicitly. Note that this is different from our proposed interpretable plausible future centerlines in Chapter 6, since they are extracted by means of physics-based heuristics, while these methods employ deep features to decode potential goals, which is a more accurate but computationally more expensive and less interpretable.

Specifically, as discussed in [12], these goal-based prediction methods follow a three-stage scheme. First, candidate goals are sampled from the lane centerlines. Second, a set of goals are selected by goal prediction. Third, trajectories are estimated conditioning on selected goals. Although these methods have achieved competitive results (in our particular case Argoverse 1 and 2), there present two main drawbacks:

1. These methods merely use a limited number of isolated goal coordinates as conditions, which contain limited information and hinder accurate motion forecasting. As goal coordinates of different distances to the road edge carry different information, using a limited number of goal coordinates as conditions constrains the full utilization of a road context.

2. The competitive performance of these methods heavily depends on the well-designed goal space, which may be violated in practice. Well-designed goal space is required

for sampling, refining, and scoring candidate goals, due to the difficulty of predicting and evaluating accurate goal coordinates. For example, vehicles candidate goals are sampled from the lane centerlines while VRUs candidate goals (particularly regarding pedestrians) are sampled from a virtual grid around themselves in TNT [18]. These hard-encoded candidate goals abide by driving rules, *e.g.* never depart far from lanes or go beyond the road's edge. However, these methods may fail once these hard-encoded candidate goals are violated in the real world.

Compared with accurate goal coordinates, a potential goal area with a relatively richer context of the road is able to provide more tolerance and better guidance for accurate MP through a soft constraint. Also, as driving history of actors is critical for goal area estimation, GANet [12] make full use of this clue for accurate localization of goal areas. For example, a fast-moving vehicle goal area may be far away, while the goal area of a stationary vehicle should be limited around itself.

Motivated by these observations, GANet builds upon LaneGCN pipeline proposing a Goal Area Network framework to predict potential goal areas and aggregate their surrounding information as conditions for MP. As aforementioned, we adopt GANet as baseline in this Chapter, including DL based goal areas estimation (Figure 7.1).

7.2.4.1. Estimate goals and context

The first stage of the Goal Areas estimation module aims to predict possible goals for the i-th actor based on X_i. We apply intermediate supervision and calculate the Smooth $\mathcal{L}_1$ loss between the best-predicted goal and the ground-truth trajectory endpoint to backpropagate, making the predicted goal close to the actual goal as much as possible. The goal prediction stage serves as a predictive test to locate goal areas, which is different from goal-based methods using the predicted goals as the final predicted trajectories endpoint.

In practice, the future behaviour of an agent in an arbitrarily complex urban scenario is highly multi-modal. For example, the agent may stop, go ahead, turn left, or turn right when approaching an intersection. Therefore, it is coherent to make a multiple-goals prediction. We construct a goal prediction header as proposed by [12] with two branches to predict E possible goals $G_{n,end} = \{g^e_{n,end}\}_{e\in[0,E-1]}$ and their confidence scores $C_{n,end} = \{c^e_{n,end}\}_{e\in[0,E-1]}$, where $g^e_{n,end}$ is the e-th predicted goal coordinates and $c^e_{n,end}$ is the e-th predicted goal confidence of the n-th actor.

We train this stage using the sum of classification loss and regression loss. Given E predicted goals, we find a positive goal $\hat{e}$ that has the minimum Euclidean distance with the ground truth trajectory's endpoint.

For classification, we use the max-margin loss:

$$L_{cls\_end} = \frac{1}{N(E-1)} \sum_{n=1}^{N} \sum_{e \neq \hat{e}} max(0, c^{e}_{n,end} + \epsilon - c^{\hat{e}}_{n,end}) \tag{7.6}$$

where N is the total number of actors and $\epsilon = 0.2$ is the margin. The margin loss expects each goal to capture a specific pattern and pushes the goal closest to the ground truth to have the highest score. For regression, we only apply the smooth L1 loss to the positive goals:

$$L_{reg\_end} = \frac{1}{N} \sum_{n=1}^{N} reg(g^{\hat{e}}_{n,end} - a^{*}_{n,end}) \tag{7.7}$$

where $a^{*}_{n,end}$ is the ground truth BEV coordinates of the n-th actor trajectory's endpoint, $reg(z) = \sum_i d(z_i)$, z_i is the i-th element of z, and $d(z_i)$ is a smooth L1 loss.

Additionally, we also try to add a "one goal prediction" module at each trajectory middle position aggregating map features to assist the endpoint goal prediction and the whole trajectory prediction. Similarly, we apply a residual MLP to regress a middle goal $g_{n,mid}$ for the n-th actor. Then, the loss term for this module is given by:

$$L_{reg\_mid} = \frac{1}{N} \sum_{n=1}^{N} reg(g_{n,mid} - a^{*}_{n,mid}) \tag{7.8}$$

where $a^{*}_{n,mid}$ is the GT BEV coordinates of the n-th actor trajectory's middle position.

Finally, total loss at the goal prediction stage is:

$$L_1 = \alpha_1 L_{cls\_end} + \beta_1 L_{reg\_end} + \rho_1 L_{reg\_mid} \tag{7.9}$$

where $\alpha_1 = 1$, $\beta_1 = 0.2$ and $\rho_1 = 0.1$, as proposed in [12].

7.2.4.2. Add deep contexts to agents and agent-to-agent update

Once different potential destinations have been predicted, we choose the predicted goal with the highest confidence among E goals as an anchor. This anchor is the approximate destination with the highest possibility that the actor may reach based on its motion history and driving context.

Since the actors future behaviour is highly uncertain, we adopt the same hyperparameter than crop maps within 6 meters of the anchor as the goal area of interest, which relaxes the strict goal prediction requirement. The actual endpoint is more likely to appear in candidate areas compared with being hit by scattered endpoint predictions. Moreover, the actor's behavior highly depends on its destination area's context, i.e., the maps and other actors. Although previous works have explored the interactions between actors, the

interactions between actors and maps in goal areas and the interactions among actors in the future have received less attention.

Thus, we retrieve the lane nodes in goal areas and apply a GoICrop module to aggregate these map node features as follows:

$$x_i' = \phi_1(x_i W_0 + \sum_j \phi_2(concat(x_i W_1, \Delta_{i,j}, y_j)W_2))W_3 \tag{7.10}$$

where x_i is the feature of i-th actor and and y_j is the feature of j-th lane node, W_i is a weight matrix, ϕ_i is a layer normalization with ReLU function, and $\Delta_{i,j} = \phi(MLP(v_i - v_j))$, where v_i denotes the anchor's coordinates of i-th actor and v_j denotes the j-th lane node's coordinates.

GoICrop serves as spatial distance-based attention and updates the goal area lane nodes' features back to the actors. We transpose x_i with W_1 as a query embedding. The relative distance feature between the anchor of i-th actor and j-th lane node are extracted by $\Delta_{i,j}$. Then, we concatenate the query embedding, relative distance feature, and lane node feature. An MLP is employed to transpose and encode these features. Finally, the goal area features are aggregated for i-th actor.

Previous motion forecasting methods usually focus on the interactions in the observation history. However, actors will interact with each other in the future to follow driving etiquette, such as avoiding collisions.

Since we have performed predictive goal predictions and gotten possible goals for each actor, our framework can model the actors' future interactions.

Hence, we utilize the predicted anchor positions and apply a GoICrop module as equation 7.10 to implicitly model actors' interactions in the future. We consider the other actors whose future anchor's distance from the anchor of i-th actor is smaller than 100 meters. In this case, y_j in equation 7.10 denotes the features of j-th actor, v_i denotes the anchor's coordinates of i-th actor, and v_j denotes the anchor's coordinates of j-th actor in $\Delta_{i,j} = \phi(MLP(v_i - v_j))$.

Finally, as performed at the end of the fusion cycle, we conduct message-passing among actor nodes by means of a Crystal-GCN block, inspired in the efficient baselines proposed in Chapter 6, to update their corresponding surrounding information.

7.2.5. Decoding module

In order to get the future trajectories with corresponding scores, as observed in Figure 7.1, we take the updated actor features X as input to predict K final future trajectories and their confidence scores in stage three. Specifically, we construct a two-branch multi-modal prediction header similar to the goal prediction stage, with one regression branch estimating the trajectories and one classification branch scoring the trajectories.

For each actor, we regress K sequences of BEV coordinates $A_{n,F} = \{(a^k_{n,1}, a^k_{n,2}, ..., a^k_{n,T})\}_{k\in[0,K-1]}$, where $a^k_{n,t}$ denotes the n-th actor's future coordinates of the k-th mode at t-th step.

For the classification branch, we output K confidence scores $C_{n,cls} = \{c^k_n\}_{k\in[0,K-1]}$ corresponding to K modes.

We find a positive trajectory of mode $\hat{k}$, whose endpoint has the minimum Euclidean distance with the ground truth endpoint.

For classification, we use the margin loss L_{cls} similar to the goal prediction stage. For regression, we apply the smooth L1 loss on all predicted steps of the positive trajectories:

$$L_{reg} = \frac{1}{NT}\sum_{n=1}^{N}\sum_{t=1}^{T} reg(a^{\hat{k}}_{n,t} - a^*_{n,t}) \tag{7.11}$$

where $a^*_{n,t}$ is the n-th actor's ground truth coordinates.

To emphasize the importance of the goal, we add a loss term stressing the penalty at the endpoint:

$$L_{end} = \frac{1}{N}\sum_{n=1}^{N} reg(a^{\hat{k}}_{n,end} - a^*_{n,end}) \tag{7.12}$$

where $a^*_{n,end}$ is the n-th actor's ground truth endpoint coordinates and $a^{\hat{k}}_{n,end}$ is the n-th actor's predicted positive trajectory's endpoint.

The loss function for training at this stage is given by:

$$L_2 = \alpha_2 L_{cls} + \beta_2 L_{reg} + \rho_2 L_{end} \tag{7.13}$$

where $\alpha_2 = 2$, $\beta_2 = 1$ and $\rho_2 = 1$.

7.2.6. Motion refinement

A second-stage motion refinement, as proposed by [134], is introduced to further explore the temporal consistency for predicting more accurate future trajectories. The goal is to reduce the offset between ground truth trajectory Y and predicted trajectory $\hat{Y}$. We define this offset as $\Delta Y = Y - \hat{Y}$. In this stage, we leverage three sources of information: 1. Preliminary predictions computed in the decoding module, 2. Prior latent information to the decoding module and 3. Past observations. Using this approach, an MLP model is trained to minimize the offset by predicting a residual R that is added to the original trajectory *i.e.*we use L_2 loss to optimize the offset as follows:

$$\mathcal{L}_{\text{off}} = ||Y - \hat{Y} - \hat{R}||_2 = ||\Delta Y - \hat{R}||_2. \tag{7.14}$$

Furthermore, we use a cosine function, denoted by Equation 7.15, to explicitly aid the model in learning the turning angle from the last observed position. It measures the difference between the ground truth angle $\theta_t = \arctan2(Y_t - X_0)$ and the predicted angle $\hat{\theta}_t = \arctan2(\hat{Y}_t - X_0)$:

$$\mathcal{L}_{\text{angle}} = \frac{1}{t_f} \sum_{t=1}^{t_f} -cos(\hat{\theta}_t - \theta_t) \tag{7.15}$$

Note that this method can be applied to the pre-trained model from previous stages, which is completely functional, as the main function is to improve the output trajectories.

7.3. Experimental Results

7.3.1. Dataset

We use the Argoverse 2 [7] dataset described in Section 2.4, where we could appreciate that, compared to Argoverse 1, is a high-quality multi-agent motion prediction dataset. For each real driving scenario we have the corresponding local HD map, past trajectories of the agents, metadata about the agents (*e.g.* the type of agent: cyclist, pedestrian, car), and topological information about the scene. Each scenario is 11 seconds long. We consider five seconds of the past trajectory (also known as motion history), and we predict the next six seconds.

7.3.2. Metrics

We follow the widely used evaluation metrics **gu2021densetntwaymo**, [50], [118]. We follow the benchmark settings and adopt widely used metrics. Table 7.1 illustrates standard metrics proposed in previous chapter (minADE and minFDE both in the uni-modal and multi-modal scenarios). Moreover, regarding the Argoverse 2 Motion Forecasting Leaderboard, we additionally study the MR, which is the ratio of predictions where none of the predicted K trajectories is within 2.0 meters of ground truth according to the endpoint's displacement error, and the Brier minimum Final Displacement Error (brier-minFDE K=6), which adds a probability-related penalty to the endpoint $\mathcal{L}_2$ distance error.

7.3.3. Implementation details

We train our model on 2 A100 GPUs using a batch size of 128 with the ADAM optimizer for 42 epochs. The initial learning rate is 1 x 10-3, decaying to 1 x 10-4 at 32 epochs. The latent dimension (regarding map and social features) in most of our experiments is 128. The number of attention heads in the social encoder and motion refinement is 8.

The training setup including loss functions follows GANet [12] official implementation as our baseline.

In terms of augmentations, we apply (i) Dropout and swapping random points from the past trajectory, (ii) point location perturbations under a $\mathcal{N}(0, 0.2)$ [m] noise distribution [118].

7.3.4. Comparative with the state-of-the-art

Tables 7.1 and 7.2 present the results obtained on the Argoverse 2 Motion Forecasting validation and test sets, respectively. We achieve near SOTA performance in both sets, which is on-pair with the most promising pipelines, while using notably less parameters. As stated throughout this work, we focus on applying efficient methods to help understand future interactions among the different agents, reducing the number of parameters and inference time.

We can appreciate in Table 7.1 the huge influence of the physical context both in terms of accuracy and runtime. GANet [12] shows the best multimodal prediction metrics, with an approximate amount of 6.2M of parameters of 1612 ms given a batch size of 128 traffic scenarios and an average number of 30 agents per scene. As expected, progressively removing the map influence (remove map from decoder, remove goal areas estimation) in the model we decrease the MP performance with a noticeable parameter decrease.

In our case, we study the influence of substituting the modified ActorNet [12], [14] social encoder proposed by GANet, which uses RNNs. Our proposal replaces these by a Linear embedding, a Positional Encoding and Encoder Transformer. Moreover, we add the aforementioned agent metadata (object type and track category), and we substitute the Actor to Actor attention of the fusion cycle for a GCN [13] operator to enhance agents global interaction. It can be appreciated how we obtained a similar performance (both with 128 latent dimension in *Ours-m*, and 64 latent in *Ours-s*), reducing the parameters and inference time.

Finally, our best model, which includes heuristic proposals that serve as a preliminar multi-modal guidance for the model and motion refinement to improve the quality of the final predictions, obtains a performance on pair with [12], reducing the number of parameters and inference time about 21% and 41% respectively. We can appreciate in Table 7.2 how our model generalizes well in the test set, with results (both in uni-modal and multi-modal prediction) up-to-pair with other state-of-the-art algorithms.

We provide advanced qualitative samples in Figure 7.4, where we show the HD Map of real traffic scenes, heuristic trajectory proposals in the form of centerlines, and the multimodal predictions from our model including their respective confidences (the higher, the most probable).

Table 7.1: Comparison of methods in the Argoverse 2 Validation Set. We show the number of parameters for each model, prediction metrics (minADE, minFDE and brier-minFDE) for the multimodal scenario (k=6) and runtime. Runtime was measured on a single GPU A100-SXM4 (using batch 128). Our experiments are indicated using †. We use as baseline method GANet [12]. We bold the best results in **black** and the second best in **blue** for each metric.

Method	Map	# Par. (M)	minADE (m) ↓	minFDE (m) ↓	brier-minFDE (m) ↓	Runtime (ms) ↓
GANet [12]	Yes	6.2	0.806	1.402	2.02	1612
GANet w/o Map Decoder [12]	Yes	5.7	0.84	1.55	2.18	1353
GANet w/o Goal Areas [12]	Yes	4.5	0.87	1.66	2.29	1134
GANet w/o map [12]	No	1.79	1.034	2.212	2.825	838
† CRAT-Pred [13]	No	0.53	1.31	2.78	3.65	223
† Ours-social: GANet w/o map [12] ActorNet → Attention Transformer	No	0.86	1.19	2.34	3.19	193
† Ours-base: GANet [12] ActorNet → Attention Transformer	Yes	5.0	0.83	1.45	2.07	923
† Ours-m: Ours-base + A2A → C-GCN + Metadata	Yes	4.74	0.82	1.43	2.05	892
† Ours-s: Ours-base + A2A → C-GCN + Metadata (64 latent size)	Yes	1.2	0.88	1.53	2.15	893
† **Ours:** Ours-m + Proposals + Motion Refinement	Yes	4.92	0.81	1.42	2.04	946

As we discussed throughout this Chapter, we designed our model to ensure realistic predictions. We can appreciate that all the predictions are plausible and constrained to the scene geometry *e.g.* lane distribution and centerlines. We believe our heuristic proposals help to regularize the model and produce realistic predictions that would ensure traffic safety. For simplicity, we only illustrate the heuristic proposals for the focal agent and ego-vehicle. We believe our software for qualitative analysis of MP models on the well-known Argoverse 2 [7] is fundamental and a core contribution.

Table 7.2: Results on the Argoverse 2 Motion Forecasting Leaderboard. The "-" denotes that this result was not reported in their paper. Some numbers are borrowed from [12]. We bold the best results in **black** and the second best in **blue** for each metric.

Method	b-minFDE ↓ (K=6)	MR ↓ (K=6)	minFDE ↓ (K=6)	minADE ↓ (K=6)	minFDE ↓ (K=1)	minFDE ↓ (K=1)	MR ↓ (K=1)
DirEC	3.29	0.52	2.83	1.26	6.82	2.67	0.73
drivingfree	3.03	0.49	2.58	1.17	6.26	2.47	0.72
LGU	2.77	0.37	2.15	1.05	6.91	2.77	0.73
Autowise.AI(GNA)	2.45	0.29	1.82	0.91	6.27	2.47	0.71
Timeformer [135]	2.16	0.20	1.51	0.88	4.71	1.95	0.64
QCNet	2.14	0.24	1.58	0.76	4.79	1.89	0.63
OPPred w/o Ensemble [129]	2.03	0.180	1.389	0.733	4.70	1.84	0.615
TENET w/o Ensemble [136]	2.01	-	-	-	-	-	-
Polkach(VILaneIter)	2.00	0.19	1.39	**0.71**	4.74	1.82	0.61
GANet	**1.969**	**0.171**	**1.352**	0.728	**4.475**	**1.775**	**0.597**
Ours	1.98	0.185	1.37	0.73	4.53	1.79	0.608

7.4. Summary

In this Chapter we solve the challenging problem of Multi-Agent MP in real driving scenarios. We present an end-to-end pipeline that combines DL and heuristic scene understanding. Our model uses as input the map of the scene, the past trajectories of the agents, and additional information about the scene geometry and agents *e.g.* type of agent, lane distribution. We propose a model that integrates attention mechanisms with GNNs, heuristic goals, and a motion refinement module to further improve temporal consistency. We achieve SOTA results on the Argoverse 2 Motion Forecasting Benchmark

reducing in millions of parameters previous methods such as GANet, and improving over LaneGCN. Our code is publicly available.

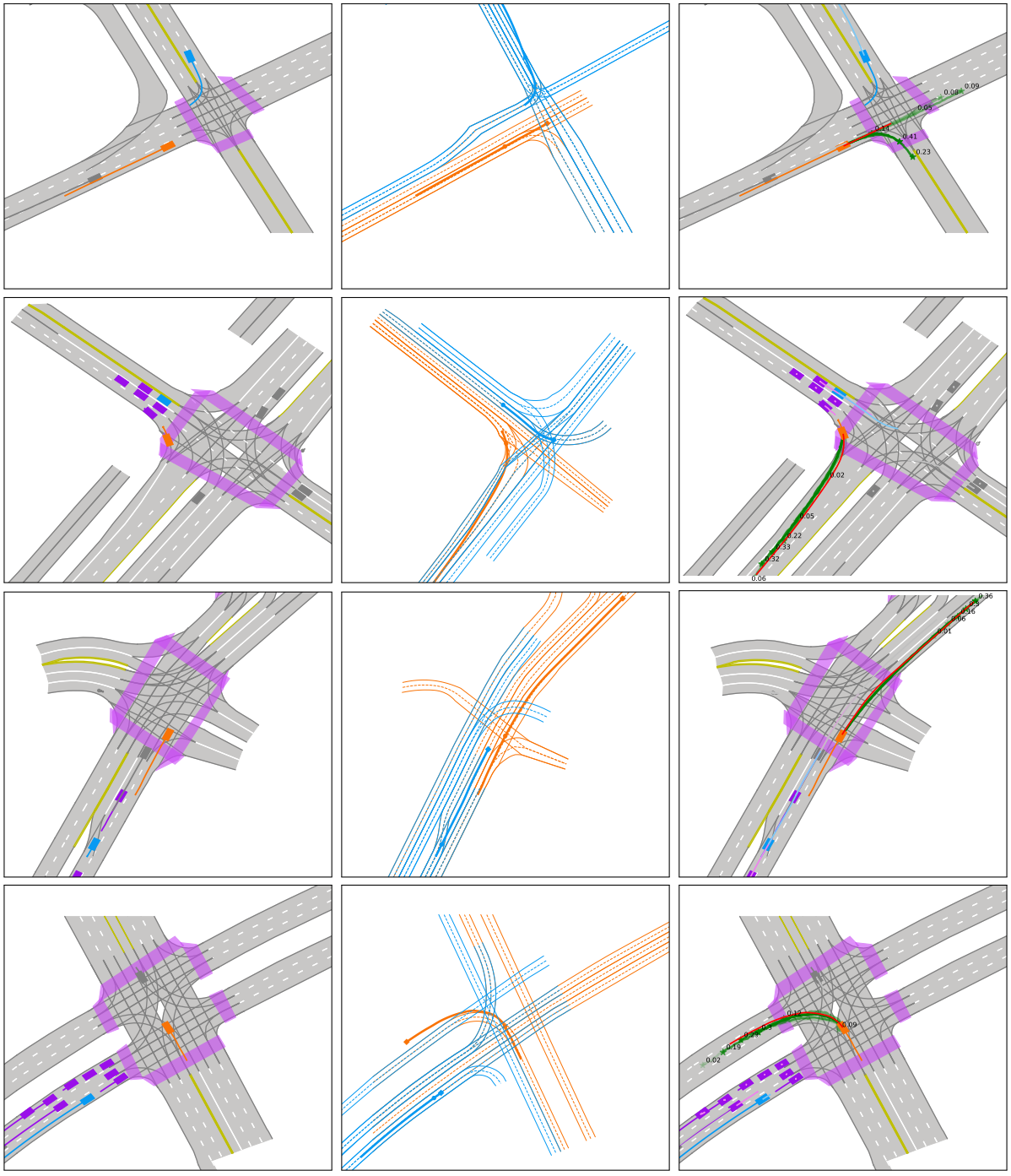

HD Map input | Heuristic lane proposals | Multi-modal (K=6) predictions

Figure 7.4: Qualitative Results on challenging scenarios in Argoverse 2 using our best model. We represent: our vehicle (**ego**), the **focal agent**, the **relevant agents** in the scene, and **other agents**. We can also see the **ground-truth** trajectory of the target agent, our **multi-modal predictions** (with the corresponding **confidences**). We also highlight the most important topology of the road, such as pedestrian crossing and boundaries mark type. We show, from left to right, a general view of the traffic scenario (including and map information), the heuristic proposals for each agent (we only include the **ego** and **focal agent** for simplicity) and the multi-modal prediction ($K = 6$) for the **focal agent**, including the corresponding confidences (the higher, the most probable)

Chapter 8

Applications in Autonomous Driving

Trabaja duro en silencio,
y deja que tu éxito
haga todo el ruido.

Autor original: Frank Ocean

8.1. Introduction

In this Chapter we detail the experiments carried out to assess the performance of our final proposal, both in terms of accuracy and computational resources (time, Hz) for real-time applications in the field of AD.

First, we integrate our prediction pipeline in the Decision-Making (DM) layer of our research group and we study its influence when computing the most optimal action for the ego-vehicle, in contrast to reactive proposals where only the past observations or current adversaries positions are required. Experimental results are obtained in the Scalable Multi-Agent Reinforcement Learning Training School (SMARTS) [137] framework based on the Simulation of Urban MObility (SUMO) [138] simulator. This integration of the prediction pipeline and the DM layer was published in the following conference paper [139]: "Augmented Reinforcement Learning with Efficient Social-based Motion Prediction for Autonomous Decision-Making", 2023 IEEE 26th International Conference on Intelligent Transportation Systems (ITSC).

Second, the prediction pipeline is integrated in the ADS of our research group using the CAr Learning to Act simulator (CARLA) [62] simulator to study the domain adaptation of our prediction model in complex scenarios of the CARLA Autonomous Driving Leaderboard [1], inspired in the well-established National Highway Traffic Safety Administration (NHTSA) typology. Since in this thesis we do not focus on the detection stage, and in the different MP datasets the agents are assumed to be tracked before feeding the network, for simplicity purposes, we will make use of a simple-yet-powerful concept such us ray-tracing

[1] https://leaderboard.carla.org/

to obtain a realistic Ground-Truth (GT) to emulate the input of multi-tracked agents provided by the different datasets. The main reason to use a ray-tracing-based filtering is to get those agents which are within a certain radius with respect to the ego-vehicle and are observed by the rays of the LiDAR sensor in such a way a SOTA sensor fusion could detect and track that object. By assuming this, we will be able to deploy and validate (since we have the past and future of the scene) our prediction pipeline in the overall architecture in an efficient and isolated way both in simulation or our real-world vehicle.

8.2. Predictions for Decision-Making

The increasing popularity of ADSs has brought with it significant challenges in ensuring safe and effective decision-making, particularly in complex urban driving scenarios [140]. RL techniques have emerged as a promising solution to address these challenges [141], outperforming ruled-based approaches that usually cannot solve complex situations [142]. They enable ADSs to learn from their interactions with the driving environment, without relying on pre-defined rules. However, RL-based approaches still face a number of limitations that can hinder their development, including issues related to state representation.

A key challenge in RL-based ADSs is the development of effective state representations that can account for the complexity of urban driving scenarios. Unlike in simpler environments, state representations for urban driving must be able to incorporate a wide range of information, including dynamic features of traffic flows and interactions among different agents. Finding ways to effectively encode this information and develop accurate state representations is essential to enabling RL-based ADSs to generalize to various scenarios and make effective driving decisions. Distilling predictive information from scene representations can aid in the development of effective decision-making policies for ADSs. By better understanding the potential consequences of different driving actions, RL-based ADSs can make more informed decisions that lead to safer and more efficient driving behaviour.

In this application we propose an approach to enhance the efficiency and generalization of RL-based ADSs in urban driving scenarios. Specifically, we introduce the use of a MP module to obtain the future positions of the ego-vehicle and the surrounding vehicles (adversaries) in the scenario. These predictions are the input to an RL-based DM module that executes high-level actions. Our approach is developed using the Proximal Policy Optimization (PPO) algorithm [143]. We carry out the evaluation in an unsignalized T-intersection scenario implemented in the SMARTS simulator, as shown in Figure 8.1, with and without the proposed state representation and provide a comparison with some baseline methods.

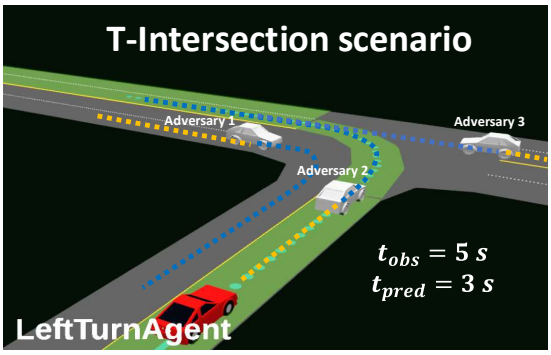

Figure 8.1: T-intersection scenario in the SMARTS simulator. The past positions of the adversaries (yellow) and the predicted trajectories (**blue**) are represented in the scenario.

This application is focused on a critical issue for RL-based ADSs, which is the state representation problem. Traditional state representations often focus on low-dimensional features such as distance to obstacles, lane positions, and vehicle velocities [144]. However, these representations may not be sufficient to capture the complex interactions among different agents and road structures in urban driving scenarios. To address the state representation problem, some methods have been proposed that use high-dimensional or learned representations, such as CNNs [145] and RNNs [146]; other methods have been proposed to use more detailed representations, such as BEV images [147], image augmentation [148] or occupancy grids [149]. These methods have shown promising results in improving the generalization and robustness of the decision-making approaches. Recently, transformer-based approaches have gained increasing attention for their ability to capture long-term dependencies and interactions among different entities in sequential data. In the context of AD, transformers have been used to reduce the computational load in end-to-end approaches [150] and anticipate future states with prediction-aware planning [151].

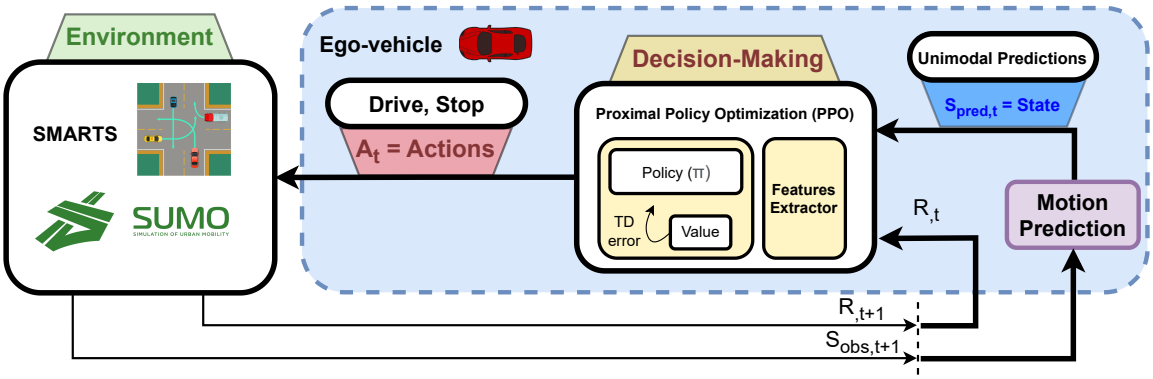

Figure 8.2: An overview of the Augmented RL with Efficient Social-based MP for Autonomous DM. The observations (both position and ID, so, trackers) of the vehicles in the scenario are obtained from the simulator. The MP module estimates the future positions of these vehicles, taking into account the most plausible score of a multimodal prediction. The decision-making module selects high-level actions based on this information. These actions are executed by the simulator, which provides a new state to the framework.

The objective of this study is to illustrate the efficacy of employing a low-dimensional state representation in conjunction with an MP method. We aim to prove that the proposed framework can lead to good performance in urban scenarios. More specifically, this application presents the following contributions:

- The **augmentation of RL-based DM techniques with MP** to improve state representation. By predicting vehicle trajectories, we can better capture the complex interactions between different agents and road structures in urban driving scenarios.
- **Higher explainability** than end-to-end methods. Intermediate states are accessible in our approach. This can help to understand the decisions made.
- We provide a **comparison with baseline methods** in a standard scenario. We demonstrate that our approach leads to some improvements in performance, particularly in scenarios with high velocities.

8.2.1. Our approach

The RL framework proposed in this work, which executes high-level decisions to solve urban driving scenarios, is represented in Figure 8.2. The past observations of the position of adversaries are obtained from the environment. This information is provided to our MP module (excluding the map for simplicity), which estimates future positions. The PPO algorithm takes these predictions and generates the decision-making output.

As observed in Figure 8.2, the overall pipeline mainly consists on two different learning processes: supervised learning for the MP module and a RL approach for the DM module. These two modules are trained separately, which allows access to the information of the predictions that feed the DM module.

8.2.1.1. Efficient Social-based Prediction stage

As observed throughout this thesis, predicting the future behaviour of traffic agents around the ego-vehicle is one of the key unsolved challenges in reaching full self-driving autonomy and it is required to be multi-modal, which means given the past motion of a particular vehicle and its surrounding scene, there may exist more than one possible future behaviour. Therefore, MP models need to cover the different choices a driver could make (*i.e.* going straight or turning, accelerations or slowing down) as a possible trajectory in the immediate future or as a probability distribution of the agents future location. In other words, when an ADS attempts to make a specific action (*e.g.* left turn, brake or accelerate), it must consider the future motion of the other vehicles, since the own future actions (also known as decision-making or behaviour planning) depends on the all possible maneuvers of the other agents of the scene for safe driving.

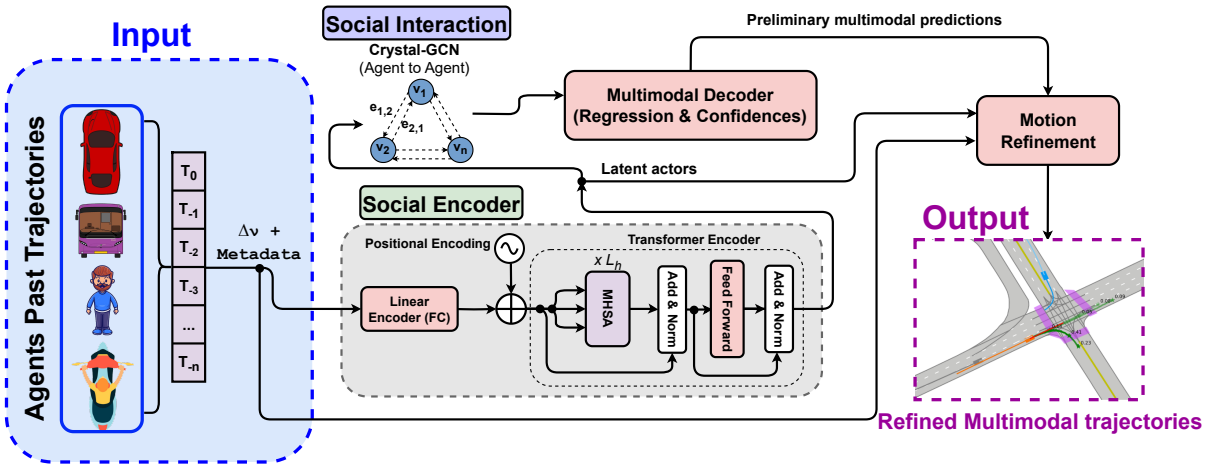

Figure 8.3: Overview of our Efficient Social-based MP. The main inputs are the relative displacements and centers (last observations) of the agents in the ego-vehicle frame. The relative displacements, agents centers and additional metadata are encoded through a transformer encoder and interactions are computed by means of a Crystal-GCN. Finally, K final future trajectories (modes) and their confidence scores are computed and refined through a multi-modal decoder and motion refinement module respectively.

Since our proposed decision-making and MP pipeline (Figure 8.2) is multi-stage to provide a more interpretable framework, we follow the principles of the Argoverse 2 Motion Forecasting dataset [7]. In particular, we take the final proposal of this thesis (Chapter 7) but excluding the map and heuristic lane proposals for simplicity. Then, this model is solely based on past trajectories (motion history, $obs_{len} = 50$) and agent metadata (in SMARTS we assume all agents are vehicles and are relevant), as observed in Figure 8.3, which output is a set of multi-modal predictions with $pred_{len} = 60$ future steps.

The Scalable Multi-Agent Reinforcement Learning Training School (SMARTS) [137] framework provides only the positions of the agents in the timestamp t. Nevertheless, in order to predict the future $pred_{len}$ trajectories of the agents, we require their corresponding obs_{len} trackers over a certain set of observations. Most vehicle prediction datasets [7] aim to predict the future behaviour of a target agent assuming the surrounding agents have been detected and tracked (so, monitored over time) and the map information is also provided. In that sense, since SMARTS provide the agents in the same order for consecutive timestamps (that is, the agent 5, unless it disappears from the scene, will be the agent 5 again in the next frame), we are able to compute a FIFO (*First Input First Output*) for each agent, not requiring data association [68] to perform this task.

On top of that, as proposed by multiple methods [14], [128], we consider only the vehicles that are observable at t=*0*, handling those agents that are not observed over the full sequence spectrum (observation length = obs_{len} + prediction length = $pred_{len}$) by concatenating a binary flag b_i^t that indicates if the agent is padded or not. In particular, we filter the static elements and track fragments scored by Argoverse 2 to get only the most relevant traffic agents, reducing the number of agents to be considered in complex traffic scenarios. Furthermore, to make the model translation and rotation invariant, the coordinate system in our model is BEV-centered of a given target agent at $t = 0$,

and we use the orientation from the target location given in the same timestamp as the positive x-axis. Note that this representation will benefit the model to have a common representation to enhance the generalization of the model and prevent overfitting. Once the scene has been translated and rotated, instead of using absolute 2D-BEV (xy plane), the input for the agent i is a series of relative displacements, as stated throughout this thesis.

Then, as stated in Chapter 7, we concatenate the agents past trajectories and additional social metadata in order to be processed by a linear embedding. Then, positional encoding is added to the output embedding explicitly to retain the information regarding the order of past trajectories and future preliminar steps. Finally, these latent features feed the transformer encoder, leveraging the self-attention mechanism and positional encoding to learn complex and dynamic patterns from long-term time series data. Once we have the latent vector of the different agents, as observed in Figure 8.3, we learn complex agent-agent interactions by means of a Crystal-GCN, which output is finally introduced into the multi-modal decoder. Taking the final actor features after motion history and agents interaction, a multi-modal prediction header outputs the final motion forecasting. For each agent, it predicts K possible future trajectories and their confidence scores. The header has two branches, a regression branch to predict the trajectory of each mode and a classification branch to predict the confidence score of each mode.

For the m-th actor, a residual block and a linear layer in the regression branch to regress the K sequences of BEV coordinates is obtained:

$$O_{m,\text{reg}} = \{(\mathbf{p}^k_{m,1}, \mathbf{p}^k_{m,2}, ..., \mathbf{p}^k_{m,T})\}_{k\in[0,K-1]} \tag{8.1}$$

where $O_{m,\text{reg}}$ is the whole set of regressions and $\mathbf{p}^k_{m,i}$ is the predicted m-th actor's BEV coordinates of the k-th mode at the i-th time step.

On the other hand, for the classification branch, a MLP to $\mathbf{p}^k_{m,T} - \mathbf{p}_{m,0}$ to get K distance embeddings is applied. Finally, each distance embedding is concatenated with the actor feature, applying a residual block and a linear layer to output K confidence scores, $O_{m,\text{cls}} = (c_{m,0}, c_{m,1}, ..., c_{m,K-1})$.

Finally, as stated in Chapter 7, a motion refinement modules takes into account the preliminary multi-modal predictions computed by the decoder, latent vector before the decoder and past trajectories (including the corresponding meta-data) to fine-tune the final trajectories by means of a regression and orientation loss.

On top of that, in this particular application in the SMARTS simulator, we take the most plausible future trajectory for each agent (both the adversaries and the ego-vehicle) in the following timestamps: *t=0*, *t=10*, *t=20* and *t=30*, which correspond to the current position and the predicted position of the corresponding agent 1, 2 and 3 seconds in the future respectively. Even though we train our prediction model following

the principles of Argoverse 2 (5s and 6s of observation and prediction respectively), given the velocities and traffic density of the experiments run in the SMARTS simulator , we believe that predicting 3s in the future is enough for this purpose to evaluate the high-level actions of decision-making layer preventing over-fitting. In future works, we will design more difficult scenarios, up-to-pair with the Argoverse 2 dataset (specially in terms of intersections or lane change behaviours at high speed) where multi-modal predictions with higher prediction horizons will be required.

8.2.1.2. Reinforcement Learning-based Decision Making

A Markov Decission Process (MDP) is a discrete-time stochastic control process that provides a mathematical framework for modelling decision-making environments. An MDP is a tuple (S, A, P, R) in which S is a set of states named state space, A is a set of actions named action space, P is the probability function and R is a reward function. An algorithm with a given state $s \in S$ takes an action $a \in A$ transitioning to s' with a probability $P(s, a, s')$, and getting a reward $R(s, a, s')$ as shown in Figure 8.2. This algorithm iterates through this loop to learn a desired behaviour.

The goal in an MDP is to find a good policy for the decision-making system. The objective is to find the optimal policy $\pi*(s)$, that maximizes the cumulative function of the future reward.

We represent the driving scenario as an MDP to develop our decision-making module. We consider the output of the MP module as an input to this module. The state space, action space, and reward functions are defined in this section.

8.2.1.2.1. State space The state is defined by the predicted trajectories of the ego-vehicle and the five closest vehicles in the scenario.

$$s_t = (K_t^{ego}, K_t^1, ..., K_t^5) \tag{8.2}$$

where $K_t^i = (x_{t_0}^i, y_{t_0}^i, x_{t_1}^i, y_{t_1}^i, x_{t_2}^i, y_{t_2}^i, x_{t_3}^i, y_{t_3}^i)$ contains the future estimations of the positions of the vehicles across a future horizon of three seconds. A representation of a state vector is shown in Figure 8.4, where the vehicles predicted positions are represented.

8.2.1.2.2. Action space We propose a discrete action space formed by two actions. A low-level controller implemented by the simulator is in charge of performing smooth driving based on these actions. These actions are focused on the ego-vehicle velocity. The first action aims to reach a desired predefined velocity and the second action reduces the velocity until the vehicle stops. The action space is defined as:

$$a = (Drive, Stop) \tag{8.3}$$

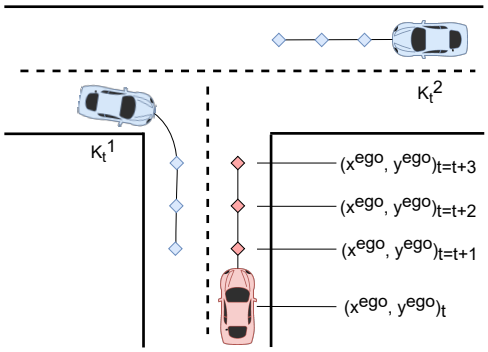

Figure 8.4: Predicted positions of the **ego-vehicle** and the **adversaries** in the next 3s.

8.2.1.2.3. Reward function The reward function is defined in terms of success or failure. A negative reward is given when there is a collision and a positive reward is given when the vehicle reaches the success point, situated at the end of the scenario.

$$r = k_v * v_{ego} + \begin{cases} 1 & if \quad sucess \\ -1 & if \quad collision \end{cases} \tag{8.4}$$

As shown in Equation 8.4, we add one more factor to the reward function to encourage the ego-vehicle to move. We propose a cumulative reward based on its longitudinal velocity. We use a constant small enough to ensure that the reward per episode is bounded between -1 and 1.

Our approach for the RL implementation (Figure 8.5) builds upon our previous research [152], where we demonstrated that incorporating a feature extractor module to a PPO algorithm yields improved metrics and faster convergence.

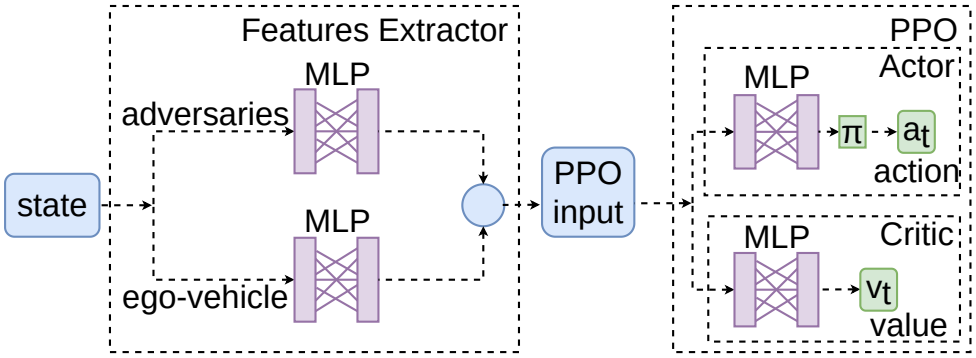

Figure 8.5: Overview of our Reinforcement Learning-based Decision-Making architecture. The neural network architecture consists of two fully connected layers followed by the concatenation of both adversaries and ego vehicle features. The resulting concatenated features are then passed through an actor-critic structure, which comprises two layers, each containing 128 neurons.

In this implementation, we introduce separate feature extractors for adversaries and the ego-vehicle, which are then concatenated into the input for the PPO algorithm. This algorithm consists of two models: the Actor, responsible for selecting an action based on the policy, and the Critic, which estimates the value function.

8.2.2. Experimental results

8.2.2.1. Driving scenario

To validate the performance of our approach, an intersection scenario is implemented in SMARTS, which is a SUMO [138] based simulation platform for research on autonomous driving.

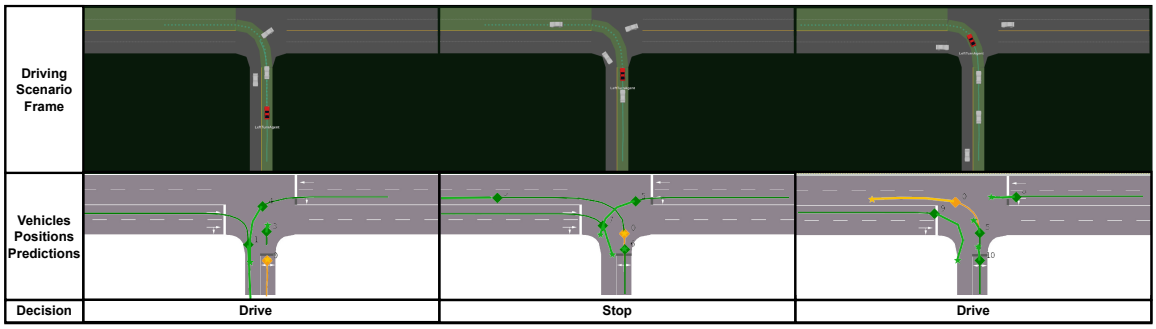

Figure 8.6: Simulation overview of our system behaviour. The red car follows the green path, and each image represents a different frame of the simulation. We also show the predicted positions below each image and the actions taken by the decision-making module.

The scenario is an urban unsignalized T-intersection. The objective is to execute a left turn maneuver in the absence of traffic signal protection, allowing the continuous flow of traffic. Fig. 8.1 illustrates the drivable area (highlighted in green) where the ego-vehicle can navigate to reach the target location. Simulations are reset under three conditions: 1) the ego-vehicle successfully reaches the target, 2) the episodic step surpasses the maximum time steps limit, and 3) the ego-vehicle collides or deviates from the drivable route.

We define different scenario configurations to test the performance of the proposed framework. First, the regular T-intersection scenario which is defined in SMARTS, where a random number of vehicles between [5-10] are spawned every minute, and the maximum velocity of these vehicles is 14 km/h. Then, we propose different configurations increasing the maximum velocity of the adversaries to 30, 60, and 90 km/h.

8.2.2.2. Evaluation Metrics

In decision-making, the success rate serves as a direct measure of the effectiveness of the RL agent in accomplishing the designated task. Besides, the average time of the episode is a common metric used in the literature. These metrics are defined as:

$$success[\%] = \frac{n_{success}}{n_{episodes}} \tag{8.5}$$

$$t_e[s] = \sum \frac{t_n}{n_{episodes}} \tag{8.6}$$

where the number of episodes n_e is 100 and simulation time is measured in seconds.

8.2.2.3. Results

To evaluate the performance of our approach we first present a comparison with the existing methods for decision-making in the literature and then an ablation study is conducted.

This first study compares the proposed approach with other existing methods for decision-making. The baseline methods used for comparison are Data-regularized Q-learning (DrQ) [148], Soft Actor-Critic (SAC) [153], and PPO. These methods have different features and serve as reference points for evaluating the proposed approach. The results presented in Table 8.1 demonstrate a higher success rate of our proposal.

Table 8.1: Comparison of the proposed framework against the existing baselines in the T-intersection scenario. The success rate S[%] and the average episode time t_e are presented.

Metric	Ours	PPO	SAC	DrQ
S[%]	**80**	70	68	78
t_e(s)	22.3	36.4	19.2	**18.2**

Two ablative studies are carried out to see how the use of motion prediction in the state representation can improve the performance of the framework. The first approach is to use just the position of the vehicles as the input to the decision-making module and the second approach is to use the locations over the past five seconds. We test the three approaches under the previously introduced configurations with different adversaries' velocities, from 15km/h to 90km/h. To correctly evaluate the performance of the decision-making system we propose different metrics that aim to provide a better comprehension of the behaviour. We believe that the success rate is still a good indicator, but we slightly modify the average time, only considering the successful episodes to calculate this metric. In addition, we include a new relevant metric: the average ego-vehicle velocity when a collision takes place v_c.

The results presented in Table 8.2 show that the use of the predicted positions in the state vector avoids more collisions as the velocities increase. Besides, the average collision velocity and the average time to complete the scenario are lower for the proposed approach.

Finally, an overview of the behaviour of our system is shown in Figure 8.6. The ego-vehicle in red follows the trajectory defined in green. Each image represents a different frame of the simulation and the respective predictions of the positions are displayed below. Besides, the action executed by the decision-making module for each frame is shown.

8.3. Domain Adaptation in CARLA simulator

In this Section we study the domain adaptation of our efficient social-based prediction model (Figure 8.3) in the CARLA simulator. As stated in previous sections, CARLA

Table 8.2: Ablation study comparing three state representations with different scenario configurations: Current positions, Past positions, and Future positions. The success rate S[%], the episode time t_e in these successful episodes, and the average velocity of collision v_c are presented.

	Metric	15 km/h	30 km/h	60 km/h	90 km/h
Future	S [%]	80	78	78	77
	t_e (s)	22.3	23.3	23.4	23.3
	v_c (km/h)	4.9	5.1	5.6	5.6
Current	S [%]	77	73	70	70
	t_e (s)	25.1	23.4	23.4	23.3
	v_c (km/h)	5.1	5.5	6.1	6.2
Past	S [%]	78	75	72	71
	t_e (s)	24.2	23.3	23.2	23.1
	v_c (km/h)	4.9	5.2	5.9	6.0

provides a realistic sensor simulation environment, including cameras, LiDAR, and other on-board sensors. On top of that, it accurately models vehicle dynamics, including realistic acceleration, braking, and steering behaviors in complex traffic scenarios with various types of vehicles, pedestrians, and cyclists, enabling motion prediction algorithms to be tested and evaluated in realistic traffic situations, such as sudden imminent collisions with another vehicle, unexpected VRU, intersections or lane change maneuver in a high-way, where the ego-vehicle must pay attention to the surrounding scene and predict its future to take the optimal action.

To this end, we take the ADS provided by the RobeSafe research group (including the global planning, perception with basic map monitoring, control and DM modules) to move the vehicle around the city in a reactive way (that is, stop in front of red traffic lights, unexpected VRU and avoid collisions, not taking into account the predictions of the model presented in this thesis) given a pre-defined route. In this case, the global routes are predefined by the CARLA Autonomous Driving Leaderboard [62], one of the main competitions around the world to evaluate ADS proposals, either end-to-end or modular-based. Since our MP pipeline require a set of obs_{len} observations per agent, *i.e.* the agent has been previously detected and tracked in such a way a buffer is filled with its past observations, a robust and reliable detection and tracking stage should be implemented to perform 360 °sensor fusion and monitor the most relevant obstacles around the ego-vehicle. Nevertheless, implementing the whole perception pipeline is out of the scope of the thesis, which is mainly focused on the prediction stage.

In that sense, as observed in Figure to validate our prediction pipeline in CARLA in real-time simulation (not in isolated traffic scenarios, as expected from a dataset), we make use of the Autonomous Driving Perception Development Kit (also referred as AD-PerDevKit), partially published (where I am a co-author) in the following conference paper [154]: "Ad perdevkit: an autonomous driving perception development kit using carla simulator and ros", 2022 IEEE 25th International Conference on Intelligent Transportation Systems (ITSC), p. 4095-4100.

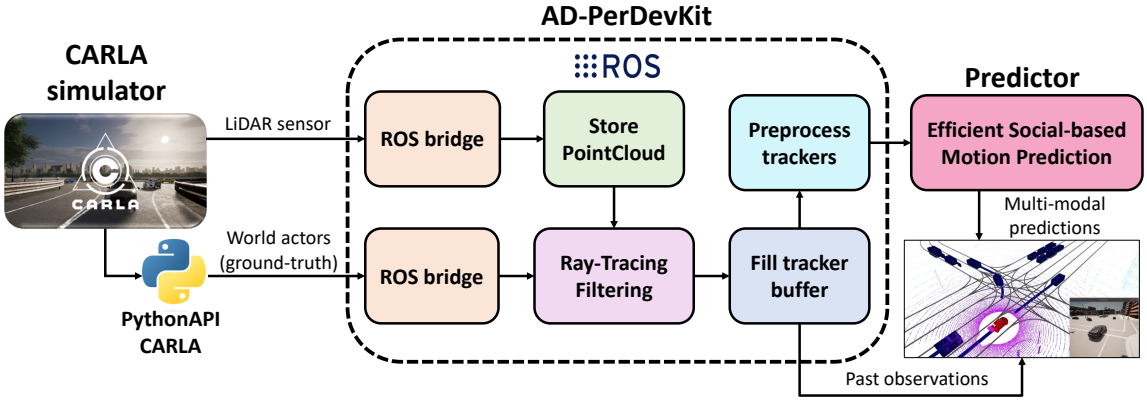

Figure 8.7: Overview of the integration of our prediction pipeline in the CARLA simulator using the AD-PerDevKit tool. The PythonAPI module is used to obtain all actors in the world. Our AD-PerDevKit performs a ray-tracing-based filtering to keep only those obstacles which are hit by at least one LiDAR ray. Past observations are considered over time for these relevant obstacles which are used to feed the social-based prediction pipeline.

8.3.1. Autonomous Driving Perception Development Kit (AD-PerDevKit)

As stated above, most SOTA MP pipelines in the field of AD require 360° DAMOT to get the past observations of the agents and then predict their future actions. Since this thesis is not focused neither in object detection nor tracking, which would involve significant complexity and effort, surpassing the intended focus of this research, utilizing ray-tracing-based ground-truth as a realistic representation of the environment is a justifiable decision.

Autonomous driving systems rely on accurate and reliable input data to make informed decisions. Ray-tracing techniques, which simulate the behavior of light in a virtual environment, provide a highly realistic representation of the surroundings. By employing ray-tracing-based ground-truth, precise information about the positions, shapes, and properties of obstacles in the environment can be generated as preliminary information before conducting the prediction stage. This approach ensures that the ADS receives high-fidelity data that closely resembles real-world conditions.

Moreover, the offline nature of the ground-truth generation process allows for flexibility in experimentation, debugging, and analysis, which can significantly benefit the development and evaluation of the prediction algorithm. For example, by storing the ground-truth of a whole scenario as a text file, do the same with the output predictions, and finally obtain the same metrics that the original dataset where the model was trained to check the domain adaptation (that is, if the model works fine or not without fine-tuning with the current environment data).

The main contribution of the AD-PerDevKit is the creation of a ground-truth generation tool for the surrounding obstacles of the ego-vehicle using CARLA and ROS. For

its implementation, the CARLA-ROS brige is used so that the simultaneous execution of CARLA and this tool is not necessary, since the execution of both programs can be very demanding due to the simulator requirements. This way it is possible to record a rosbag (a file with all the ROS messages) with the GT information, so that only an area around the ego-vehicle is analyzed and not the whole obstacles in the CARLA runtime.

The messages created by CARLA contain the information of the different objects of the environment in relation to the map on which it is being used. However, to be used independently, the obstacles must be referenced to the ego-vehicle. Therefore, it is necessary to perform the different transformations to go from a coordinate system based on the map to a coordinate system based on the ego-vehicle.

8.3.1.1. Ray-Tracing-based Filtering

One main issue for the GT calculation is that CARLA always render all the objects, even when they are not visible by the camera, LiDAR or Radar, which is a problem for any training or validation process. In other words, it is necessary to calculate the visibility of the objects from the vehicle, since, otherwise, when proceeding with the evaluation, the precision of the models would be reduced due to not being able to detect some occluded or invisible objects. As aforementioned, to solve that calculation of object visibility (*i.e.* an object that could be preliminarily observed by a SOTA sensor fusion module), we make use of the ray-tracing paradigm.

There are many studies about ray tracing that solve this issue. These techniques [155], [156] are computationally very expensive so it is very difficult to implement them in real-time. In that sense, we propose a method using directly the point-cloud calculated by the simulator. Regarding this, a vehicle will be considered as visible, as long as a point of the LiDAR point-cloud is found inside an object, in the same way as it is done in the nuScenes dataset [56].

Moreover, it is important to note that this tool is designed to work either for offline or online GT generation. On the other hand, one of the most important and delicate parts for the real-time use of this application is efficiency, so it is necessary to perform a method similar to the SOTA in terms of ray-tracing, but with low computational cost. Therefore, it was decided to use the latest point-cloud processed by our custom Robot Operating System (ROS) bridge to filter the objects in the environment given a frequency of 10 Hz (standard in the AD industry, and particularly in the CARLA Autonomous Driving Leaderboard). For the implementation of this operation, vectorization of the operations is necessary, as computation needs to be done in less than 10^{-2} seconds. It must be noted that only vehicles and pedestrians are considered for our purposes, since CARLA also provides the traffic lights and other traffic infrastructure as World agents or actors. The steps to be performed are the summarized in Algorithm 8.1, where a maximum distance of 120 m is considered to filter the furthest agents:

Algorithm 8.1: Ray-tracing-based filtering algorithm to perform object visibility in the AD-PerDevKit

Input : LiDAR raw data and CARLA World objects
Output: Bounding box parameters of visible agents

Transform LiDAR raw data and CARLA World objects into ROS format to enhance matrix operations and interpretability.

Remove objects further than the maximum LiDAR distance.

Delete points in the point cloud with heights higher or lower than the objects in the surroundings.

Function $f_{\text{visible\_bb}}(\text{bb}, \text{points})$:

    return np.logical_and(

        np.logical_and(bb[0] $-\frac{\text{bb[3]}}{2} \leq$ np.array(points[:, 0]),

        np.array(points[:, 0]) $\leq$ bb[0] $+\frac{\text{bb[3]}}{2}$,

        bb[1] $-\frac{\text{bb[4]}}{2} \leq$ np.array(points[:, 1])),

        np.logical_and(np.array(points[:, 1]) $\leq$ bb[1] $+\frac{\text{bb[4]}}{2}$,

        bb[2] $-\frac{\text{bb[5]}}{2} \leq$ np.array(points[:, 2]),

        np.array(points[:, 2]) $\leq$ bb[2] $+\frac{\text{bb[5]}}{2}$))

Select visible objects having at least one point in the pointcloud, considering the rotation of different objects.

If pointcloud data is available:

    $points\_in\_bb \leftarrow f_{\text{visible\_bb}}$((obj.position_x, obj.position_y,

                obj.position_z, obj.l, obj.w, obj.h), self.pointcloud)

    $n\_points\_in\_bb \leftarrow$ np.add.reduce($points\_in\_bb$)

8.3.2. Experimental results

Once we have calculated the 360° visible objects in a frame t, as additional preprocessing steps the AD-PerDevKit tool fills a buffer with the past positions of the corresponding agent (simulating a real-world buffered Multi-Object Tracker). Note that if the buffer of an agent was created and in a given frame t it is occluded, the observation at that particular timestamp (in the same way than computed in previous Chapters) is filled with zeros and the binary flag b_i^t set to 1, indicating that the observation t of the agent i has been padded.

Nevertheless, since the proposed prediction model has been trained in Argoverse 2 using an observation length of $obs_{len} = 50$ (*i.e.* 5s of motion history regarding a frequency of 10 Hz). Then, calculating the predictions with only 2 or 3 observations would not make sense, since even though there are several agents in Argoverse 1 and Argoverse 2 with only few observations (for example, an object is relevant in the scene since it is relevant to the ADS in $t = 0$, with only has 4 observations because suddenly appeared in the traffic scenario), most agents should not be predicted with such a low number of observations. To this end, we filter those obstacles with a number of observations less than a certain threshold, set to 30 in this case. Figure 8.8 depicts an example in Town03 of the AD-PerDevKit output while driving our ADS in the CARLA simulator. We illustrate the past observations (until $obs_{len} = 50$) of the relevant agents such as **vehicles** (cars, vans, trucks, buses) and **VRUs** (cyclists, motorcyclists and pedestrians), as well as the **ego-vehicle** observations. All agents have their corresponding identifier.

In terms of prediction, model will be able to predict only if the ego-vehicle has at least two observations, since to compute the rotation angle, at least the current and past observations are required. Moreover, **multi-modal predictions** are calculated for each agent (including the ego-vehicle, treated as a standard agent, not taking into account the CMP paradigm as explained in Chapter 2). Note that for visualization purposes, we avoid plotting the ego-vehicle predictions, other agents modes with a confidence value lower than a certain threshold, in this case set to 0.2. The remaining predictions will be sorted in terms of opacity based on their confidence: the higher the transparency, the less probable the future mode or behavior will be, as illustrated throughout the thesis. Furthermore, even though in CARLA our ego-vehicle is a gray Lincoln MKZ 2017, in the RVIZ tool, for visualization purposes, it is represented as the red vehicle. Note that, in all traffic scenarios, the model should be able to differentiate between static and dynamic objects, *i.e.* the model must reason which agents should keep their position in future frames (*e.g.* agents stopped in front of a red traffic light or stop) and which agents, even though they are currently stopped, must be predicted since ahead vehicles have started moving. Dynamic agents, as expected, are predicted in all different situations.

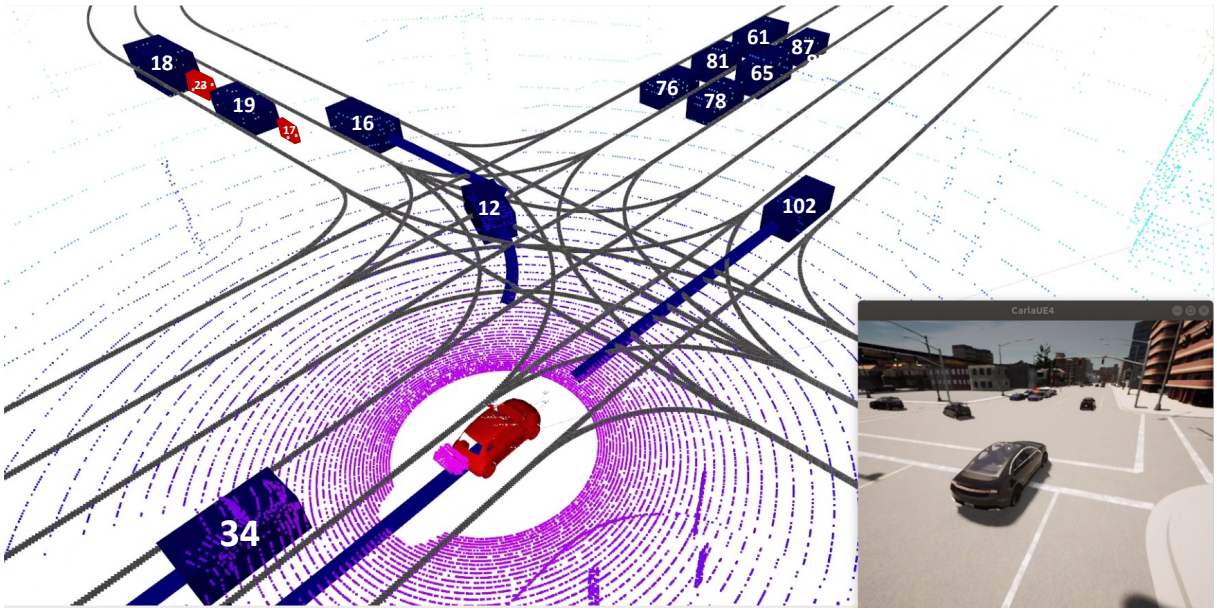

Figure 8.8: Ray-tracing-based filtering example and buffered MOT in the RVIZ simulator. Past observations (until $obs_{len} = 50$) of the relevant agents such as **vehicles** (cars, vans, trucks, buses) and **VRUs** (cyclists, motorcyclists and pedestrians), as well as the **ego-vehicle** observations. All agents have their corresponding identifier.

Experiments were run in a PC desktop computer consisting of an AMD Ryzen 9 5900X 12-Core Processor (overclocked to 3.7 GHz), NVIDIA 3090 RTX Ti and 32 GB of RAM (3200 MHz). To qualitatively validate our prediction pipeline, we have designed several interesting use cases in the CARLA simulator using the OpenScenario tool, inspired in the NHTSA where a prediction algorithm is of vital importance to take the optimal action

Table 8.3: Summary of use cases conducted in the CARLA to study the domain adaptation of our efficient social-based MP algorithm

Scenario ID	Town	Use case highlights	Actors in the world	Ego max-vel [km/h]	minADE (K=6) ↓	Threshold min observations
1	03	Stop + 4-ways intersection	120	25.2	1.96	30
2	04	Crowded highway	180	54	2.52	30
3	01	Red Traffic Light + Unexpected VRU	100	25.2	1.78	3
4	03	Crowded roundabout	160	36	2.81	30

in the short/long term, being essential to improve the safety and comfort of both the ego-vehicle and the surrounding environment. As aforementioned, map information is not included in the model for simplicity due to the noticeable amount of work to adapt the HD map format and heuristic lane proposals extraction (as proposed in Chapter 7) to a completely different environment. Furthermore, as trained in Argoverse 1 and 2, observations are received at a frequency of 10 Hz from the simulator.

Table 8.3 summarizes the proposed use cases, including the following features: Scenario ID, CARLA simulator town where it was conducted, use case highlights, total number of actors in the world, ego-vehicle speed, and minADE K=6, which is the most representative MP metric throughout this thesis, and a threshold of minimum of number of observations to start predicting an agent. Note that the number of actors in the CARLA is the recommended traffic density for the corresponding town in the CARLA Autonomous Driving Leaderboard to avoid unnecessary blockouts specially in crowded roads and intersections.

In order to evaluate the model in the different scenarios, we store the buffers of all observed objects at frame t in a *csv* file. Then, after the traffic scenario has finished, we have $obs_{len} = 50$ observations at frame t per agent, which is the input required by the prediction network in Argoverse 2. Furthermore, it is important to take into account that the GT for each timestamp t must be a set of $pred_{len} = 60$ 2D BEV positions in global coordinates. To this end, as a preprocessing step, given a timestamp (so, its corresponding *csv* file), we gather the future positions of the agents observed in the current file. If an agent has not been observed at a particular frame in the prediction horizon (*i.e.* the agent was not observed in the $39-th$ future step out of 60), that position of the GT is masked in such a way it will not be compared with the output of our model. Finally, after having the GT of the whole scenario and predictions per frame, we follow standard practices to compute the minADE and minFDE metrics (both in the uni-modal and multi-modal scenario). As observed in Figures 8.10, 8.13, **??** and 8.19, at the end of the scenarios the metrics are closed to zero since the number of future steps start decreasing from $frames_{total} - 60$, in such a way we can only compare our predictions with the nearest future steps (from long-term to short-term, because other positions of the GT are masked). Further details and code to generate the GT and calculate the metrics may be found in the final open-source [2] proposal of this thesis.

[2] https://github.com/Cram3r95/argo2goalmp

8.3.2.1. Scenario 1: Stop and 4-ways intersection in Town03

Figures 8.9, 8.10 and 8.11 show the ego-vehicle conducting a stop maneuver and 4-ways intersection in Town03. The number of agents in the world is set to 120, the maximum velocity for the ego-vehicle is 25.4 km/h, and the minimum number of observations is set to 30. As observed in Figure 8.10, the mean value of the minADE K=6 metric is 1.96, which is noticeable higher than the results obtained in Argoverse 2 with our proposed model without map information (multi-modal K=6 minADE = 1.19). However, it may be appreciated that most values are up-to-pair with the validated model (1.19) since the average value is greatly increased due to the large error from frames $\simeq$ 700 to $\simeq$ 800 when agents start moving after the corresponding traffic lights change from red to green, and the uncertainty in the prediction stage becomes noticeable higher.

Regarding the stop maneuver (Figures 8.11a and 8.11b at frame t), according to the traffic rules, the ego-vehicle must stop regardless if there are opponents around, so prediction is not required for the first stop. Nevertheless, predicting future behavior is absolutely necessary after making the first stop in order to safely merge into the new lane. It can be observed how the model proposes curved trajectories from straight past trajectories, as well as multi-modality, fundamentally in terms of different velocity profiles. This is because the model understands, based on the deep social features of the scene, that there are not several clearly distinct directions as is the case with an intersection. On the other hand, in the case of the 4-ways intersection, it can be clearly seen how the model is capable of understanding the difference between static objects (waiting behind a red traffic light, so predictions are calculated in the same site than observations), and dynamic objects. For example, agent number 392 (green Chevrolet Impala in Figures 8.11c, 8.11d at frame $t + 240$) presents multi-modality in terms of different possible directions (turn left or go straight) since the model understands that the agent is in an intersection given the surrounding agents and past observations, even though map information is not included. On the other hand, 2 seconds (20 frames) in the future the model reasons that agent 392 has left the intersection and makes multi-modal predictions with different speed profiles in a single direction.

8.3.2.2. Scenario 2: Crowded highway in Town04

Figures 8.12, 8.13 and 8.14 illustrate a crowded highway scenario in Town04. The number of agents in the world is set to 180, the maximum velocity for the ego-vehicle is 54 km/h, and the minimum number of observations is set to 30. This situation can be interpreted as a traffic jam, a standard situation when approaching a metropolis in the morning at work time. In this case, we may observe that the model does not compute multi-modal predictions towards different directions, but, as expected, it understands that all vehicles are driving in the same direction (either forward or reverse way) and the multi-modal prediction is computed in terms of different velocity. profiles (that is, the

agent can continue with the same velocity, suddenly break or accelerate in the mid/long term).

The mean minADE K=6 metric throughout the scenario and in general most values throughout the whole scenario are higher than the previous use case (2.52 vs 1.96) whilst from human perspective, a traffic jam should be easier to be predicted than an intersection since most agents present a similar velocity towards the same direction (either forward or reverse way). In that sense, one of the advantages of using our proposed AD-PerDevKit pipeline to compute realistic object trackers is that we realize about one of the most important concerns when driving in the AD field: object occlusion. Due to the large amount of agents in relatively small areas, LiDAR rays are not able to hit the corresponding agents, specially those which are further away from the ego-vehicle. Then, a lot of padding data is introduced to the network at the same time, so the model is not able to properly reason what is happening around. To this end, a possible solution could be integrating the object tracking and motion predictor in the same loop in order to use the most plausible predictions from previous timestamps as object observations if the sensor fusion module and tracker in the short-term cannot estimate the current position of the agent.

8.3.2.3. Scenario 3: Red Traffic Light and Unexpected VRU in Town01

Figures 8.15, **??** and 8.17 illustrate an urban scenario in Town01 where the ego-vehicle is initially stopped in front of a red traffic light, then turn left in a 3-ways intersection and finally must predict the future behaviour of an unexpected VRU (in this particular case, a kid suddenly appears running towards the road from behind a CocaCola vending machine). The number of agents in the world is set to 100, the maximum velocity for the ego-vehicle is 25.2 km/h.

Moreover, as discussed throughout this thesis, predicting the behaviour of VRUs, such as cyclists or pedestrians, is one of the most critical aspect of an ADS to be deployed and scaled to real-world applications in urban scenarios. In that sense, unlike other use cases, in this particular case the minimum number of observations is set to 3. The reason is simple: In order to predict the future actions of a challenging unexpected VRU who suddenly appears behind an obstacle (*e.g.* a wall, van, vending machine, etc.), we need to reduce the minimum number of observations to get predictions on time in order to perform an emergency break (note that in these experiments the predictions do not feed the DM module, but our reactive ADS, which includes map monitoring, is able to deal with the unexpected situation).

The mean minADE K=6 metric (1.78) of the whole scenario is worse than the reference in Argoverse 2 (1.19), but the actual metric in most frames is noticeable smaller than the mean. The model struggles from frame $t = 400$ to $t = 600$ when the ego-vehicle turns left and suddenly faces an unexpected VRU. In terms of the 3-ways intersection, Figures

8.17a, 8.17b and Figures 8.17c, 8.17d depict the traffic scenario at frame t and $t + 20$ respectively. In that sense, the vehicle 423 is approaching to the intersection. Since the model lacks of map information, it predicts keeping straight and turning right. Then, 2s in the future, due to its past motion (velocity and orientation, which are implicit in the relative displacements), the model correct computes all predictions in the same direction with different velocity profiles.

Finally, at the end of the scenario the ego-vehicle faces the unexpected VRU (Figures 8.17e, 8.17f and Figures 8.17g, 8.17h depict the traffic scenario at frame $t+145$ and $t+147$ respectively). Despite the fact that the model only has 3 observations out of $obs_{len} = 50$ to start predicting (remaining observations are padded with zeros), preliminary intentions are correctly computed with the corresponding velocity. Moreover, 2 frames later, due to the lack of past information, the model cannot decide a particular behaviour for the kid and still predicts the future actions in completely different directions, which is coherent given the nature of agent.

As observed, even though the model struggles in a particular moment of the traffic scenario, changing the minimum number of observations from 30 to 3 only increases the error at the beginning of the sequence when the model misses past information from the agents. However, in steady state (that is, when most of the agents have the observation buffer filled), the prediction accuracy is similar to the previous use cases.

An interesting point of view for future works could be how to assign the optimal minimum number of observations in the pipeline, or if it can depend on the agent type or potential risks associated to the traffic situation. Better predictions are usually associated to enriched past information (*i.e.* more data), so for vehicles it make sense to have at least 30 observations. Nevertheless, for VRUs, even though the model has been trained with way more past observations, it should predict the agent behaviour as fast as possible in spite of the fact that several modes are computed in non-plausible or non-sense directions.

8.3.2.4. Scenario 4: Crowded roundabout in Town03

Figures 8.19, 8.19 and 8.20 illustrate one of the most challenging traffic situations in urban scenarios, that is, a roundabout full of agents in Town03, considering incoming, outcoming and present agents in the current time-stamp. The number of agents in the world is set to 160, the maximum velocity for the ego-vehicle is 36 km/h, and the minimum number of observations is set to 30.

To help the behavioural and local planning modules to take the optimal action, the model clearly predicts the circular motion of the agents, either for the agents that are in the roundabout with different velocity profiles or even for the incoming agents which are going to get into the roundabout and probably intersect with the trajectory of our ego-vehicle if the adversary does not respect the give-way traffic signal.

The mean minADE K=6 metric (2.81) of the whole scenario is the worst among all proposed scenarios, due to the huge difficulty of predicting the future motion of the agents in a roundabout without map information. There are some agents (such as 405 and 289) which are turning left (roundabout direction is counter-clockwise) and once they leave the roundabout, they are turning right, which is quite difficult to predict without the geometrical constraints, as well as semantic and topological information, of the road.

Moreover, in a similar way to the Scenario 2 (crowded highway), due to the large amount of agents (either vehicles or VRUs), as well as the fountain in the middle of the roundabout, there are many occlusions (*e.g.* object 376 in Figure 8.20b) which generate way more discontinuous past trajectories than in the training dataset, making difficult the generalization of the model. Conducting transfer learning and fine-tuning the model with CARLA scenarios could be an option to help the models understand high-complex situation in an enhanced way.

As observed, understanding this complex situation and taking account all different scenarios, from least dangerous to most optimistic, is the key to build a robust and reliable architecture.

8.4. Summary

In this Chapter we have evaluated our efficient social-based prediction model, where the incorporation of map information has been avoided for simplicity purposes, since the model has been evaluated in two frameworks, the SMARTS and CARLA simulators respectively, with a map graph structure way different to Argoverse 2.

In terms of the decision-making application, the prediction module must calculate the future positions of vehicles within the scenario to improve a Reinforcement Learning-based Decision Making module. The results of the study demonstrate that our approach achieves significant performance improvements, particularly in scenarios involving high velocities.

On the other hand, we have successfully integrated the prediction algorithm in our ADS in simulation using CARLA and studied the domain adaptation of the algorithm from a static dataset (Argoverse 2) to an hyper-realistic environment, using some scenarios inspired in the well-established NHTSA typology. Given the amount of work and complexity required to develop an efficient and accurate 360 °DAMOT pipeline, we make use of the AD-PerDevKit pipeline to generate a realistic GT given a ray-tracing-based filtering algorithm and some pre-processing steps to obtain a buffer of past observations for each agent, removing those agents with a number of observations lower than a certain threshold, as a preliminary stage before feeding the prediction module. As observed, the model is able to compute multi-modal predictions in terms of different directions and velocity profiles, or even predicting the trajectories in the same point for agents stopped

for a while, understanding the past motion and complex interactions among the agents and corresponding neighbours.

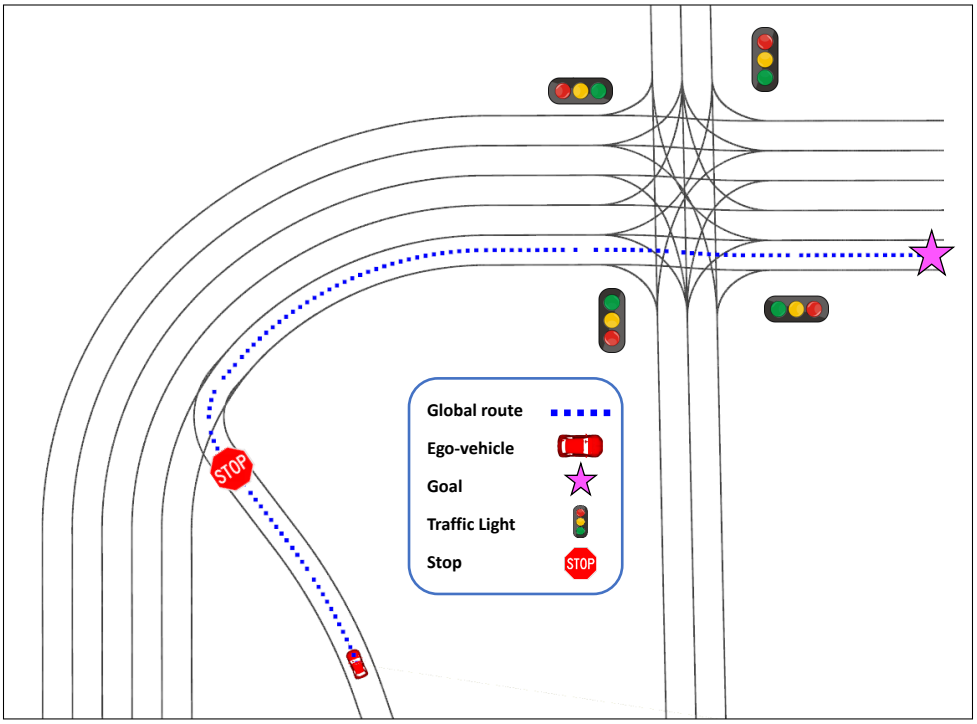

Figure 8.9: Scenario 1 overview: Stop and 4-ways intersection

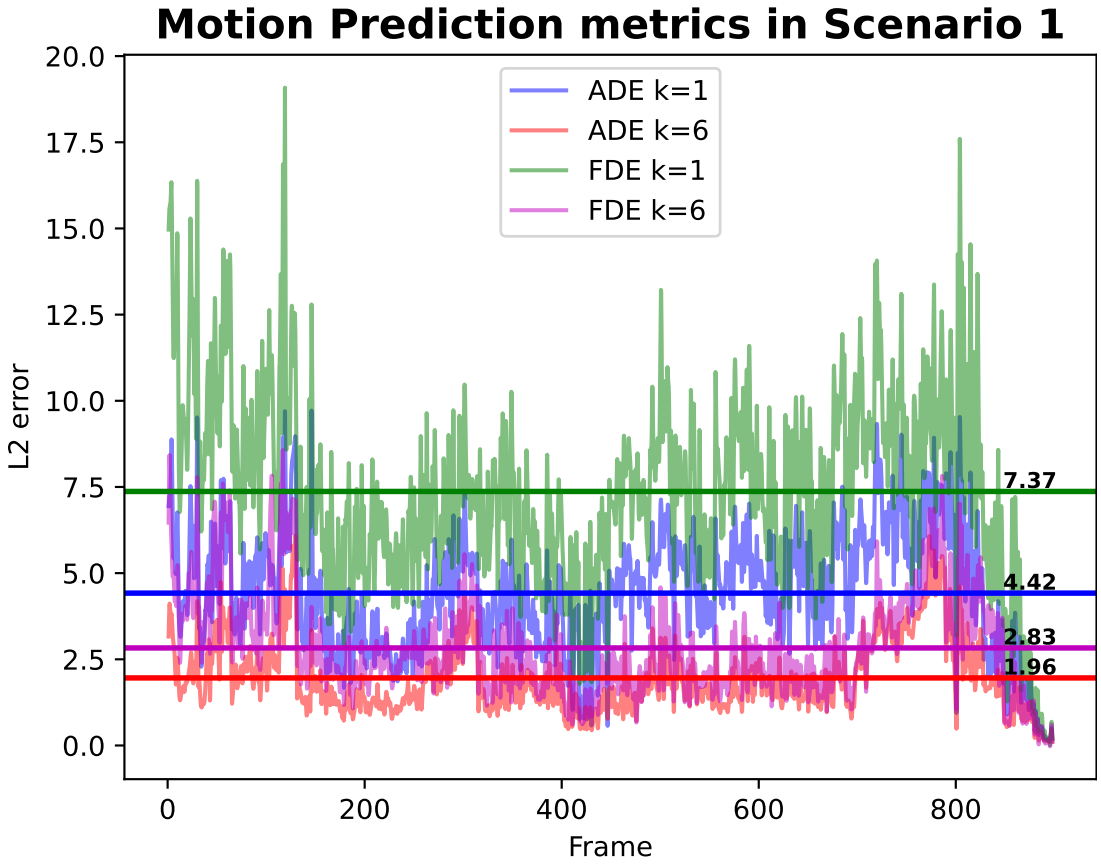

Figure 8.10: Scenario 1 quantitative results. Constant lines represent the mean value for the corresponding metric throughout the whole scenario.

(a) CARLA at frame t

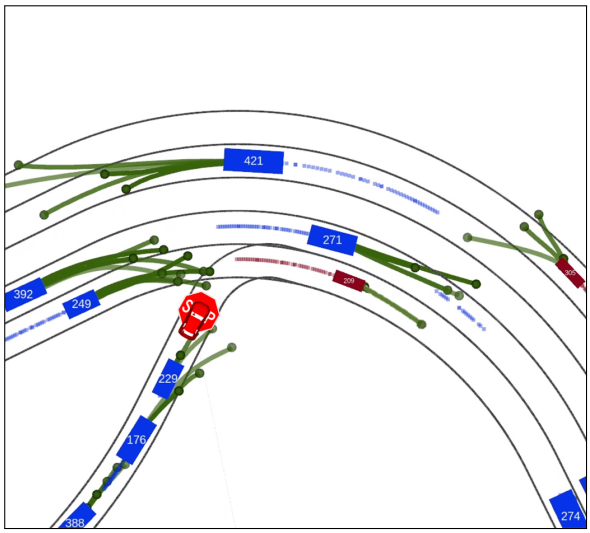

(b) RVIZ at frame t

(c) CARLA at frame $t + 240$

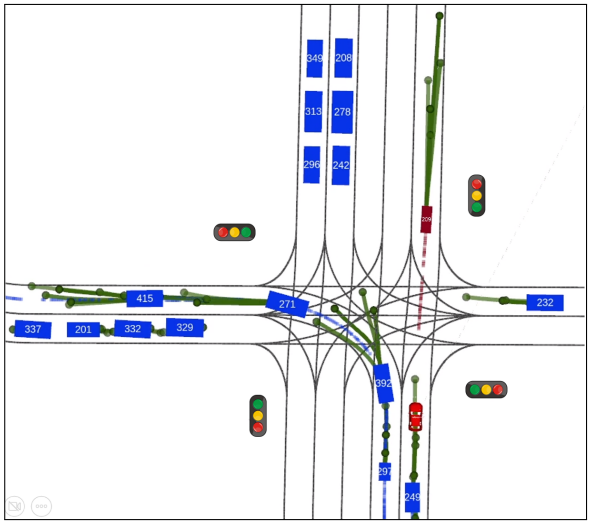

(d) RVIZ at frame $t + 240$

(e) CARLA at frame $t + 260$

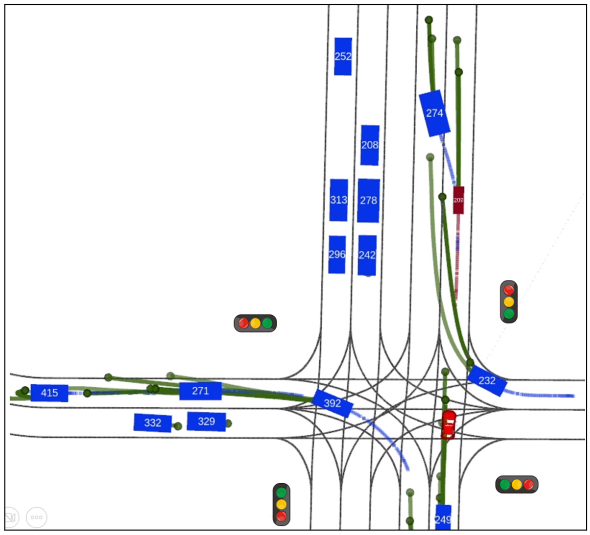

(f) RVIZ at frame $t + 260$

Figure 8.11: Scenario 1 frames of interest

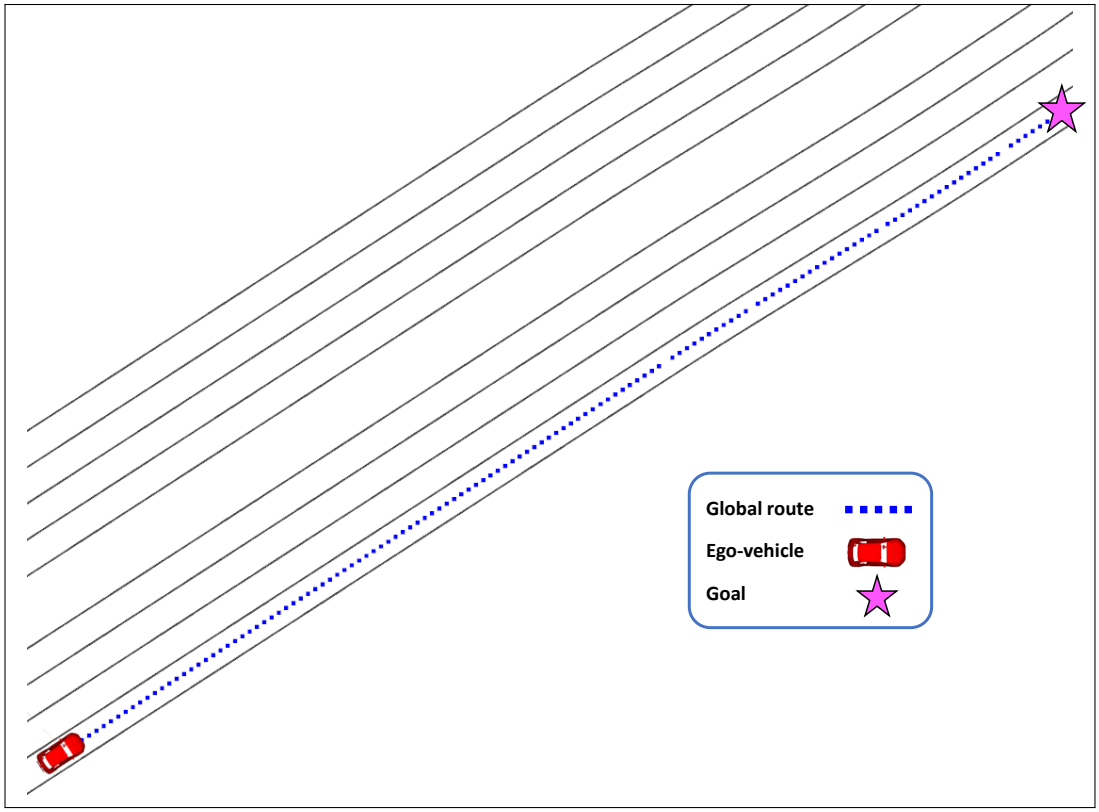

Figure 8.12: Scenario 2 overview: Crowded highway

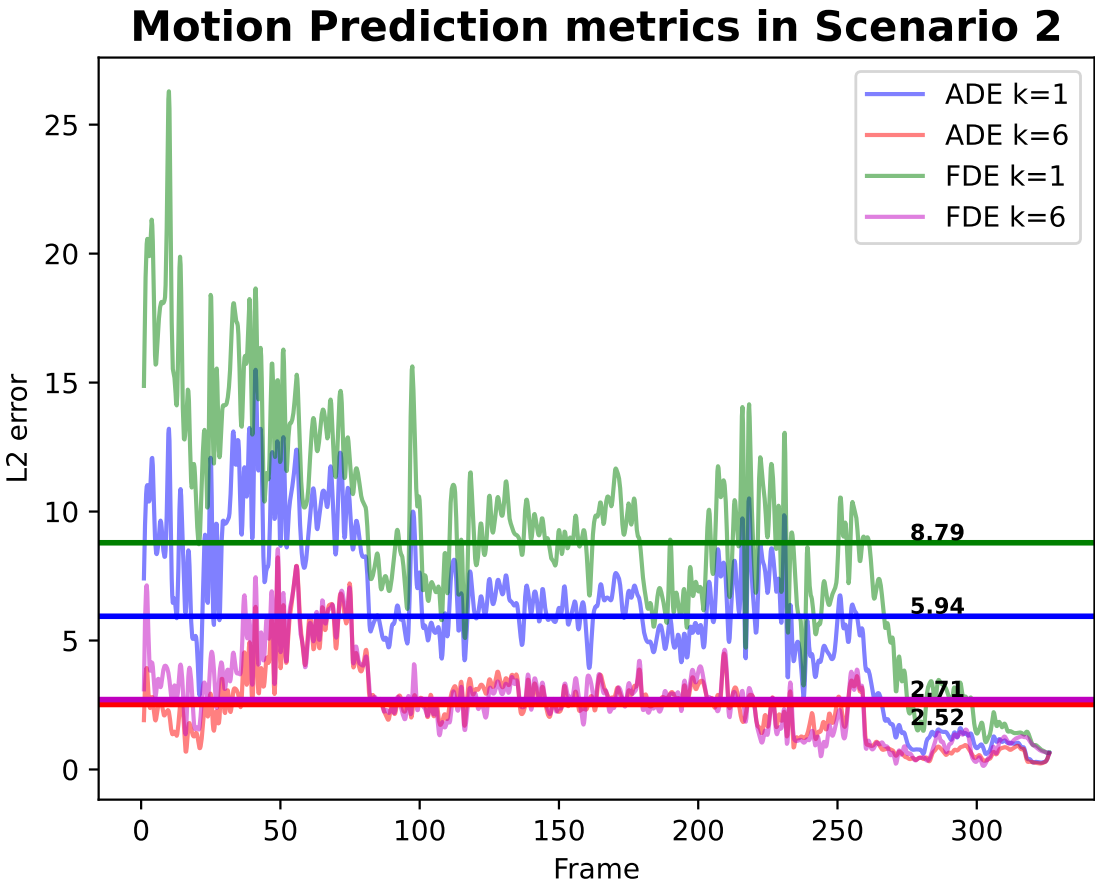

Figure 8.13: Scenario 2 quantitative results. Constant lines represent the mean value for the corresponding metric throughout the whole scenario.

(a) CARLA at frame t

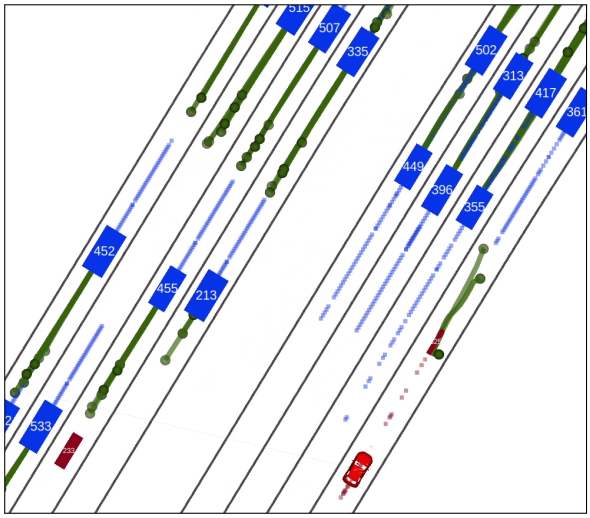

(b) RVIZ at frame t

(c) CARLA at frame $t + 15$

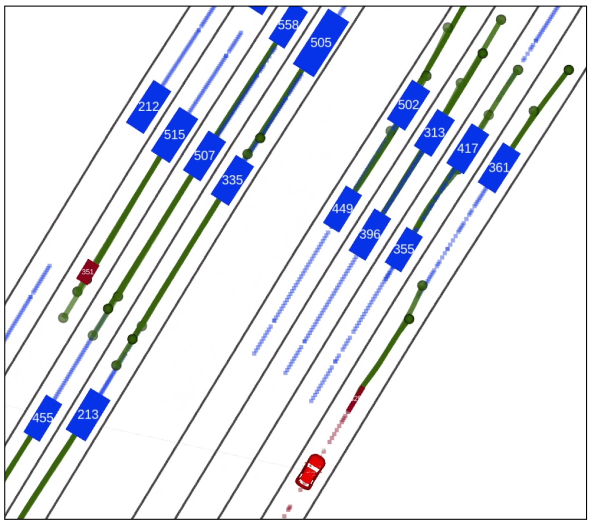

(d) RVIZ at frame $t + 15$

(e) CARLA at frame $t + 30$

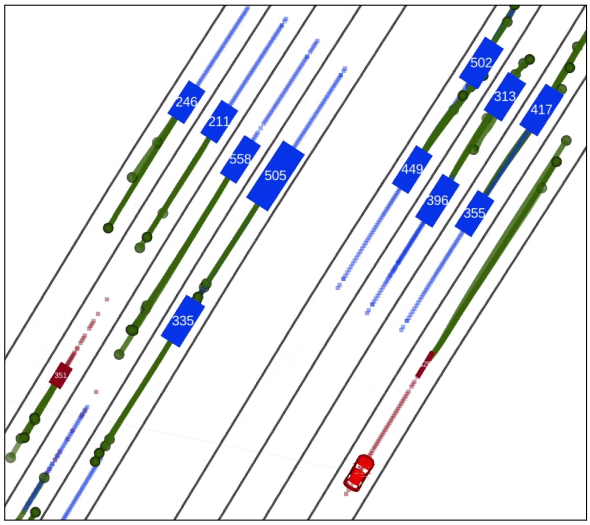

(f) RVIZ at frame $t + 30$

Figure 8.14: Scenario 2 frames of interest

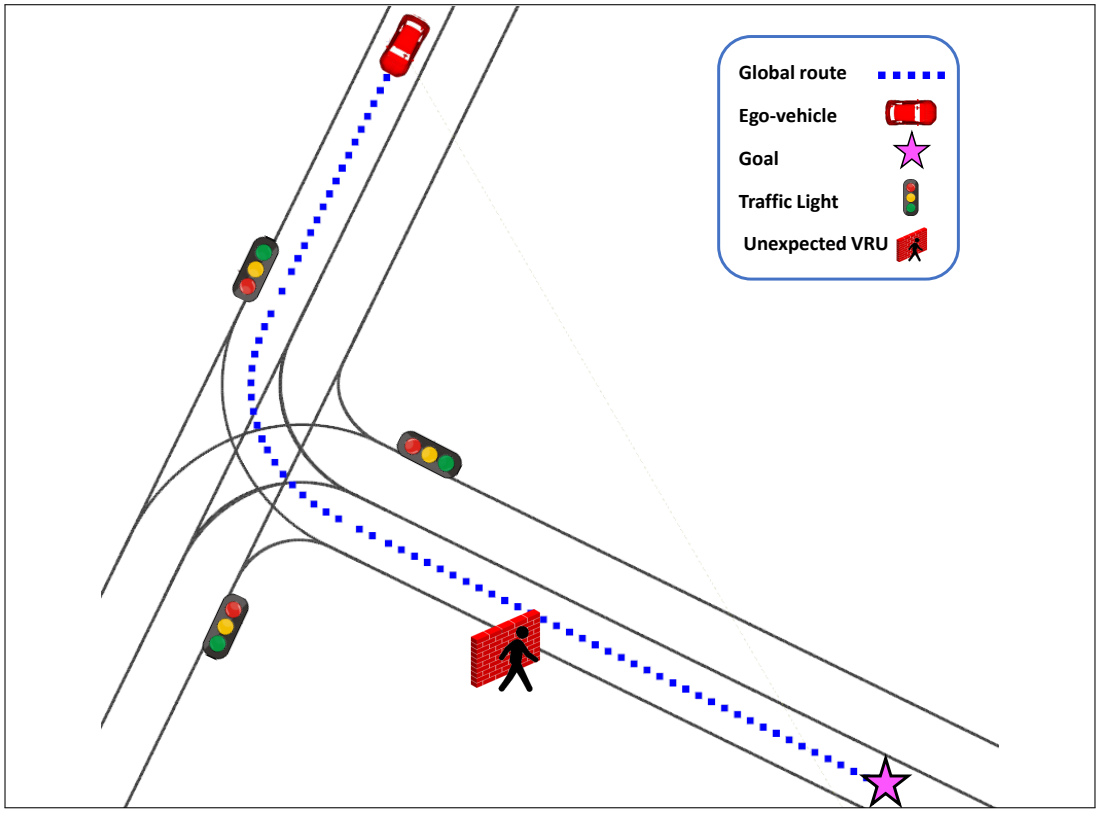

Figure 8.15: Scenario 3 overview: Red Traffic Light and Unexpected VRU

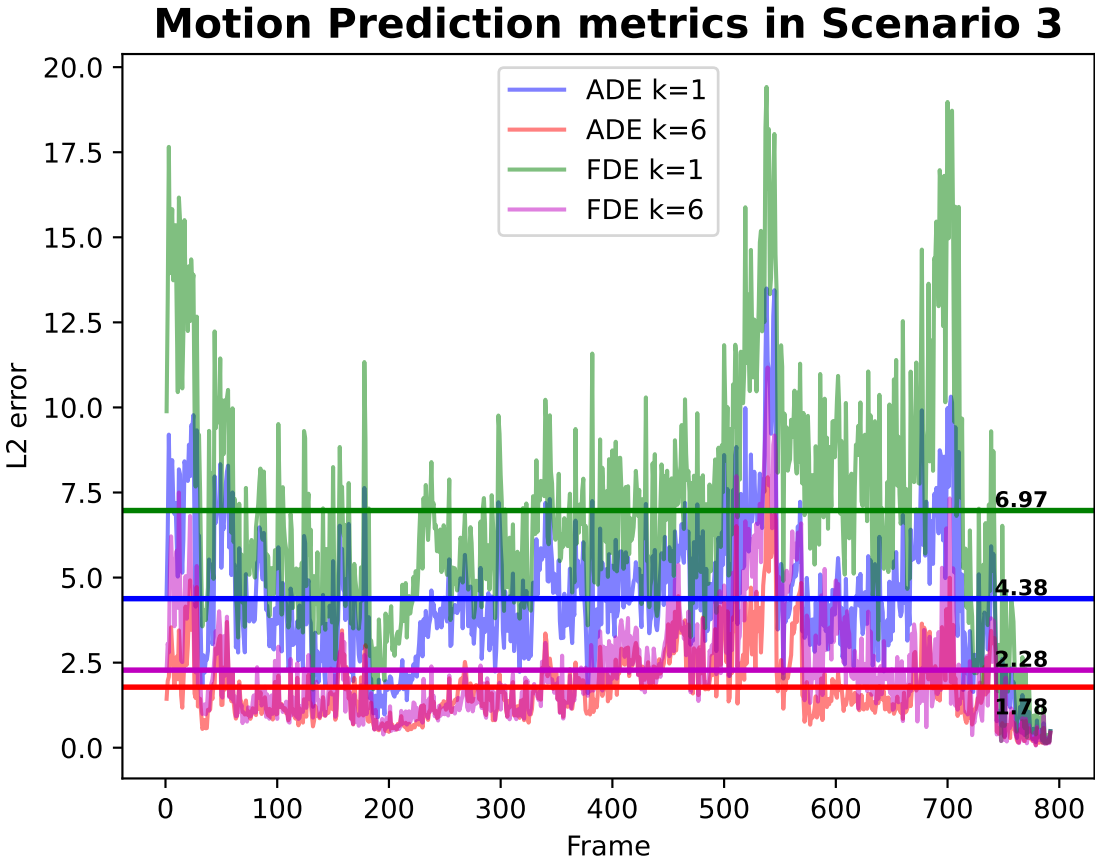

Figure 8.16: Scenario 3 quantitative results. Constant lines represent the mean value for the corresponding metric throughout the whole scenario.

(a) CARLA at frame t

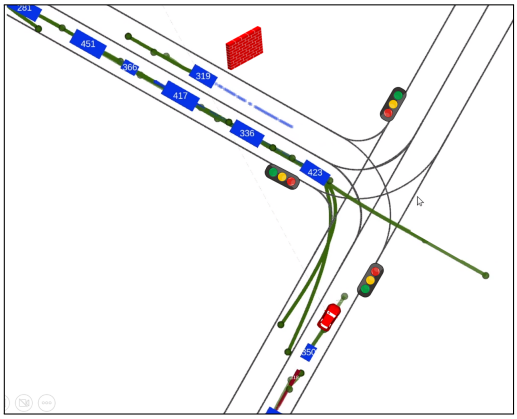

(b) RVIZ at frame t

(c) CARLA at frame $t + 5$

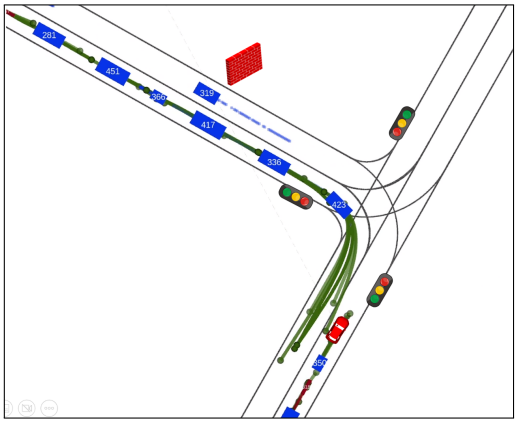

(d) RVIZ at frame $t + 5$

(e) CARLA at frame $t + 145$

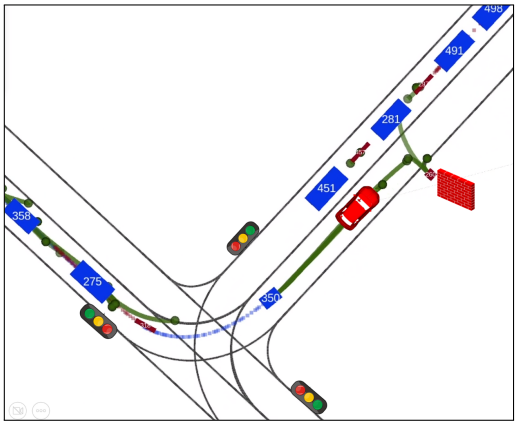

(f) RVIZ at frame $t + 145$

(g) CARLA at frame $t + 147$

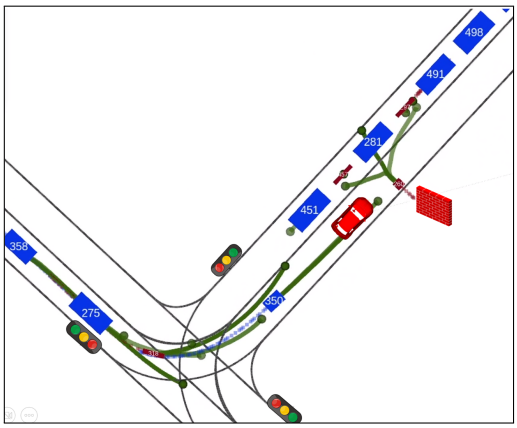

(h) RVIZ at frame $t + 147$

Figure 8.17: Scenario 3 frames of interest

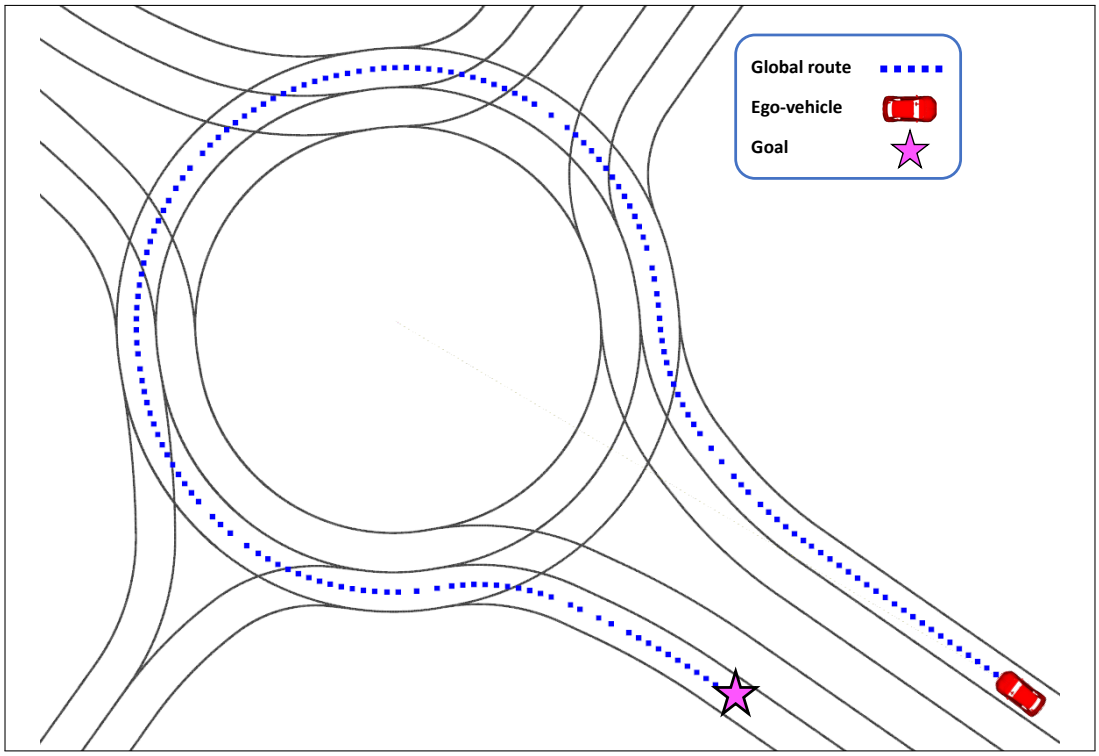

Figure 8.18: Scenario 4 overview: Crowded roundabout

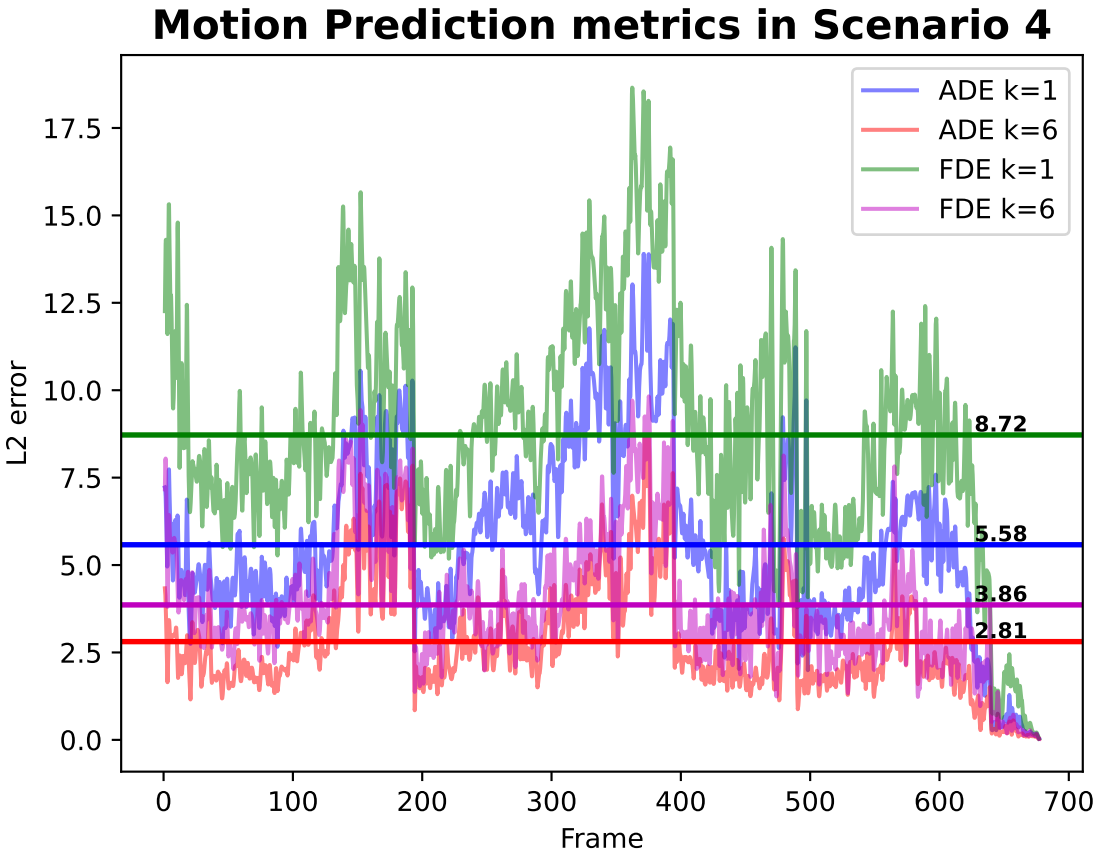

Figure 8.19: Scenario 4 quantitative results. Constant lines represent the mean value for the corresponding metric throughout the whole scenario.

(a) CARLA at frame t

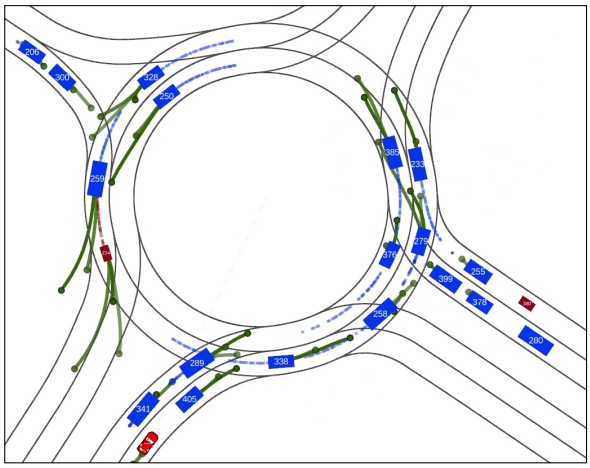

(b) RVIZ at frame t

(c) CARLA at frame $t + 40$

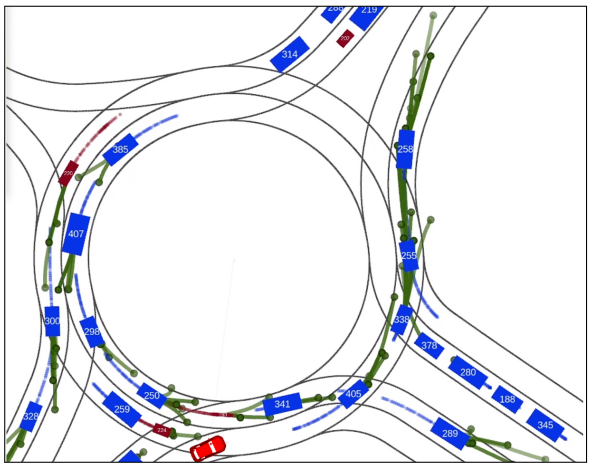

(d) RVIZ at frame $t + 40$

(e) CARLA at frame $t + 80$

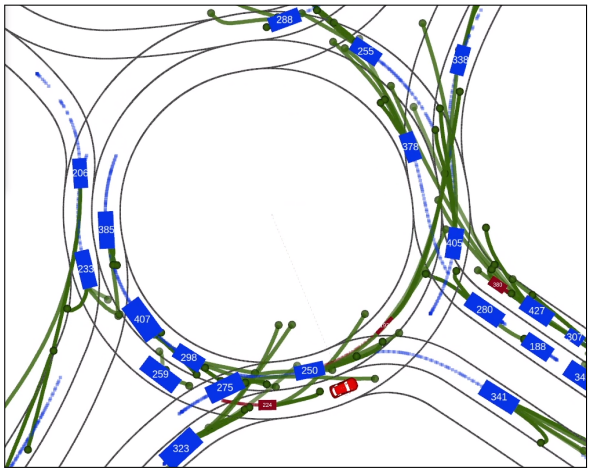

(f) RVIZ at frame $t + 80$

Figure 8.20: Scenario 4 frames of interest

Chapter 9

Conclusions and Future Works

A más ver, mis valientes hobbits.
Mi labor ha concluido.
Aquí, al fin, a la orilla del mar,
llega el adiós a nuestra Compañía.
No os diré no lloréis,
pues no todas las lágrimas son amargas.

Discurso de despedida de Gandalf
El Señor de los Anillos: El Retorno del Rey

9.1. Conclusions

In this thesis, a series of interaction-aware motion prediction methods for scene understanding in the field of Autonomous Driving, covering both the single-agent motion prediction and multi-agent motion prediction use cases from the uni-modal and multi-modal perspectives focusing on long-term (from 3 to 6 s) prediction horizon, including social and physical information.

In Chapter 2 we review the contextual factors and the classification of the most important physics-based and Deep Learning (DL)-based methods for Motion Prediction (MP) in the Autonomous Driving (AD) field. Moreover, we study the literature of the State-of-the-Art (SOTA) databases and simulators to validate the algorithms.

In Chapter 3, we study the theoretical background to deeply understand the proposed methods and their validation in the remaining Chapters.

Once the technical background and related works are presented, in Chapter 4 we introduce a simple-yet-powerful tracking-by-detection pipeline, based on traditional techniques such as Kalman Filter (KF) for state estimation, Hungarian Algorithm (HA) for data association and map-based filtering, that computes the trackers over time in the traffic scenario to feed the subsequent predictions. We conclude here that filtering non-relevant objects by means of the monitored area (most relevant lanes around the Autonomous

Driving Stacks (ADSs)) can reduce the inference time and computational complexity of the overall pipeline.

Then, the thesis focuses on Deep Learning (DL)-based MP in Chapter 5 and 6, where we validate our algorithms in the Argoverse 1 Motion Forecasting dataset and Chapter 7, where we move to the Argoverse 2 Motion Forecasting, the most challenging and recent vehicle MP dataset in the literature, progressively introducing State-of-the-Art (SOTA) mechanisms to encode the complex traffic scenarios, agents interactions and the most representative features of the map information.

Chapter 5 proposes a conditional Generative Adversarial Network (cGAN) prediction algorithm to compute uni-modal future trajectories which uses as generator a Long Short-Term Memory (LSTM) based encoder-decoder with Multi-Head Self-Attention (MHSA), where the concatenation of the past motion, encoded by a LSTM, and plausible target points, encoded by a Multilayer Perceptron (MLP), represents the condition to the network.

Chapter 6 proposes several efficient baselines, introducing the use of Graph Neural Networks (GNNs) to powerfully encode agent interactions and preprocess preliminary trajectories from the map using a heuristic method to obtain simple-yet-useful centerlines with only geometric information to avoid full HD map preprocessing, that serve as preliminary trajectories. We realize that using encoder transformers instead of recurrent networks or standard MLP presents some benefits, since, as stated in Chapter 6, despite having more parameters, recurrent neural networks such as Long Short-Term Memory (LSTM) or Gated Recurrent Unit (GRU) are non-parallelizable due to their sequential structure so the overall training and hence time is higher than transformers-based approaches.

Taking these previous baselines into consideration, the final model of the thesis improves upon the previous ones by incorporating enhancements in the heuristic method, including topological and semantic information of interest about lanes (such as lane boundaries information, presence of intersection or lane mark type), Deep Learning (DL)-based map encoding by means a Graph Convolutional Network (GCN), fusion-cycle of physical and social features, deep learning-based estimation of final positions on the road, aggregation of the surrounding environment, and refinement of predictions to enhance the quality of the final multi-modal predictions in an elegant and efficient manner.

In all our models, specially in the last one, we can appreciate how they generalize well in unknown traffic scenarios, with up-to-pair regressions metrics (both in uni-modal and multi-modal prediction) while noticeably reducing the inference time and number of parameters compared to other SOTA algorithms.

Then, the final proposal is validated in several applications in Chapter 8, taking into account only its social version, due to the difficulty of adapting the map preprocessing and format in different datasets or simulators), such as decision-making or holistic integration

in a hyper-realistic simulator with other vehicle layers, as a preliminary step towards its implementation in an actual autonomous vehicle. Particularly, in our different tests, run in the SMARTS and CARLA simulators, we successfully realize how the overall pipeline can leverage the predictions, specially in challenging situations, to avoid a collision or perform smoother trajectories in complex scenarios where only detecting and tracking the objects over time would not be enough to understand the surrounding scenario and compute the optimal decision.

We hope that our open-source proposals can serve as a solid baseline on which others can build on to advance the State-of-the-Art (SOTA) in fusing perception data and map information to perform real-time Motion Prediction (MP) and Decision-Making (DM) evaluation in arbitrarily complex urban scenarios.

9.2. Future Works

The field of vehicle Motion Prediction for Autonomous Driving is continuously evolving, and several promising future directions can be anticipated. These potential advancements aim to enhance the accuracy, reliability, and safety of motion prediction algorithms, ultimately leading to more efficient and robust Autonomous Driving Systems. Although significant research has been conducted in trajectory prediction and path planning in recent years, there are still numerous aspects that require further investigation in the future:

- **Enhanced Scene Representation and Encoding**: Various methods have been proposed to encode driving scenes using different representations, such as graphs or rasterized top-view maps. However, the absence of a unified representation hampers the generalization of prediction methods for large-scale deployment in real-world autonomous vehicles. Graph-based representations show promise in accommodating heterogeneous objects and their inter-dependencies through directed edges. To enhance graph-based scene representation and encoding, three important steps can be pursued and improved in future works: constructing the graph with proper connections, assigning node and edge features appropriately, and designing graph operators to handle scene graph heterogeneity, leveraging advancements in heterogeneous graph neural networks.

- **Probabilistic Modeling**: Incorporating probabilistic methods into vehicle motion prediction algorithms can help quantify uncertainty and improve the reliability of predictions. By estimating probability distributions over future trajectories, autonomous systems can make more informed decisions, taking into account the likelihood of different outcomes. Probabilistic modeling also enables better risk assessment and planning in uncertain and dynamic traffic scenarios.

- **Predictive Planning**: The integration of MP into the planning module (stated as Conditional Behaviour Prediction in Chapter 2) is crucial for improving decision-making and motion control in ADS. Predictive planning is a worthwhile avenue to explore, addressing challenges such as handling prediction uncertainty, studying the relationship between prediction and planning, and designing scalable predictive planners for predictors with different known uncertainties. Additionally, investigating learning-based motion planners that can be combined with data-driven predictions holds great potential, although the current limitations in explainability and reliability require attention.

- **Interpretability and explainability** are critical aspects of vehicle motion prediction in autonomous driving that require further exploration in future works. While the accuracy and performance of prediction models have improved significantly, understanding and explaining the reasoning behind their predictions remain challenging. Several directions for future research in explainability and interpretability are: Model transparency and visualization (Developing methods to make prediction models more transparent and interpretable is crucial), Rule-based models (Investigating rule-based approaches can provide interpretable predictions in vehicle motion prediction), Feature importance analysis (Conducting feature importance analysis can help identify the most influential factors in vehicle motion prediction), Context-aware explanations (Future research should aim to develop context-aware explanation methods that not only provide predictions but also explain the reasoning behind them in the context of the surrounding environment), Uncertainty estimation and trust assessment (Future works should focus on developing techniques to estimate and communicate prediction uncertainties effectively) and Human-machine interaction (To enhance user trust and acceptance, future research should explore methods for effective human-machine interaction in vehicle motion prediction).

- **Transfer Learning**: Transferring knowledge from one driving scenario to another can significantly improve the efficiency of vehicle motion prediction. By training models on diverse datasets and environments, and then fine-tuning them for specific scenarios, researchers can reduce the reliance on large amounts of scenario-specific training data. Transfer learning allows predictions to generalize across different driving conditions, leading to more robust and adaptable autonomous systems.

- **Human-Centric Approaches**: Understanding human intentions and incorporating social norms in motion prediction is crucial for ensuring safe and harmonious interactions between autonomous vehicles and human drivers or pedestrians. Future works may involve the development of algorithms that can interpret and predict human behavior accurately. This can be achieved by leveraging techniques from computer vision, natural language processing, and social sciences to capture and model human intentions, gestures, and communication cues.

- **Knowledge-Distillation** in vehicle motion prediction is an emerging area that holds promise for reducing reliance on map information and enhancing the generalizability of prediction models. By leveraging the knowledge acquired from more complex models or human experts, knowledge distillation enables the transfer of valuable insights to smaller and more lightweight models. Here are several potential future directions for employing knowledge distillation in vehicle motion prediction to reduce dependency on map information: Model compression for map-free prediction (Knowledge-Distillation can be applied to compress large-scale map-based prediction models into smaller models that can make accurate predictions without explicit map information), Expert knowledge transfer (Knowledge-Distillation can facilitate the transfer of expert knowledge to prediction models), Reinforcement learning with model distillation (Reinforcement learning techniques combined with knowledge distillation can be employed to train models that can learn to predict vehicle motions without explicit map information), Data augmentation techniques (By synthesizing additional training samples using map-based models, the prediction models can learn from a more diverse range of scenarios, including situations without map information), Self-supervised learning for map-free prediction (Knowledge distillation can be combined with self-supervised learning techniques to train prediction models without relying on explicit map information).

In conclusion, extensive effort is needed in some interesting areas such as scene representation and encoding, probabilistic modeling, predictive planning, interpretability and explainability, transfer learning, human-centric approaches or even knowledge-distillation to further advance the performance (both in terms of regression and efficiency) of MP algorithms in the field AD as a preliminary stage before feeding the subsequent decision-making, local planning and motion control layers in an ADS, contributing to the development of more efficient and reliable autonomous driving systems.

List of Publications

The following publications (both journal papers and conference contributions) correspond to first author or main co-author. For a complete view of all publications derived from the thesis: All publications [1].

Journal Papers

- **Gomez-Huelamo, C.**, Conde, M. V., Barea, R., Ocala, M, & Bergasa, L. M. (2023). Efficient Baselines for Motion Prediction in Autonomous Driving. Transactions on Intelligent Transportation Systems. In submission.
- **Gomez-Huelamo, C.**, Del Egido, J., Bergasa, L. M., Barea, R., Lopez-Guillen, E., Araluce, J., & Antunes, M. (2022). 360º real-time and power-efficient 3D DAMOT for autonomous driving applications. Multimedia Tools and Applications, 81(19), 26915-26940
- **Gómez-Huélamo, C.**, Del Egido, J., Bergasa, L. M., Barea, R., López-Guillén, E., Arango, F., ... & López, J. (2021). Train here, drive there: Ros based end-to-end autonomous-driving pipeline validation in carla simulator using the nhtsa typology. Multimedia Tools and Applications, 1-28

Conference Contributions

- **Gómez-Huélamo, C.**, Conde, M. V., Gutiérrez-Moreno R, Barea, R., Llamazares A., Antunes M., & Bergasa, L. M. (2022, October). Efficient Context-Aware Graph Transformer for Vehicle Motion Predictio. In 2023 IEEE 26th International Conference on Intelligent Transportation Systems (ITSC). IEEE.
- Gutiérrez-Moreno R., **Gómez-Huélamo, C.**, Barea. R, López-Guillén E., Arango F., Ortiz, M., & Bergasa, L. M. (2023, October). Augmented Reinforcement Learning with Efficient Social-based Motion Prediction for Autonomous Decision-Making. In 2023 IEEE 26th International Conference on Intelligent Transportation Systems (ITSC). IEEE.

[1] https://scholar.google.es/citations?user=OWwoG6EAAAAJ&hl=es

- **Gómez-Huélamo, C.**, Conde, M, Barea, R. & Bergasa, L. M. (2023, June). Improving Multi-Agent Motion Prediction with Heuristic Goals and Motion Refinement. In Proceedings of the IEEE/CVF Conference on Computer Vision and Pattern Recognition (CVPR) (pp. 5322-5331). IEEE

- **Gómez-Huélamo, C.**, Conde, M. V., Ortiz, M., Montiel, S., Barea, R., & Bergasa, L. M. (2022, October). Exploring Attention GAN for Vehicle Motion Prediction. In 2022 IEEE 25th International Conference on Intelligent Transportation Systems (ITSC) (pp. 4011-4016). IEEE

- Diaz-Diaz, A., Ocaña, M., Llamazares, Á., **Gómez-Huélamo, C.**, Revenga, P., & Bergasa, L. M. (2022, June). HD maps: Exploiting OpenDRIVE potential for Path Planning and Map Monitoring. In 2022 IEEE Intelligent Vehicles Symposium (IV) (pp. 1211-1217). IEEE.

- **Gómez-Huélamo, C.**, Diaz-Diaz, A., Araluce, J., Ortiz, M. E., Gutiérrez, R., Arango, F., ... & Bergasa, L. M. (2022, June). How to build and validate a safe and reliable Autonomous Driving stack? A ROS based software modular architecture baseline. In 2022 IEEE Intelligent Vehicles Symposium (IV) (pp. 1282-1289). IEEE.

- **Gómez–Huélamo, C.**, Bergasa, L. M., Gutiérrez, R., Arango, J. F., & Díaz, A. (2021, July). Smartmot: exploiting the fusion of hdmaps and multi-object tracking for real-time scene understanding in intelligent vehicles applications. In 2021 IEEE Intelligent Vehicles Symposium (IV) (pp. 710-715). IEEE.

- Gutiérrez, R., Arango, J. F., **Gomez-Huélamo, C.**, Bergasa, L. M., Barea, R., & Araluce, J. (2021, July). Validation Method of a Self-Driving Architecture for Unexpected Pedestrian Scenario in CARLA Simulator. In 2021 IEEE Intelligent Vehicles Symposium (IV) (pp. 1144-1149). IEEE.

- Del Egido, J., **Gómez-Huélamo, C.**, Bergasa, L. M., Barea, R., López-Guillén, E., Araluce, J., ... & Antunes, M. (2020, November). 360 real-time 3d multi-object detection and tracking for autonomous vehicle navigation. In Advances in Physical Agents II: Proceedings of the 21st International Workshop of Physical Agents (WAF 2020), November 19-20, 2020, Alcalá de Henares, Madrid, Spain (pp. 241-255). Cham: Springer International Publishing.

- **Gómez-Huélamo, C.**, Del Egido, J., Bergasa, L. M., Barea, R., López-Guillén, E., Arango, F., ... & López, J. (2021). Train here, drive there: Simulating real-world use cases with fully-autonomous driving architecture in carla simulator. In Advances in Physical Agents II: Proceedings of the 21st International Workshop of Physical Agents (WAF 2020), November 19-20, 2020, Alcalá de Henares, Madrid, Spain (pp. 44-59). Springer International Publishing.

- **Gómez-Huélamo, C.**, Del Egido, J., Bergasa, L. M., Barea, R., Ocana, M., Arango, F., & Gutiérrez-Moreno, R. (2020, September). Real-time bird's eye view multi-object tracking system based on fast encoders for object detection. In 2020 IEEE 23rd International Conference on Intelligent Transportation Systems (ITSC) (pp. 1-6). IEEE.
- **Gómez-Huelamo, C.**, Bergasa, L. M., Barea, R., López-Guillén, E., Arango, F., & Sánchez, P. (2019, October). Simulating use cases for the UAH Autonomous Electric Car. In 2019 IEEE Intelligent Transportation Systems Conference (ITSC) (pp. 2305-2311). IEEE.

Bibliography

[1] S. Taxonomy, "Definitions for terms related to driving automation systems for on-road motor vehicles (j3016)", Technical report, Society for Automotive Engineering, Tech. Rep., 2016.

[2] J. F. Arango, L. M. Bergasa, P. A. Revenga, *et al.*, "Drive-by-wire development process based on ros for an autonomous electric vehicle", *Sensors*, vol. 20, no. 21, p. 6121, 2020.

[3] A. Ranga, F. Giruzzi, J. Bhanushali, *et al.*, "Vrunet: Multi-task learning model for intent prediction of vulnerable road users", *arXiv preprint arXiv:2007.05397*, 2020.

[4] E. Yurtsever, J. Lambert, A. Carballo, and K. Takeda, "A survey of autonomous driving: Common practices and emerging technologies", *IEEE access*, vol. 8, pp. 58 443–58 469, 2020.

[5] I. Gog, S. Kalra, P. Schafhalter, M. A. Wright, J. E. Gonzalez, and I. Stoica, "Pylot: A modular platform for exploring latency-accuracy tradeoffs in autonomous vehicles", in *2021 IEEE International Conference on Robotics and Automation (ICRA)*, IEEE, 2021, pp. 8806–8813.

[6] M.-F. Chang, J. Lambert, P. Sangkloy, *et al.*, "Argoverse: 3d tracking and forecasting with rich maps", in *Proceedings of the IEEE/CVF conference on computer vision and pattern recognition*, 2019, pp. 8748–8757.

[7] B. Wilson, W. Qi, T. Agarwal, *et al.*, "Argoverse 2: Next generation datasets for self-driving perception and forecasting", *arXiv preprint arXiv:2301.00493*, 2023.

[8] T. Salzmann, B. Ivanovic, P. Chakravarty, and M. Pavone, "Trajectron++: Dynamically-feasible trajectory forecasting with heterogeneous data", in *Computer Vision–ECCV 2020: 16th European Conference, Glasgow, UK, August 23–28, 2020, Proceedings, Part XVIII 16*, Springer, 2020, pp. 683–700.

[9] T. Gilles, S. Sabatini, D. Tsishkou, B. Stanciulescu, and F. Moutarde, "Home: Heatmap output for future motion estimation", in *2021 IEEE International Intelligent Transportation Systems Conference (ITSC)*, IEEE, 2021, pp. 500–507.

[10] T. Gilles, S. Sabatini, D. Tsishkou, B. Stanciulescu, and F. Moutarde, "Gohome: Graph-oriented heatmap output for future motion estimation", in *2022 International Conference on Robotics and Automation (ICRA)*, IEEE, 2022, pp. 9107–9114.

[11] B. Varadarajan, A. Hefny, A. Srivastava, *et al.*, "Multipath++: Efficient information fusion and trajectory aggregation for behavior prediction", in *2022 International Conference on Robotics and Automation (ICRA)*, IEEE, 2022, pp. 7814–7821.

[12] M. Wang, X. Zhu, C. Yu, *et al.*, "Ganet: Goal area network for motion forecasting", *arXiv preprint arXiv:2209.09723*, 2022.

[13] J. Schmidt, J. Jordan, F. Gritschneder, and K. Dietmayer, "Crat-pred: Vehicle trajectory prediction with crystal graph convolutional neural networks and multi-head self-attention", in *2022 International Conference on Robotics and Automation (ICRA)*, IEEE, 2022, pp. 7799–7805.

[14] M. Liang, B. Yang, R. Hu, *et al.*, "Learning lane graph representations for motion forecasting", in *Computer Vision–ECCV 2020: 16th European Conference, Glasgow, UK, August 23–28, 2020, Proceedings, Part II 16*, Springer, 2020, pp. 541–556.

[15] C. Tang and R. R. Salakhutdinov, "Multiple futures prediction", *Advances in neural information processing systems*, vol. 32, 2019.

[16] N. Rhinehart, R. McAllister, K. Kitani, and S. Levine, "Precog: Prediction conditioned on goals in visual multi-agent settings", in *Proceedings of the IEEE/CVF International Conference on Computer Vision*, 2019, pp. 2821–2830.

[17] S. Khandelwal, W. Qi, J. Singh, A. Hartnett, and D. Ramanan, "What-if motion prediction for autonomous driving", *arXiv preprint arXiv:2008.10587*, 2020.

[18] H. Zhao, J. Gao, T. Lan, *et al.*, "Tnt: Target-driven trajectory prediction", in *Conference on Robot Learning*, PMLR, 2021, pp. 895–904.

[19] Y. Huang, J. Du, Z. Yang, Z. Zhou, L. Zhang, and H. Chen, "A survey on trajectory-prediction methods for autonomous driving", *IEEE Transactions on Intelligent Vehicles*, vol. 7, no. 3, pp. 652–674, 2022.

[20] N. Kaempchen, B. Schiele, and K. Dietmayer, "Situation assessment of an autonomous emergency brake for arbitrary vehicle-to-vehicle collision scenarios", *IEEE Transactions on Intelligent Transportation Systems*, vol. 10, no. 4, pp. 678–687, 2009.

[21] R. Pepy, A. Lambert, and H. Mounier, "Reducing navigation errors by planning with realistic vehicle model", in *2006 IEEE Intelligent Vehicles Symposium*, IEEE, 2006, pp. 300–307.

[22] R. Miller and Q. Huang, "An adaptive peer-to-peer collision warning system", in *Vehicular Technology Conference. IEEE 55th Vehicular Technology Conference. VTC Spring 2002 (Cat. No. 02CH37367)*, IEEE, vol. 1, 2002, pp. 317–321.

[23] J. Hillenbrand, A. M. Spieker, and K. Kroschel, "A multilevel collision mitigation approach—its situation assessment, decision making, and performance tradeoffs", *IEEE Transactions on intelligent transportation systems*, vol. 7, no. 4, pp. 528–540, 2006.

[24] R. E. Kalman, "A new approach to linear filtering and prediction problems", 1960.

[25] N. Kaempchen, K. Weiss, M. Schaefer, and K. C. Dietmayer, "Imm object tracking for high dynamic driving maneuvers", in *IEEE Intelligent Vehicles Symposium, 2004.*, IEEE, 2004, pp. 825–830.

[26] B. Jin, B. Jiu, T. Su, H. Liu, and G. Liu, "Switched kalman filter-interacting multiple model algorithm based on optimal autoregressive model for manoeuvring target tracking", *IET Radar, Sonar & Navigation*, vol. 9, no. 2, pp. 199–209, 2015.

[27] V. Lefkopoulos, M. Menner, A. Domahidi, and M. N. Zeilinger, "Interaction-aware motion prediction for autonomous driving: A multiple model kalman filtering scheme", *IEEE Robotics and Automation Letters*, vol. 6, no. 1, pp. 80–87, 2020.

[28] A. Broadhurst, S. Baker, and T. Kanade, "Monte carlo road safety reasoning", in *IEEE Proceedings. Intelligent Vehicles Symposium, 2005.*, IEEE, 2005, pp. 319–324.

[29] K. Okamoto, K. Berntorp, and S. Di Cairano, "Driver intention-based vehicle threat assessment using random forests and particle filtering", *IFAC-PapersOnLine*, vol. 50, no. 1, pp. 13 860–13 865, 2017.

[30] Y. Wang, Z. Liu, Z. Zuo, Z. Li, L. Wang, and X. Luo, "Trajectory planning and safety assessment of autonomous vehicles based on motion prediction and model predictive control", *IEEE Transactions on Vehicular Technology*, vol. 68, no. 9, pp. 8546–8556, 2019.

[31] A. Gupta, J. Johnson, L. Fei-Fei, S. Savarese, and A. Alahi, "Social gan: Socially acceptable trajectories with generative adversarial networks", in *Proceedings of the IEEE conference on computer vision and pattern recognition*, 2018, pp. 2255–2264.

[32] S. Casas, W. Luo, and R. Urtasun, "Intentnet: Learning to predict intention from raw sensor data", in *Conference on Robot Learning*, PMLR, 2018, pp. 947–956.

[33] A. Alahi, K. Goel, V. Ramanathan, A. Robicquet, L. Fei-Fei, and S. Savarese, "Social lstm: Human trajectory prediction in crowded spaces", in *Proceedings of the IEEE conference on computer vision and pattern recognition*, 2016, pp. 961–971.

[34] J. Mercat, T. Gilles, N. El Zoghby, G. Sandou, D. Beauvois, and G. P. Gil, "Multi-head attention for multi-modal joint vehicle motion forecasting", in *2020 IEEE International Conference on Robotics and Automation (ICRA)*, IEEE, 2020, pp. 9638–9644.

[35] J. Gao, C. Sun, H. Zhao, *et al.*, "Vectornet: Encoding hd maps and agent dynamics from vectorized representation", in *Proceedings of the IEEE/CVF Conference on Computer Vision and Pattern Recognition*, 2020, pp. 11 525–11 533.

[36] J. Ngiam, V. Vasudevan, B. Caine, *et al.*, "Scene transformer: A unified architecture for predicting future trajectories of multiple agents", in *International Conference on Learning Representations*, 2022.

[37] S. Casas, A. Sadat, and R. Urtasun, "Mp3: A unified model to map, perceive, predict and plan", in *Proceedings of the IEEE/CVF Conference on Computer Vision and Pattern Recognition*, 2021, pp. 14 403–14 412.

[38] T. Phan-Minh, E. C. Grigore, F. A. Boulton, O. Beijbom, and E. M. Wolff, "Covernet: Multimodal behavior prediction using trajectory sets", in *Proceedings of the IEEE/CVF Conference on Computer Vision and Pattern Recognition*, 2020, pp. 14 074–14 083.

[39] N. Lee, W. Choi, P. Vernaza, C. B. Choy, P. H. Torr, and M. Chandraker, "Desire: Distant future prediction in dynamic scenes with interacting agents", in *Proceedings of the IEEE conference on computer vision and pattern recognition*, 2017, pp. 336–345.

[40] F. Marchetti, F. Becattini, L. Seidenari, and A. D. Bimbo, "Mantra: Memory augmented networks for multiple trajectory prediction", in *Proceedings of the IEEE/CVF conference on computer vision and pattern recognition*, 2020, pp. 7143–7152.

[41] Y. Biktairov, M. Stebelev, I. Rudenko, O. Shliazhko, and B. Yangel, "Prank: Motion prediction based on ranking", *Advances in neural information processing systems*, vol. 33, pp. 2553–2563, 2020.

[42] H. Cui, V. Radosavljevic, F.-C. Chou, *et al.*, "Multimodal trajectory predictions for autonomous driving using deep convolutional networks", in *2019 International Conference on Robotics and Automation (ICRA)*, IEEE, 2019, pp. 2090–2096.

[43] Y. Chai, B. Sapp, M. Bansal, and D. Anguelov, "Multipath: Multiple probabilistic anchor trajectory hypotheses for behavior prediction", *arXiv preprint arXiv:1910.05449*, 2019.

[44] T. Buhet, E. Wirbel, A. Bursuc, and X. Perrotton, "Plop: Probabilistic polynomial objects trajectory prediction for autonomous driving", in *Conference on Robot Learning*, PMLR, 2021, pp. 329–338.

[45] N. Rhinehart, K. M. Kitani, and P. Vernaza, "R2p2: A reparameterized pushforward policy for diverse, precise generative path forecasting", in *Proceedings of the European Conference on Computer Vision (ECCV)*, 2018, pp. 772–788.

[46] H. Cui, T. Nguyen, F.-C. Chou, *et al.*, "Deep kinematic models for kinematically feasible vehicle trajectory predictions", in *2020 IEEE International Conference on Robotics and Automation (ICRA)*, IEEE, 2020, pp. 10 563–10 569.

[47] Y. B. Can, A. Liniger, O. Unal, D. Paudel, and L. Van Gool, "Understanding bird's-eye view of road semantics using an onboard camera", *IEEE Robotics and Automation Letters*, vol. 7, no. 2, pp. 3302–3309, 2022. DOI: 10.1109/LRA.2022.3146898.

[48] R. Mahjourian, J. Kim, Y. Chai, M. Tan, B. Sapp, and D. Anguelov, "Occupancy flow fields for motion forecasting in autonomous driving", *IEEE Robotics and Automation Letters*, 2022.

[49] B. Ivanovic, K.-H. Lee, P. Tokmakov, *et al.*, "Heterogeneous-agent trajectory forecasting incorporating class uncertainty", *arXiv preprint arXiv:2104.12446*, 2021.

[50] W. Zeng, M. Liang, R. Liao, and R. Urtasun, "Lanercnn: Distributed representations for graph-centric motion forecasting", in *2021 IEEE/RSJ International Conference on Intelligent Robots and Systems (IROS)*, IEEE, 2021, pp. 532–539.

[51] W. Zeng, W. Luo, S. Suo, *et al.*, "End-to-end interpretable neural motion planner", in *Proceedings of the IEEE/CVF Conference on Computer Vision and Pattern Recognition*, 2019, pp. 8660–8669.

[52] B. Triggs, "Motion planning for nonholonomic vehicles: An introduction", 1993.

[53] W. Zhan, L. Sun, D. Wang, *et al.*, "Interaction dataset: An international, adversarial and cooperative motion dataset in interactive driving scenarios with semantic maps", *arXiv preprint arXiv:1910.03088*, 2019.

[54] H. John, Z. Guido, B. Luca, *et al.*, "One thousand and one hours: Self-driving motion prediction dataset", *arXiv preprint arXiv: 2006.14480*, 2020.

[55] S. Ettinger, S. Cheng, B. Caine, *et al.*, "Large scale interactive motion forecasting for autonomous driving: The waymo open motion dataset", in *Proceedings of the IEEE/CVF International Conference on Computer Vision*, 2021, pp. 9710–9719.

[56] H. Caesar, V. Bankiti, A. H. Lang, *et al.*, "Nuscenes: A multimodal dataset for autonomous driving", in *Proceedings of the IEEE/CVF conference on computer vision and pattern recognition*, 2020, pp. 11 621–11 631.

[57] A. Malinin, N. Band, G. Chesnokov, *et al.*, "Shifts: A dataset of real distributional shift across multiple large-scale tasks", *arXiv preprint arXiv:2107.07455*, 2021.

[58] S. Kim, H. Jeon, J. Choi, and D. Kum, "Improving diversity of multiple trajectory prediction based on map-adaptive lane loss", *arXiv preprint arXiv:2206.08641*, 2022.

[59] P. Kaur, S. Taghavi, Z. Tian, and W. Shi, "A survey on simulators for testing self-driving cars", *arXiv preprint arXiv:2101.05337*, 2021.

[60] R. F. Benekohal and J. Treiterer, "Carsim: Car-following model for simulation of traffic in normal and stop-and-go conditions", *Transportation research record*, vol. 1194, pp. 99–111, 1988.

[61] M. Tideman and M. Van Noort, "A simulation tool suite for developing connected vehicle systems", in *2013 IEEE Intelligent Vehicles Symposium (IV)*, IEEE, 2013, pp. 713–718.

[62] A. Dosovitskiy, G. Ros, F. Codevilla, A. Lopez, and V. Koltun, "Carla: An open urban driving simulator", in *Conference on robot learning*, PMLR, 2017, pp. 1–16.

[63] A. Sanders, *An introduction to unreal engine 4*. AK Peters/CRC Press, 2016.

[64] N. Koenig and A. Howard, "Design and use paradigms for gazebo, an open-source multi-robot simulator", in *Intelligent Robots and Systems, 2004.(IROS 2004). Proceedings. 2004 IEEE/RSJ International Conference on*, IEEE, vol. 3, 2004, pp. 2149–2154.

[65] G. Rong, B. H. Shin, H. Tabatabaee, *et al.*, "Lgsvl simulator: A high fidelity simulator for autonomous driving", in *2020 IEEE 23rd International Conference on Intelligent Transportation Systems (ITSC)*, IEEE, 2020, pp. 1–6.

[66] J. Haas, "A history of the unity game engine", *Diss. WORCESTER POLYTECHNIC INSTITUTE*, 2014.

[67] R. Lattarulo, J. Pérez, and M. Dendaluce, "A complete framework for developing and testing automated driving controllers", *IFAC-PapersOnLine*, vol. 50, no. 1, pp. 258–263, 2017.

[68] H. W. Kuhn, "The hungarian method for the assignment problem", *Naval research logistics quarterly*, vol. 2, no. 1-2, pp. 83–97, 1955.

[69] G. Bishop, G. Welch, *et al.*, "An introduction to the kalman filter", *Proc of SIGGRAPH, Course*, vol. 8, no. 27599-23175, p. 41, 2001.

[70] R. Schubert, E. Richter, and G. Wanielik, "Comparison and evaluation of advanced motion models for vehicle tracking", in *2008 11th international conference on information fusion*, IEEE, 2008, pp. 1–6.

[71] S. Hochreiter and J. Schmidhuber, "Long short-term memory", *Neural computation*, vol. 9, no. 8, pp. 1735–1780, 1997.

[72] I. Goodfellow, J. Pouget-Abadie, M. Mirza, *et al.*, "Generative adversarial networks", *Communications of the ACM*, vol. 63, no. 11, pp. 139–144, 2020.

[73] A. Mino and G. Spanakis, "Logan: Generating logos with a generative adversarial neural network conditioned on color", in *2018 17th IEEE International Conference on Machine Learning and Applications (ICMLA)*, IEEE, 2018, pp. 965–970.

[74] A. Vaswani, N. Shazeer, N. Parmar, *et al.*, "Attention is all you need", *Advances in neural information processing systems*, vol. 30, 2017.

[75] Z. Wu, S. Pan, F. Chen, G. Long, C. Zhang, and S. Y. Philip, "A comprehensive survey on graph neural networks", *IEEE transactions on neural networks and learning systems*, vol. 32, no. 1, pp. 4–24, 2020.

[76] D. E. Rumelhart, R. Durbin, R. Golden, and Y. Chauvin, "Backpropagation: The basic theory", *Backpropagation: Theory, architectures and applications*, pp. 1–34, 1995.

[77] H. Robbins and S. Monro, "A stochastic approximation method", *The annals of mathematical statistics*, pp. 400–407, 1951.

[78] J. Duchi, E. Hazan, and Y. Singer, "Adaptive subgradient methods for online learning and stochastic optimization.", *Journal of machine learning research*, vol. 12, no. 7, 2011.

[79] F. Zou, L. Shen, Z. Jie, W. Zhang, and W. Liu, "A sufficient condition for convergences of adam and rmsprop", in *Proceedings of the IEEE/CVF conference on computer vision and pattern recognition*, 2019, pp. 11 127–11 135.

[80] M. D. Zeiler, "Adadelta: An adaptive learning rate method", *arXiv preprint arXiv:1212.5701*, 2012.

[81] D. P. Kingma and J. Ba, "Adam: A method for stochastic optimization", *arXiv preprint arXiv:1412.6980*, 2014.

[82] X. Weng, J. Wang, D. Held, and K. Kitani, "3d multi-object tracking: A baseline and new evaluation metrics", in *2020 IEEE/RSJ International Conference on Intelligent Robots and Systems (IROS)*, IEEE, 2020, pp. 10 359–10 366.

[83] H.-k. Chiu, J. Li, R. Ambruş, and J. Bohg, "Probabilistic 3d multi-modal, multi-object tracking for autonomous driving", in *2021 IEEE International Conference on Robotics and Automation (ICRA)*, IEEE, 2021, pp. 14 227–14 233.

[84] C. Gómez–Huélamo, L. M. Bergasa, R. Gutiérrez, J. F. Arango, and A. Díaz, "Smartmot: Exploiting the fusion of hdmaps and multi-object tracking for real-time scene understanding in intelligent vehicles applications", in *2021 IEEE Intelligent Vehicles Symposium (IV)*, IEEE, 2021, pp. 710–715.

[85] K. Wong, Y. Gu, and S. Kamijo, "Mapping for autonomous driving: Opportunities and challenges", *IEEE Intelligent Transportation Systems Magazine*, vol. 13, no. 1, pp. 91–106, 2020.

[86] M. Dupuis, M. Strobl, and H. Grezlikowski, "Opendrive 2010 and beyond–status and future of the de facto standard for the description of road networks", in *Proc. of the Driving Simulation Conference Europe*, 2010, pp. 231–242.

[87] A. Sadeghian, V. Kosaraju, A. Sadeghian, N. Hirose, H. Rezatofighi, and S. Savarese, "Sophie: An attentive gan for predicting paths compliant to social and physical constraints", in *Proceedings of the IEEE/CVF conference on computer vision and pattern recognition*, 2019, pp. 1349–1358.

[88] J. Hong, B. Sapp, and J. Philbin, "Rules of the road: Predicting driving behavior with a convolutional model of semantic interactions", in *Proceedings of the IEEE/CVF Conference on Computer Vision and Pattern Recognition*, 2019, pp. 8454–8462.

[89] A. Diaz-Diaz, M. Ocaña, Á. Llamazares, C. Gómez-Huélamo, P. Revenga, and L. M. Bergasa, "Hd maps: Exploiting opendrive potential for path planning and map monitoring", in *2022 IEEE Intelligent Vehicles Symposium (IV)*, IEEE, 2022, pp. 1211–1217.

[90] M. Quigley, K. Conley, B. Gerkey, *et al.*, "Ros: An open-source robot operating system", in *ICRA workshop on open source software*, Kobe, Japan, vol. 3, 2009, p. 5.

[91] H. Tverberg, "A proof of the jordan curve theorem", *Bulletin of the London Mathematical Society*, vol. 12, no. 1, pp. 34–38, 1980.

[92] A. Bewley, Z. Ge, L. Ott, F. Ramos, and B. Upcroft, "Simple online and realtime tracking", in *2016 IEEE international conference on image processing (ICIP)*, IEEE, 2016, pp. 3464–3468.

[93] A. Geiger, P. Lenz, and R. Urtasun, "Are we ready for autonomous driving? the kitti vision benchmark suite", in *2012 IEEE Conference on Computer Vision and Pattern Recognition*, IEEE, 2012, pp. 3354–3361.

[94] K. Bernardin and R. Stiefelhagen, "Evaluating multiple object tracking performance: The clear mot metrics", *EURASIP Journal on Image and Video Processing*, vol. 2008, pp. 1–10, 2008.

[95] X. Weng and K. Kitani, "A baseline for 3d multi-object tracking", *arXiv preprint arXiv:1907.03961*, vol. 1, no. 2, p. 6, 2019.

[96] A. H. Lang, S. Vora, H. Caesar, L. Zhou, J. Yang, and O. Beijbom, "Pointpillars: Fast encoders for object detection from point clouds", in *Proceedings of the IEEE/CVF conference on computer vision and pattern recognition*, 2019, pp. 12 697–12 705.

[97] W. Zhang, H. Zhou, S. Sun, Z. Wang, J. Shi, and C. C. Loy, "Robust multi-modality multi-object tracking", in *Proceedings of the IEEE/CVF International Conference on Computer Vision*, 2019, pp. 2365–2374.

[98] E. Baser, V. Balasubramanian, P. Bhattacharyya, and K. Czarnecki, "Fantrack: 3d multi-object tracking with feature association network", in *2019 IEEE Intelligent Vehicles Symposium (IV)*, IEEE, 2019, pp. 1426–1433.

[99] X. Weng and K. Kitani, "Monocular 3d object detection with pseudo-lidar point cloud", in *Proceedings of the IEEE/CVF International Conference on Computer Vision Workshops*, 2019.

[100] J.-M. Jullien, C. Martel, L. Vignollet, and M. Wentland, "Openscenario: A flexible integrated environment to develop educational activities based on pedagogical scenarios", in *2009 Ninth IEEE International Conference on Advanced Learning Technologies*, IEEE, 2009, pp. 509–513.

[101] C. Gómez-Huélamo, J. Del Egido, L. M. Bergasa, *et al.*, "Train here, drive there: Ros based end-to-end autonomous-driving pipeline validation in carla simulator using the nhtsa typology", *Multimedia Tools and Applications*, pp. 1–28, 2021.

[102] P. Dendorfer, A. Osep, and L. Leal-Taixé, "Goal-gan: Multimodal trajectory prediction based on goal position estimation", in *Proceedings of the Asian Conference on Computer Vision*, 2020.

[103] S. Pellegrini, A. Ess, K. Schindler, and L. Van Gool, "You'll never walk alone: Modeling social behavior for multi-target tracking", in *2009 IEEE 12th international conference on computer vision*, IEEE, 2009, pp. 261–268.

[104] A. Lerner, Y. Chrysanthou, and D. Lischinski, "Crowds by example", *Comput. Graph. Forum*, vol. 26, pp. 655–664, Sep. 2007. DOI: 10.1111/j.1467-8659.2007.01089.x.

[105] J. Amirian, J.-B. Hayet, and J. Pettré, "Social ways: Learning multi-modal distributions of pedestrian trajectories with gans", in *Proceedings of the IEEE/CVF Conference on Computer Vision and Pattern Recognition Workshops*, 2019.

[106] X. Li, X. Ying, and M. C. Chuah, "Grip: Graph-based interaction-aware trajectory prediction", in *2019 IEEE Intelligent Transportation Systems Conference (ITSC)*, IEEE, 2019, pp. 3960–3966.

[107] A. Vemula, K. Muelling, and J. Oh, "Social attention: Modeling attention in human crowds", in *2018 IEEE international Conference on Robotics and Automation (ICRA)*, IEEE, 2018, pp. 4601–4607.

[108] C. Gómez-Huélamo, M. V. Conde, M. Ortiz, S. Montiel, R. Barea, and L. M. Bergasa, "Exploring attention gan for vehicle motion prediction", in *2022 IEEE 25th International Conference on Intelligent Transportation Systems (ITSC)*, IEEE, 2022, pp. 4011–4016.

[109] C. Tang, W. Zhan, and M. Tomizuka, "Exploring social posterior collapse in variational autoencoder for interaction modeling", *Advances in Neural Information Processing Systems*, vol. 34, pp. 8481–8494, 2021.

[110] M. Ahmed, R. Seraj, and S. M. S. Islam, "The k-means algorithm: A comprehensive survey and performance evaluation", *Electronics*, vol. 9, no. 8, p. 1295, 2020.

[111] *Argoverse benchmark*, https://eval.ai/web/challenges/challenge-page/454/evaluation, Accessed: 2022-03-19.

[112] L. Fang, Q. Jiang, J. Shi, and B. Zhou, "Tpnet: Trajectory proposal network for motion prediction", in *Proceedings of the IEEE/CVF Conference on Computer Vision and Pattern Recognition*, 2020, pp. 6797–6806.

[113] C. Gómez-Huélamo, M. V. Conde, R. Gutiérrez, R. Barea, Á. Llamazares, and L. M. Antunes Miguel Bergasa, "Efficient context-aware graph transformer for vehicle motion prediction", in *2023 IEEE 26th International Conference on Intelligent Transportation Systems (ITSC)*, IEEE, 2023.

[114] T. Xie and J. C. Grossman, "Crystal graph convolutional neural networks for an accurate and interpretable prediction of material properties", *Physical review letters*, vol. 120, no. 14, p. 145 301, 2018.

[115] N. Djuric, H. Cui, Z. Su, *et al.*, "Multixnet: Multiclass multistage multimodal motion prediction", in *2021 IEEE Intelligent Vehicles Symposium (IV)*, IEEE, 2021, pp. 435–442.

[116] R. S. Ross, "Planning minimum-energy paths in an off-road environment with anisotropic traversal costs and motion constraints", NAVAL POSTGRADUATE SCHOOL MONTEREY CA, Tech. Rep., 1989.

[117] A. Savitzky and M. J. Golay, "Smoothing and differentiation of data by simplified least squares procedures.", *Analytical chemistry*, vol. 36, no. 8, pp. 1627–1639, 1964.

[118] M. Ye, T. Cao, and Q. Chen, "Tpcn: Temporal point cloud networks for motion forecasting", in *Proceedings of the IEEE/CVF Conference on Computer Vision and Pattern Recognition*, 2021, pp. 11 318–11 327.

[119] Y. Liu, J. Zhang, L. Fang, Q. Jiang, and B. Zhou, "Multimodal motion prediction with stacked transformers", in *Proceedings of the IEEE/CVF Conference on Computer Vision and Pattern Recognition*, 2021, pp. 7577–7586.

[120] N. Deo and M. M. Trivedi, "Convolutional social pooling for vehicle trajectory prediction", in *Proceedings of the IEEE Conference on Computer Vision and Pattern Recognition Workshops*, 2018, pp. 1468–1476.

[121] Q. Li, Z. Han, and X.-M. Wu, "Deeper insights into graph convolutional networks for semi-supervised learning", in *Thirty-Second AAAI conference on artificial intelligence*, 2018.

[122] Z. Zhou, L. Ye, J. Wang, K. Wu, and K. Lu, "Hivt: Hierarchical vector transformer for multi-agent motion prediction", in *Proceedings of the IEEE/CVF Conference on Computer Vision and Pattern Recognition*, 2022, pp. 8823–8833.

[123] P. Bhattacharyya, C. Huang, and K. Czarnecki, "Ssl-lanes: Self-supervised learning for motion forecasting in autonomous driving", in *Conference on Robot Learning*, PMLR, 2023, pp. 1793–1805.

[124] R. Walters, J. Li, and R. Yu, "Trajectory prediction using equivariant continuous convolution", *arXiv preprint arXiv:2010.11344*, 2020.

[125] J. Gu, Q. Sun, and H. Zhao, "Densetnt: Waymo open dataset motion prediction challenge 1st place solution", *arXiv preprint arXiv:2106.14160*, 2021.

[126] B. He and Y. Li, "Multi-future transformer: Learning diverse interaction modes for behaviour prediction in autonomous driving", *IET Intelligent Transport Systems*, 2022.

[127] C. Katrakazas, M. Quddus, W.-H. Chen, and L. Deka, "Real-time motion planning methods for autonomous on-road driving: State-of-the-art and future research directions", *Transportation Research Part C: Emerging Technologies*, vol. 60, pp. 416–442, 2015, ISSN: 0968-090X. DOI: https://doi.org/10.1016/j.trc.2015.09.011. [Online]. Available: https://www.sciencedirect.com/science/article/pii/S0968090X15003447.

[128] C. Gómez-Huélamo, M. V. Conde, R. Barea, and L. M. Bergasa, "Improving multi-agent motion prediction with heuristic goals and motion refinement", in *Proceedings of the IEEE/CVF Conference on Computer Vision and Pattern Recognition*, 2023, pp. 5322–5331.

[129] C. Zhang, H. Sun, C. Chen, and Y. Guo, "Banet: Motion forecasting with boundary aware network", *arXiv preprint arXiv:2206.07934*, vol. 2, 2022.

[130] T.-Y. Lin, P. Dollár, R. Girshick, K. He, B. Hariharan, and S. Belongie, "Feature pyramid networks for object detection", in *Proceedings of the IEEE conference on computer vision and pattern recognition*, 2017, pp. 2117–2125.

[131] D. I. Shuman, S. K. Narang, P. Frossard, A. Ortega, and P. Vandergheynst, "The emerging field of signal processing on graphs: Extending high-dimensional data analysis to networks and other irregular domains", *IEEE signal processing magazine*, vol. 30, no. 3, pp. 83–98, 2013.

[132] T. N. Kipf and M. Welling, "Semi-supervised classification with graph convolutional networks", *arXiv preprint arXiv:1609.02907*, 2016.

[133] F. Yu and V. Koltun, "Multi-scale context aggregation by dilated convolutions", *arXiv preprint arXiv:1511.07122*, 2015.

[134] M. Liu, H. Cheng, L. Chen, *et al.*, "Laformer: Trajectory prediction for autonomous driving with lane-aware scene constraints", *arXiv preprint arXiv:2302.13933*, 2023.

[135] T. Gilles, S. Sabatini, D. Tsishkou, B. Stanciulescu, and F. Moutarde, "Thomas: Trajectory heatmap output with learned multi-agent sampling", *arXiv preprint arXiv:2110.06607*, 2021.

[136] Y. Wang, H. Zhou, Z. Zhang, *et al.*, "Tenet: Transformer encoding network for effective temporal flow on motion prediction", *arXiv preprint arXiv:2207.00170*, 2022.

[137] M. Zhou, J. Luo, J. Villella, *et al.*, *Smarts: Scalable multi-agent reinforcement learning training school for autonomous driving*, Nov. 2020. [Online]. Available: https://arxiv.org/abs/2010.09776.

[138] M. Behrisch, L. Bieker, J. Erdmann, and D. Krajzewicz, "Sumo - simulation of urban mobility: An overview", in *in SIMUL 2011, The Third International Conference on Advances in System Simulation*, 2011, pp. 63–68.

[139] R. Gutiérrez, C. Gómez-Huélamo, R. Barea, E. López-Guillén, F. Arango, and L. M. Bergasa, "Augmented reinforcement learning with efficient social-based motion prediction for autonomous decision-making", in *2023 IEEE 26th International Conference on Intelligent Transportation Systems (ITSC)*, IEEE, 2023.

[140] E. Yurtsever, J. Lambert, A. Carballo, and K. Takeda, "A survey of autonomous driving: Common practices and emerging technologies", *CoRR*, vol. abs/1906.05113, 2019. arXiv: 1906.05113. [Online]. Available: http://arxiv.org/abs/1906.05113.

[141] B. R. Kiran, I. Sobh, V. Talpaert, *et al.*, "Deep reinforcement learning for autonomous driving: A survey", *CoRR*, vol. abs/2002.00444, 2020. arXiv: 2002.00444. [Online]. Available: https://arxiv.org/abs/2002.00444.

[142] L. Zhu, F. R. Yu, Y. Wang, B. Ning, and T. Tang, "Big data analytics in intelligent transportation systems: A survey", *IEEE Transactions on Intelligent Transportation Systems*, vol. 20, no. 1, pp. 383–398, 2019. DOI: 10.1109/TITS.2018.2815678.

[143] J. Schulman, F. Wolski, P. Dhariwal, A. Radford, and O. Klimov, "Proximal policy optimization algorithms", *CoRR*, vol. abs/1707.06347, 2017. arXiv: 1707.06347. [Online]. Available: http://arxiv.org/abs/1707.06347.

[144] R. Gutiérrez-Moreno, R. Barea, E. López-Guillén, F. Arango, N. Abdeselam, and L. M. Bergasa, "Hybrid decision making for autonomous driving in complex urban scenarios", in *2023 IEEE Intelligent Vehicles Symposium (IV)*, 2023.

[145] C. Hoel, K. Wolff, and L. Laine, "Automated speed and lane change decision making using deep reinforcement learning", *CoRR*, vol. abs/1803.10056, 2018. arXiv: 1803.10056. [Online]. Available: http://arxiv.org/abs/1803.10056.

[146] T. Tram, A. Jansson, R. Grönberg, M. Ali, and J. Sjöberg, "Learning negotiating behavior between cars in intersections using deep q-learning", *CoRR*, vol. abs/1810.10469, 2018. arXiv: 1810.10469. [Online]. Available: http://arxiv.org/abs/1810.10469.

[147] Z. Zhang, A. Liniger, D. Dai, F. Yu, and L. V. Gool, *End-to-end urban driving by imitating a reinforcement learning coach*, 2021. arXiv: 2108.08265 [cs.CV].

[148] I. Kostrikov, D. Yarats, and R. Fergus, *Image augmentation is all you need: Regularizing deep reinforcement learning from pixels*, 2021. arXiv: 2004.13649 [cs.LG].

[149] M. Moghadam and G. H. Elkaim, *A hierarchical architecture for sequential decision-making in autonomous driving using deep reinforcement learning*, 2019. arXiv: 1906.08464 [cs.RO].

[150] G. Li, Y. Qiu, Y. Yang, *et al.*, "Lane change strategies for autonomous vehicles: A deep reinforcement learning approach based on transformer", *IEEE Transactions on Intelligent Vehicles*, vol. 8, no. 3, pp. 2197–2211, 2023. DOI: 10.1109/TIV.2022.3227921.

[151] R. Valiente, M. Razzaghpour, B. Toghi, G. Shah, and Y. P. Fallah, *Prediction-aware and reinforcement learning based altruistic cooperative driving*, 2022. arXiv: 2211.10585 [cs.RO].

[152] R. Gutiérrez-Moreno, R. Barea, E. López-Guillén, J. Araluce, and L. M. Bergasa, "Reinforcement learning-based autonomous driving at intersections in carla simulator", *Sensors*, vol. 22, no. 21, 2022, ISSN: 1424-8220. DOI: 10.3390/s22218373. [Online]. Available: https://www.mdpi.com/1424-8220/22/21/8373.

[153] T. Haarnoja, A. Zhou, K. Hartikainen, *et al.*, *Soft actor-critic algorithms and applications*, 2019. arXiv: 1812.05905 [cs.LG].

[154] J. de la Peña, L. M. Bergasa, M. Antunes, F. Arango, C. Gómez-Huélamo, and E. López-Guillén, "Ad perdevkit: An autonomous driving perception development kit using carla simulator and ros", in *2022 IEEE 25th International Conference on Intelligent Transportation Systems (ITSC)*, IEEE, 2022, pp. 4095–4100.

[155] J. Knodt, J. Bartusek, S.-H. Baek, and F. Heide, *Neural ray-tracing: Learning surfaces and reflectance for relighting and view synthesis*, 2021. arXiv: 2104.13562 [cs.CV].

[156] S. M. Koksbang and S. Hannestad, "Studying the precision of ray tracing techniques with szekeres models", *Physical Review D*, vol. 92, no. 2, 2015, ISSN: 1550-2368. DOI: 10.1103/physrevd.92.023532. [Online]. Available: http://dx.doi.org/10.1103/PhysRevD.92.023532.